

Marine Propeller Roughness Penalties

Mohamed Ahmed Mosaad

Naval Architecture and Shipbuilding
August 1986

NEWCASTLE UNIVERSITY LIBRARY

086 11537 3

Thesis 3111

University of Newcastle upon Tyne
Newcastle upon Tyne NE1 7RU

A Thesis submitted to the University of Newcastle upon Tyne for the
Degree of Doctor of Philosophy

ABSTRACT

The main objective of the project is to investigate the influence of surface roughness of marine propeller blades on propulsive power. The work has involved studies in the concept and practice of surface roughness measurement and characterisation as well as application of boundary layer theory for the analysis of propeller flow and propeller-ship hull flow interaction.

From extensive measurements of the surface topography of in-service propellers, a standard measurement procedure using different commercially available propeller-surveying instruments is described.

A development of turbulent boundary layer procedures has been made to determine sufficiently accurately the increment of drag coefficient of propeller blade sections due to propeller blade surface roughness. The roughness function used for this integral boundary layer analysis is derived using, principally, Musker's experimental data.

In addition, an experimental determination of the roughness function of a replicated propeller surface using a rotor apparatus has been carried out and described in detail.

The turbulent boundary layer procedures require a knowledge of the surface variation of pressure over the propeller blade. For this purpose a program based on Riegels method has been used to give the velocity distribution for a given propeller section geometry. This is used with the boundary layer procedures for developing a complete program "PROFNESS" to calculate the increment of drag coefficient of the blade section. Results from different propellers analysed indicate that the power penalty is proportional to the relative blade roughness to the $1/3$ power.

An investigation has been made to compare the increment of frictional coefficient for a flat plate and propeller section profiles. It is shown that a "rough" flat plane calculation is quite adequate for such work.

The use of a flat plate analogue as a reference to calculate the skin friction resistance of both propeller and hull surfaces is considered. It is shown that the proposed solution of flat plate momentum integral equations provides a valid, simple and practical solution to the problem of predicting the hull and propeller roughness drag penalties. It also provides, particularly for ship hull resistance, a strong support for the ITTC Correlation Line, not only, and importantly, in regard to its slope, but also its level.

For shipowners and operators who may not wish to access advanced computer programs, a simplified method has been proposed to calculate the propeller roughness penalties. There is a good agreement between the two

simplified and detailed propeller analysis methods.

The propeller roughness penalties, which can be obtained from either the simplified or the more rigorous method, can be related to the Rubert Propeller Comparator Gauges in order to quantify the benefits and justify the cost of the blade surface roughness.

Analytical procedures have been included which can be used to calculate the combined effects on ship performance of propeller blade and ship hull surface roughnesses.

ACKNOWLEDGEMENTS

The Author is indebted to Dr. R. L. Townsin, Head of Naval Architecture & Shipbuilding Department, and Dr. E. J. Glover whose supervision, continuous encouragement, suggestions and discussion contributed to the success of this work.

The Author wishes to thank the following companies and individuals for facilitating the measurements of propeller surfaces and providing valuable data and information:

- International Paint Company (specially Mr. Alex Milne).
- Stone Manganese Marine Limited.
- Shell International Marine Limited.
- Admiralty Marine Technology Establishment.
- Mr. D. F. Jones of Underwater Maintenance Co. Ltd.
- Dr. T. E. Svensen and Mr. D. Byrne of BMT.
- Rank Taylor Hobson Ltd. and Rubert & Co. Limited.

The help received from colleagues in the Ship Performance Group at Newcastle (SPG), Mr. D. Spencer and Mr. B. Chuah, is also acknowledged with gratitude. Special thanks are due to Mr. J. S. Medhurst who was a stimulating source of help and encouragement during his period as a member of the SPG.

I am deeply grateful to my wife whose patience and continuous support helped me to carry out this work.

The Author was financially supported by the Egyptian Government and by 1983/84 & 1984/85 ORS Awards from the Vice-Chancellors and Principals of the Universities of the United Kingdom.

CONTENTS

1	INTRODUCTION	1
2	CHARACTERISTICS OF PROPELLER SURFACE ROUGHNESS	8
2.1	Roughness Definition	8
2.2	Surface Roughness Characterisation	9
2.2.1	The Representation of the Surface Roughness	9
2.2.2	Statistical Height Descriptors	12
2.2.3	Extreme-value Height Descriptors	14
2.2.4	Texture Parameters	17
2.2.5	Spectral Analysis of Surface Profiles	18
2.3	Methods of Measurement or Assessment of Propeller Roughness	26
2.3.1	Propeller Roughness Comparator	28
2.3.2	Portable Stylus Machine	29
2.3.3	The Bench Stylus Machine	30
2.3.4	Replication	32
2.4	ROUGHNESS OF PROPELLER IN SERVICE	36
2.4.1	Review of Propeller Roughness Measurements	36
2.4.2	Causes of Propeller Roughness	42
2.5	BLADE SURFACES AND THEIR MAINTENANCE	45
2.5.1	Initial Surface Finish	45
2.5.2	Maintenance of Propeller	47

2.5.3	Propeller Coating	48
2.5.4	Costs of Polishing the Propeller	49
2.6	ANALYSIS OF MEASUREMENTS	51
2.6.1	Measurement of Rubert Comparator Gauges	51
2.6.2	Measurements of Poole River Propeller Surface	57
3	THE TURBULENT BOUNDARY LAYER ON ROUGH SURFACE	69
3.1	INTRODUCTION	69
3.2	THE MOMENTUM INTEGRAL EQUATION	71
3.3	THE VELOCITY PROFILE FOR TWO-DIMENSIONAL TURBULENT FLOW	73
3.4	THE LOW RANGE OF REYNOLDS NUMBER	79
3.5	CHARACTERISTIC PARAMETERS OF THE BOUNDARY LAYER	80
3.6	PROPOSED WORK AND GOVERNING BOUNDARY LAYER EQUATIONS ON ROUGH SURFACE	82
3.6.1	The Momentum Integral Equation	84
3.6.2	The Entrainment Equation	85
3.6.3	The Wall Equation	86
3.6.4	The Starting Conditions	87
3.6.5	Calculation of the Blade Section Drag Increment	88
3.6.6	Testing the Boundary Layer Integral Method	89
4	THE HYDRODYNAMIC ROUGHNESS FUNCTION FOR PROPELLERS	91
4.1	ROUGHNESS DRAG CHARACTERIZATION	91
4.1.1	Introduction	91
4.1.2	Derivation of Colebrook-White Roughness Function	99
4.1.3	Musker's Roughness Parameter	101

4.2	LABORATORY EVALUATION OF IN-SERVICE PROPELLER ROUGHNESS	
	FUNCTION	115
4.2.1	Introduction	115
4.2.2	Newcastle University Rotor Apparatus	117
4.2.3	Smooth Rotor Experiments	120
4.2.4	Rough Rotor Experiments	122
5	CALCULATION OF PROPELLER FLOW AND PROPELLER CHARACTERISTICS . . .	135
5.1	BLADE SECTION VELOCITY DISTRIBUTIONS	135
5.2	THE SHIP WAKE FIELD	138
5.2.1	Introdution	138
5.2.2	Nominal and Effective Wake	138
5.2.3	Formation and Determination of Wake	139
5.3	BASIC PROPELLER CHARACTERISTICS	140
5.4	EFFECTS OF PROPELLER ROUGHNESS UPON PROPELLER CHARACTERISTICS	141
5.5	THE EFFECT OF PROPELLER ROUGHNESS ON SHIP SPEED AND POWER	145
5.5.1	Power Penalty	145
5.5.2	Speed Penalty	147
5.6	APPLICATION STUDIES	150
5.6.1	Program "PROFNESS"	150
5.6.2	Case Studies	157
5.6.3	Comparison of Flat Plane and Section Profile Roughness Drag Penalty	169

6 SIMPLIFIED METHODS FOR THE ESTIMATION OF HULL AND PROPELLER

ROUGHNESS PENALTIES	173
6.1 ADDED RESISTANCE OF HULL ROUGHNESS	173
6.1.1 Introduction	173
6.1.2 The Hull Roughness Allowance	176
6.1.3 The ITTC Ship Correlation Line	177
6.1.4 Proposed Smooth Friction Line	179
6.2 BOUNDARY LAYER PREDICTION METHOD ON ROUGH FLAT PLANE	187
6.2.1 Introduction	187
6.2.2 Summary of the Method	188
6.2.3 Discussion and Applications	191
6.2.4 Approximate Equations	193
6.3 A SIMPLIFIED METHOD TO DETERMINE THE EFFECT OF PROPELLER ROUGHNESS ON SHIP POWER	208
6.3.1 Calculation of Thrust and Torque Coefficient of Equivalent Profile	208
6.3.2 Change of Thrust and Torque Coefficient Due to Propeller Roughness	211
6.3.3 Average Propeller Roughness APR	215
6.3.4 Applications and Economic Evaluations of Propeller Maintenance	217
6.4 COMBINED EFFECT OF PROPELLER AND HULL ROUGHNESSES ON THE SHIP PERFORMANCE	225
6.4.1 The Effect of Hull Roughness upon the Propulsion Factors	225
6.4.2 Estimation of Combined Propeller and Hull Roughness	

Penalties	229
7 CONCLUSIONS AND RECOMMENDATIONS	236
Appendix A : PROPELLER ROUGHNESS MEASUREMENT	249
Appendix B : POOLE RIVER SURFACE ROUGHNESS PROFILES	251
Appendix C : ALGORITHM SOLUTION OF THE BOUNDARY LAYER INTEGRAL EQUATIONS	257
Appendix D : ESTIMATING THE BOUNDARY LAYER THICKNESS	259
Appendix E : ROTOR EXPERIMENTS DATA	261
Appendix F : SUMMARY OF THE RIEGELS METHOD	265
Appendix G : PROPELLER/HULL ROUGHNESS PENALTIES - NUMERICAL EXAMPLE	267

LIST OF FIGURES

Figure -----		Page -----
(1.1)	Outline of Propeller Roughness Analytical Model.....	7
(2.1a)	Profiles and their associated Height Distribution showing the effects of Skewness and Kurtosis.....	15
(2.1b)	Extreme Height Descriptors.....	15
(2.2)	Two different Textures having approximately the same Roughness Amplitude.....	19
(2.3a)	Construction of the Autocovariance Function.....	21
(2.3b)	The Exponential Autocorrelation Function.....	21
(2.4a)	High-Spot Count.....	25
(2.4b)	Peak Count Wavelength.....	25
(2.5)	Ship Propeller Roughness Gauge.....	27
(2.6)	A Photograph of Rank Taylor-Hobson Surtronic 3 and its Parameter Module.....	34
(2.7)	A Photograph of the Surface Metrology Equipment.....	35
(2.8)	Changing of Propeller Roughness with Hull Condition...	41
(2.9)	Effect of Long Wavelength Cutoff on Ratio R_t/R_a	56
(2.10)	The Effect of Long Wavelength Cutoff on Roughness Height Parameters.....	63
(2.11)	The Effect of Long Wavelength Cutoff on Slope, Skewness	

	and Kurtosis.....	64
(2.12)	The Effect of Long Wavelength Cutoff on Roughness Texture Parameters.....	65
(2.13)	The Effect of Digitizing Intervals on Roughness Height Parameters.....	66
(2.14)	The Effect of Digitizing Intervals on Slope, Skewness and Kurtosis.....	67
(2.15)	The Effect of Digitizing Intervals on Roughness Texture Parameters.....	68
(3.1)	Demonstration of the Normalizing Conditions Given by Equation (3.10).....	78
(3.2)	Overall Skin Friction Coefficient For Smooth Flat Plate	90
(4.1)	The Logarithmic Law of the Wall and the Roughness Function.....	92
(4.2)	The Roughness Function.....	93
(4.3)	Nine Different Painted Surfaces Obeying Single Colebrook-White Curve.....	98
(4.4)	Exponential Plot of Musker's Roughness Function for R173-Surface Correlated with h'	107
(4.5)	Exponential Plot of Musker's Roughness Function for R253-Surface Correlated with h'	108
(4.6)	Exponential Plot of Musker's Roughness Function for R345-Surface Correlated with h'	109
(4.7)	Exponential Plot of Musker's Roughness Function for R420-Surface Correlated with h'	110
(4.8)	Exponential Plot of Musker's Roughness Function for R550-Surface Correlated with h'	111
(4.9)	Exponential Plot of Roughness Function from the Five Musker Surfaces Correlated with h'	112
(4.10)	Roughness Function from the Five Musker Surfaces Correlated with $R_a(2.0)$ and $B^*(0.5)$	113
(4.11)	Exponential Plot of Roughness Function from the Five Musker Surfaces Using $R_a(2.0)$ and $B^*(0.5)$	114
(4.12)	Newcastle University Rotor Apparatus.....	125

(4.13)	Torque/Speed Plots of Smooth Rotor Experiments.....	126
(4.14)	Smooth Friction Plots of Rotor Experiments.....	127
(4.15)	Photograph of "Poole River" Replicated Surface Applied on a Cylinder of the Rotor.....	128
(4.16)	Torque/Speed Plots of "Poole River" Experiments.....	129
(4.17)	Friction Plots of "Poole River" Experiments.....	130
(4.18)	"Poole River" Roughness Function Correlated with h'	131
(4.19)	"Poole River" Roughness Function Correlated with $Ra(2.5)$ and Pc	132
(5.1)	Velocity Distribution of Blade Section at 0.7R for "VLCC" Propeller.....	137
(5.2)	Speed and Force Diagram.....	143
(5.3)	Effect of Propeller Roughness upon K_T , K_Q and η_0	144
(5.4)	Speed-Power Relationship.....	148
(5.5)	Local Skin Friction Coefficient of Blade Section at 0.7R for "VLCC" Propeller.....	153
(5.6)	Flow Diagram of "PROFNESS".....	154
(5.7)	Model Wake Distribution of "VLCC" Propeller.....	161
(5.8a)	Roughness Effects on Only the Outer Half of a Propeller Blade (Power Penalty).....	162
(5.8b)	Roughness Effects on Only the Outer Half of a Propeller Blade (Speed Penalty).....	163
(5.9)	Power Penalty Due to Propeller Roughness.....	164
(5.10)	Increment of C_f for a Flat Plate.....	171
(5.11)	Effect of Pressure Distribution on Drag Penalty.....	172
(6.1)	Assumption of $2/C_f \sim R_\theta$ Relationship Below $R_\theta = 425$	183
(6.2)	Integration of Coles Results.....	184
(6.3)	Flowchart of the Program "RFPBL".....	190
(6.4)	"RFPBL" Smooth Friction Results.....	197

(6.5)	Flowchart of the Program "FPBL".....	198
(6.6)	Universal Law of the Wall Plots.....	199
(6.7)	Hull Skin Coefficient C_F as a Function of R_n With R_h as a Parameter ($m = 22.5$).....	200
(6.8)	Propeller Skin Coefficient C_F as a Function of R_n With R_h as a Parameter ($m = 9.02$).....	201
(6.9)	Hull Drag Penalty C_F Versus $(AHR/L)^{1/3}$ With R_n as a Parameter ($m = 22.5$).....	202
(6.10)	Propeller Drag Penalty C_F Versus $(h'/c)^{1/3}$ With R_n as a Parameter ($m = 9.02$).....	203
(6.11)	Results of C_F Obtained From "PROFNESS" and "FPBL" at 0.7R Blade Section For 4 Types of Propeller.....	204
(6.12)	Comparision of "FPBL" Results With Expermental Data.....	205
(6.13)	C_F Versus $(AHR/LPP)^{1/3}$ For 4 Types of Ships Using "FPBL" Prediction Method.....	206
(6.14)	$C_F \sim (h'/c)^{1/3}$ Plots of Propeller Foils and Their Equivelant Flat Plate.....	207
(6.15)	Propeller Power Penalty of "Product Carrier".....	220
(6.16)	Propeller Power Penalty of "VLCC".....	221
(6.17)	Propeller Power Penalty of "Container Ship".....	222
(6.18)	Propeller Power Penalty of "Car Ferry".....	223
(6.19)	Propeller Power Penalty of "Frigate".....	224

NOMENCLATURE

AHR	=	Average Hull Roughness (μm)
APR	=	Average Propeller Roughness (μm)
BAR	=	Blade area ratio
B_0	=	A constant in the skin friction equation ($B_0 = 5.0$)
B_1	=	Smooth wall law constant ($B_1 = 0.129$)
c	=	Blade section chord (m)
Cl	=	Rough wall constant in roughness function
C_{AA}	=	The weather allowance coefficient
C_D	=	Blade section drag coefficient
ΔC_D	=	Increment to drag coefficient due to roughness
C_e	=	Entrainment Function, $f(H^*)$
C_f	=	Local skin friction coefficient, $C_f = \tau_w / 0.5 \rho U_s^2$
C_F	=	Overall skin friction coefficient, $C_F = \text{Drag} / 0.5 \rho L v^2$
ΔC_F	=	Increment in C_F due to roughness
C_L	=	Lift coefficient of propeller blade section
ΔC_L	=	Change in lift coefficient
C_p	=	Pressure coefficient of propeller blade section
C_R	=	Residual resistance coefficient

- C_T = Total resistance coefficient of ship
 C_{vis} = Total viscous resistance coefficient
 D = Propeller diameter (m) or drag force (N)
 h = An arbitrary measure of roughness having the dimension of length (μm)
 h' = Musker's roughness parameter (μm)
 h^* = Combined centre line average and peak count roughness parameter, $h^* = Ra (2.5) Pc$ (μm)
 H_{12} = Boundary layer shape parameter, $H_{12} = \delta^*/\delta$
 H^* = Entrainment shape parameter, $H^* = (\delta - \delta^*)/\theta$
 J = Advance coefficient of propeller
 K = Van Karman constant, $K = 0.41$
 K_Q = Torque coefficient of the propeller
 ΔK_{QD} = Change in K_Q due to drag
 ΔK_{QL} = Change in K_Q due to lift
 K_T = Thrust coefficient of the propeller
 ΔK_{TD} = Change in K_T due to drag
 ΔK_{TL} = Change in K_T due to lift
 Ku = Kurtosis of the height distribution
 $(1+k)$ = Form factor
 L = Ship length, between perpendiculars, (m)
 m = Grigson's roughness parameter, $m = B1/C1$
 $m_0, m_2 \& m_4$ = Spectral moments (see text)
 n = Speed index or propeller revolutions per second
 P = Power delivered to the propeller (KW or hp)
 Pc = Peak count (see text)
 P/D = Pitch ratio

$\Delta P/P$	=	Power penalty (%)
Q	=	Section torque (N.m)
r	=	Radius of propeller element
R	=	Ship resistance (N or KN)
R_a	=	Centre line average roughness height, CLA, (μm)
R_h	=	Roughness Reynolds number, $R_h = h'U_s/\nu$
R_n	=	Reynolds number based on chord or length
R_q	=	Root mean square roughness height (μm)
R_t	=	Peak-to-trough roughness height (μm)
R_{tm}	=	Mean peak-to-trough roughness height (μm)
R_θ	=	Reynolds number based on momentum boundary layer thickness
RPM	=	Propeller revolutions per minute
S	=	Wetted surface area of ship (m^2)
S_a	=	Mean slope of the surface profile
S_c	=	Propeller material yield stress (MN/m^2)
S_k	=	Skewness of the height distribution
SHP	=	Shaft horse power
t	=	Thrust deduction fraction
T	=	Propeller thrust (N)
t/c	=	Blade section thickness to chord ratio
U_s	=	Streamwise velocity at edge of boundary layer
u	=	Streamwise velocity inside the boundary layer
u^*	=	Friction velocity, $u^* = \sqrt{\tau_w/\rho}$
v	=	Free stream velocity (m/s)
v_s	=	Ship speed (m/s or knots)
v_a	=	Propeller advance speed (m/s)

w_k	=	Coles' wake function
w_T	=	Wake fraction (Taylor)
x	=	Length along a surface from the leading edge (m)
x	=	Non-dimensional radius of propeller
x_h	=	Non-dimensional propeller hub radius
y	=	Distance normal to surface inside the boundary layer
z	=	Number of propeller blades
α	=	Texture parameter (see text)
α	=	Angle of incidence of flow to propeller section (Deg)
β	=	Advance angle (Deg)
β_i	=	Hydrodynamic pitch angle (Deg)
B^*	=	Correlation length (see text)
δ	=	Boundary layer thickness
δ^*	=	Displacement boundary layer thickness
η_D	=	Quasi-propulsive coefficient
η_H	=	Hull efficiency
η_0	=	Open water propeller efficiency
η_R	=	Relative rotative efficiency
η_s	=	Shaft transmission efficiency
η_{tot}	=	Total propeller efficiency
θ	=	Momentum boundary layer thickness
λ_{pc}	=	Peak count wavelength (mm or μm)
π	=	Coles' wake strength parameter
ρ	=	Density of fluid (Kg/m ³)
τ_w	=	Wall shear stress (N/m ²)
ν	=	Kinematic viscosity of fluid (m ² /s)

Φ = Face pitch angle (Deg)

χ = Nikuradse's roughness function

ω = $\sqrt{C_f/2}$ = u^*/U_s

CHAPTER ONE

INTRODUCTION

Fuel efficiency is one of the principal factors in today's ship technology, particularly through the maintenance of underwater surfaces. This is compatible with the evidence that new coating systems have been developed and are likely to continue to be developed in order to meet the demand for high standard of new hull smoothness. This demand is indeed the outcome of the extensive investigations of hull roughness and its impact on ship performance.

Ships with rough hulls often also have rough propellers, although the causes of the surface deterioration are different. Most attention has been given to the hull roughness problem however. It has often been cited that a rough hull condition is the cause of reduction in performance in ship operation. However, in practice a significant contribution to the reduction in performance may well be as a result of the propeller roughness. Alternatively, in absolute terms, propeller roughness is less important than hull roughness, but in terms of energy loss per unit area, propeller roughness is significantly more important. In economic terms, high return of a relatively cheap investment can be obtained by propeller maintenance standards.

Little work has been undertaken to relate propeller roughness with ship performance and much of that in recent years. The Ship Performance

Group at Newcastle University has been working on the problems of propeller roughness and by 1982 the foundation for further research work was established. At this point the Author joined the Group.

Ship operators are keen on keeping the cost of operation low, and they are interested to have a simple and practical procedure to quantify the benefits of the propeller maintenance. However, the problem is compounded by the range of topics which must be covered to meet the needs of the ship operator. The subject also deserves additional study to cover some interests in the academic field. Topics include:

1. The measurement and characterisation of blade surface roughness and the importance of the role of the texture parameters in assessing the surface roughness measure.
2. The hydrodynamic roughness function and its experimental evaluation.
3. Boundary layer prediction methods to calculate the drag penalty of propeller blade sections due to propeller blade surface roughness.
4. Calculation of the velocity distribution about the propeller blade section as a pre-requisite for the boundary layer procedures.
5. The incorporation of the section roughness drag contribution into a propeller analysis procedure.
6. The effect of the propeller roughness on shaft power.
7. The combined effects of both propeller blade and hull surface roughnesses on ship performance.

From the above topics, the Author has established his plan in developing the present work. Owing to the diversity of topics involved

in this work, review of the relevant literature, particular aims and achievements are discussed in individual chapters of the thesis.

Chapter 2 presents a discussion of the basic concepts and practice of the surface measurement and characterisation. This includes the general problems of describing and quantifying the surface measurements as well as the technical methods of measuring or assessing propeller surface roughness. The main causes of propeller surface deterioration are given together with descriptions of the proper treatment that a new and in-service propeller should receive. An important part of this Chapter is also the laboratory measurements of true replicas of propeller blade surfaces, namely, the six Rubert Comparator Gauges and the surface of "Poole River", a cast iron bladed propeller of 3.75 m in diameter, built for a Collier in 1949 to operate from the Tyne and Wear at 9.5 knots. A novel method of replication technique is used in reproducing the last surface. By this technique, many copies are produced not only for the roughness measurements but also to apply onto cylinders for drag tests. The analysis of the surface topography shows the importance of the long wavelength cutoff in measuring the height roughness parameters and provides reliable texture parameters which can be used for propellers. Additionally, a standard propeller roughness survey using either a stylus instrument or a comparator gauge is described.

Chapter 3 deals with the prediction of boundary layers to calculate the roughness drag penalty of propeller blade sections. The turbulent mean velocity profile of Coles [1] is used together with some

modifications which are introduced in order to make it valid for both low and high Reynolds number. The use of this modified velocity profile to derive the parameters in the boundary layer equations led to an improvement in the slope of the flat plate smooth friction line. The Colebrook-White roughness function [2] is used and Musker's roughness parameter [3] is adopted.

The complexities of the boundary layer equations defy any analytical solution, and so recourse must be made to semi-empirical methods. This implies that data from flow experiments relating to a particular rough surface should be used. In a review of boundary layer experiments, Chapter 4 shows that most of the engineering surfaces obey a particular form of the roughness function. This has been confirmed when the Author analysed nine sets of drag measurements of different coated surfaces. Although they have different roughnesses the data shows that all are Colebrook-White surfaces. From the experimental data of Musker, empirical relations have been found to use in the prediction methods. The Rubert propeller gauges have been carefully studied and their Musker's parameter values are re-evaluated. In addition a simpler version of Musker's 4-parameters h' is described in terms of only 2-parameters, which can be found using a portable stylus instrument.

In the same Chapter, novel experimental work is described to demonstrate the role of propeller roughness in augmenting the propeller section drag, using a rotor apparatus. A smooth-rotor experiment has also been performed to establish an appropriate base for comparison. The

experimental technique used to measure both the smooth and rough rotor drag is described. The roughness function so obtained shows trends similar to those of Colebrook-White type.

The boundary layer procedures require a knowledge of the surface variation of pressure over the propeller blade. In Chapter 5, the method used is that of Riegels-Wittich [4] and adopted by Patience [5] to suit the marine propeller flow. This is incorporated with the boundary layer prediction method to give a complete program "PROFNESS" which can be used to calculate the roughness drag penalty for a given blade section geometry. The program is used on different types of propellers and the results of the roughness penalty are then transformed to a power penalty using the Burrill's vortex analysis method [6]. Figure (1.1) shows the logic followed in Chapters 3, 4 and 5.

An investigation has been made to compare the increased section drag for a rough flat plane and a propeller section aerofoil for varying values of Reynolds number. From the results it was discovered that the effect of pressure distribution about the aerofoil section on boundary layer characteristics, for moderately roughened propellers, is not significant. This implies that a rough flat plane calculation is quite adequate for such work.

Following the above encouraging conclusion an attempt is made, in Chapter 6, to develop a "rough" flat plate solution in order to calculate the hull and propeller roughness penalty. The method is intended to

provide a valid, simple and practical solution to the problem of predicting the roughness drag. Meanwhile a new form of smooth friction line based on analytical solution of Coles' friction data [7] is proposed. This solution provides a strong support to the ITTC correlation line, not only in regard to its slope but also its level. In addition, a simplified method has been proposed to determine the effect of propeller roughness on ship performance. There is good agreement between the power penalty calculated using the two simplified methods and the more rigorous method of Chapter 5.

A rough propeller is often accompanied by a rough hull with corresponding changes in resistance and wake characteristics. The combined effect of these factors upon propeller efficiency is therefore examined. It is also shown that the total power penalty associated with a rough propeller operating behind a rough hull can be calculated by summing each of the propeller and hull power penalties together.

Finally, the conclusions drawn from the investigation are presented in Chapter 7.

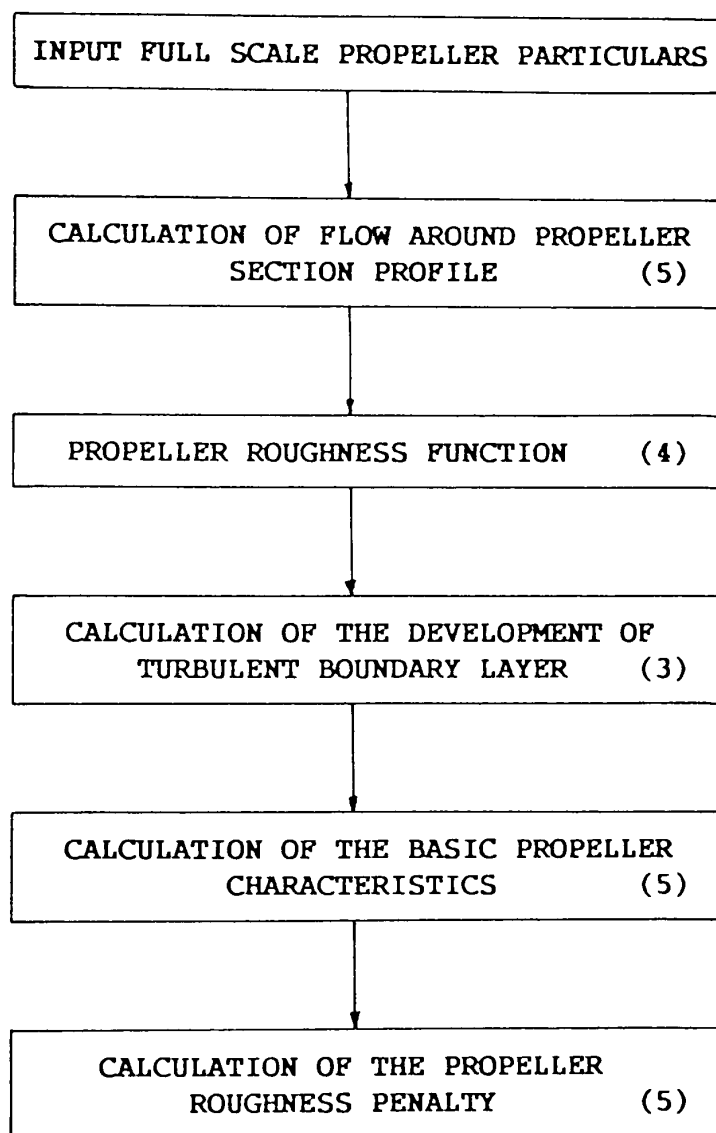


Figure (1.1) Outline of Propeller Roughness Analytical Model

(Figures in Brackets Refer to Chapters of the Thesis)

CHAPTER TWO

CHARACTERISTICS OF PROPELLER SURFACE ROUGHNESS

2.1 ROUGHNESS DEFINITION

Surface irregularities which can be seen and felt, are generally associated with machining processes. This has long attracted attention, and the first demand was for a better method of assessing them than by the customary finger nail.

It is well known that surface topography can be described by three different types of irregularity which are recognized as: roughness, waviness, and errors of form. The waviness is called "secondary texture" and may be described as a long wavelength periodic variation in surface height. In practice, waviness may be caused by inaccuracies in the cutting-tool machine, vibration, heat treatment or a badly trued grinding wheel.

Having the knowledge to define the waviness, then the roughness may be defined as the irregularities in the surface texture which are inherent in the production process, but excluding waviness and errors of form. However, this form of description is not very acceptable because for a complete texture of the surface, it is not possible to separate each contributing cause by instruments.

In order to quantify the surface roughness, an application must be defined. Having a knowledge of the application enables a measurement to be planned and in particular for it to be decided to what bandwidth of surface features the information collected should refer. Thomas [8] has demonstrated that, for most random surfaces there are no definite regions which can be separately considered as roughness, waviness or errors of form. Alternatively, two parameters are required to define the surface, one defining the height variation and the other a spatial or texture parameter, defining how heights vary in the plane of the surface.

2.2 SURFACE ROUGHNESS CHARACTERISATION

2.2.1 The Representation of the Surface Roughness

It is well known that a real surface represents a three-dimensional random structure. In other words, in order to gain a complete knowledge of the surface one should look at a three-dimensional representation. Such representations of surface roughness are being developed and sophisticated instrumentation has become a reality in small laboratories for workshop specimens.

However, questions may be raised of how far the accuracy of surface measurement needs to go, taking into account the needs of quality control and economic constraints. It would be impracticable to measure 100 locations from a ship hull or even 12 from a propeller in 3-D as an everyday quality control check.

Since the early development of surface metrology, it has been standard practice to examine the characteristics of rough surfaces from their measured surface profiles. In this work, single profiles or averages of several isolated profiles will be used for the analysis of propeller surface roughness. The advances in computer and microelectronic technology have enabled extensive use of digital methods in most modern surface roughness instruments. This allows more sophisticated analysis to be carried out with high accuracy and more economically.

Sampling of a roughness profile as a measure of roughness is still based on the original concept of considering a sample length deemed long enough to represent the roughness but short enough to ignore the undulations of possible waviness. Removal of these wavelengths is known as "filtering".

In spite of the usefulness and impressiveness of modern instruments, there is today still a lack of universally accepted standard measures of roughness. It is very difficult to compare roughness parameters evaluated from different sorts using instruments specifically designed to conform to certain standards. For example, various national standards might adopt the same parameter name for different roughness measures or, equally confusing, have different parameter names for the same roughness measurement.

Nearly all the parameters are affected by either the long wavelength filter or the short wavelength filter. If electronic or digital

filtering of the signal from the stylus head is not used, the long wavelength filtering is set by trace length and the short wavelength is fixed by the diameter of the stylus itself. It is very often the case that the instrument has a selection of standard long wavelength cutoff available and the length of the profile trace, at the "sampling length", is a multiple of it.

For ship hull roughness, the almost universal measure parameter, $R_t(50)$ has a long wavelength or, high pass cutoff, of 50 mm. Musker [3] has suggested that 2.0 mm is a more hydrodynamically significant cutoff. The International Standards for propeller roughness specify a high pass cutoff of 0.8 mm. This is thought to be too short for hydrodynamic work where cutoffs of 2.0, 2.5 and even 5.0 mm are in common use.

The choice of long and short wavelength cutoffs can radically alter the numerical values of roughness parameters evaluated from the roughness profile. Therefore, the long and short wavelength cutoffs and the type of filtering process, if any, should be specified with the measurements.

It is now generally accepted that two-parameter representation of roughness is required in the correlation between surface roughness and hydrodynamic drag. Surface profiles may be analysed by statistical techniques to produce various roughness parameters to describe both the roughness heights as well as the surface texture parameter. Thomas [9] has described the height parameters by two kinds of descriptor:

- Statistical height descriptors.

- Extreme-value height descriptors.

All height descriptors or the average parameters depend on the long wavelength cutoff or sample length. Extreme-value height descriptors along with the texture parameters are influenced by stylus diameter or, in the case of digital analysis the digitising interval.

2.2.2 Statistical Height Descriptors

The most universally used height descriptor is the average roughness, R_a , which is also known as the centre line average, CLA. It is easy to measure and can be defined as the average absolute deviation from mean line over one sampling length. This value usually averaged over several consecutive sampling lengths, depending on the standard used. For a sampling length L , R_a is defined as:

$$R_a = 1/L \int_0^L |z| dx \quad (2.1)$$

where, z is a height measured normal to the centre line. For the symmetrical Gaussian distribution, which is a good approximation for many surface structures,

$$R_a = 0.8 \sigma \quad (2.2)$$

where, σ is the root mean square surface roughness.

The root mean square σ or R_q is a more sensitive descriptor than R_a , especially to the longer wavelengths in the profile. It is defined as the root mean square deviation from profile mean over sampling length,

$$R_q = \left[\frac{1}{L} \int_0^L z^2 dx \right]^{1/2} \quad (2.3)$$

In terms of the surface height distribution, r.m.s. is equivalent to the standard deviation. Alternatively, it is the square root of the variance or second moment of the probability density function, $p(z)$.

The two other height parameters often found in the literature are the skewness, S_k and the kurtosis, K_u , of the height distribution. The skewness is a useful parameter for the measuring of the asymmetry of the distribution and can be defined as:

$$S_k = \frac{1}{R_q^3} \int_{-\infty}^{\infty} z^3 p(z) dz \quad (2.4)$$

It is the third moment of the distribution and has a value of zero for Gaussian surfaces. The skewness is also a useful measure of the relative prominence of peaks and valleys. In theory it is potentially very important in hydrodynamic roughness drag, since the peaks are intuitively much more important hydrodynamically.

The kurtosis is the fourth moment of the height distribution and represents the peakiness of the distribution. It is a measure of the sharpness of the peaks and valleys. It is usually written in normalised

form:

$$Ku = 1/Rq^4 \int_{-\infty}^{\infty} z^4 p(z) dz \quad (2.5)$$

The symmetric Gaussian distribution has kurtosis of three. Distributions with kurtosis greater than three are called "leptokurtic" in which the profile is very peaky. When the kurtosis is less than three (platykurtic) the peaks of the profile become plateaus and the valleys plains. Figure (2.1a) show the effects of skewness and kurtosis on surface profiles.

In practical application, skewness and kurtosis are relatively more difficult to evaluate and have large sample variations. They are described as statistically inefficient [8]. Moreover, measurements on a propeller surface indicate that its height distribution is nearly Gaussian so that these two parameters are relatively unimportant.

2.2.3 Extreme-value Height Descriptors

The extreme height parameters are commonly used in engineering surfaces and their numerical values are influenced by the sampling interval. Statistically they are all so similar that one parameter would probably be sufficient to describe their features as shown in Figure (2.1b).

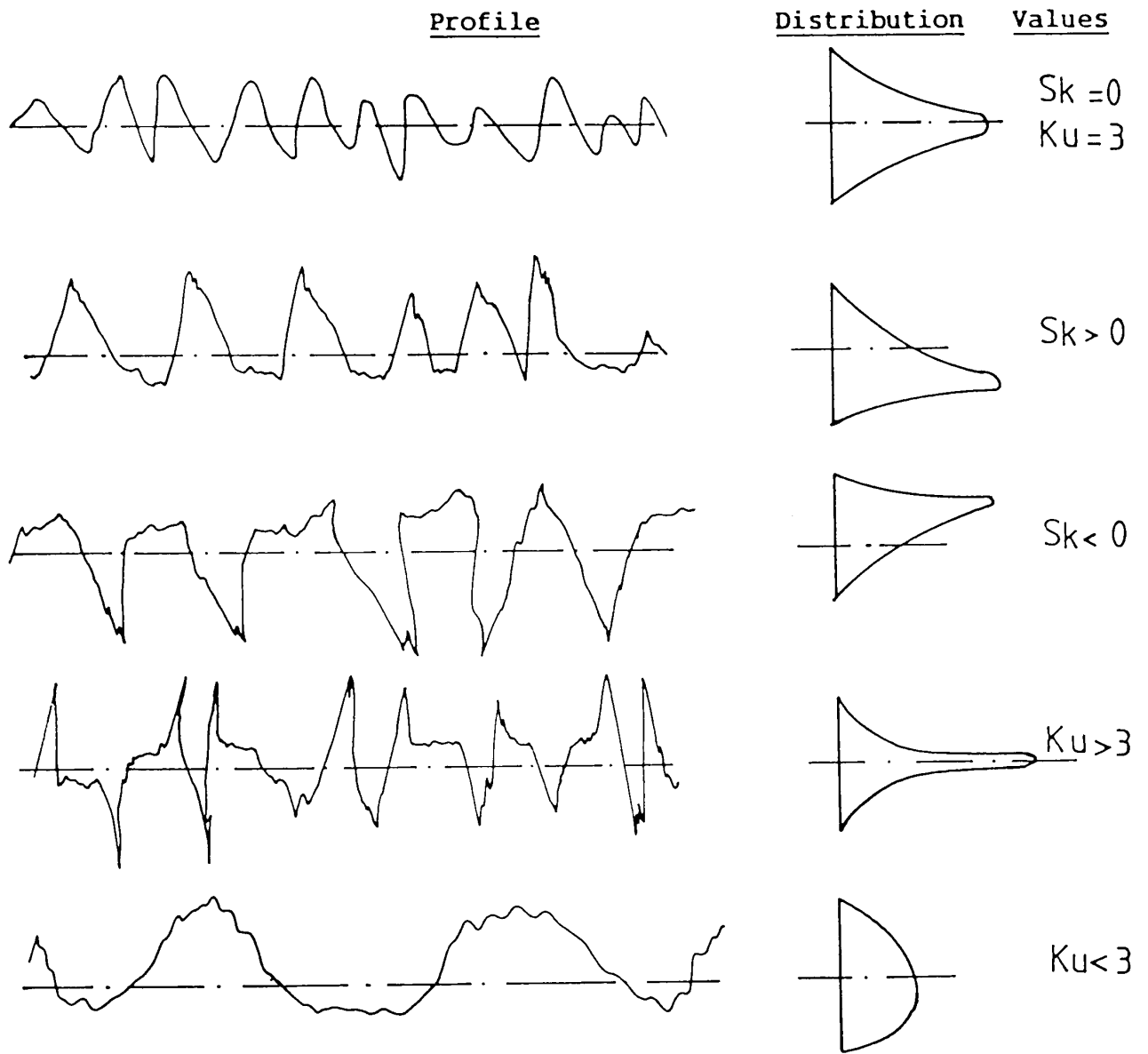


Figure (2.1a) Profiles and their associated Height Distribution showing the effects of Skewness and Kurtosis

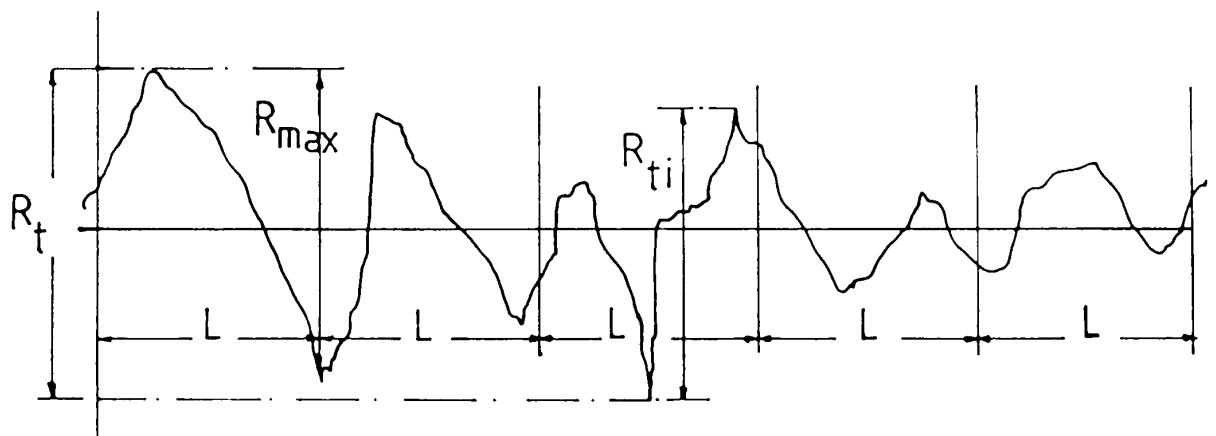


Figure (2.1b) Extreme Height Descriptors

A fundamental parameter is the peak to valley height, R_{ti} , which is the absolute value of the separation between the highest peak and lowest valley over the i th sample of length L , measured normal to the mean line. If N consecutive samples are taken, the distance between the highest peak and the lowest valley within all the samples is R_t . The mean of the R_{ti} over N samples is known as the mean peak valley height, R_{tm} , defined by:

$$R_{tm} = 1/N \sum_{i=1}^N R_{ti} \quad (2.6)$$

This parameter, $R_{tm}(50)$, was made popular by BSRA and its Hull Roughness Analyser [10] .

The mean apparent amplitude MAA, as originally defined by Lackenby [11] in association with the Wall Roughness Gauge involved an analysis of the profile by drawing envelope curves touching the highest peaks and lowest troughs in each 50 mm length. Byrne [12] showed that the same result could be obtained by drawing lines parallel to the mean slope yielding $R_t(50)$. The SPG defines the average $R_t(50)$ from each profile as Mean Hull Roughness MHR and then the Average Hull Roughness AHR over the whole hull as the average value of MHR which is equivalent to the original MAA. Thus,

$$AHR = 1/m \sum MHR \quad (m = \text{measurement stations}) \quad (2.7)$$

When $N=5$, R_{ti} then becomes the average peak to valley height R_z defined in the German standard DIN 4762,

$$Rz(DIN) = 1/5 \sum_{1}^{5} R_{ti} \quad (2.8)$$

The last extreme-value parameter based on peak to valley heights is the maximum peak to valley height, R_{max} , which is the largest value of the separation of the highest and lowest peaks in 5 consecutive sampling lengths.

Finally there is the ISO extreme height parameter, $Rz(ISO)$, which is called ten point height. It is defined as the mean separation of 5 highest peaks and 5 lowest valleys in one sampling length,

$$Rz(ISO) = 1/5 \left[\sum_{1}^{5} P_i - \sum_{1}^{5} V_i \right] \quad (2.9)$$

and the conditions $P_i > 0$, $V_i < 0$ should be satisfied.

2.2.4 Texture Parameters

The texture or spatial parameters give a description of the variation of the profile in the plane of the surface. Most texture parameters are statistically related to one another and they are strongly dependent on short wavelength cutoff. In digital methods this is equal to or larger than twice the sampling interval. According to the Nyquist criterion, the minimum rate of sampling required to define the waveform completely is about half of the smallest wavelength to be measured.

The mean slope of the surface profile is an important texture parameter and is often used in hydrodynamics. It is defined as the mean absolute profile slope over sampling length and its mathematical form is

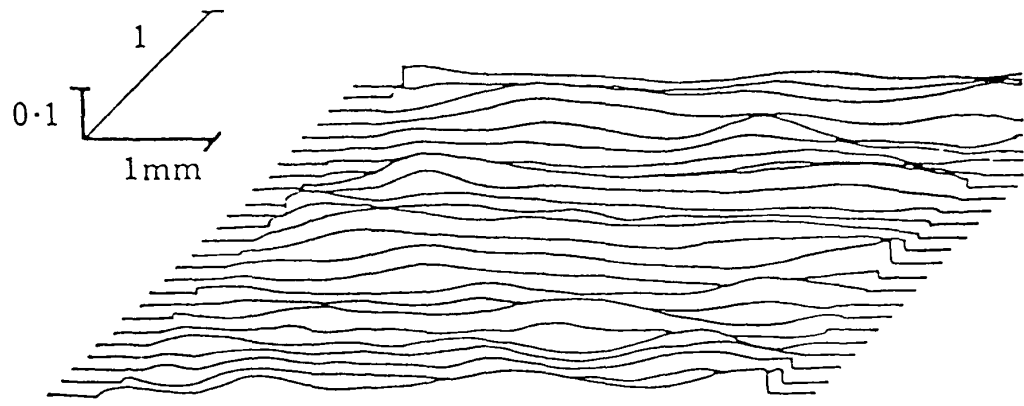
$$S_a = 1/L \int_0^L |dz/dx| dx \quad (2.10)$$

In order to specify the mean slope of the profile, it is safest to specify the sampling interval because as the former is reduced the value of the slope will increase. Figure (2.2) shows two surfaces having nearly the same height parameter, R_{tm} , but very different textures or slopes. There can be no doubt that the greater the slope the greater the hydrodynamic drag.

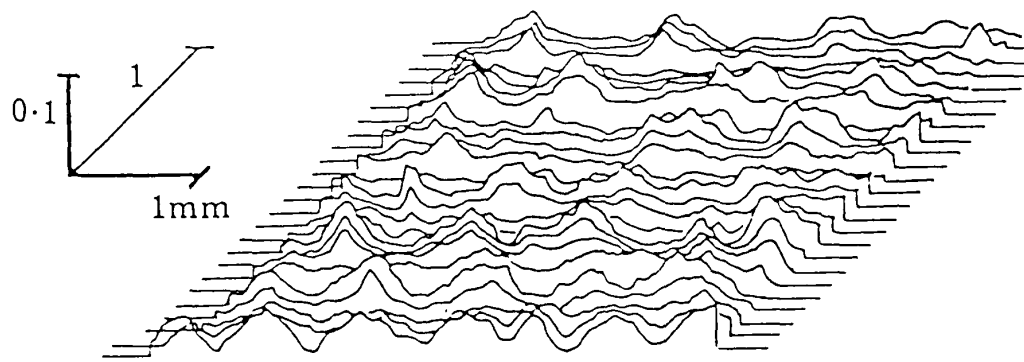
Other commonly used texture parameters suggested include the mean profile curvature or the second differential of the profile, and various random process parameters such as the correlation length and the so-called the Bandwidth Parameter. All these are functions of the peak and zero-crossing densities and their mathematical definitions are discussed in the next section.

2.2.5 Spectral Analysis of Surface Profiles

The application of random-process theory to surface roughness has been extremely informative and there are different ways to carry out the spectral analysis. Only an introduction to a few of the more elementary ideas of the subject will be outlined in the present section.



(a)



(b)

Figure (2.2) Two different Textures having approximately the same Roughness Amplitude

The autocovariance function (ACVF), or its normalized form, the autocorrelation function (ACF), are the most popular means of representing spatial variation. The ACVF, Figure (2.3a) is defined as:

$$R(\tau) = \lim_{L \rightarrow \infty} \frac{1}{L} \int_0^L z(x) z(x+\tau) dx \quad (2.11)$$

where L is the sample length. This equation can be written in a more statistical form:

$$R(\tau) = E \{ z(x) z(x+\tau) \} \quad (2.12)$$

where $E \{ \}$ denotes an expectation, i.e an average value of $z(x)z(x+\tau)$.

The ACF is simply the ACVF normalized by the square of the r.m.s. roughness. Thus :

$$\zeta(\tau) = R(\tau) / \sigma^2 \quad (2.13)$$

A simple exponential form has been found to fit the ACF for many random surfaces and is given as

$$\zeta(\tau) = \exp(-\tau / B^*) \quad (2.14)$$

where, $1/B^*$ is the decay rate of the function at the origin [Figure (2.3b)].

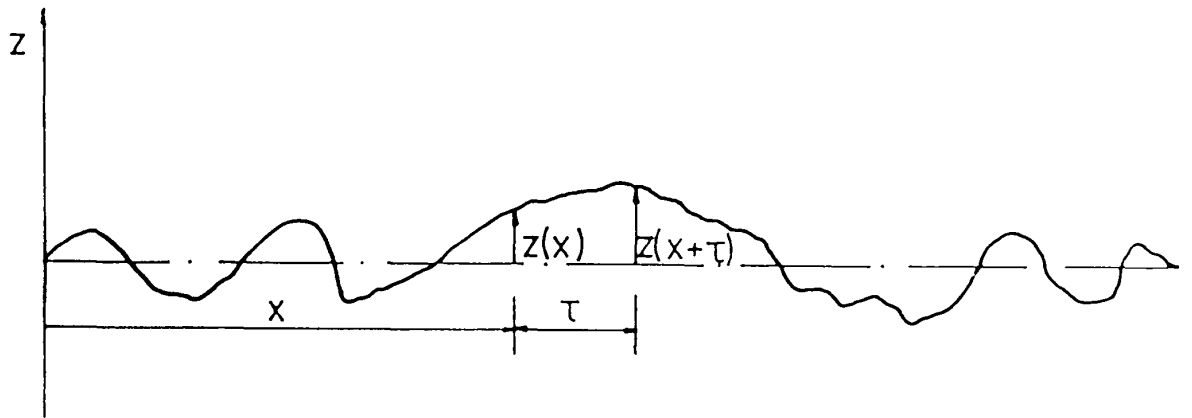


Figure (2.3a) Construction of the Autocovariance Function

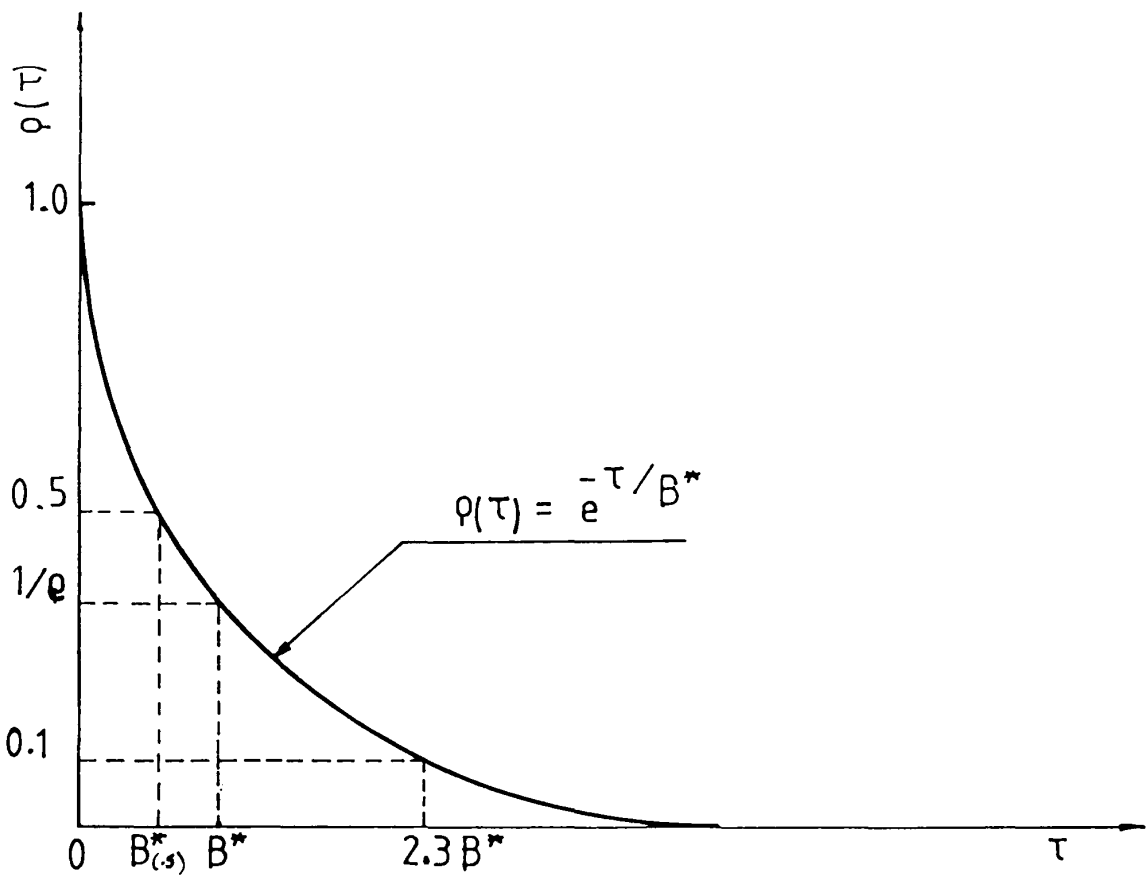


Figure (2.3b) The Exponential Autocorrelation Function

The correlation length B^* is defined as the distance over which the ACF decays to a certain value of 0.1 or $1/e=0.368$ or 0.5, depending on the application. In general B^* is not an intrinsic surface parameter, however, it can be used to define the spatial properties of the surface roughness.

Power spectrum is another form of spatial representation of the surface properties; which is defined as the variation of the power spectral density function with the frequency. It is determined usually either via the ACF or with the use of band-pass filters. In both cases the variability in the assessment of any parameter, measured from a given sample length, is governed largely by the product of the bandwidth of the profile and the duration of the sample, as illustrated by Thomas [8] .

The power spectral density function (PSDF) can be defined in a number of ways. The usual one is as the Fourier transform of the autocovariance function (ACVF):

$$G(\omega) = 1/2\pi \int_{-\infty}^{\infty} R(\tau) e^{-i\omega\tau} d\tau \quad (2.15)$$

A useful inverse to equation (2.15) is used for the situation when the PSDF is known and the ACVF is required:

$$R(\tau) = \int_{-\infty}^{\infty} G(\omega) e^{i\omega\tau} d\omega \quad (2.16)$$

The moments of the profile PSDF are defined as :

$$m_n = \int_{-\infty}^{\infty} G(\omega) \omega^n d\omega \quad (2.17)$$

The first three even moments of the above equation, m_0 , m_2 and m_4 are the variances of the distributions of profile heights, slopes and curvatures respectively. These are usually used to find a number of useful surface statistics. Probably the most fundamental spatial parameters is Nayak [13] bandwidth parameter, α , defined as:

$$\alpha = m_0 m_4 / m_2^2 \quad (2.18)$$

This parameter has found an application in rough surface hydrodynamics [14]. Generally, its numerical value depends on the bandwidth used in any analysis. A more simple method to estimate α directly from the profile without performing any spectral analysis as described in [15] is as follows:

the density of zero-crossing is given by,

$$D_0 = 1/\pi \left(m_2/m_0 \right)^{1/2} \quad (2.19)$$

and the density of extremes (peaks or valley) is given by,

$$D_e = 1/\pi \left(m_4/m_2 \right)^{1/2} \quad (2.20)$$

Therefore, the value of α can be estimated by,

$$\alpha = [D_e/D_o]^2 \quad (2.21)$$

Such a parameter is generally useful for measuring newer or smoother surfaces and could be used in testing ship antifoulings or propeller surface finish.

The density of zero crossings is twice the profile high spot count, HSC, which is the density of zero up crossings, see Figure (2.4a). The mean separation of the excursions above the mean line, measured over the sample length is known as the mean high-spot spacing, S_m . Alternatively, S_m can be defined as:

$$S_m = 1 / HSC \quad (2.22)$$

The Peak Count Wavelength, λ_{pc} is a similar parameter to S_m , and defined in [16] as twice the sample length divided by the number of times that the profile crosses completely through an envelope of amplitude R_a centred about the mean line [Figure (2.4b)]. Thus:

$$\lambda_{pc} = \frac{2 \text{ sample length}}{\text{No. of crossings}} \quad (2.23)$$

If more than one cutoff length is included in the sample then the average value or R_a for the profile length is calculated and this amplitude is applied to each sample length.

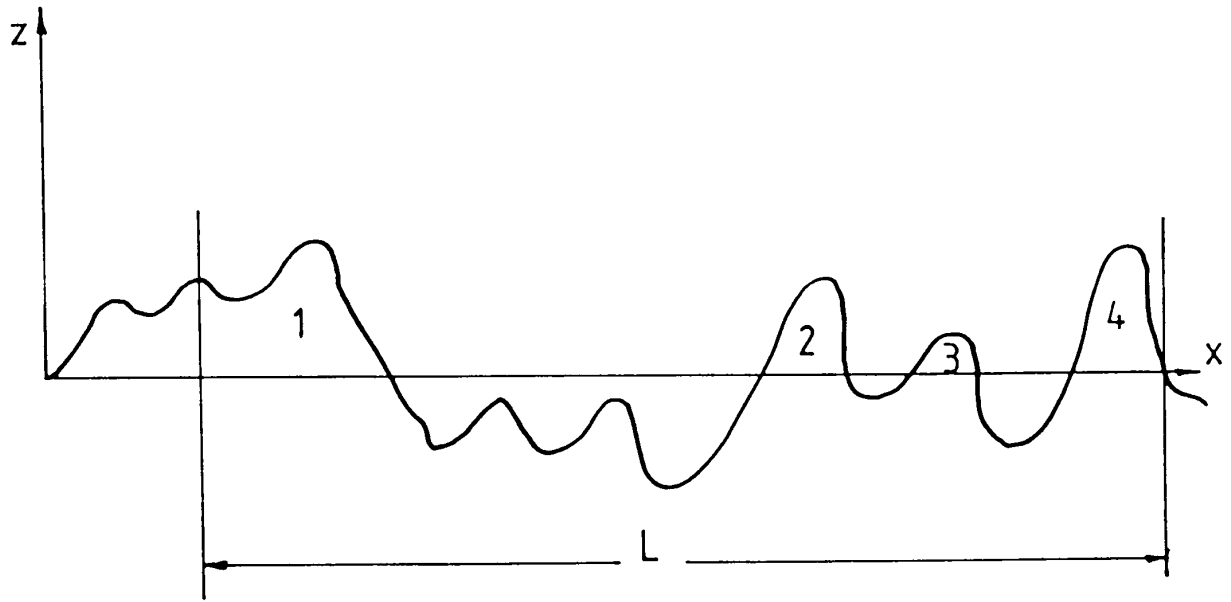


Figure (2.4a) High-Spot Count

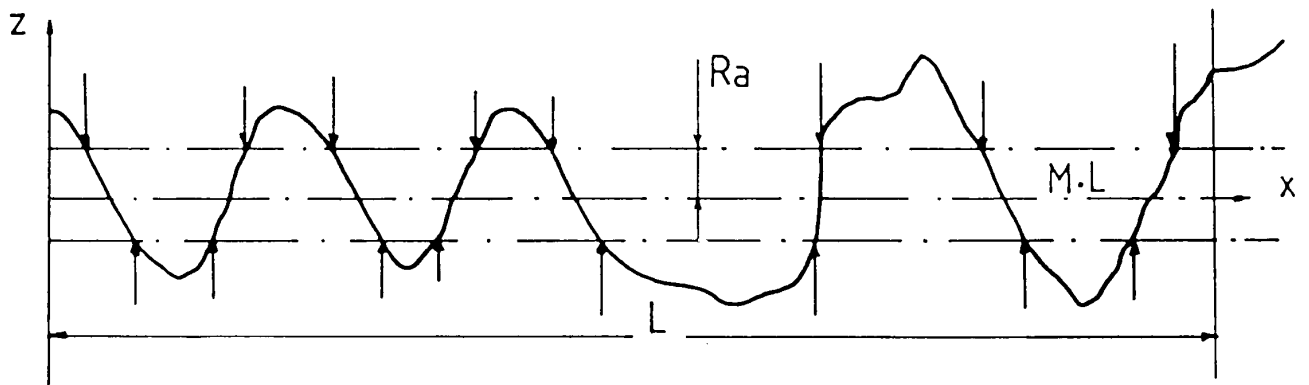


Figure (2.4b) Peak Count Wavelength

It is worth notice that, the above definition of λ_{pc} is slightly different from the one defined in the Hand-Held Rank Taylor Hobson Surtronic 3, used for propeller roughness measurement. In this case only one peak count is registered for each complete double crossing of the envelope. Thus the definition of peak count wavelength becomes:

$$\lambda_{pc} = \frac{\text{sample length}}{Pc} \quad (2.24)$$

where, Pc is the number of peak-valley pairs per unit length projected through a bandwidth equal to the measured Ra centred on the mean line.

2.3 METHODS OF MEASUREMENT OR ASSESSMENT OF PROPELLER ROUGHNESS

The propeller blade surface roughness may be measured by one of the following ways:

1. Using a propeller roughness comparator.
2. Using a portable stylus instrument.
3. Taking a replica of the surface and measuring it under a bench stylus machine.

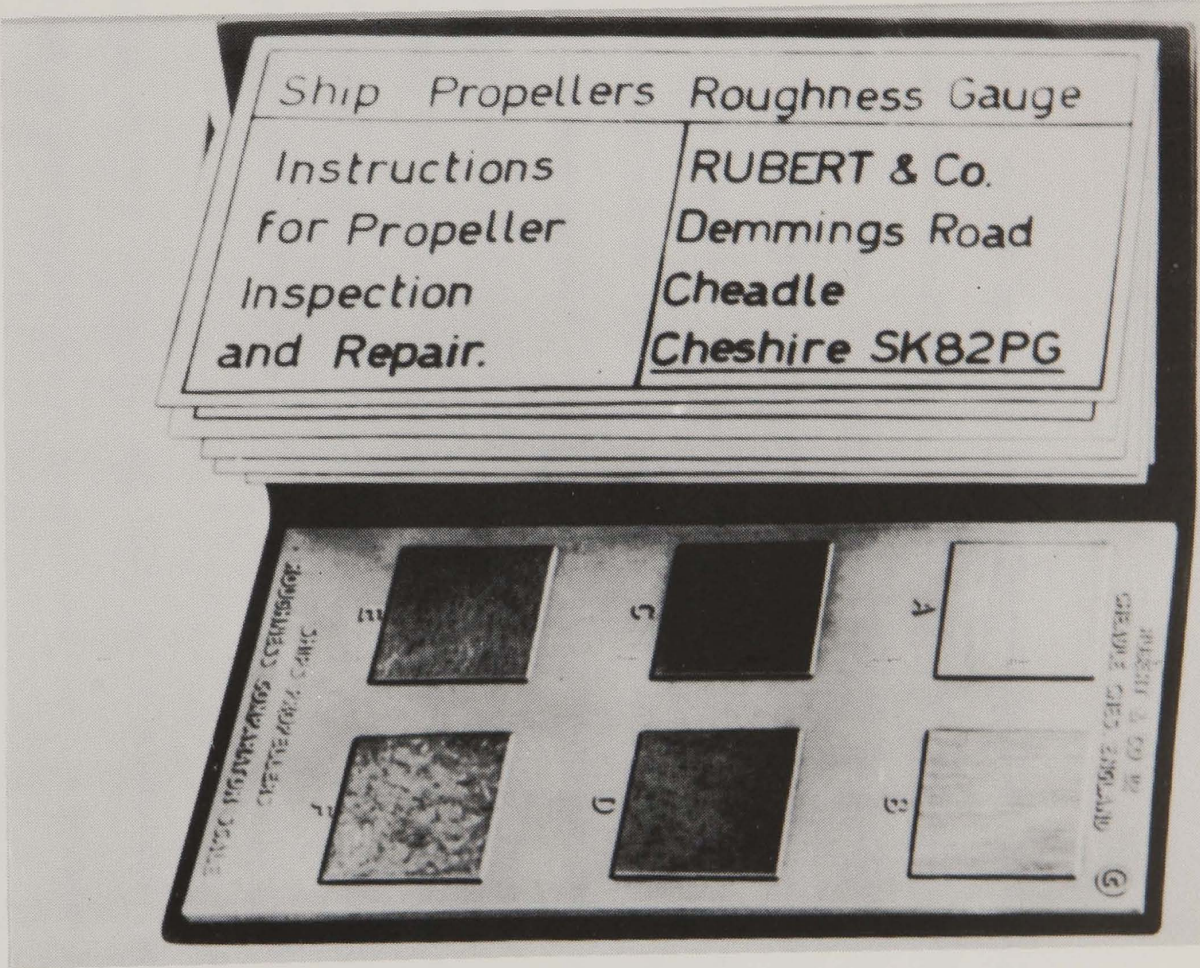


Figure (2.5) Ship Propellers Roughness Gauge.

2.3.1 Propeller Roughness Comparator

It is a simple method by which the propeller surface can be compared with a surface of known roughness. This type of tactile and visual comparison can be made by using the Rubert propeller roughness comparator. It consists of six specimens (A,B,C,D,E&F) of surface finish ranging from Ra=1 micron to Ra=30 microns. These surfaces are exact replicas of the surface of actual propeller blades. Specimens A and B are replicas of the surface roughness of new or reconditioned propeller blades to be used as a standard for comparison with similar surface roughness taken from propellers eroded by periods of service. Specimens C,D,E and F can be used to assess and report upon the propeller blade surface condition after periods of service.

The benefits of this comparator are that it is relatively inexpensive, can be carried in the pocket and a special version can be used underwater by divers if required. A photograph of the Rubert gauges is shown in Figure (2.5).

Research has shown the human finger is a very valuable and sensitive metrology instrument. However, comparators have their limitations on accuracy especially at the higher roughness where the change in successive steps becomes large. Therefore, large errors are likely when assessing blade roughness by this means. Fortunately, this error is reduced when transposing the result to estimating the power penalty since the relationship between the power penalty and the surface roughness is

described by one third power relationship. For example, a 30% error in measuring surface roughness would result in less than 10% error in the estimation of power penalty.

In order to carry out detailed calculation on the effect of propeller surface roughness upon ship power, a drag-roughness correlation is needed. For this purpose extensive measurement of Rubert comparator gauges has been carried out and is discussed later in section (2.6).

2.3.2 Portable Stylus Machine

Portable stylus systems which can be taken and used anywhere are required to measure the propeller roughness in certain circumstances. The Rank Taylor-Hobson Surtronic 3 is the most versatile and compact instrument which can be used equally well in propeller workshops or on the propeller on shaft in drydock. This instrument records Ra in micron or micro inches if preferred, over a range of cutoff lengths.

Surtronic 3 measures five sampling lengths in each traverse and the average of the five sampled Ra is displayed. There are as yet no internationally agreed standards of cutoff for the use of propeller surfaces measure. Whilst a choice of value from cutoff of 0.25, 0.8 or 2.5 mm can be used for most newly machined surfaces, a value of 2.5 mm is more realistic to define the surface topography for fluid drag calculation. Stone Manganese Marine Limited (S.M.M.Ltd.) have standardised on the Surtronic 3 instrument using a cutoff length of 2.5

mm for both new and old propellers.

Additional parameters can be provided by the parameter module which can be coupled directly to the display-traverse unit on the baseplate. The parameter module can also be positioned away from the display-traverse unit by using the connecting lead supplied. The peak count, P_c , used as a texture parameter in measuring the blade surface roughness, is provided per unit length (inch). This instrument may be considered too delicate for dock bottom use and it is not possible for underwater use. However, it can be used for the routine check in drydock if sufficient care is taken. Figure (2.6) shows a photograph of the Surtronic 3, and its Parameter Module.

A standard procedure for the measurement of propeller blade surface roughness, using the Surtronic plus its parameter module, is proposed by the Ship Performance Group and already accepted by S.M.M.Ltd. Rubert comparator gauges underwater or in dock can also be used for such work. A specification of this procedure is given in Appendix A.

2.3.3 The Bench Stylus Machine

A sophisticated system of modern instruments in conjunction with microcomputer and associated software is also used in the present work. A photograph of the surface metrology equipment are shown in Figure (2.7). This is made available by courtesy of International Paint Co. Ltd. It consists of a Ferranti Surfcom bench stylus machine with two

alternative skidless styli. One, a large spherical stylus intended primarily for film thickness measurements. The other is much smaller, 3 micron truncated pyramid stylus for the detailed measurement of surface topography.

The Surfcom has three modules:

1. The measuring table carrying the stylus, traversing gearbox and specimen platform.
2. The indication unit with range and manual cutoff switches, zero and gain adjustments, analogue meter.
3. A chart recorder.

The Surfcom is connected to a digital interface which sends measured data on line to a PET microcomputer for analysis. A second chart recorder is also available which can be used to produce better plots than the Ferranti machine. Unfortunately, it is very slow and is therefore not really suitable for surface metrology work. There is also a tractor printer on which hard copies of the results may be obtained.

The software VARICUT84 [17] written for this system has facilities for carrying out a sequential measurement of a number of profiles on the same specimen. For a single profile, a large number of roughness parameters are computed and displayed on the VDU instantly. The operator may choose to print these calculation if required.

The processing capacity of the CBM PET computer on which the VARICUT84 runs is insufficient to carry out any form of spectral analysis. However, a transferring link was designed to pass data files from the PET to the Newcastle University Computer for use by the Ship Performance Group in hydromechanics roughness analysis.

2.3.4 Replication

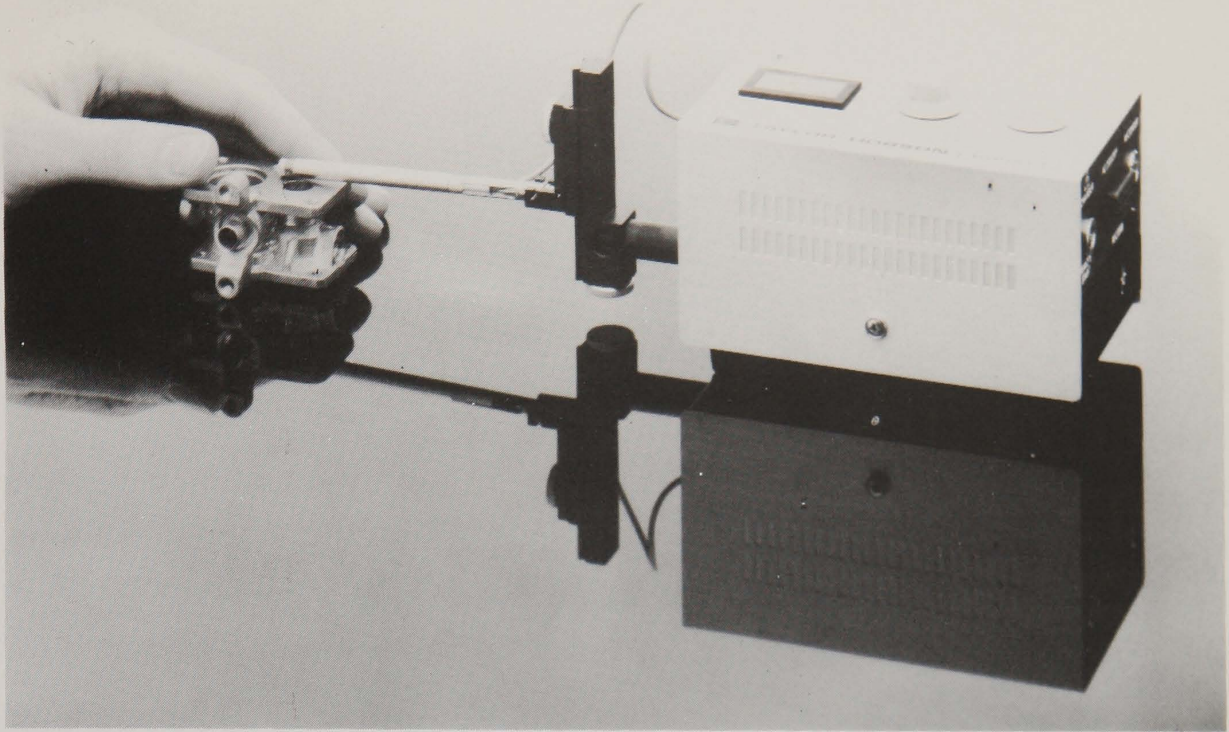
The main objective of copying a sample area of propeller surface in the workshop or drydock is to obtain a flat replica of the original surface roughness. A single stage process method, using a piece of acetate flooded with acetone, has been described extensively elsewhere [18] . It is a quick method to use. To obtain a flat replica surface, only small areas of propeller blade can be copied. The roughness is usually measured with stylus instruments. Before processing the data, it has to be remembered that the surface is a negative replica.

A two stage process is needed to obtain a nominally flat positive replica. Rotating cylinder drag measurement (see later) requires the use of positive replica surfaces, which can also be used with stylus instruments for measuring the surface topography. A "negative" replica of the propeller surface is taken by applying thixotropic silicon rubber compound to the blade, using either a paint brush or a pallet knife. This should be done after the surface to be measured is cleaned of contamination and fouling, if any, and then dried.

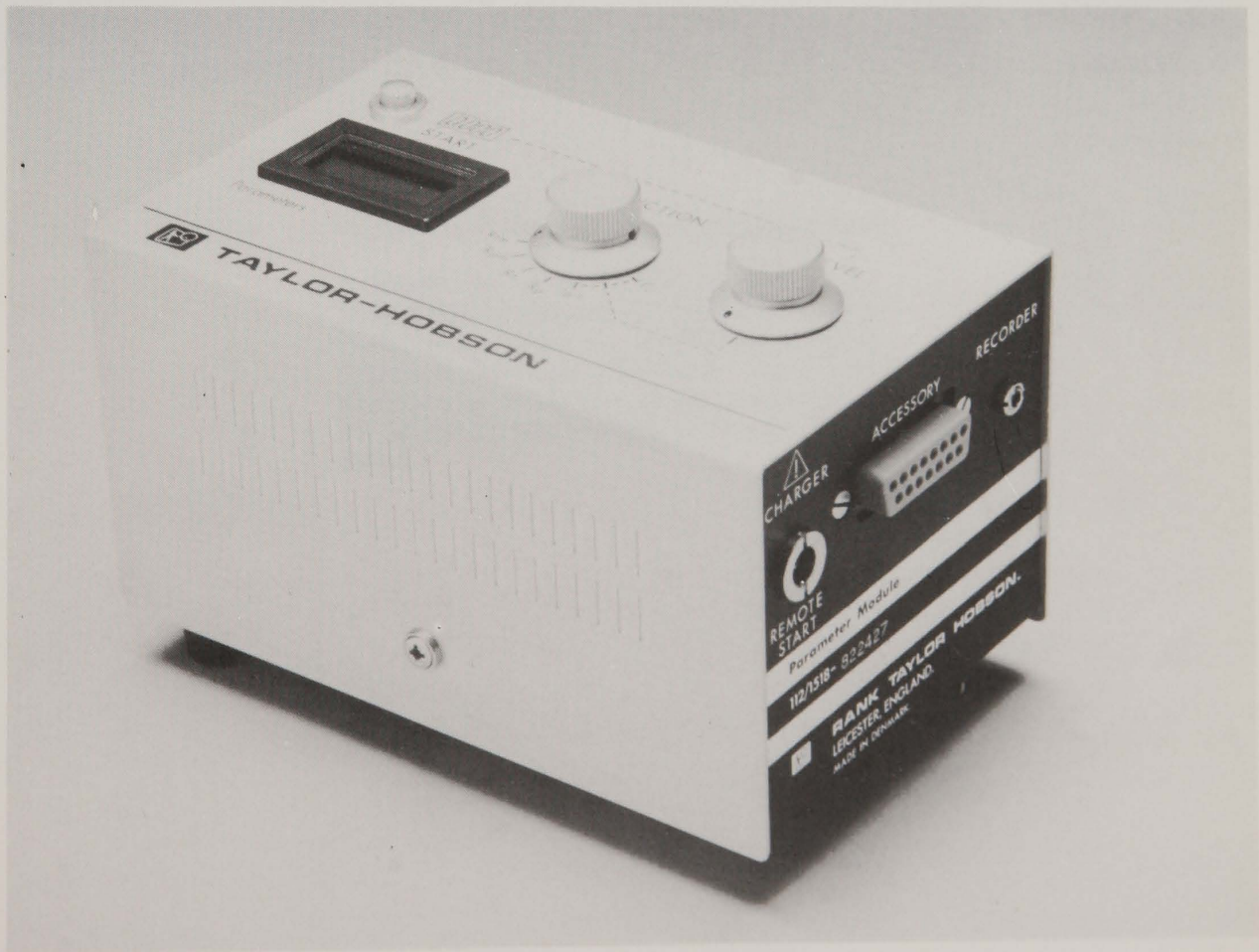
The silicon rubber has an excellent dimensional stability and contour-following properties and is nonstick. Its replica has been found to be extremely accurate if the paste was applied correctly; i.e. by freeing any air-bubbles that may be trapped. Some considerable length of time should also be allowed for the paste to set before peeling from the blade. In order to cover the circumferential surface area of the cylinder using a relatively small propeller surface area, more silicon copies are preferred.

After several hours the rubber can be peeled from the blade and taken to the workshop. There it is placed face down on a machined table and more silicon rubber applied to the back to give a nominal flat horizontal datum. The negative is then placed face up on the table and as many positive copies as required are made using a solventless flexible polyurethane elastomer. The elastomer positives are attached to the cylinders using more elastomer as an adhesive.

The surface topography of these elastomer positive panels are measured using the computerised Ferranti "Surfcom" stylus profilometer.



Display unit and pick-up head.



Parameter Module.

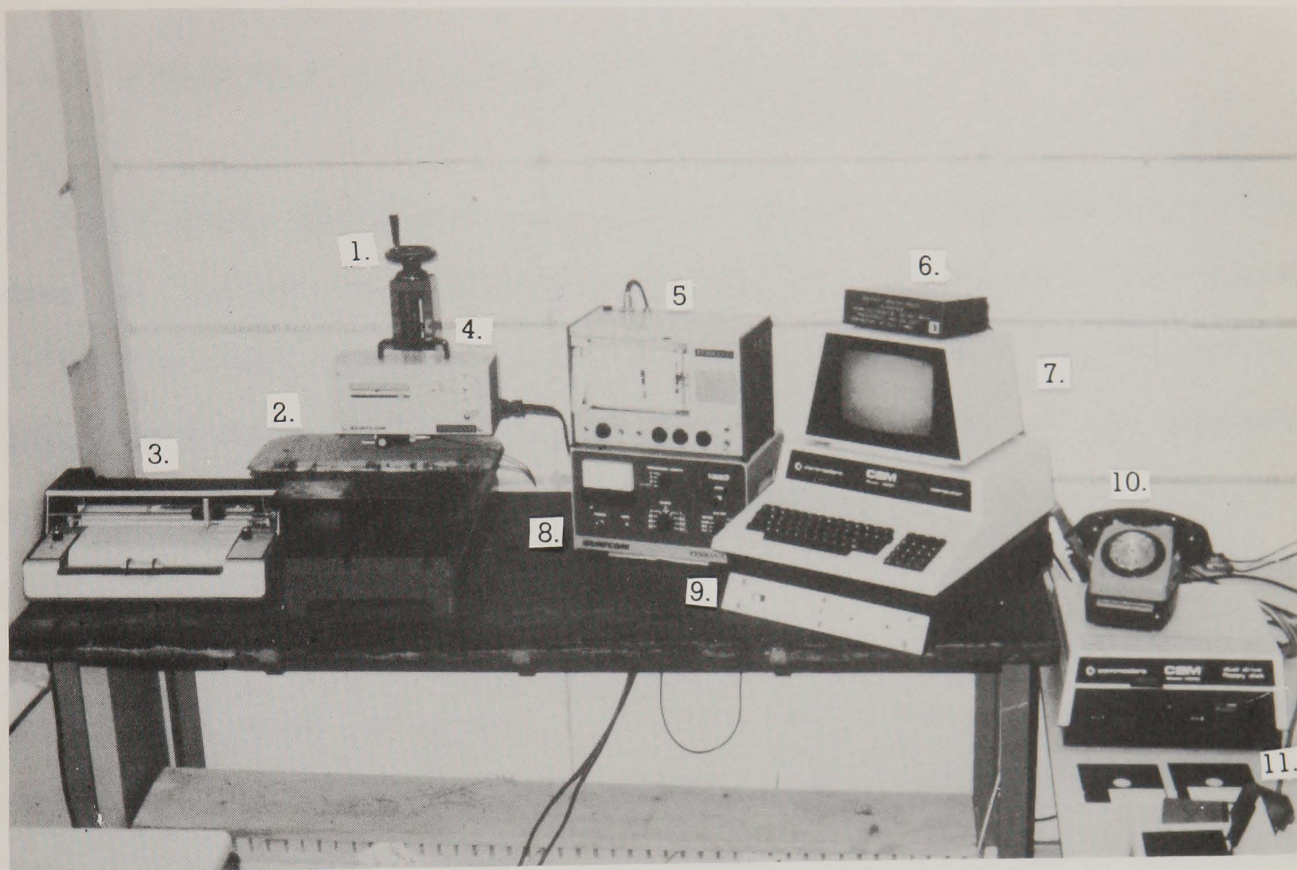


Figure (2.7) Surface Metrology Equipment

1. Measuring table. 2. Ship hull test plate.
3. Backup chart recorder. 4. Stylus & gear-box.
5. Chart recorder. 6. IEEE 488/RS232 interface.
7. Microcomputer. 8. 'SURFCOM' control unit.
9. Analog/digital converter.
10. MODEM (for transfer of data)
11. Disc drive.

2.4 ROUGHNESS OF PROPELLER IN SERVICE

2.4.1 Review of Propeller Roughness Measurements

Surprisingly enough there are very few propeller roughness measurement data in international technical publications. Furthermore, the records in the few cases that have been published are not always complete and are often compounded by confusion mainly in the definition of the roughness parameters used.

In 1963 Wellman [19] published a number of roughness measurements made on new and used propellers. He concluded that the blade surface roughness for both new and used propellers was similar in nature to that of a uniformly sanded surface. From measurements on 43 new propellers he obtained Ra values of 5 to 10 microns. He suggested that these new propeller blades were generally quite smooth. However, there were considerable differences in the surface texture when entering service. Such observations are very important to show that propeller surfaces have a different texture from uniform sand described above. It must also be pointed out that better quality of propeller surface finish can be easily achieved in practice than the 5 to 10 microns quoted above. Typical values of Ra of about 1.2 microns have been obtained during the measurement of a new propeller at S.M.M.Ltd.

With regard to the increase in roughness with time, Wellman has shown that there is an appreciable deterioration of the propeller surface

condition after only seven months in operation. Unfortunately, he did not give the type of alloy metal used in the propellers under investigation. Therefore it is difficult to generalise whether similar deterioration would occur on propellers made from other materials. Wellman also found that, the roughness is usually greater on the outer radii of the blades on both face and back.

Broersma and Tasseron [20] described the roughness for a large number of new propellers in terms of H_{max} . Although the sample length was not quoted, Grigson [21] suggested that their H_{max} can be related to MAA, which corresponds to $R_t(50)$. Consequently, the specially finished blades had an average of MAA of 3 microns and the normally finished ones of 10 microns. These give a good agreement with the new propeller measured by the the Author at S.M.M.Ltd. ($R_a=1.2\mu m$, $P_c=115$). Broersma and Tasseron quoted some interesting results from the measurement of used propellers which also indicated that the roughness increased with the propeller's time in service. Unfortunately, this was not a systematic study of how propeller roughness characteristics change with service time.

Further measurements made by Sinclair [22], showed an increase in R_a of 10 to 12 microns within 3 years for "Bronze" propeller. He also remarked upon the lack of regular servicing of propellers.

Milne [21] reported some measurements of the roughness of large screws using the BSRA Hull Roughness Analyser. The values he obtained were

thought to be underestimates of the true figures owing to the use of an unsuitable design of probe.

Byrne et al [23] gave some very useful information from extensive surveys of propellers in service. They expressed the average roughness in terms of the unweighted mean values of $R_{tm}(2.5)$ and the texture parameter α . The general conclusion was both R_{tm} and α tend to increase with time in service. The initial rate of increase of $R_{tm}(2.5)$ ranges from almost nil to about 15 $\mu\text{m}/\text{year}$, with about 8 $\mu\text{m}/\text{year}$ being most frequent. For the texture parameter, α , the average initial rate of increase is about 2.5 $\mu\text{m}/\text{year}$.

In case of re-polishing the propellers, Byrne et al noted that the decreases in $R_{tm}(2.5)$ were accompanied by increases in α . However, a stable deteriorating rate of the surface texture has been indicated. Their analysis did not relate to propeller material, size, loading, cathodic protection, or other factors which would be expected to influence the roughening rate. However, their conclusion that changes in roughness occur most rapidly in the outer half of the blades, agree with that of Wellman. They also found that roughening affects the back more than the face.

Patience [24] has published R_a values for propellers which have been in service for periods of 12-24 months. It is interesting to note that according to these values the roughness has increased rapidly from the centre of the propeller, of 3 μm , outwards to the blade tips, of 20 μm .

In general terms, Patience showed that Ra values of 30 μm for propellers after 12 months in service have also been measured.

The most recent results have been reported by Meyne et al [25] Over a period of 1.5 years they measured about 91 marine propellers and 12 inland waterway propellers using principally the Rubert comparator gauge. Although they presented good propeller surveys, their conclusion that propellers become smoother after entering service seems to be in error. Patience pointed out in his discussion of the paper that Meyne et al might have misinterpreted the numerical values of the ISO propeller roughness measures of peak valley average (PVA) and Ra.

Meyne assumed that all new propellers manufactured before 1981 would be made to class 1 finish of ISO.R.484 1966, which requires a PVA of less than 9 μm . However, Meyne and his co-authors appeared to have misread the standard and took it as less than 9 μm Ra. In table 1 of the appendix I of their paper, a factor of 3.7 is given which can be used in converting from Ra to PVA. This means that the ISO 1966 roughness value of 9 μm is equivalent to about 2.4 μm Ra. Consequently, most of the propellers they measured had a rougher surface than the ISO recommendation prior to 1981 contrary to their original conclusion.

However, it may be possible that there is an initial smoothing of the propeller upon entry into service. Ground surfaces, such as the new propeller blades tend to have fewer sharp peaks than relatively shallow valleys. These peaks can be eroded and a smoothing of the surface

results over an initial period for a short time.

Although there are no details of the propellers running time in Meyne et al's data, they did quote the condition of the hull in qualitative terms. It was therefore decided to study the variation of propeller roughness with hull condition. In Figure (2.8) the propeller roughness as measured at $x=0.7$ midchord is plotted against hull condition. A glance at the results in the former figure provides an expected conclusion that, on the whole, smooth hulls have smooth propellers. Alternatively, it might be said that in general, newer ships have smoother hulls than much older ships and indeed newer propellers are smoother. This again opposes Meyne's conclusion, that propellers had become smoother in service. Furthermore, the roughness measurements on those propellers belonging to the "smooth hull" have a mean value of $3.5 \mu\text{m Ra}$. This is quite close to the ISO R484 value of $9 \mu\text{m PVA}$ for new propellers of class 1 standard.

In the quest for smoother propellers it is appropriate to look at the best available propeller alloys which will remain relatively smooth in service. Accordingly, analysis was performed on all propellers attached to the "fairly smooth" hull condition. The test showed that the manganese bronze propellers were significantly rougher than those containing Ni-Al alloys as illustrated in Figure (2.8).

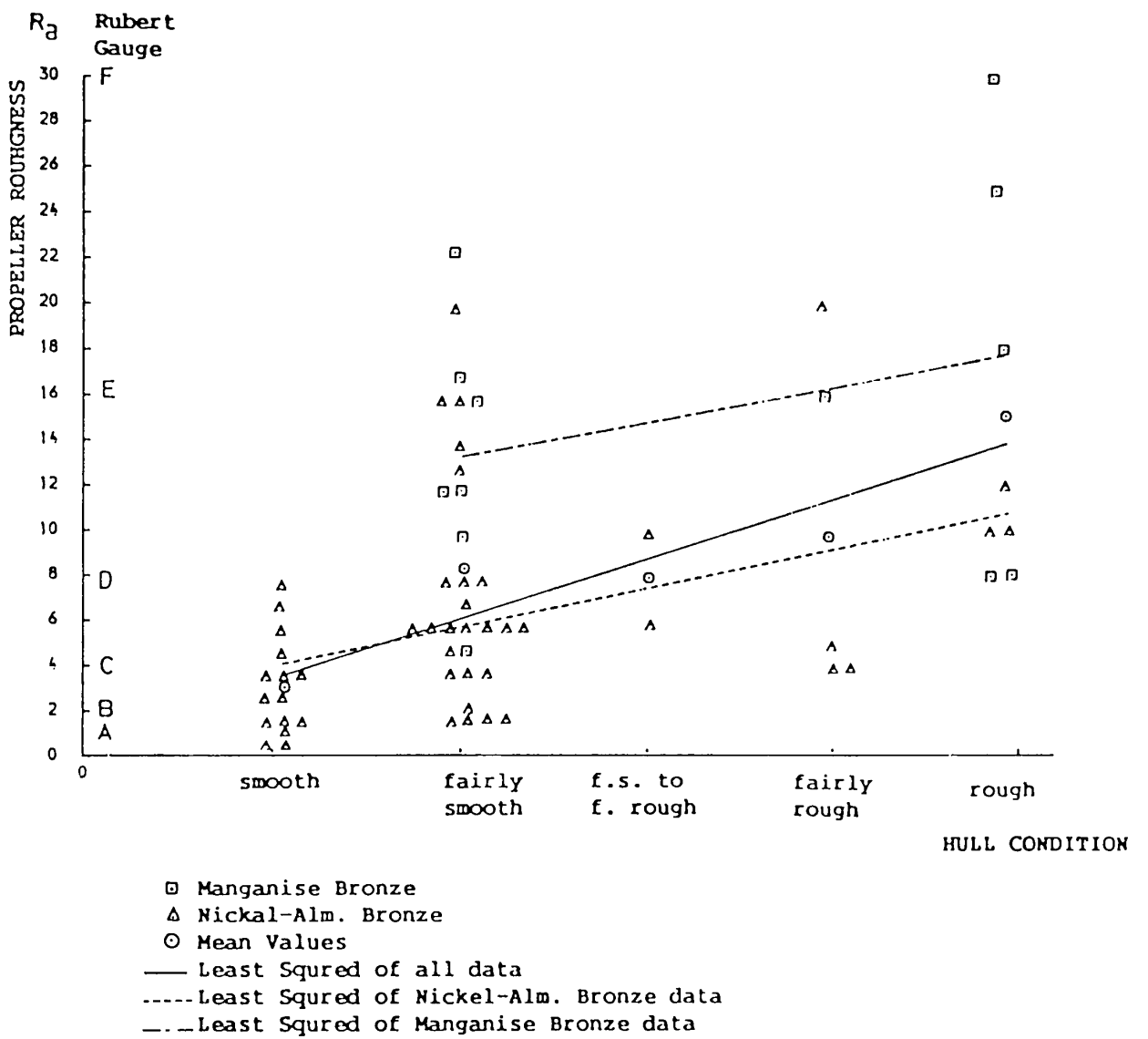


Figure (2.8) Changing of Propeller Roughness with Hull Condition

2.4.2 Causes of Propeller Roughness

The causes of surface roughness on propeller blades may be classified as follows :

- Corrosion - chemical and electrochemical.
- Impingement attack.
- Cavitation erosion.
- Improper maintenance.

Corrosion is probably the main cause of propeller deterioration. It occurs on both sides of the blades, particularly in outer half regions, where the speeds are very high relative to the water. The effects of bronze propeller corrosion and associated phenomena are outlined by Callis [26] . After a new propeller is fitted and immersed in sea water it becomes the cathode in the hull-propeller electrolytic cell. During the fitting-out period of the ship a thin, hard and strongly adherent coating of magnesium and calcium carbonates is formed on all propeller surfaces. In service, this chalk film is normally worn away at the outer parts of the propeller. At these local parts which become relatively small anodic areas with respect to the other large cathodic areas, and still covered with chalk, are subject to abnormal wastage by corrosion. Alloys such as Nikalium or Superston have about one half to one third the rate of deterioration as Manganese Bronze, Cast steels or Cast iron. However, this deterioration can be minimised by the adoption of properly designed and maintained cathodic protection systems.

Impingement attack, as described by Patience [24] , usually happens at the leading edge and the outer part of the propeller blades where the circumferential velocities are highest. Generally, it is a type of surface damage which has a widespread distribution of fairly shallow depressions. Normally, in order to withstand such attacks proper alloys such as Superston and Nikalium, can be used. Stainless steels are highly resistant to this type of attack, but mild steel and cast iron have very poor resistance.

Cavitation erosion is usually a concentrated and localised damage, particularly near the tip on the back of the blade. It is highly dependent on the propeller pressure distribution and the wake flow. With the most modern designs of propeller the resulting erosion is relatively small and generally negligible even after years of service. However, it is advisable to examine blade surfaces carefully for indications of cavitation erosion during the early service life of the propeller. So that if necessary, modification of blade sections may be adopted. It is to be noted that these modifications can not be regarded as a routine part of the propeller surface maintenance. Cavitation effects and preventions are specialised areas of study which will not be dealt with here.

Poor quality grinding may worsen the blade roughness which will in turn cause an increase in high wavenumber roughness due to scratching of the surface. At the same time, interference with the accurate dimensions of the blade leading edge form can seriously impair performance.

During hull painting, a propeller is always subject to splashes of conventional anti-corrosive or anti-fouling paints, which increase the surface roughness of the blade. Protection from grit-blasting should be given to the propeller by covering the blades with a layer of grease before the painting. This coating should be stripped off before the propeller goes into service.

It should be borne in mind that propellers also suffer from fouling which may cause a more considerable effect than that of roughness. However, the effects of propeller fouling are very difficult to quantify since there is a lack of theoretical and experimental work on the subject. Experimental work has been done by Kan et al [27] to investigate the characteristics of fouled propeller. From his results, it can be seen that the effects of propeller fouling in terms of power penalty are much greater than those of surface roughness.

The majority of marine growth on the propeller surface are of animal type, acorn barnacles and tubeworms being the most frequently encountered. Propeller fouling usually occurs during the fitting-out period or when the ship is in port. When the ship gets into service, large amounts of this fouling are likely to be removed from the outer parts of the blade. However, the influence of the small amount left near the boss of the propeller can not be ignored. There are also secondary effects of propeller fouling in which the blade surface never regains its original smoothness until the propeller is properly cleaned.

2.5 BLADE SURFACES AND THEIR MAINTENANCE

2.5.1 Initial Surface Finish

It is a normal procedure that the surface finish of the merchant ship propeller should satisfy the requirements of ISO class 1 criterion. However, some confusion has arisen between the 1966 standard and the existing one. The normal finish of propeller roughness to ISO standards is given in Table (2.1). It should also be remembered that the longwave cutoff for both standards is 0.8 mm.

TABLE (2.1)

ISO Surface Finish Standards

Standard	Year	class S	class I	Units
ISO R484	1966	3	9	$\mu\text{m } R_t$
ISO R484/1	1981	3	6	$\mu\text{m } R_a$

It is very difficult to say that ISO intended to reduce the standard of propeller finish in the latest version at the same time as the importance of a high standard is more appreciated. More likely, the change in units between the two standards may cause some confusion. This was the case in [25] when the two standards were used as equal numerically.

Examination of the ISO requirements was undertaken by the Author with other members of the Ship Performance Group at Newcastle and the results

and recommendations are reported in [28] . From this study a factor of 4 has been deduced to convert approximately the numerical values of R_a to R_t . On this basis the 1966 standard for class I which used R_t would be equivalent to a value of $2.3 \mu m R_a$. This is certainly much better than the 1981 class I standard and even better than the 1981 class S specified for finer propeller finish. Consequently, the current 1981 standard for propeller surface finish is a step backward as far as improvement of ship fuel consumption and propeller hydrodynamic smoothness are concerned.

An average value of 1.6% power can be saved, as will be seen later from the case studies, if the new propeller is finished at $2 \mu m R_a$ which can be easily achieved.

It is recommended therefore, that for all merchant ship propellers a standard of ISO class I should be specified for manufacturing tolerances, but with the 1981 class S standard of finish. It should be borne in mind that this standard is readily achievable in practice with the use of normal finishing methods at no extra cost [28] . It is also possible to reduce the roughness base even more than the proposed standard. In this case, the surface finish can be specified to meet the 1966 class S standard, which is equivalent to $0.8 \mu m R_a$. This generally gives a reduction in power of approximately 0.3% corresponding to the 1981 class S standard. It is also true that roughness creates yet more roughness, but in this particular case other factors must be given consideration. Firstly, there is a higher initial propeller cost for the additional finishing time involved. Secondly, very little performance may be gained

due to the quicker deterioration of this finer finish during transport, storage or the fitting-out period.

2.5.2 Maintenance of Propeller

It is usually recommended that the propeller should be cleaned and polished when a ship is drydocked. However, the periods between these routines have recently tended to extend to as long as three years. It is therefore recommended that additional intermediate servicing be given consideration during the inter-docking intervals, and preferably to be carried out every year.

There are obvious advantages in polishing just the outer parts of the blades. This can be done simply by trimming the ship, while in port, to expose the blades for such treatment with the ship afloat. However, the complete propeller can be easily polished underwater to a high standard in few hours. Modern equipment and technique used by specialist propeller maintenance companies [29] have made considerable progress towards this purpose. The technique is to polish the propeller twice, once with a coarse abrasive and next with a fine grade. The results have been measured many times and frequently the finish is better than Rubert gauge "A" surface. More benefits of underwater polishing can be summarised as follows:

- The equipment is portable which can be provided at any location on request.
- The cost of polishing underwater is approximately half that of

carrying out a comparable job in drydock.

- The time is dependent on size and condition of the propeller, but generally a four or five bladed propeller of 6.5 m diameter takes five to six hours to polish twice using two grades of abrasive.
- In some cases, polishing afloat may save time during the busy drydock period and consequently cost. Moreover, there is no need to protect the propeller from drips, spatter and overspray during paint application, if the polishing is carried out after dry docking.

Whatever the method, it is essential that polishing the propeller should be carried out by propeller specialists who are aware of the requirements of the designer. For the propeller designer it is important to choose the propeller dimensions, blade thickness, etc. to suit the conditions of propeller maintenance without affecting the blade strength as well as the propeller performance. It is also beneficial for the operator to remember "little and often" as a maintenance rule gives a satisfactory life of propeller.

2.5.3 Propeller Coating

The basic use of using coverings or coatings on propellers is to reduce the costly results of cavitation erosion damage. However, its advantages of smoothness and freedom from fouling are now recognized.

Results of extensive laboratory research on covering systems [30] show that some coating materials have a maintainable fine surface finish and

can be used on conventional bronze propellers in service. This indicates that in the absence of anticipated cavitation, the benefits of smoothness and permanent anti-fouling protection might repay the development of such coatings. More research work in this area is highly recommended.

2.5.4 Costs of Polishing the Propeller

The cost of grinding and polishing a propeller varies widely. In general, a rough propeller will cost more to grind and polish than a smoother one. However, the real cost depends also on other factors such as the local cost of labour, cost of transporting specialists, or cost of removing the propeller to enable downhand work, etc. It is therefore not unreasonable for assessment purposes to assume an average rate of \$180 per square metre of blade surface area as a typical cost of all propeller service in a drydock. For a propeller with a very slight deterioration of surface condition, the polishing is simple and the cost may well be less. Typical costs for a complete propeller polish, back and face, are given in Table (2.2) for two ship types [28] .

TABLE (2.2)

The Polishing Costs

Ship	64,000 DWT Bulker	1400 TEU Container
Diameter	6900 mm	7000 mm
Blade Area	19.24 sq.m	24.55 sq. m
Cost	\$6730	\$8590

The cost of polishing afloat for the reasons described before is much less than that of carrying out in drydock. A typical price list is given in Table (2.3) as suggested by Jones [29] .

TABLE (2.3)

Costs of Polishing Afloat

Propeller Diameter (m)	Price (£)
up to 5.00	1500
5.25	1560
5.50	1710
5.75	1870
6.00	2050
6.25	2200
6.50	2390
6.75	2575
7.00	2775
Greater than 7.0	3000

The prices tabulated above are based very roughly on average rate of £60.0 per m² of the developed area. Approximate calculation of that area, if not given, may be based on 0.6 of the disc area. It should also be noted that these prices apply to vessels within Port Limits, at ballast draught.

It is strongly recommended, whatever the method, that changes in propeller roughness should be measured before and after polishing. There is indeed a need for such measurements to be reported clearly and accurately, not only for the operator's immediate concern but also for continuing research investigation into the mechanism and magnitude of the propeller roughness and drag relationship.

2.6 ANALYSIS OF MEASUREMENTS

The propeller replicas of the Rubert comparator card and "Poole River" were measured, using the computerised Ferranti "Surfcom" stylus profilometer. This was carried out in the surface metrology laboratory in International Paints Co. Ltd in Felling. The analysis of the profiles was carried out using the computer software "SURFPACK" developed by Medhurst of the Ship Performance Group. SURFPACK is a very sophisticated package which incorporates routines for the computation of various roughness parameters and graphical presentation of the data.

2.6.1 Measurement of Rubert Comparator Gauges

The six propeller type surfaces of the Rubert gauges (A - F) were extensively measured. On each surface four profiles were recorded to measure, however, some surfaces had so much curvature that complete sets of profiles were not possible. Approximately 3600 points were sampled in each profile at a digitizing interval of 5 microns. These surfaces were also measured using the Surtronic 3 stylus instrument complete with its parameter module for measuring the peak count. The measurements are given in Table (2.4). The mean values of $R_a(2.5)$ and $R_t(2.5)$ for the six gauges are also given in Table (2.5), as quoted by Messrs Rubert. These values were derived from 10 measurements on each surface, 5 longitudinal and 5 transverse.

Table (2.4)

 Rubert Ship Propeller Roughness Gauge
 (length parameters in μm)

Rubert Surface	Ra	Pc	Ra	Pc	Ra	Pc
A	0.75	61	0.97	111	0.88	106
B	1.6	187	1.68	116	1.6	152
C	4.2	71	4.1	78	4.1	58
D	8.1	74	6.3	84	8.0	66
E	16.2	38	22.4	20	14.0	36
F	33.2	25	28.8	20	31.1	20

 Directions
 of traverse

Table (2.5)

 Measurements of Propeller Comparator as quoted by Messers Rubert

Specimen	Ra	Rz
A	0.65	5.0
B	1.92	12.0
C	4.70	32.0
D	8.24	51.0
E	16.60	97.0
F	29.90	154.0

The ultimate objective of these measurements is to quantify approximately the effect of each type of propeller roughness. The methodology will be described in more detail later. Briefly, we wish to derive from the surface measurement results Musker's h' for each surface so that it can be used in the estimation of the propeller roughness penalty. At the same time the surfaces were studied in detail to explore the relative merits of the various surface roughness parameters and the relationships between them.

Since Rubert gauge D is typical of the condition of many ship propellers in service, it was therefore decided to choose it for extensive study. A profile representing this surface was examined at four long wavelength filters 0.25, 0.8, 2.5 and 8.0 mm each at 3 digitizing intervals 10, 25 and 50 microns. A summary of the results of the six Rubert surfaces are set out in Table (2.6). The Digitizing interval is 50 microns and the long wavelength filter is 2.0 mm digital Butterworth [31] , equivalent to the long wavelength filter used in the Surtronic 3.

Table (2.6)

Surface Statistics of the Rubert Gauge
(length parameters in μm)

Rubert Surface	Ra	Rq	R _t	Sa	Sk	Ku	λ_{pc}	B*(.5)	α
A1	0.70	0.87	3.68	0.86	-0.107	2.72	470	49.4	2.91
A2	0.77	0.97	4.28	1.19	-0.271	2.89	320	31.2	2.15
A3	0.77	0.96	4.16	1.10	-0.131	3.35	310	27.8	4.95
A4	1.04	1.36	5.99	1.20	-0.246	3.95	480	100.0	4.92
B1	1.35	1.88	8.26	1.67	-1.181	5.91	470	43.3	2.89
B2	1.70	2.23	11.30	2.70	-0.419	4.25	330	25.8	1.80
C1	3.95	5.30	25.5	4.6	-0.301	3.94	500	48.9	2.95
C2	4.15	5.10	24.4	5.6	-0.270	3.62	360	40.4	2.65
D1	8.02	9.7	40.0	10.1	-0.282	2.6	380	35.4	2.4
D2	8.02	9.8	40.2	9.0	-0.272	2.51	470	57.2	3.4
D3	7.93	9.9	44.4	8.4	-0.252	3.41	610	49.1	3.15
D4	7.32	9.2	39.3	8.3	-0.465	3.18	430	49.2	3.09
E1	14.80	19.9	78.6	12.7	0.312	3.91	740	99.8	5.57
E2	18.69	23.4	96.2	13.5	0.465	3.17	830	113.0	6.93
F1	21.5	28.0	112.0	14.9	-0.375	3.25	800	127.0	7.87
F2	26.3	35.1	141.0	16.1	-0.530	4.12	910	146	8.52
F3	34.8	41.0	149.0	15.8	-0.030	2.25	1330	212	13.60
F4	27.4	34.5	127.0	15.6	-0.080	2.54	1250	161	9.71

The present results confirm the finding of Nayak [13] that all the three spatial parameters λ_{pc} , $B^*(0.5)$ and α can be related, thus

$$\lambda_{pc} = 8.8 B^*(0.5) \quad (2.25)$$

and

$$B^*(0.5) = 16 \alpha \quad (2.26)$$

Similarly the three height parameters, R_a , R_q , and R_t appear to be related as follows:

$$R_a = \sqrt{2/\pi} R_q \quad (2.27)$$

and

$$R_t = 4.3 R_q \quad (2.28)$$

An approximate scale of transformation has been provided by Byrne [23] to use in converting from $R_a(0.8)$ or $R_a(2.5)$ to $R_t(2.5)$. Thomas [32] has shown that all the three height parameters, depend on the long wavelength cutoff and for many surfaces their values increase as the square root of the cutoff. Results of the measurement of grade D in Table (2.7) show that its surface roughness is different and there is no simple mathematical relationship between the numerical values of its height parameters and the long wavelength cutoffs. The influence of long wavelength cutoff is shown in Figure (2.9).

In conclusion, it seems from the above results that it is possible to replace any height parameter with another, at the same cutoff, in

calculating h' for these propeller surfaces, if required. The texture parameters λ_{pc} and $B^*(0.5)$ are relatively insensitive to the digitizing interval, in which the results given in Table (2.8) show great reliability. However, a look at this table may suggest that the bandwidth parameter, α , is an unsuitable parameter to measure the texture of such surfaces.

Table (2.7)

Height Parameters for Profile D Pass 1 as a Function of
Long Wavelength Cutoff and the Digitizing Interval

Parameter	Digitizing Interval(μm)	Long Wave Cutoff, mm			
		0.25	0.8	2.5	8.0
Ra	10.0	4.99	7.29	8.46	9.26
	25.0	5.10	7.35	8.5	8.76
	50.0	-	7.6	8.2	8.35
Rq	10.0	6.35	8.99	10.37	11.56
	25.0	6.59	9.11	10.38	10.66
	50.0	-	9.15	9.92	10.17
R _t	10.0	21.70	37.23	50.17	78.22
	25.0	20.36	37.19	48.77	61.14
	50.0	-	31.95	42.11	50.84
R _t /Ra	10.0	4.35	5.10	5.93	8.45
	25.0	3.99	5.05	5.74	6.98
	50.0	-	4.20	5.13	6.09

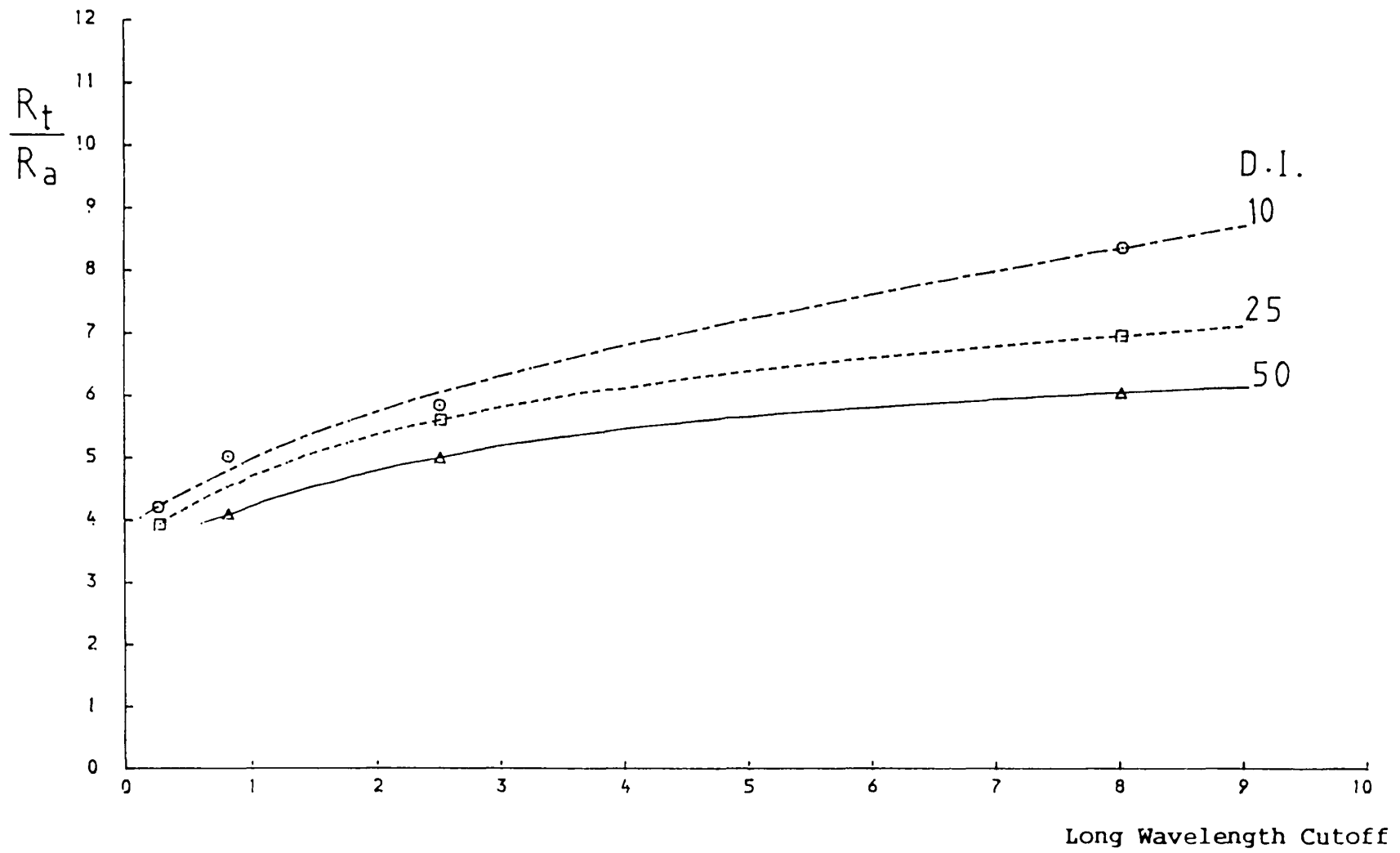


Figure (2.9) Effect of Long Wavelength Cutoff on Ratio R_t/R_a

Table (2.8)

Texture Parameters for Profile D Pass 1 as a Function of Long Wavelength Cutoff and the Digitizing Interval

Parameter	Digitizing Interval(um)	Long Wave Cutoff, mm			
		0.25	0.8	2.5	8.0
α	10.0	6.35	10.29	14.0	14.5
	25.0	2.44	3.15	4.93	4.32
	50.0	-	-	2.5	4.32
λ_{pc}	10.0	160.0	270.0	360.0	340.0
	25.0	190.0	280.0	370.0	300.0
	50.0	-	280.0	380.0	360.0
$\beta^*(0.5)$	10.0	23.8	34.8	43.2	43.6
	25.0	23.0	30.4	36.4	38.5
	50.0	-	30.4	36.8	37.3

2.6.2 Measurements of Poole River Propeller Surface

Five panels of the in-service Poole River propeller surface were replicated from the same negative replica of the surface used in the rotor cylinder experiments (see later). Extensive roughness measurements were carried out on these panels. On each 10 cm x 10 cm panel, five roughness profiles at 12.5 μm digitizing interval and 12 mm sampling length were recorded giving 25 profiles in all, (see Appendix B).

Each profile was examined at four long wavelength cutoffs of 2.0, 2.5, 5 and 10 mm and at three different digitizing intervals of 12.5, 25 and 50 μm . The averaged results are presented in Tables (2.9) and (2.10) as well as Figures (2.10)-(2.15). The standard deviations show the variations about the mean for each of these computed parameters.

The aim of these measurements is to see whether it is possible to relate these statistically evaluated parameters to the frictional drag of the surface. Visual inspection suggests that, unlike new propeller surfaces, the present surface is quite different from a typical engineering one. The roughness distribution is more rugged and less homogeneous. In other words, the roughness distribution is unlikely to be Gaussian and two-parameter correlation between surface roughness and hydrodynamic drag is required. It was therefore decided that a detail study of the changes in surface statistics with respect to changes in long and short wavelength cutoffs might be interesting in itself and could help to throw some light on the eventual choice of roughness parameters and wavelength cutoffs for use in the final roughness-drag correlation attempt.

Analysis of the results shows that the effect of increasing the long wavelength cutoff or the sample length, is generally to increase the mean and variation of height roughness parameters. Moreover, the increase in the ratio of various height parameters results from an increase in long wavelength cutoff, and is larger as the former cutoff increases from 5 mm to 10 mm. It can be seen also that the skewness and kurtosis are highly sensitive to the long wavelength cutoff and their values decrease as this cutoff increases. On the other hand, the slope parameter is more insensitive to the long wavelength cutoff.

In Table (2.10) three sets of mean and standard deviations of 9 parameters are set out. The effect of varying sample interval from 12.5

μm to $50 \mu\text{m}$ on the mean and scatter of R_a , R_q , R_t , λ_{pc} and $B^*(0.5)$ is negligible. For the slope and the bandwidth parameter α , their mean values increase as sampling interval decreases. The large variations of skewness and kurtosis show them to be unreliable parameters.

For the purpose of comparison it is desirable to know the relationships between some of the various values of the present parameters. These are shown in Tables (2.11) and (2.12). The three height parameters R_a , R_q and R_t can be related, from Table (2.12), as follows:

$$R_a = 0.74 R_q \quad (2.29)$$

and

$$R_t = 3.60 R_q \quad (2.30)$$

The relationship between the texture parameters λ_{pc} and $B^*(0.5)$ similarly appear to be related as:

$$\lambda_{pc} = 6.0 B^*(0.5) \quad (2.31)$$

Whilst in the case of the bandwidth parameter α , it is very difficult to draw any consistent conclusion.

Although the initial visual inspection suggested differently, the measured parameters of Rubert gauges and Poole River propeller surface only differ slightly except for the values of slope and kurtosis. The

relationship between the height parameters are very similar in both surfaces, but the texture parameters are slightly different. The values of the slope are smaller in the Poole River surface than those of Rubert gauges, whilst the kurtosis appears to have much greater values for the Poole River propeller surface.

Table (2.9)

Surface Statistics of Poole River
for Different Long Wavelength Cutoffs

Surface Roughness Parameter	Long Wavelength Cutoffs (DI=50 μ m)			
	2.0 mm	2.5 mm	5.0 mm	10.0 mm
Ra	8.64 \pm 2.92	11.28 \pm 2.89	20.44 \pm 6.55	26.48 \pm 11.40
Rq	11.73 \pm 5.18	15.54 \pm 4.73	26.43 \pm 8.80	32.50 \pm 14.10
R _t	39.36 \pm 14.3	52.21 \pm 13.3	96.72 \pm 27.6	146.70 \pm 14.10
Sa	4.08 \pm 1.32	4.44 \pm 1.09	4.62 \pm 1.18	4.73 \pm 1.11
Sk	0.03 \pm 0.71	-0.04 \pm 0.58	-0.09 \pm 0.80	-0.09 \pm 0.66
Ku	4.42 \pm 2.41	4.92 \pm 2.30	3.57 \pm 2.7	3.18 \pm 2.3
λ_{pc} (mm)	1.37 \pm 0.34	1.62 \pm 0.38	2.71 \pm 0.7	4.1 \pm 1.95
B*(0.5)	185.6 \pm 43.8	248.75 \pm 66.9	441.9 \pm 163	492.4 \pm 177
α	10.14 \pm 5.3	10.24 \pm 4.31	31.0 \pm 25.3	41.6 \pm 32.2

Table (2.10)

Surface Statistics of Poole River
for Different Digitizing Interval

Surface Roughness Parameter	Digitizing Interval (Long Cutoff=2.5 mm)		
	12.5 μ m	25.0 μ m	50.0 μ m
Ra	11.17 \pm 3.06	11.2 \pm 3.2	11.28 \pm 2.89
Rq	15.38 \pm 4.79	14.8 \pm 5.36	15.54 \pm 4.73
R _t	56.70 \pm 14.9	54.15 \pm 16.3	52.51 \pm 13.34
Sa	6.67 \pm 1.16	5.65 \pm 1.2	4.44 \pm 1.09
Sk	-0.06 \pm 0.62	0.01 \pm 0.62	-0.04 \pm 0.58
Ku	5.0 \pm 2.5	4.0 \pm 2.2	4.92 \pm 2.3
λ_{pc} (mm)	1.49 \pm 0.3	1.58 \pm 0.38	1.62 \pm 0.38
B*(0.5)	290.2 \pm 98.7	249.2 \pm 59.8	248.75 \pm 66.90
α	82.0 \pm 48.4	57.0 \pm 28.5	10.24 \pm 4.31

Table (2.11)

Surface Statistics Relations of Poole River
at Different Long Wavelength Cutoffs

Surface Roughness Ratio	Long Wavelength Cutoffs (DI=50 μ m)			
	2.0 mm	2.5 mm	5.0 mm	10.0 mm
Ra/Rq	0.737	0.725	0.77	0.814
R _t /Rq	3.34	3.38	3.66	4.5
R _t /Ra	4.53	4.66	4.75	5.52
$\lambda_{pc}/B^*(0.5)$	7.40	6.50	6.13	8.3
B*(0.5)/ α	18.00	24.0	14.0	11.8

Table (2.12)

Surface Statistics Relations of Poole River
at Different Digitizing Interval

Surface Roughness Ratio	Digitizing Interval (Long Cutoff=2.5 mm)				
	12.5 μ m	25.0 μ m	50.0 μ m	A.M.	S.D.
Ra/Rq	0.726	0.757	0.726	0.74	0.02
R _t /Rq	3.69	3.660	3.380	3.60	0.17
R _t /Ra	5.08	4.95	4.65	4.90	0.22
$\lambda_{pc}/B^*(0.5)$	5.13	6.34	6.50	6.00	0.75
B*(0.5)/ α	3.50	4.40	24.0	8.30	7.80

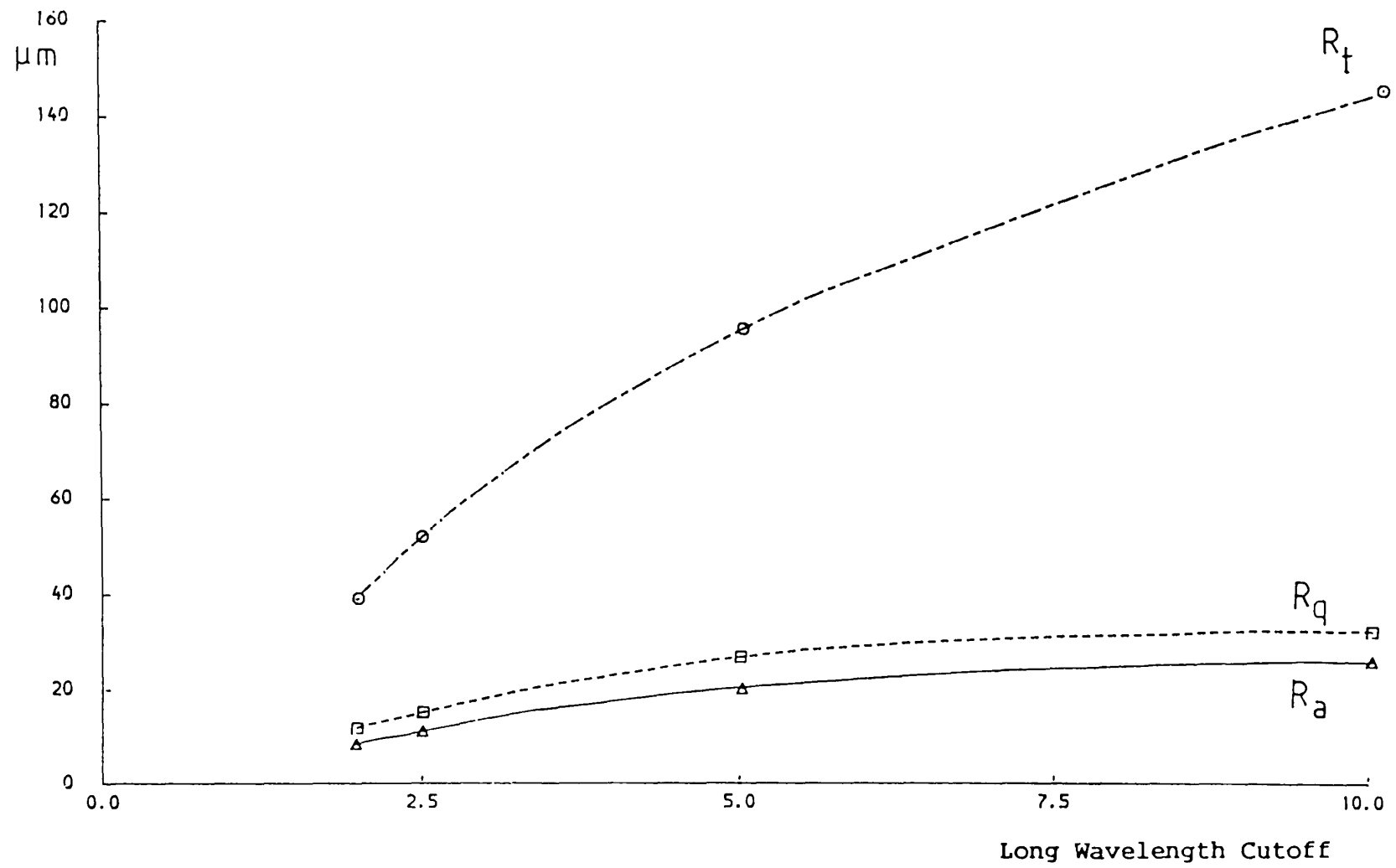


Figure (2.10) The Effect of Long Wavelength Cutoff on Roughness Height Parameters

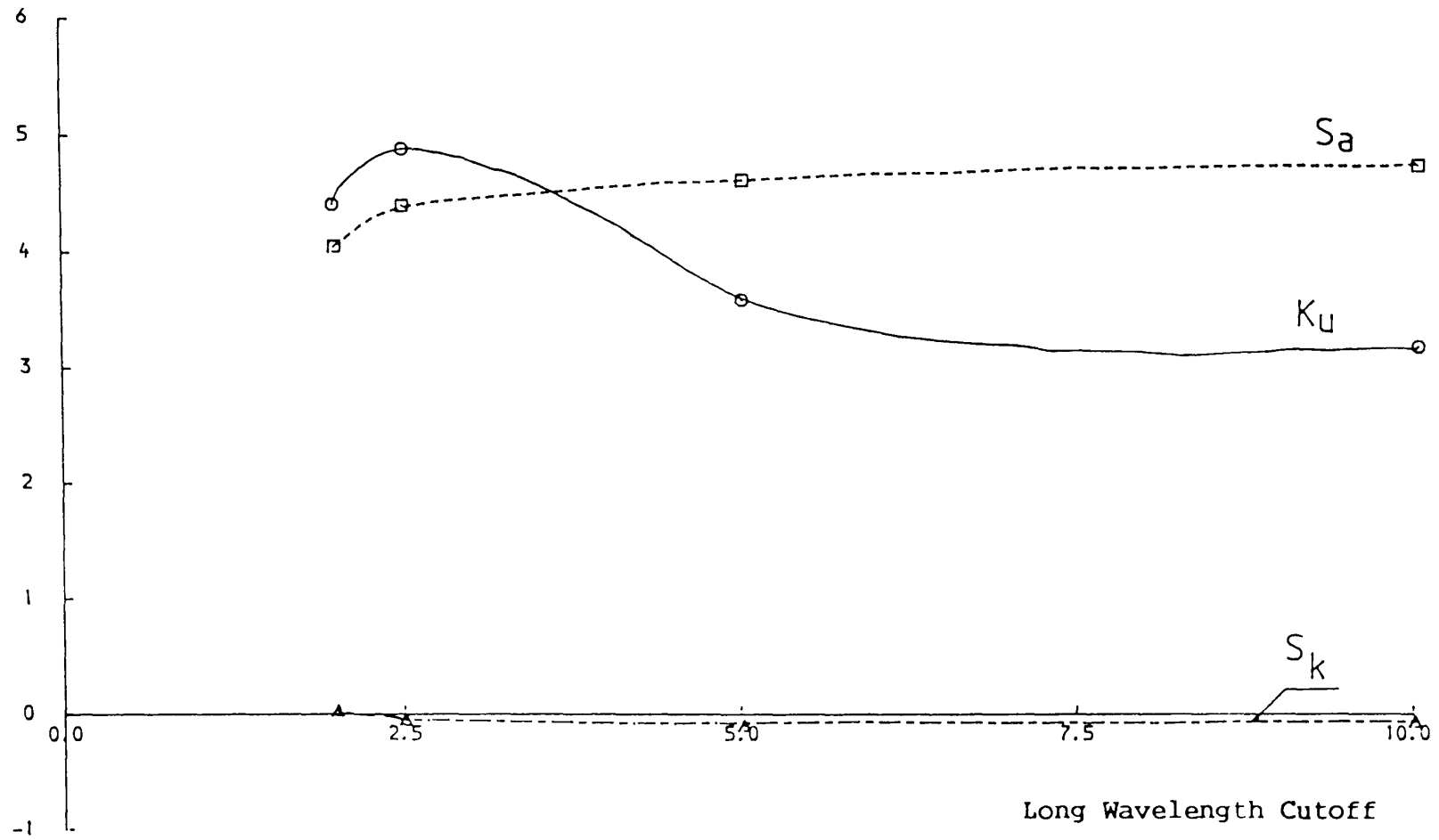


Figure (2.11) The Effect of Long Wavelength Cutoff on Slope, Skewness and Kurtosis

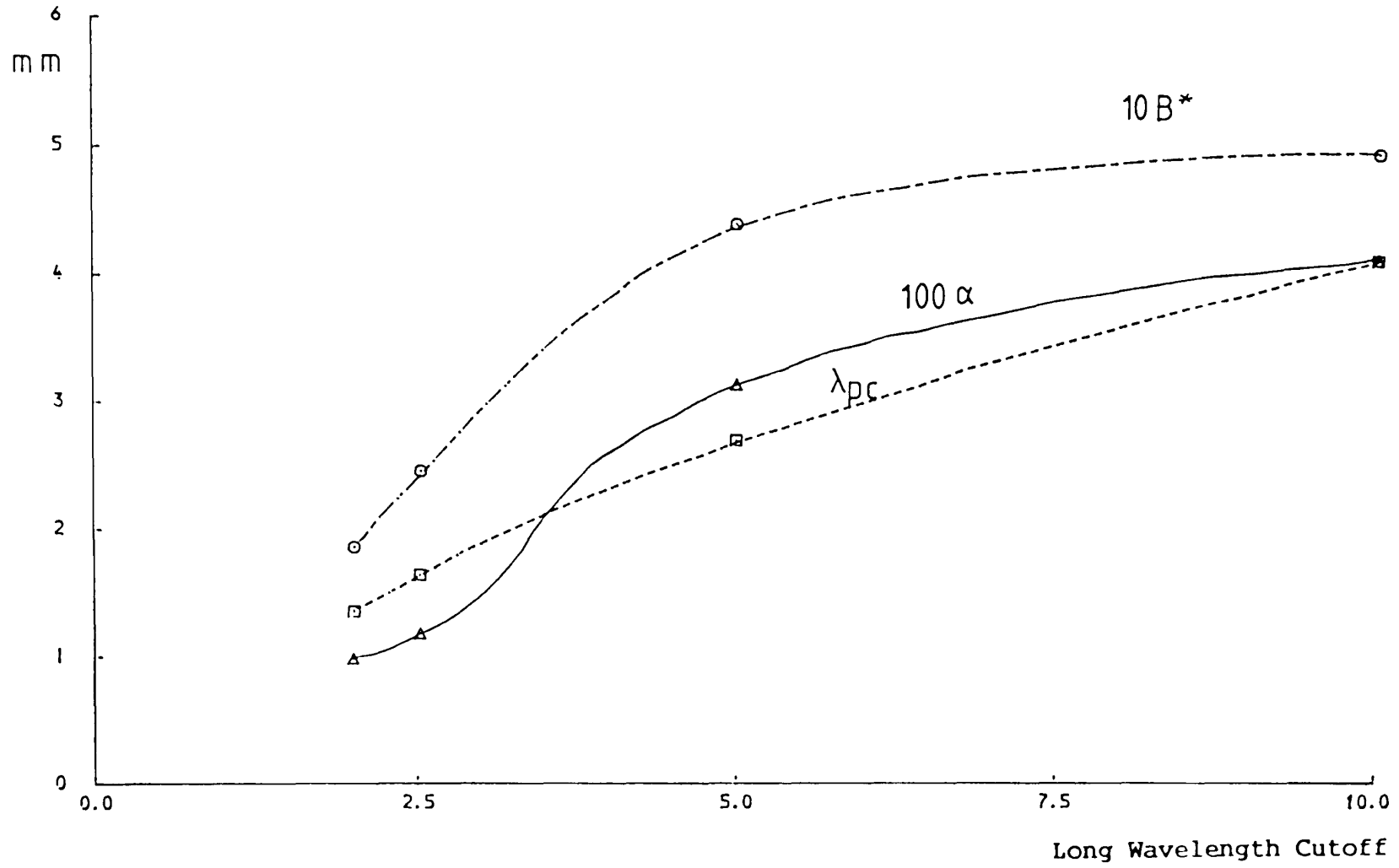


Figure (2.12) The Effect of Long Wavelength Cutoff on Roughness Texture Parameters

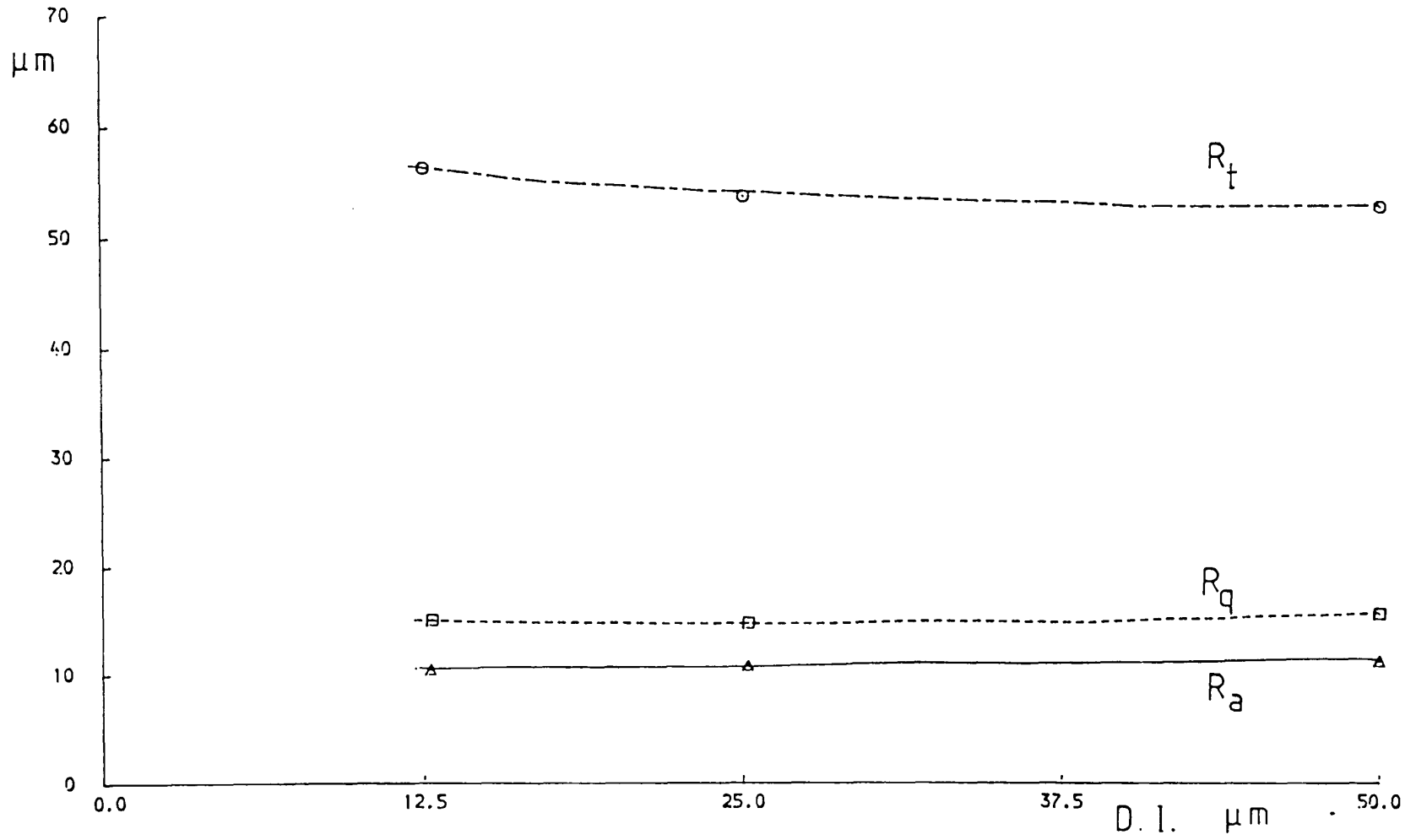


Figure (2.13) The Effect of Digitizing Intervals on Roughness Height Parameters

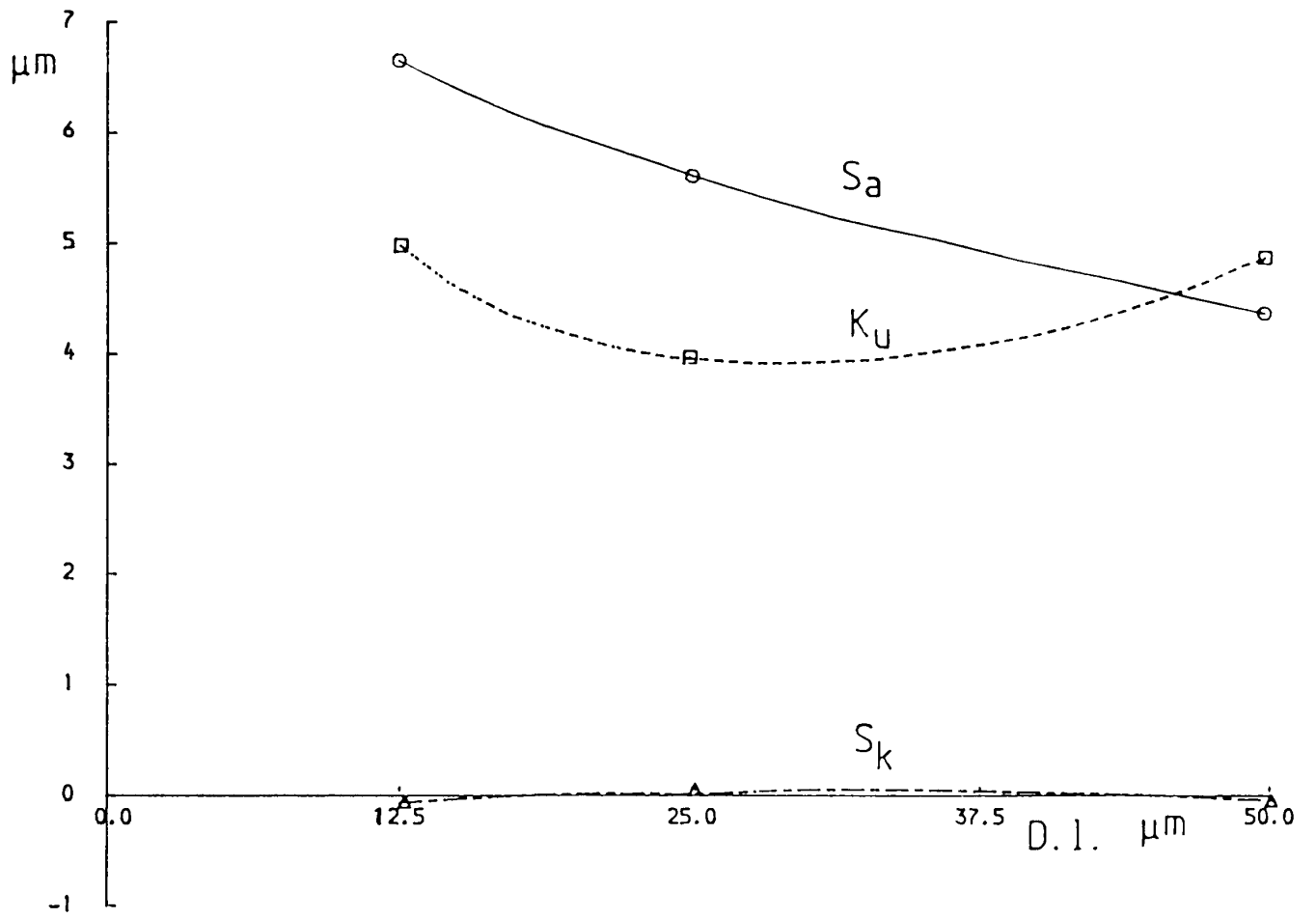


Figure (2.14) The Effect of Digitizing Intervals on Slope, Skewness and Kurtosis

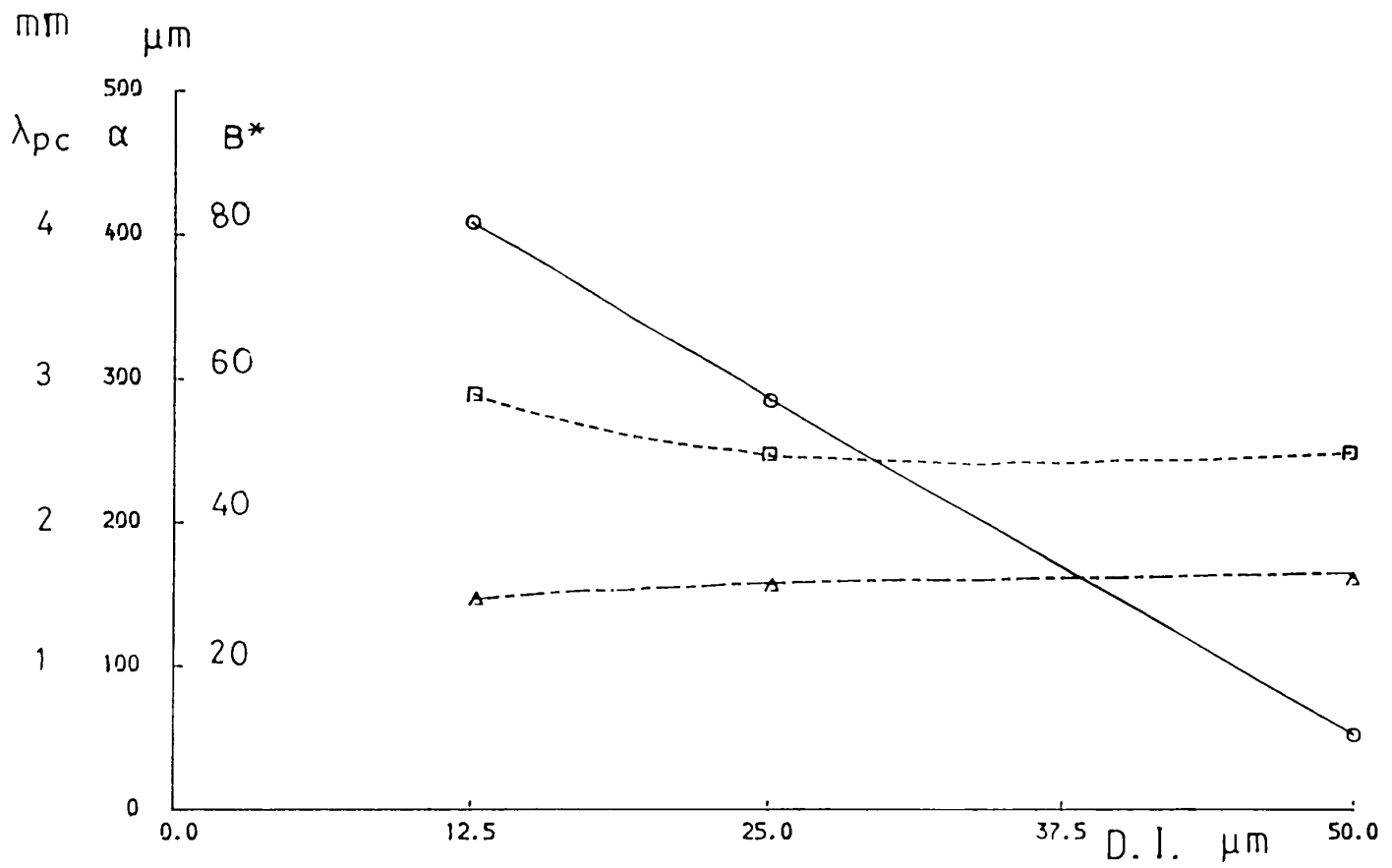


Figure (2.15) The Effect of Digitizing Intervals on Roughness Texture Parameters

CHAPTER THREE

THE TURBULENT BOUNDARY LAYER ON ROUGH SURFACE

3.1 INTRODUCTION

In recent years much attention has been given to the problem of propeller blade surface roughness and its effects on profile drag, particularly in operating conditions. It is recognised that a satisfactory method of calculating the propeller roughness drag is needed.

The most important parameters affecting the profile drag are, the section shape, the surface finish and the Reynolds number. In addition, other parameters such as the laminar-turbulent transition point and lift coefficient may also influence the propeller drag. However, there is no doubt that the flow in the wake of a ship is turbulent in nature, the flow over the propeller sections can therefore be assumed to be turbulent right from the leading edge. Moreover, for most propeller design, the lift coefficient does not vary very much, so its effect on drag penalty may be assumed to be constant.

Profile drag consists partly of skin friction, which is equal to the sum of all shearing stresses on the surface of the aerofoil, and partly of form or pressure drag, which arises from the normal pressure distribution. An approximate relationship between the skin friction and

profile drag, which has been given by Squire and Young [33] , may be used to calculate C_D from C_F . The problem then becomes one of calculating the rough turbulent skin friction or boundary layer in a pressure gradient.

One of the goals of the boundary layer theory is to enable quantitative prediction of the boundary layer development on a surface in a given flow field. The complexities of the governing equations for turbulent flows defy any analytical solution and the problem may be tackled only by semi-empirical methods. An analysis of the experimental data is needed in order to develop the required empirical relations. This implies that for experimental studies of boundary layers, sometimes certain quantities which have not been measured have to be calculated from approximate equations based on some simplifying assumptions. The method attempted here, is concerned with the prediction of boundary layer of any arbitrary aerofoil blade section when its pressure distribution is given.

Attempts to predict the growth of the turbulent boundary layer in different flow conditions have been made by many workers in the past 50 years. No complete theoretical solution has yet been found due to the difficulties in obtaining a clear picture of the mechanism of turbulent motion and until the early 70's the concept of roughness and its effect have not been adequately treated. The well known Schlichting formula of rough plates [34] , obtained by conversion of Nikuradse's pipe experiments is recommended by 1978 ITTC to estimate the drag coefficient of propeller blade sections as a function of the blade roughness. This formula has recently been used by Kresic [35] to predict the propeller

performance with regard to in-service blade roughness. Unfortunately, Schlichting's formula does not account for the flow in the transition region. Experiments by Colebrook-White and Altshul showed that the different resistance behaviours are exhibited by industrial surfaces with different types of roughness in the transition zone. Consequently, it may be difficult to apply Schlichting's formula for calculating the propeller drag penalty.

In this work, the local skin friction equation of Coles [1] for two-dimensional flow in a pressure gradient is used. Some modifications are introduced into Coles' velocity law in order to make it valid for both low and high Reynolds number. This modified velocity profile is used to derive the other boundary layer parameters with the help of boundary layer equations. The Colebrook roughness function is used and Musker's h' roughness parameter is adopted. The roughness function is discussed in detail in chapter 4.

3.2 THE MOMENTUM INTEGRAL EQUATION

Turbulent flow has an extremely complex flow structure. Mathematically, it is often expressed as a series of partial differential equations, often known as Navier-Stokes Equations. In practice they can not be solved by exact methods. Therefore, many approximate solutions were developed. The first approximate solution for this problem was due to Von Karman [36] , who put forward his well known momentum equation:

$$d\theta/dx + (2 + H12) 1/U_S dU_S/dx \theta = \tau_w/\rho U_S^2 \quad (3.1)$$

where

$$H12 = \delta^*/\theta \quad , \quad \tau_w/\rho U_S^2 = C_f/2$$

This equation is valid for laminar, turbulent, compressible and incompressible flows for plane and rotational symmetrical arrangements.

There are a number of integral prediction methods for approximate calculation of the turbulent boundary layer based on the momentum equation. The method used in this work is based on Musker and Lewkowicz [37] and its modification by the Ship Performance Group at Newcastle University [38] .

The momentum equation (3.1) can be used to calculate the development of the local skin friction coefficient on an aerofoil in a wind tunnel. For this the external velocity gradient and the velocity distribution inside the boundary layer need to be measured. However, in order to predict the development of C_f on any arbitrary aerofoil shape, more information is required to calculate the variable coefficients $H12$ and $\tau_w/\rho U_S^2$ as well as the external velocity gradient $U_S(x)$.

3.3 THE VELOCITY PROFILE FOR TWO-DIMENSIONAL TURBULENT FLOW

Before introducing the effects of surface roughness, it is important to examine the "state of the art" understanding of the velocity profile over a smooth surface.

Experience with turbulent shear flow shows that the flow very near to the wall behaves like a laminar flow, thus

$$\tau_w/\rho = \mu du/dy \quad (3.2)$$

In this case, the mean velocity profile can be described by the following simple linear function,

$$u/u^* = f(yu^*/\nu) \quad (3.3)$$

It should be noted that the mean velocity profile given by equation (3.3) is valid only for a very thin layer of y/δ less than 0.1 (δ is the boundary layer thickness). For values of $yu^*/\nu > 50$, the velocity distribution has the following universal logarithmic form:

$$u/u^* = 1/K \ln yu^*/\nu + B_0 \quad (3.4)$$

This equation is usually known as the "Inner Law" or "law of the wall", in which K and B_0 are constants to be determined experimentally.

For values of $y/\delta > 0.1$, the mean velocity profile in a turbulent shear flow may be generalised by the formula:

$$u/u^* = f(yu^*/\nu) + p(x,y) \quad (3.5)$$

where $p(x,y)$ is an arbitrary function depending on the flow condition. For a uniform flow over a flat plate, this function was found experimentally [1] to be:

$$p(x,y) = g(\Pi, y/\delta) \quad (3.6)$$

where Π is the Coles' wake strength.

Substituting equation (3.6) into equation (3.5) yields:

$$u/u^* = f(yu^*/\nu) + g(\Pi, y/\delta) \quad (3.7)$$

which represents the mean velocity profile in terms of the argument y/δ . For $yu^*/\nu > 50$, the velocity distribution is described by velocity defect law which can be rewritten as:

$$(U_S - u)/u^* = F(\Pi, y/\delta) \quad (3.8)$$

with

$$u = U_S \quad \text{at} \quad y = \delta$$

Clauser [39] used the definition "equilibrium boundary layer" to describe the flow with a defect law in which the parameter Π is constant.

The validity of the universal velocity defect law extends right to the region of the wall flow provided that the thickness of the sublayer is sufficiently small compared with the total boundary layer thickness. Therefore, to establish the defect law, the mean velocity profile must have the form of equation (3.5).

An extensive survey of experimental data at large Reynolds numbers leads to the conclusion that the function $p(x,y)$ can be described by a universal function $w_k(y/\delta)$, which is called the wake function [1] ; and hence, equation (3.5) may be written as:

$$u/u^* = [1/K \ln yu^*/\nu + B_0] + \Pi(x)/K w_k(y/\delta) \quad (3.9)$$

where

$w_k(y/\delta)$ is a function referred to the "law of the wake".

K and B_0 have generally accepted "universal" values of 0.41 and 5.0, respectively.

The above velocity profile has two universal functions, one is the law of the wall and the other is the law of the wake as given by the first and the second terms in the right hand side of the equation, respectively.

In order to study the hypothesis of a universal wake function, it is necessary to define δ and state some normalizing factor for w_k . The minimum value of w_k is at $y/\delta=0$ and the maximum value will occur very nearly at $y/\delta=1$ and the area under the curve, Figure (3.1), is equal to unity. Hence, the normalizing conditions may be expressed as follows:

$$\begin{array}{l}
w_k(0) = 0 \quad , \quad w_k(1) = 2.0 \\
\text{and} \\
\int_0^2 (y/\delta) dw_k = \int_0^1 w_k(y/\delta) d(y/\delta) = 1.0
\end{array}
\left. \vphantom{\int_0^2} \right\} \dots\dots\dots(3.10)$$

An analytical fit to the wake function has been given by Hinze [40] :

$$w_k = 1 - \cos(y/\delta) \tag{3.11}$$

Although equation (3.11) is usually used in the literature, a more convenient polynomial expression has been given by Moses [41] :

$$w_k = 6(y/\delta)^2 - 4(y/\delta)^3 \tag{3.12}$$

Unfortunately, if it is used in equation (3.9), it leads to a discrepancy in the slope at the edge of the boundary layer as discussed by Bull [42] .

Granville [43] has shown that using a modification function :

$$\Gamma = (y/\delta)^2 - (y/\delta)^3 \tag{3.13}$$

could give more accurate expression for the wake function. Combining equations (3.4), (3.12) and (3.13) gives the velocity profile described by Musker [3] :

$$u/u^* = 1/K \ln yu^*/\nu + B_0 + \pi/K [6(y/\delta)^2 - 4(y/\delta)^3] \\ + 1/K (y/\delta)^2 (1-y/\delta) \quad (3.14)$$

However, studying the wake function in the above equation does not satisfy all Coles' assumptions, [see equation (3.10)]. On the other hand Strehle [44] developed another formula for the wake function:

$$w_k(y/\delta) = 2.7(y/\delta)^2 + 14.3(y/\delta)^3 - 30(y/\delta)^4 + 20.5(y/\delta)^5 - 5(y/\delta)^6 \quad (3.15)$$

A mathematical correlation for equation (3.15) has been carried out [45] in order to satisfy the normalizing condition. The final result is given as:

$$w_k(y/\delta) = 2.124(y/\delta)^2 + 14.344(y/\delta)^3 - 30.027(y/\delta)^4 \\ + 20.527(y/\delta)^5 - 4.968(y/\delta)^6 \quad (3.16)$$

Returning to equation (3.9) and using the definition of the boundary layer thickness by the condition; $u=U_S$ for $y=\delta$. The velocity defect law in the outer part of the boundary layer may be written:

$$(U_S - u)/u^* = -1/K \ln(y/\delta) + \pi/K [2 - w_k(y/\delta)] \quad (3.17)$$

or

$$U_S - u = -u^*/K \ln(y/\delta) + \pi/K u^* [1 - w_k(y/\delta)] \quad (3.18)$$

Now, the wake function w_k satisfies the normalizing condition equation (3.10). Dividing equation (3.18) by U_S and re-arranges to solve for u/U_S ,

$$u/U_S = 1 + \omega [1/K \ln(y/\delta) - 2\pi/K] + \omega\pi/K w_k(y/\delta) \quad (3.19)$$

where

$$u^* = \sqrt{\tau_w/\rho}$$

$$C_f/2 = (u^*/U_S)^2 = \tau_w/\rho U_S^2 = \omega^2$$

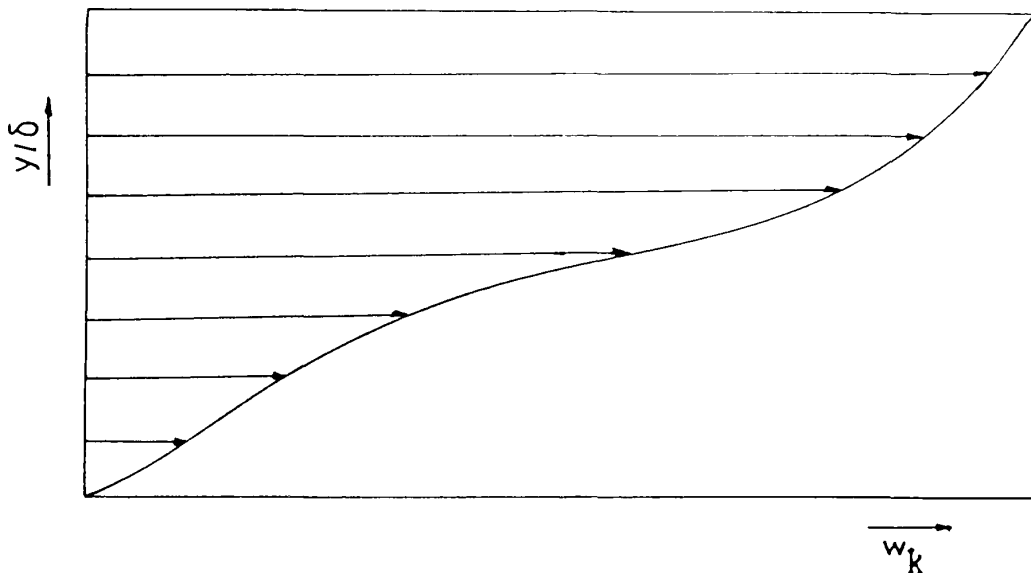


Figure (3.1) Demonstration of the Normalizing Conditions Given by Equation (3.10)

3.4 THE LOW RANGE OF REYNOLDS NUMBER

Whilst naval architecture authorities can agree about values of C_F at high Reynolds number there is still a divergence of view concerning C_F values for $Rn < 10^6$. The existence of the difference in slope between turbulent flow curves obtained by experimental and boundary layer prediction methods in the low range of Reynolds' number is still a matter for much debate. The Author believes that the experiment curve below $Rn=10^6$ represents an arbitrary condition of mixed laminar and turbulent flow. It may be difficult to obtain turbulent flow in the boundary layer at the extreme leading edge. Consequently, it is desirable to find, if possible, the curve representing complete turbulence in the low Reynolds' number range.

It is widely accepted that the velocity profile for turbulent boundary layer at high Reynolds number, outside the viscous sublayer, is adequately described by equation (3.9). However, if the momentum thickness Reynolds number, R_θ , is less than about 6000, the velocity profiles are quite different from those at higher values of R_θ . If K and B_0 in equation (3.9) are presumed to remain constant, then the wake component is observed to decrease significantly with decreasing R_θ . Coles [7] has shown that this wake component disappears completely at about $R_\theta=425$.

In order to modify the velocity laws to account for the lower Reynolds number range similarity, Simpson [46] has suggested that the wake component be unchanged and the constants K and B_0 in the law of the wall, vary with R_θ as :

$$K(R_\theta) = K (6000/R_\theta)^{0.125} \quad (3.20)$$

$$B_0(R_\theta) = R_\theta^{0.125} (7.9 - 0.737 \ln R_\theta) \quad (3.21)$$

Equation (3.20) and (3.21) are used for $600 < R_\theta < 6000$.

3.5 CHARACTERISTIC PARAMETERS OF THE BOUNDARY LAYER

The displacement thickness is defined by:

$$\delta^* = \int_0^\delta (1 - u/U_s) dy \quad (3.22)$$

or in the dimensionless form as:

$$\delta^*/\delta = \int_0^1 (1 - u/U_s) d(y/\delta) \quad (3.23)$$

From equation (3.19) and substituting in equation (3.23), yields:

$$\delta^*/\delta = -1/K \omega \left[\int_0^1 \ln(y/\delta) d(y/\delta) - 2\pi \int_0^1 d(y/\delta) + \pi \int_0^1 w_k(y/\delta) d(y/\delta) \right] \quad (3.24)$$

By integrating the above equation by parts, the first and the third

terms have the following solutions:

$$\int_0^1 \ln(y/\delta) d(y/\delta) = -1 \quad \text{and} \quad \int_0^1 w_k(y/\delta) d(y/\delta) = 1$$

hence,

$$\delta^* = \delta \omega G1 \quad (3.25)$$

where,

$$G1 = 1/K (1 + \pi)$$

The momentum thickness is defined as:

$$\theta = \int_0^{\delta} u/U_s (1 - u/U_s) dy \quad (3.26)$$

and also can be written as

$$\theta/\delta = \int_0^1 u/U_s (1 - u/U_s) d(y/\delta) \quad (3.27)$$

which can be expanded into the following form:

$$\theta/\delta = \int_0^1 (1 - u/U_s) d(y/\delta) - \int_0^1 (1 - u/U_s)^2 d(y/\delta) \quad (3.28)$$

i.e

$$\begin{aligned} \theta/\delta = \delta^*/\delta - \omega^2/k^2 \int_0^1 \{ \pi^2 [2 - w_k(y/\delta)]^2 - 2\pi [2 - w_k(y/\delta)] \ln(y/\delta) \\ + [\ln(y/\delta)]^2 \} d(y/\delta) \end{aligned} \quad (3.29)$$

or

$$\theta/\delta = \delta^*/\delta - 2\omega^2/k^2 (1 + k1 \pi + k2 \pi^2) \quad (3.30)$$

where,

$$K1 = - \int_0^1 [2 - w_k(y/\delta)] \ln(y/\delta) d(y/\delta) = 1.6$$

$$K2 = 1/2 \int_0^1 [2 - w_k(y/\delta)]^2 d(y/\delta) = 0.761$$

Therefore, equation (3.30) can be written as follows:

$$\theta = \omega \delta (G1 - \omega G2) \quad (3.31)$$

where,

$$G2 = 2/K^2 (1 + 1.6\pi + 0.761\pi^2)$$

and the shape parameter, $H12 = \delta^*/\delta$, may take the following form

$$H12 = G1 / (G1 - \omega G2) \quad (3.32)$$

3.6 PROPOSED WORK AND GOVERNING BOUNDARY LAYER EQUATIONS ON ROUGH SURFACE

In two-dimensional boundary layer theory, the streamline is considered as one of a number of parallel streamlines along a longitudinally curved section of infinite width. In this work, each radial section of the propeller blade is assumed to be an infinite aerofoil, with no convergence of streamlines and the effects of cross-flow are neglected.

From the previous survey, the wake function which was described by Musker, approximated to Coles' wake law, does not satisfy the normalizing conditions given by Coles. Although the Coles' velocity distribution,

equation (3.9), is in good agreement with the experimental data at large Reynolds number, but deviates for boundary layers at Re less than 6000. The proposed method incorporates the varying forms of the constants K and B_0 given by Simpson and the new wake function into the velocity profile.

For the prediction of the boundary layer, 3 equations are required. The first is the Von Karman momentum integral equation which was derived from Navier-Stokes equation. The second is the wall equation in transitional Colebrook-White flow. The third is the "entrainment" equation. Head [47] proposed that the rate at which the fluid is entrained by the turbulent boundary is a function of the local free-stream velocity and the shape parameter H^* , where:

$$H^* = (\delta - \delta^*)/\theta \quad (3.33)$$

The well known "entrainment equation" he derived has the form of,

$$1/U_S \, d/dx \, U_S (\delta - \delta^*) = 0.0306 (H^* - 3.0)^{0.653} \quad (3.34)$$

Many workers in the field have produced good results using the entrainment method and variants of it. One proponent who demonstrates successfully its applicability is Dvorak [48]. He shows that the entrainment function of Head is not dependent on the wall region conditions. Strictly speaking, the entrainment is essentially an outer-region phenomenon and is valid for rough surfaces.

The boundary layer method described here has been programmed in FORTRAN and a simple flow diagram is presented in chapter 5 to show the sequence of all the calculations. In the following sections, the governing equations and algorithms for their solution are outlined.

3.6.1 The Momentum Integral Equation

The momentum equation for the boundary layer, equation (3.1) may be rewritten as:

$$d\theta/dx + \theta (H_{12}+2) 1/U_S dU_S/dx = \omega^2 \quad (3.35)$$

where,

$$1/\omega = \sqrt{2/C_f} = U_S/u^*$$

By differentiating equation (3.31) w.r.t. x , yields:

$$d\theta/dx = f_{11} d\delta/dx + f_{12} d\pi/dx + f_{13} d\omega/dx \quad (3.36)$$

where,

$$f_{11} = \omega (G_1 - \omega G_2)$$

$$f_{12} = \omega \delta (1/K - \omega G_3)$$

$$f_{13} = \delta (G_1 - 2\omega G_2)$$

$$G_3 = 1/K^2(3.044\pi + 3.2)$$

$$dG_1/dx = 1/K d\pi/dx \quad [\text{from } G_1 \text{ equation (3.25)}]$$

$$dG_2/dx = G_3 d\pi/dx \quad [\text{from } G_2 \text{ equation (3.31)}]$$

Substituting for θ , $d\theta/dx$ and H_{12} , equation (3.34) the momentum equation may be reduced to the following form:

$$f_{11} \frac{d\delta}{dx} + f_{12} \frac{d\pi}{dx} + f_{13} \frac{d\omega}{dx} = f_{14} \quad (3.37)$$

where,

$$f_{14} = \omega^2 - \omega\delta(3G_1 - 2\omega G_2) \frac{1}{U_S} \frac{dU_S}{dx}$$

3.6.2 The Entrainment Equation

For thin boundary layer, the Head's Entrainment Equation takes the following form:

$$\frac{1}{U_S} \frac{d}{dx} [U_S(\delta - \delta^*)] = C_e \quad (3.38)$$

where C_e is an empirical function of H^* .

The term $(\delta - \delta^*)$ can be found from equation (3.25),

$$\delta - \delta^* = \delta (1 - \omega G_1) \quad (3.39)$$

and hence equation (3.38) becomes:

$$\frac{d}{dx} [(1 - \omega G_1)\delta] + \delta (1 - \omega G_1) \frac{1}{U_S} \frac{dU_S}{dx} = C_e \quad (3.40)$$

which can be reduced to the form:

$$f_{21} \frac{d\delta}{dx} + f_{22} \frac{d\pi}{dx} + f_{23} \frac{d\omega}{dx} = f_{24} \quad (3.41)$$

where,

$$f_{21} = (1 - G_1)$$

$$f_{22} = -\omega\delta/K$$

$$f_{23} = -\delta G_1$$

$$f_{24} = \delta (\omega G_1 - 1) \frac{1}{U_S} \frac{dU_S}{dx} + C_e$$

3.6.3 The Wall Equation

For smooth wall boundary layer, the law of the wall takes the form of equation (3.4). For a rough surface and outside the logarithmic region where the law of the wake applies,

$$u/u^* = 1/K \ln(\gamma u^*/\delta) + B_0 - \Delta u/u^* + \pi/K w_k(\gamma/\delta) \quad (3.42)$$

where,

$$\Delta u/u^* = 1/K (C_1/B_1 hu^*/\gamma + 1) \quad (3.43)$$

at the edge of the boundary layer, $w_k(1)=2.0$, thus,

$$U_S/u^* = 1/K \ln(\delta u^*/\gamma) + B_0 - \Delta u/u^* + 2\pi/K \quad (3.44)$$

For a surface in transitional Colebrook-White flow, equation (3.44) may be rewritten as:

$$1/\omega = 1/K \ln(\delta U_S \omega / \nu) + B_0 + 2\pi/K - 1/K \ln(C1/B1 h \omega U_S / \nu + 1) \quad (3.45)$$

which can be differentiated w.r.t. x and reduced to the form:

$$f_{31} \frac{d\delta}{dx} + f_{32} \frac{d\pi}{dx} + f_{33} \frac{d\omega}{dx} = f_{34} \quad (3.46)$$

where,

$$f_{31} = 1/K \cdot 1/\delta$$

$$f_{32} = 2/K$$

$$f_{33} = 1/\omega^2 + 1/K \left[1/\omega - \left(\frac{C1/B1 h U_S / \nu}{C1/B1 h U_S \omega / \nu + 1} \right) \right]$$

$$f_{34} = 1/K \left[\frac{C1/B1 h \omega / \nu}{C1/B1 h U_S \omega / \nu + 1} - 1/U_S \right] dU_S/dx$$

The boundary layer equations derived before, (3.37), (3.41) and (3.46), have been solved in terms of $d\delta/dx$, $d\pi/dx$ and $d\omega/dx$ using Cramer's rule. This gave a set of differential equations which can be solved numerically for δ , π and ω by the 4th-Range-Kutta method (Appendix C).

3.6.4 The Starting Conditions

In order to start the numerical integral solution, initial values of the dependent variables θ or δ , H_{12} or π and ω are required. For the present work two initial variables are selected, δ and π . The third variable, ω is calculated using the wall friction equation (3.45).

In the case of smooth surface the roughness function, $\Delta u/u^*$, is zero. For a rough surface equation (3.43) is used and its empirical constants will be discussed in chapter 4.

In the computer program, the starting value of δ is calculated using a power law flat method of Sayre and Duerr [49], see Appendix D. Fortunately this method is not very sensitive to the starting value of π which is selected to be equal 0.45 in both smooth and rough surfaces.

3.6.5 Calculation of the Blade Section Drag Increment

For each step of calculation the local skin friction coefficient, C_f , the frictional drag force, D_i , is calculated as follows:

$$D_i = 1/2 C_f \rho U_{S_i}^2 x_i \quad (3.47)$$

The total drags over the section length are integrated to obtain the overall skin friction coefficient in both smooth and rough conditions for face and back surfaces as follows:

$$C_F = \frac{\text{Total Drag}}{1/2 \rho V^2 \sum x_i} \quad (3.48)$$

where

$$V^2 = V_S^2 (1-w_T)^2 + (2\pi n r/60)^2$$

The drag coefficient, C_D , of each surface is evaluated from the following formula by Squire and Young,

$$C_D = C_F [1/(1-1.16 t/c)] \quad (3.49)$$

and hence,

$$\Delta C_D = C_D (\text{rough}) - C_D (\text{smooth})$$

where ΔC_D is the section drag increment due to propeller roughness.

3.6.6 Testing the Boundary Layer Integral Method

The present boundary layer method, included in "PROFNESS", is based on "NUSTREAM", in which the Author proposes the modification given at low Reynolds number range. "NUSTREAM" has been successfully tested in the work published in 1984 [38] as an adequate method to calculate the difference in resistance between smooth and rough surfaces. The Author here is concerned with the results of the modifications made to the Coles' velocity law in order to be valid for both low and high Reynolds number ranges. The result of using "PROFNESS" for a smooth flat plane is shown in Figure (3.2). It is also shown that the slope of the skin friction line has been improved and agrees reasonably well with the ITTC ship-model correlation line.

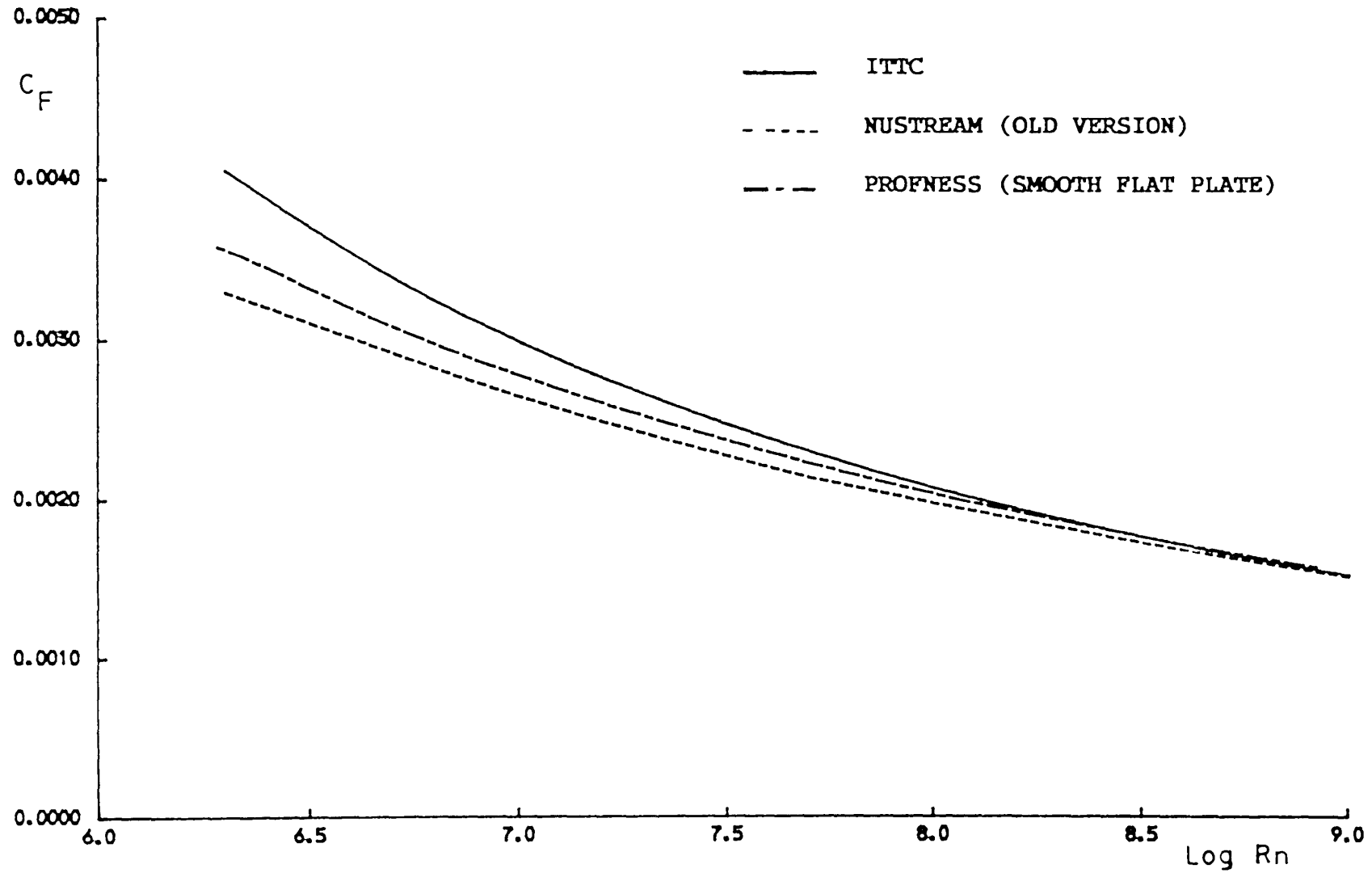


Figure (3.2) Overall Skin Friction Coefficient For Smooth Flat Plate

CHAPTER FOUR

THE HYDRODYNAMIC ROUGHNESS FUNCTION FOR PROPELLERS

4.1 ROUGHNESS DRAG CHARACTERIZATION

4.1.1 Introduction

Rough surfaces produce considerably larger values of skin friction in turbulent flow than smooth ones. This implies that the velocity gradient near the rough surface is less steeper than that near a smooth one. It follows, therefore, that the logarithmic law for velocity distribution is shifted downwards by a constant amount $\Delta u/u^*$ as demonstrated by Hama [50]. Figure (4.1) shows the velocity ratio u/u^* has been plotted against $\ln(yu^*/\nu)$ and hence the logarithmic law may have the following form:

$$u/u^* = 1/K \ln(yu^*/\nu) + B_0 - \Delta u/u^* \quad (4.1)$$

Hama also made the very important discovery that $\Delta u/u^*$ is a unique function of the Roughness Reynolds Number, hu^*/ν , where h is a height measure of the surface roughness as shown in Figure (4.2). This function is independent of the external pressure gradient which implies that its measure in a pipe flow could be related to a boundary layer for a particular surface.

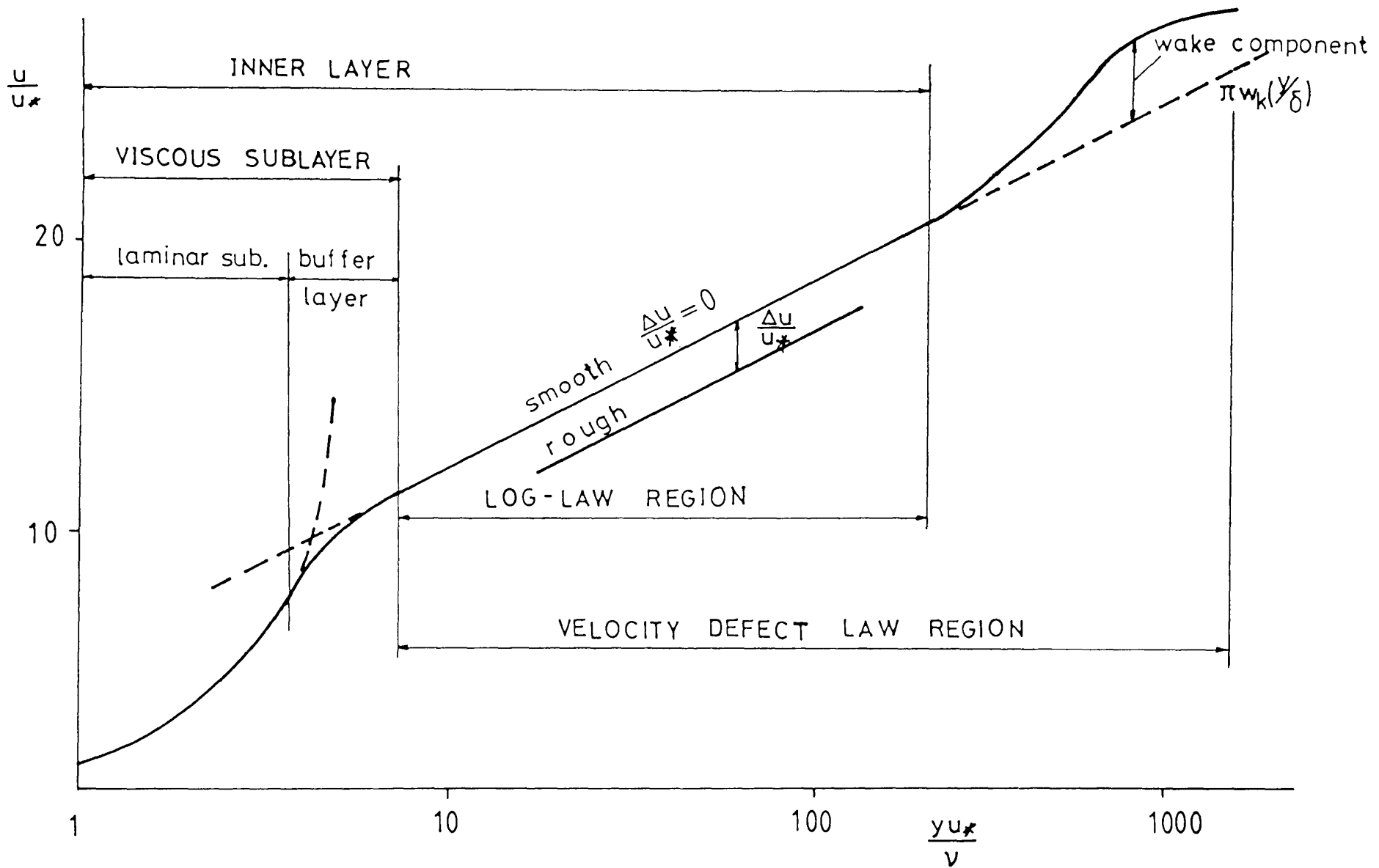


Figure (4.1) The Logarithmic Law of the Wall and the Roughness Function

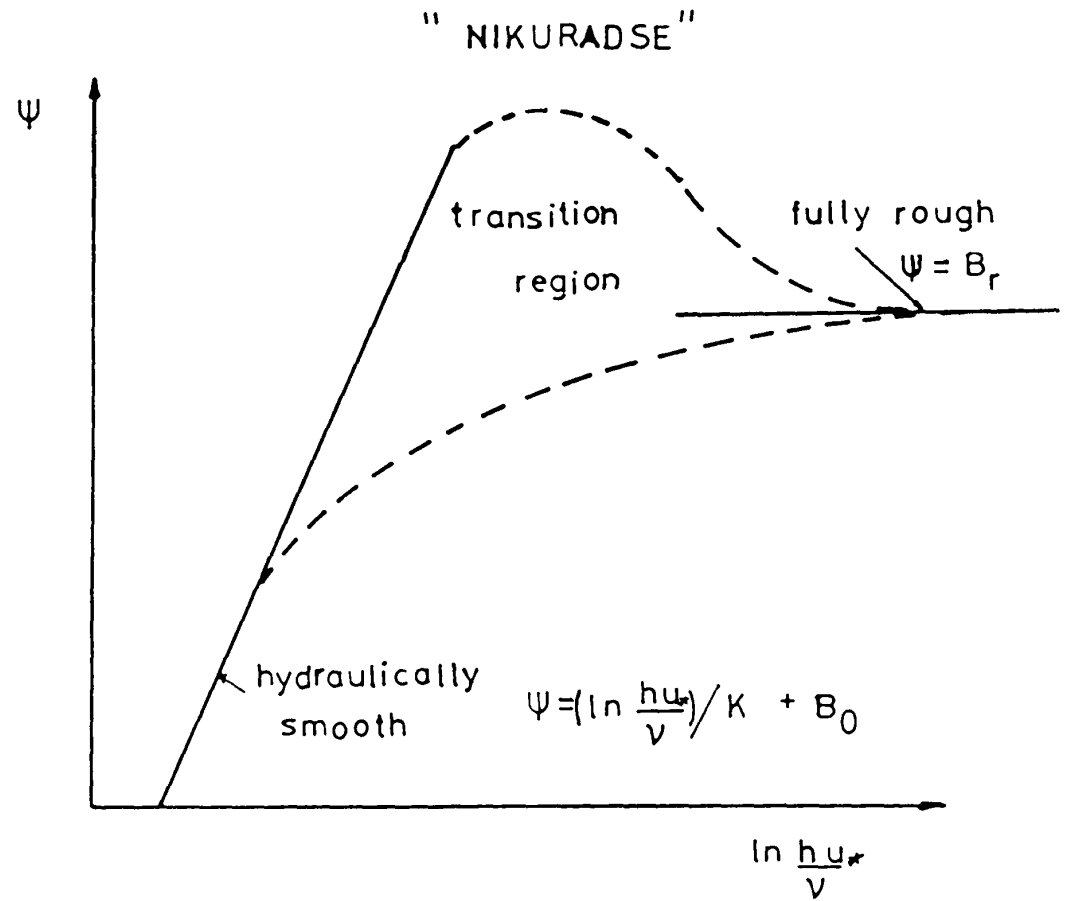
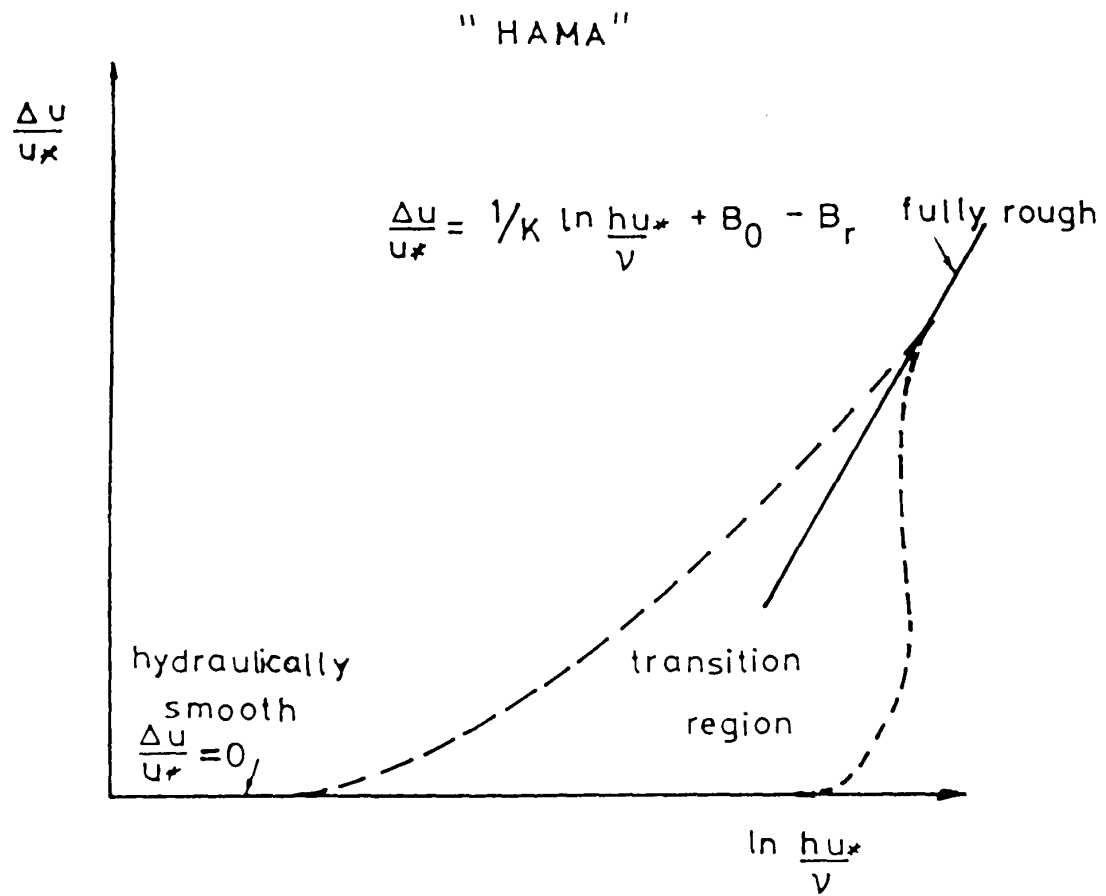


Figure (4.2) The Roughness Function

A correlation is therefore required to link the chosen measure of roughness with the function $\Delta u/u^*$. An early attempt to correlate the hydrodynamic behaviour of rough surface with a measure of their topography was by Nikuradse [51] on close-packed sand grains. He used the logarithmic law in a slightly different form:

$$u/u^* = 1/K \ln y/h + \chi \quad (4.2)$$

where χ is another form of the roughness function and takes the form:

$$\chi = 1/K \ln(hu^*/\nu) + B_0 - \Delta u/u^* \quad (4.3)$$

The roughness obtained by Nikuradse with sand can be said to be of maximum density. In many practical applications the roughness density is considerably smaller, and such roughness characterisation can no longer be applicable to "engineering" surfaces.

Colebrook and White [2] investigated surfaces of various topographies by cementing assemblies of grains to tubes. The grains were evidently more angular in shape and less uniform in size distribution than of Nikuradse's surfaces. Colebrook [52] concluded that the roughness function of a range of engineering surfaces in flow is an asymptotic fit to both "hydraulically smooth" and "fully rough". Experiments of Altshul [53] showed also that the nature of the resistance behaviour of engineering surfaces is basically different from that of sand grain roughness.

Although the roughness functions were derived from the above work for use in pipes only, they have been extended to cover rough wall boundary layers. Recently Musker [3] , Grigson [54] and Townsin [38] have described the Colebrook-White roughness as follows:

$$\Delta u/u^* = 1/K \ln (C1/B1 hu^*/\nu + 1) \quad (4.4)$$

where K and B1 are "universal" constants (0.41 and 0.129 respectively) endorsed by the 1968 STANFORD Conference and C1 is a constant dependent upon the measure of roughness used. The ratio B1/C1 is the parameter m used by Grigson which may be found from drag measurements of a replicated surface. A derivation of equation (4.4) is given in the next section.

In chapter 2 it is shown that, surfaces having the same roughness "height" but different "texture" could have very different drags in similar flow conditions. Musker, using 5 sample hull surfaces inside pipes, showed that a single roughness height parameter, like $R_t(50)$, is inadequate to characterise the behaviour of an irregularly rough surface in fluid flow. He found much better correlation by using the r.m.s. height, $R_q(2.0)$, including a measure of the spacing of the asperities. He then proposed the following roughness parameter:

$$h' = R_q (1 + a Sa) (1 + b Sk Ku) \quad (4.5)$$

where a and b are empirical constants and the mean slope Sa based on a digitizing interval equal to the correlation length. It has been shown

also that increasing S_a , S_k and K_u are likely to increase drag.

The Author has analysed nine sets of drag measurements of different hull surfaces made by Kauczynski and Walderhang [55], Musker [3] and Johansson [56]. The roughness function so obtained from these measurements collapsed on a single Colebrook-White curve as shown in Figure (4.3). Table (4.1) contains the data and the results from all the nine surfaces.

Table (4.1)

Colebrook-White Hull Surfaces

Surface	Flow Experiments	MHR	m
K205	test of plates in water	205	28
K117	tunnel by Kauczynski	117	25
K083	and Walderhang	083	41
R173	Musker's pipe test flow	173	31
R253		253	96
R345		345	30
R420		420	75
R550		550	18
J132	Johansson's cavitation tunnel test	132	26

Grigson [21] has shown that the nature of the roughness of propeller surfaces must be Colebrook-White, similar to other types of industrially rough surfaces. He then calculated the drag coefficient of propeller blades in terms of the mean apparent amplitude, MAA , and his texture parameter m . He also demonstrated that the propeller blade surfaces have

a worse topography than the worst coated surfaces examined by Musker.

Byrne [14] re-analysed Musker's data using $R_t(50)$ instead of $R_q(2.0)$ and using α as a texture parameter. He also established an alternative hull roughness function of the form:

$$\Delta u/u^* = 1/K \ln [R_t(50)u^*/\nu^{1/t} + 1] \quad (4.6)$$

where

$$t = 55 (\alpha_{av}/\alpha)^{4.5}$$

$$\alpha_{av} = 0.013 R_t(50) + 1.8$$

This approach has been extended to propellers [23] on the basis of $R_t(2.5)$ to give,

$$\Delta u/u^* = 1/K \ln [R_t(2.5)u^*/\nu^{1/t1} + 1] \quad (4.7)$$

where $t1$ is a texture parameter given by

$$t1 = 11 (\alpha_{av}/\alpha)^{4.5}$$

The measurements of Rubert surfaces, in chapter 2, showed that α is very sensitive to the digitizing interval. This makes it unsuitable as a roughness spatial measure since its numerical value may depend on the instrument used.

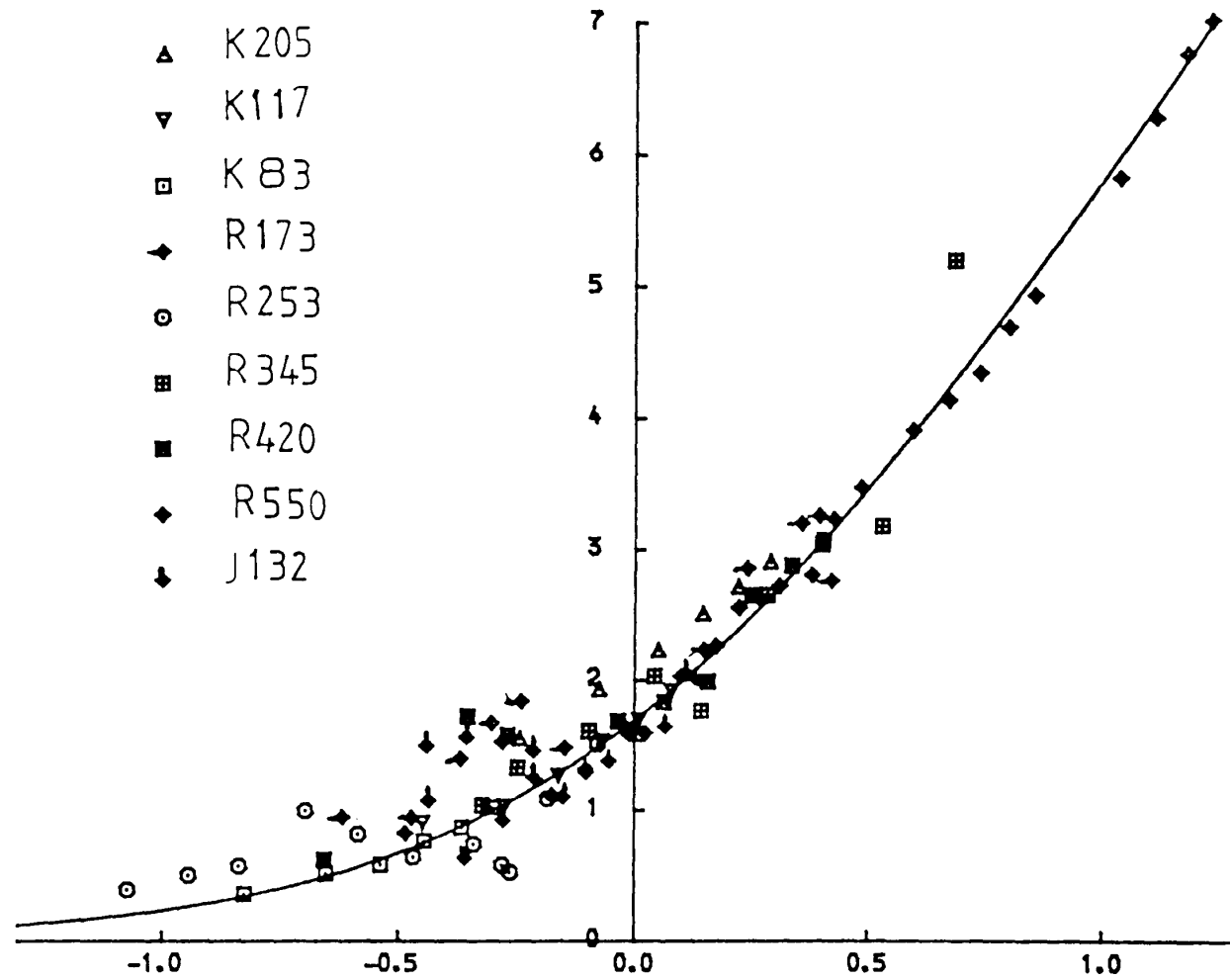


Figure (4.3) Nine Different Painted Surfaces Obeying Single Colebrook-White Curve

4.1.2 Derivation of Colebrook-White Roughness Function

It is desirable that the roughness function should be semi-empirical in nature. It can be determined by considering the law of the wall in its simplest form:

$$u/u^* = 1/K \ln y + C \quad (4.8)$$

or

$$u/u^* = 1/K (\ln y - \ln y') \quad (4.9)$$

where C is a constant and can be written in a form of $(1/K \ln y')$; and y' is the distance from the wall in which the laminar sublayer thickness lies on smooth surface and can be determined from the dimensional analysis as:

$$y' = B_1 \nu / u^* \quad (4.10)$$

where B_1 is a constant.

In the case of the fully rough flow, the flow and the surface friction are independent of Reynolds number and y' should be a function of the roughness height h ,

$$y' = C_1 h \quad (4.11)$$

where C_1 is a constant.

For surfaces in transitional flow, where the effect of both viscosity and surface roughness influence the drag, the representation of y' between hydraulically smooth and completely rough surfaces can be described by adding the two equations (4.10) and (4.11) to give

$$y' = C_1 h + B_1 \nu / u^* \quad (4.12)$$

or

$$y' = h [C_1 + B_1 / (u^* h / \nu)] \quad (4.13)$$

Substituting equation (4.13) into equation (4.9) yields

$$\left[\frac{u}{u^*} \right]_{\text{trans}} = 1/K [\ln(\gamma u^* / \nu) - \ln(C_1 h u^* / \nu + B_1)] \quad (4.14)$$

The law of the wall for smooth surfaces,

$$\left[\frac{u}{u^*} \right]_{\text{smooth}} = 1/K \ln(\gamma u^* / \nu) + B_0 \quad (4.15)$$

may be re-written as:

$$\left[\frac{u}{u^*} \right]_{\text{smooth}} = 1/K [\ln(\gamma u^* / \nu) - \ln B_1] \quad (4.16)$$

where

$$B_0 = -1/K \ln B_1 = 5.0$$

In Hama's notation, the downward shift in the velocity profile due to roughness, $\Delta u / u^*$, may be described by

$$\Delta u / u^* = \left(\frac{u}{u^*} \right)_{\text{trans.}} - \left(\frac{u}{u^*} \right)_{\text{smooth}} \quad (4.17)$$

This gives the Colebrook-White roughness function equation (4.4)

$$\Delta u/u^* = 1/K \ln (C_1/B_1 hu^*/\nu + 1)$$

where K and B₁ are the universal constants, and C₁ is a constant correlating the chosen measure of roughness and the hydrodynamic behaviour of the surface.

4.1.3 Musker's Roughness Parameter

Rough propeller surfaces may be geometrically similar to those of hulls and have Colebrook-White roughness function. However, caution must be expressed about extrapolation of results of work on ship hulls to the propeller scale. This is particularly so in the case of newly-ground propeller surfaces which bear some of the characteristics of the regular and sharp edged roughnesses of Streeter [57]. As propellers become rougher the regular roughness due to machining tends to be replaced by a more random surface approaching the Colebrook White type. Consequently, the extrapolation of Musker's result on ship hulls to the propeller scale may be used. Moreover, the combined height and texture parameter in Musker's h' gives a more complete representation of propeller surface roughness. However, the choice of these parameters is somehow restricted by what is available in commercial propeller-surveying instruments. Accordingly, a replication technique and laboratory instrumentation are required to determine the statistical parameters in h' . A much simpler version is therefore required involving, say two parameters, one height, the other texture.

To use h' as a measure of propeller roughness, the corresponding Grigson's m for each of Musker's five hull replicas has been obtained in Figures from (4.4) to (4.9), using Grigson's notation in equation (4.4) as:

$$\Delta u/u^* = 1/K \ln (h^+/m + 1) \quad (4.18)$$

where

$$h^+ = h'u^*/\nu$$

Musker's h' is essentially the product of height and slope. Although the skewness, Sk , and the kurtosis, Ku , are included in the values of h' used in this study, they are both statistically unreliable [8]. On this basis the Ship Performance Group [58] proposed a simplified version of h' of the form:

$$h' = Rq (1 + 0.3 Sa) \quad (4.19)$$

This equation has been adopted on the basis that the skewness and kurtosis have no significant effect and that the departures from unity in the term $(1 + b Sk Ku)$ may be neglected for most Musker's surfaces. To this end, the use of h' still means the need of surface replication and laboratory techniques to determine the surface parameters.

It was previously mentioned in chapter 2 that most of texture parameters are strongly influenced by the digitizing interval. Following the examination of Rubert D, the λ_{pc} and $\beta^*(0.5)$ showed great reliability

and they are highly correlated to each other; thus Musker's h' can be related to them.

The mean slope is related to the mean wavelength λ_a [8] by

$$S_a = 360 R_a / \lambda_a \quad (4.20)$$

and for Gaussian surfaces R_a is related to R_q as:

$$R_a = \sqrt{2/\pi} R_q \quad (4.21)$$

From the equations (4.20), (4.21) and (4.19), h' may be expressed in the form:

$$h' \propto R_a^2 / \lambda_a \quad (4.22)$$

A similar correlation parameter $(R_a / \sqrt{\lambda_{pc}})$ is given by Vorburger [16], which is essentially the square root of equation (4.22).

Unfortunately, Musker did not record the peak count wavelength λ_{pc} , but he did note the correlation length $B^*(0.5)$. In Table (4.2) the correlation lengths for each of the five replicas are given and it can be seen that they are quite similar. The Author with other members of the Ship Performance Group [28] have re-examined Musker's data using $B^*(0.5)$ instead of λ_a in equation (4.22) at three long wavelength cutoffs, 50, 10 and 2 mm. At the 2 mm cutoff, as shown in Figure (4.10), the points fall

reasonably close to a single Colebrook-White curve.

Table (4.2)

 Correlation lengths for Musker's Surfaces
 at 2 mm long wavelength cutoff

Surface	Ra(2.0)	B*(0.5)	m
R173	13.0	350	4.67
R253	12.0	300	7.00
R345	26.0	390	6.67
R420	19.0	440	9.09
R550	40.0	320	9.17

In a similar manner Musker's data are replotted in Figure (4.11) using Ra(2.0) and B*(0.5) instead of h'. On this basis m was found to be 0.17 with a correlation coefficient, $r^2=0.985$, in which Musker's original h' can be rewritten in the following form:

$$h' = 53 Ra^2(2.0)/B*(0.5) \quad (4.23)$$

In Table (4.3) a comparison is shown between h' given by equation (4.5) and that of equation (4.23) for each of Musker's five ship hull replicas. Since λ_{pc} was found to be almost proportional to the correlation length as shown in equation (2.25), h' may have the form:

$$h' = 466 Ra^2(2.0)/\lambda_{pc} \quad (4.24)$$

According to the ISO standard long wavelength cutoff for roughness

measurements, Ra was scaled to reflect a 2.5 mm cutoff instead of 2.0 mm

$$h' = 373 Ra^2(2.5)/\lambda_{pc} \quad (4.25)$$

Using the definition of λ_{pc} equation (2.24) for the Surtronic 3

$$\lambda_{pc} = 25400/Pc \quad (\text{micron}) \quad (4.26)$$

equation (4.25) can be written, for the Surtronic 3 only, as:

$$h' = 0.0147 Ra^2(2.5) Pc \quad (4.27)$$

where Pc is the number of peak valley pairs per inch.

Table (4.3)

Comparison Methods of h' Values		
Surface	h' Eq(4.5)	h' Eq(4.23)
R173	31	26
R253	17.3	25
R345	90	92
R420	52.5	43
R550	267	265

When the Rubert comparator has to be used, its surface parameters need to be related to Musker's h'. In chapter 2 the Rubert comparator

surfaces are measured in great detail. As a result, h' has been established for each surface using the above different forms as shown in Table (4.4). It can be seen that there is some agreement between the different forms presented.

Table (4.4)

 Values of Musker's h' for Rubert Surfaces
 using four methods

Rubert Surface	Method (1)	Method (2)	Method (3)	Method (4)	SPG [58]
A	1.32	0.80	0.82	1.1	1.2
B	3.4	4.1	2.95	5.4	2.5
C	14.8	19.8	18.4	17.3	24
D	49.2	70.4	62	61	59
E	160	140	167	133	185
F	252	249	331	311	276

- (1) $h' = Rq(2.0)(1+0.5Sa)(1+0.2KuSk)$.
 (2) $h' = 53 Ra^2(2.0)/\beta^*(0.5)$.
 (3) $h' = 466 Ra^2(2.0)/\lambda_{pc}$.
 (4) $h' = 0.0147 Ra^2(2.5)Pc$

In conclusion, Musker's h' can be estimated readily by either the two-parameter portable stylus instrument or by a Rubert comparator.

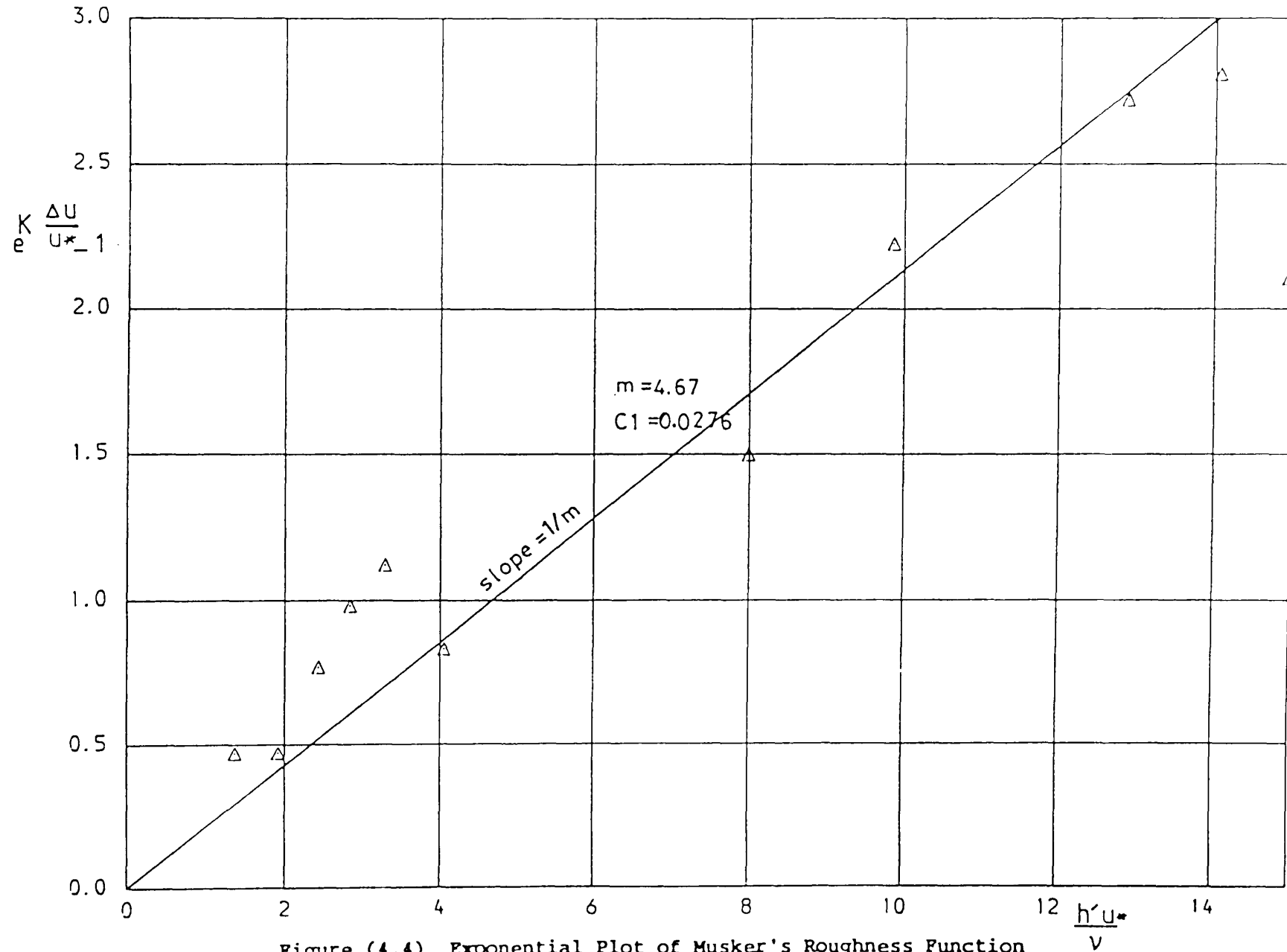


Figure (4.4) Exponential Plot of Musker's Roughness Function for R173-Surface Correlated with h'

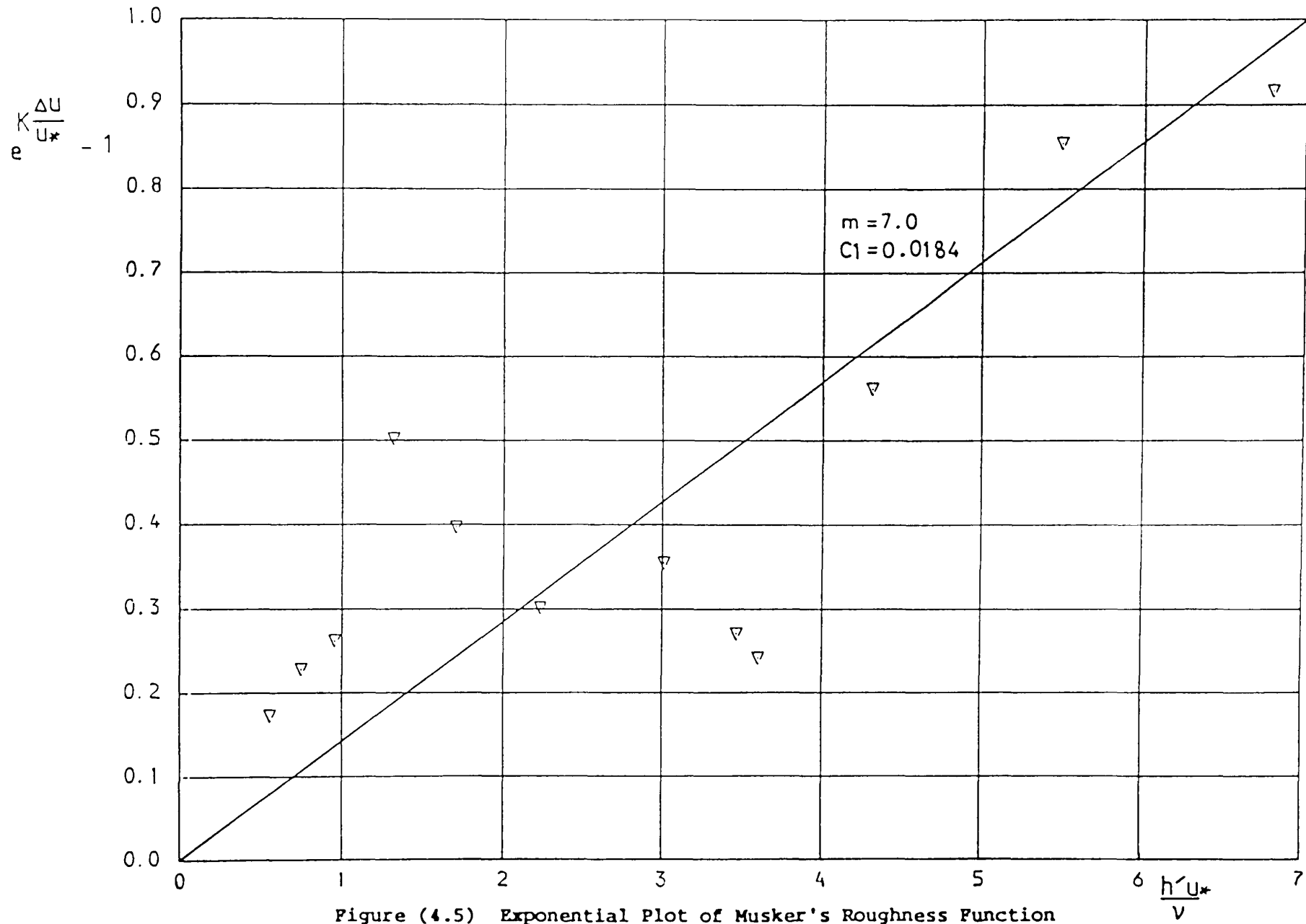


Figure (4.5) Exponential Plot of Musker's Roughness Function for R253-Surface Correlated with h'

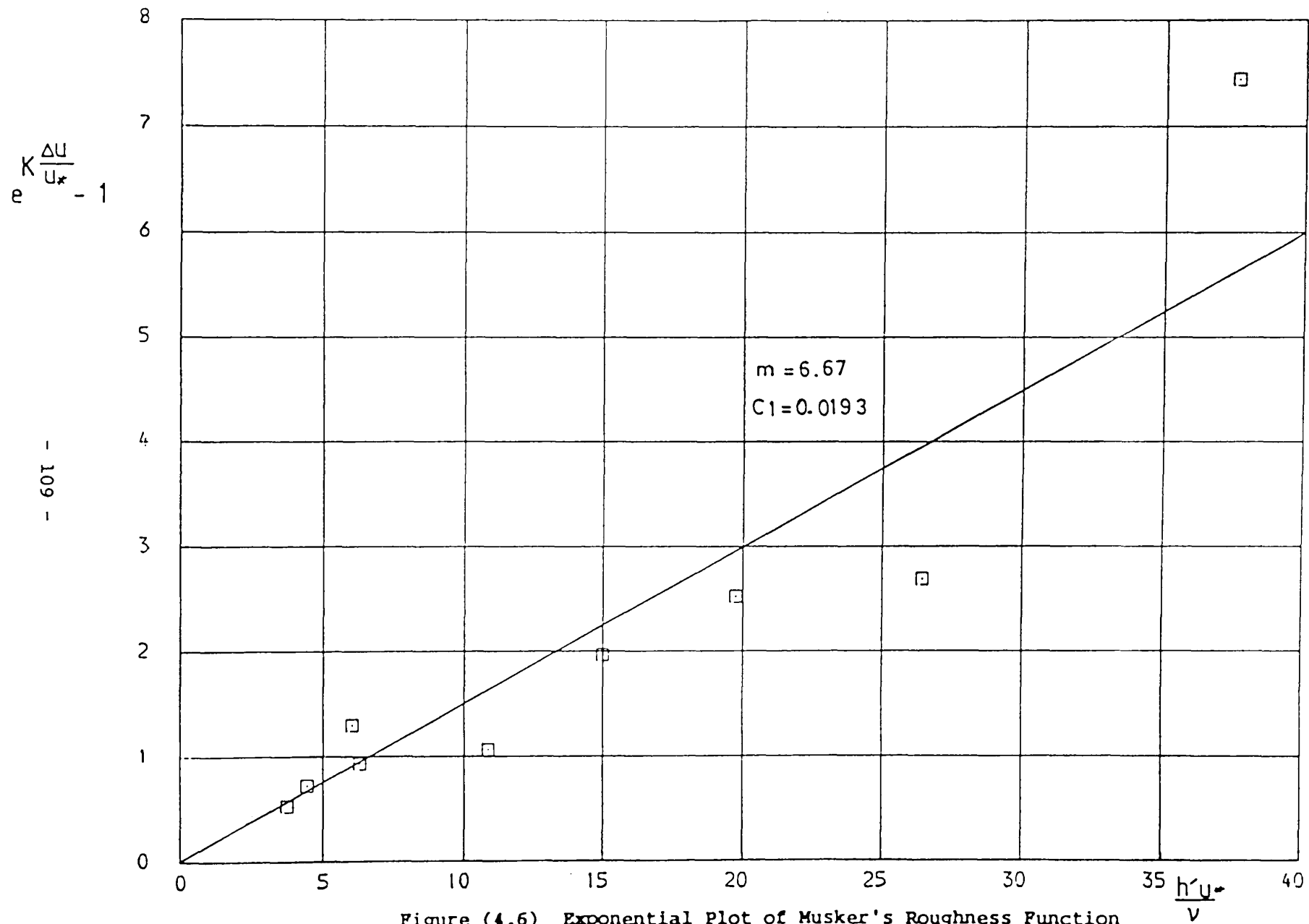


Figure (4.6) Exponential Plot of Musker's Roughness Function for R345-Surface Correlated with h'

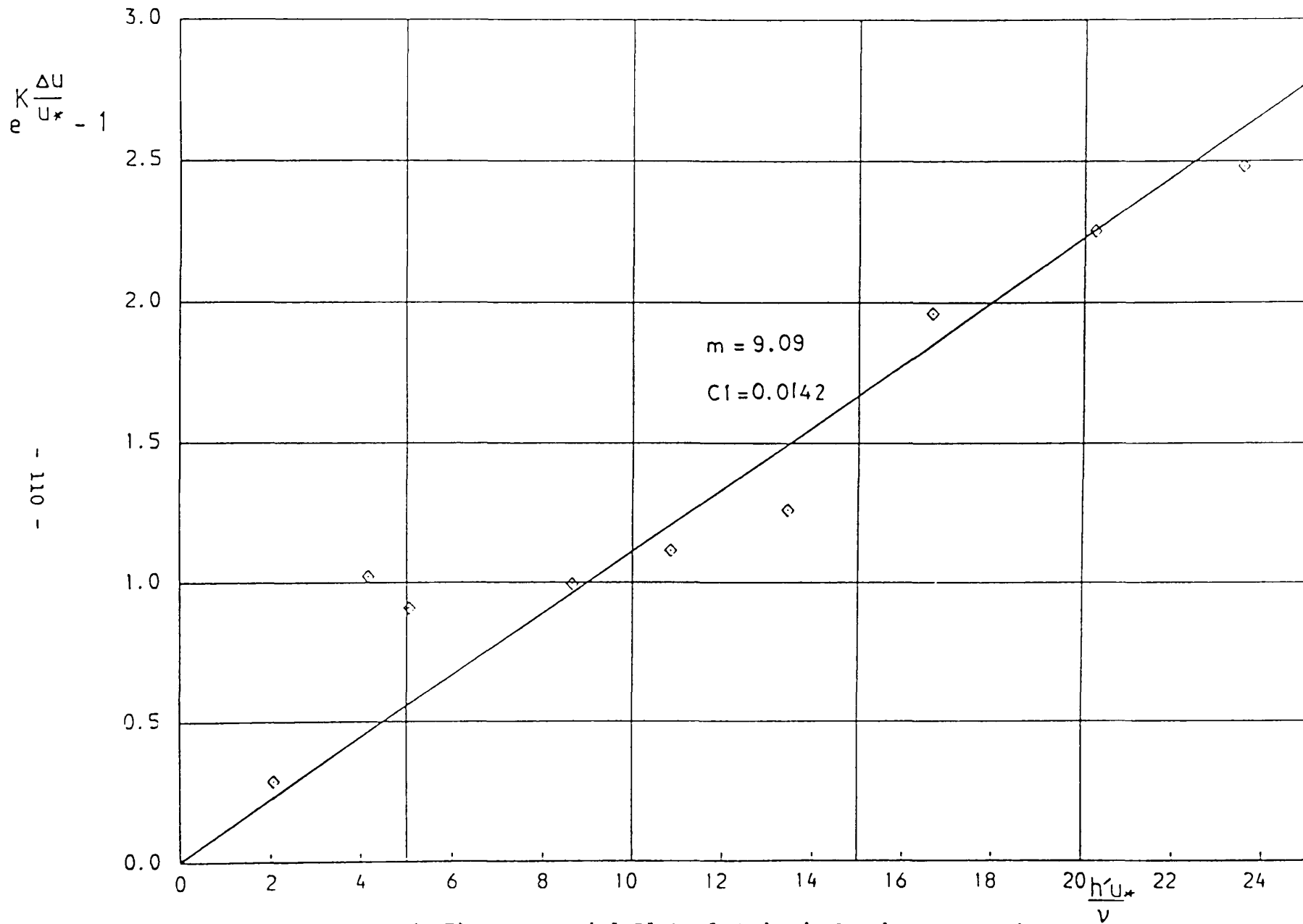


Figure (4.7) Exponential Plot of Musker's Roughness Function for R420-Surface Correlated with h'

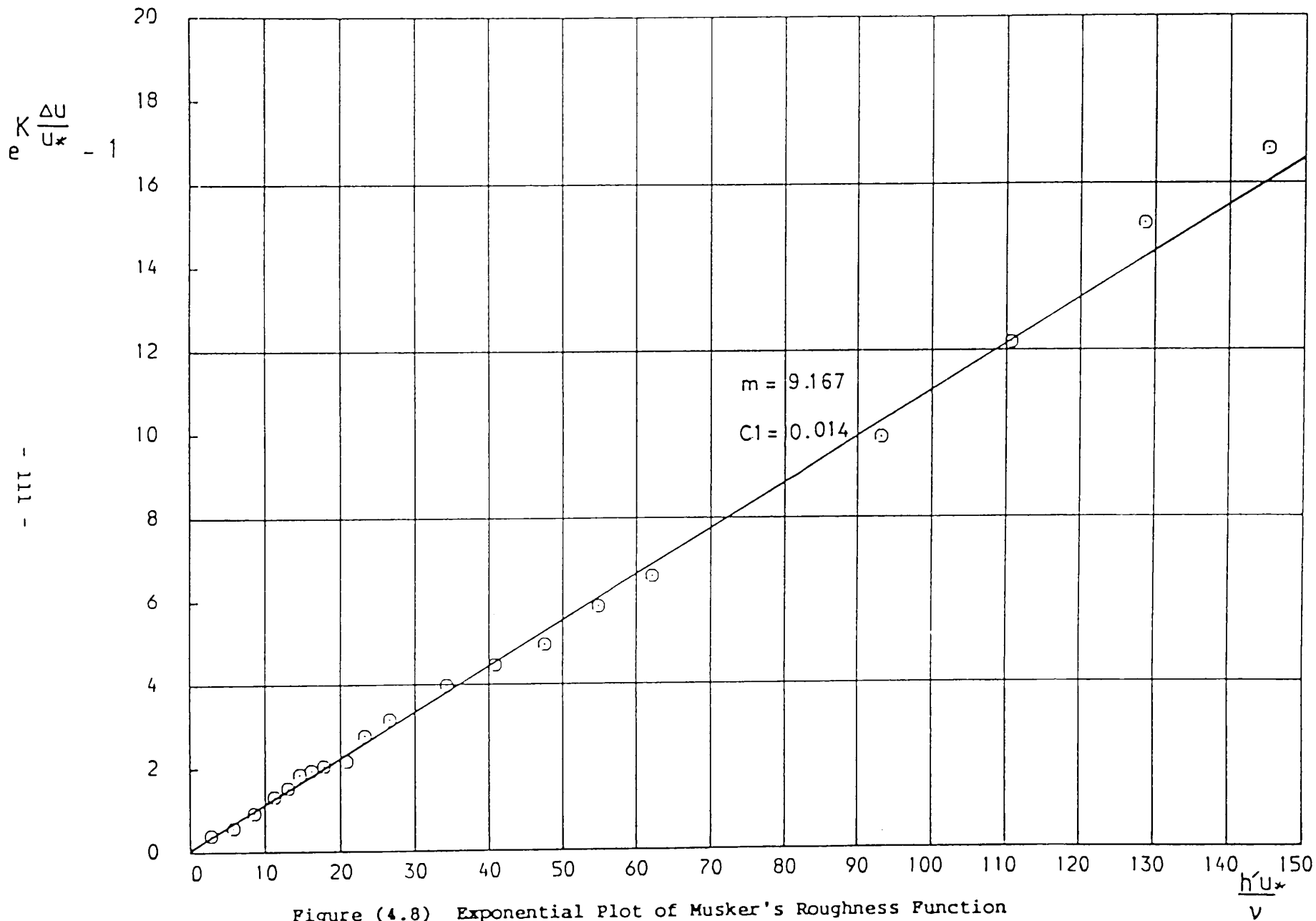


Figure (4.8) Exponential Plot of Musker's Roughness Function for R550-Surface Correlated with h'

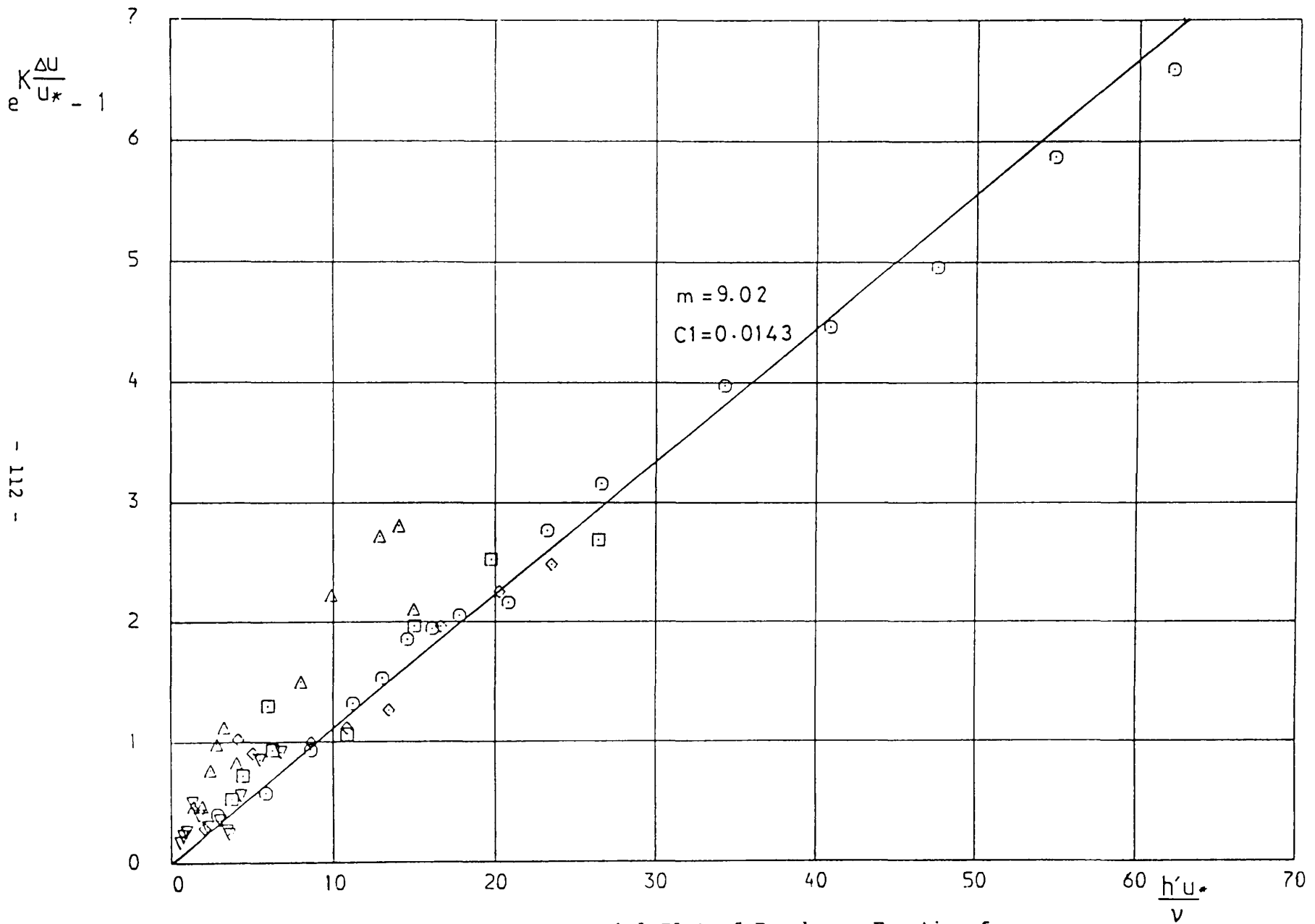


Figure (4.9) Exponential Plot of Roughness Function from the Five Musker Surfaces Correlated with h'

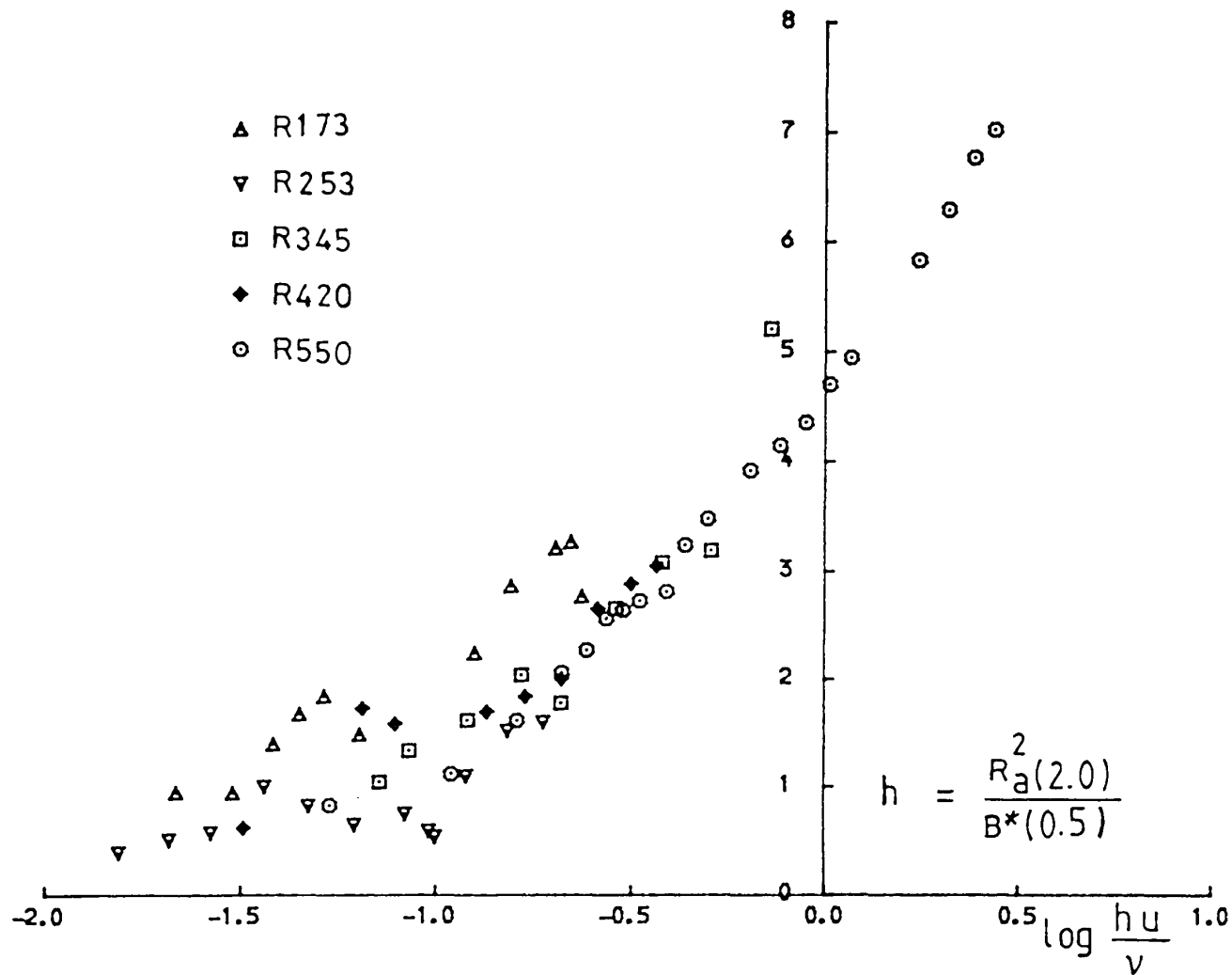


Figure (4.10) Roughness Function from the Five Musker Surfaces Correlated with Ra(2.0) and B*(0.5)

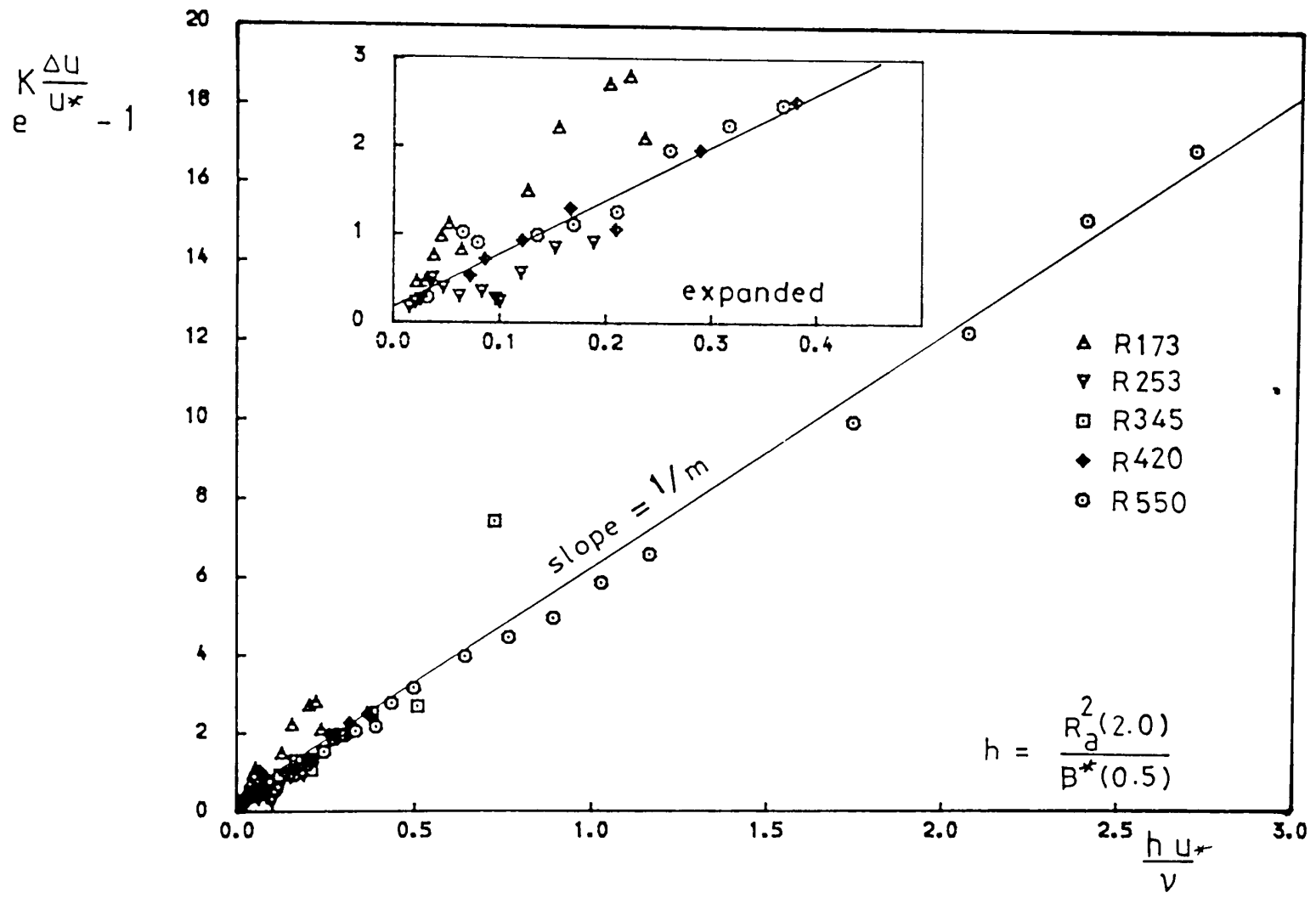


Figure (4.11) Exponential Plot of Roughness Function from the Five Musker Surfaces Using Ra(2.0) and B*(0.5)

4.2 LABORATORY EVALUATION OF IN-SERVICE PROPELLER ROUGHNESS FUNCTION

4.2.1 Introduction

To relate the propeller roughness measurement to power penalty, small scale trials or experimental relationships between surface topography and skin friction must be carried out. Although the effect on skin friction of various roughness geometries has been studied extensively, and attempts made to correlate experimental results with those obtained in service, none of such work has particularly dealt with propeller surface roughness. The aim of the present experimental work is to further understanding of the role which propeller roughness plays in the development of the propeller section drag. In addition, it was intended to determine the roughness function of a particular propeller surface, as an example, using a rotating cylinder apparatus.

In fact there are different laboratory methods which can be used to evaluate the roughness function. The method of towing a flat plane to measure directly the skin friction can be used to confirm or to find the drag penalty of a particular surface roughness. Unfortunately, it does not give the direct measurement of the roughness function. The velocity profiles in the boundary layer of the moving plane are necessary. There is also the consideration of the edge effects which should be taken into account.

Flow through pipes is also convenient for extracting the roughness function. However, there are some disadvantages which can be summarised as follows:

1. A long test section of about 50 to 100 times the pipe diameter is required.
2. Large pumping capacity and hence high costs.
3. Velocity profile measurements which are required take considerable experimental time and skill.
4. Replicating the surface inside a relatively small bore of pipe is very difficult.
5. Possible misalignment at the joints would lead to experimental errors.

Open water channels (flume experiments) can be used to study the roughness function. However, a limited range of Reynolds number can be achieved.

In addition to the above plan flow methods, two rotating systems can also be used. These are the rotating disc and the rotating cylinder. In both methods, direct evaluation of the roughness function can be obtained by measuring the torque and the speed of rotation only. Rotating disc has the disadvantage that the friction velocity varies with the diameter and hence problems in relating the torque to the roughness Reynolds number.

Perhaps the most convenient method of measuring the roughness function directly is the rotating cylinder. This type of experiment has been criticised on the ground that the flow is inherently unstable and end effects at the top and bottom of the cylinder lead to experimental errors. The Ship Performance Group at Newcastle has eliminated most of these problems by careful design of the rotor apparatus and devising a method involving shortening the cylinder.

4.2.2 Newcastle University Rotor Apparatus

There is no doubt that experiments on rotating cylinders can be made to establish the hydrodynamic roughness function for a particular rough surface. This is demonstrated by the work of Theodorsen and Regier [59] and Smith and Townsend [60] which shows that fluid flow between rotating cylinders and plane wall flows are very similar and a simple mathematical analogy between the two types of flow can be found. However, it is necessary before using a particular apparatus to prove its capability for performing such work. For this purpose, work on Newcastle rotor apparatus has been carried out by Medhurst [61]. It shows that on the wall of the inner and outer cylinders a thin boundary layer is formed, while the flow in the middle (about 85% of the annular gap) is inviscid and follows the form $uR = \text{constant}$. Inside the boundary layers the velocity profile follows the logarithmic friction law. The slope and the intercept of this logarithmic law are found to be the same as for the plane flow.

An attempt has been also made by Medhurst to predict the performance of the rotor, using the Dorfman theory of concentric rotating cylinders [62]. On this basis, Medhurst derived a resistance law of the inner smooth cylinder in the form:

$$U_1/u^* = 6.19 \log(R_1 u^*/\nu) - 5.383 \quad (4.28)$$

His preliminary test on the smooth rotor showed that the theoretical prediction of equation (4.28) is quite different than that obtained from the experimental data. However, experiments on close-packed sand grain surface of the Nikuradse type have been carried out to evaluate the performance of the rotor in the light of Nikuradse's well known roughness function. The results indicated the ability of the rotor apparatus to quantify reasonably the roughness function. Moreover, this roughness function can be obtained directly from torque/speed measurements without the need for velocity distribution traverses.

In view of the above, the smooth surface resistance law of the rotor may appear to be less critical, since our main purpose is to investigate the roughness function and differences only are considered.

The apparatus, see Figure (4.12), consists of a sectional rotor with three lengths of test surface, each of length 200 mm. The rotor is manufactured from PVC pressure pipe with nominal diameter of 320 mm. The procedure devised by Townsin is to carry out the experiments in two stages. The first is to measure the torque for a rotor of length 600 mm

(Long Rotor) and the second for a rotor of length 400 mm (Short Rotor), in which the top cover is positioned 200 mm lower than for the 'Long Rotor'. On the assumption that the 'end effects' are the same for both experiments, the difference in torque ΔT will represent the torque of the centre length piece of the 'Long Rotor'. The technical and experimental problems of this apparatus are discussed by Medhurst [61] in detail.

To establish the rotor experimental friction law whether for smooth or rough surface, ΔT can be expressed as:

$$\Delta T = F R_1 \quad (4.29)$$

Here F is the frictional force of the centre section cylinder, and if A is the surface area of it, the wall shear stress can be defined as:

$$\tau_w = F / A \quad (4.30)$$

use of equations (4.29) and (4.30) gives τ_w in the form of:

$$\tau_w = \Delta T / 2\pi R_1^2 L \quad (4.31)$$

where L is the length of the centre test cylinder (200 mm).

By definition, the friction velocity u^* is:

$$u^* = \sqrt{\tau_w / \rho} \quad (4.32)$$

yields

$$u^* = \sqrt{\Delta T / 2 \pi \rho R_1^2 L} \quad (4.33)$$

since

$$U_1/u^* = \sqrt{2 / C_f} \quad \text{and} \quad U_1 = 2 \pi R_1 N / 60$$

C_f can be found to be:

$$C_f = 900 \Delta T / \rho \pi^3 R_1^4 N^2 L \quad (4.34)$$

or

$$C_f = \tau_w / 0.5 \rho U_1^2 \quad (4.35)$$

4.2.3 Smooth Rotor Experiments

The smooth rotor experiments have been carried out in order to obtain a basis for comparison with rough surfaces. The intention was to produce a surface texture similar to that of a new propeller surface with Rubert grade A. The PVC cylinders have been carefully coated with epoxy white base. Using fine grain wet and dry emery paper, the cylinders were then hand polished while being rotated at constant speed. Such treatment means that the surface has been subjected to an equivalent machining process and is no longer of painted surface texture. The roughness of the surface was estimated using the Rubert gauge and found to be between grade A and grade B; i.e. an order of magnitude of about one micron of Ra(2.5).

Measurements of the torque were made at speeds from 100 to 900 RPM for both long and short rotors. Sufficient interval of time were allowed to

obtain a steady readout from the tachometer. Starting-up the rotor on all occasions is done gradually to ensure that the tachometer is not overloaded. Readings of water temperature are also made in order to account for the changes in the kinematic viscosity and hence the Reynolds number.

Records of torque/speed curves are tabulated in Appendix E and shown in Figure (4.13). The data has been analysed and the results are given in Table (4.5). Figure (4.14) also shows plots of U_1/u^* against $\log(R_1u^*/\nu)$ and C_f against $\log(R_1U_1/\nu)$ for the smooth centre section of the long rotor. A linear regression equation is then found in the following form:

$$U_1/u^* = 8.81 \log(R_1u^*/\nu) - 1.13 \quad (4.36)$$

with a correlation coefficient R^2 of 0.628. Clearly the surface is hardly proved to be a hydraulically smooth, but it may represent a relatively smooth commercial surface. Accordingly, the friction law given by equation (4.36) is considered as an appropriate base to establish the hydrodynamic roughness function.

4.2.4 Rough Rotor Experiments

The experiments on the rough "Poole River" surface consisted of replicating the surface, measuring the roughness characteristics and taking the torque/speed readings. Replicating and measuring the surface of "Poole River" have already discussed in chapter 2 and only the drag measurements are dealt with here. A photograph of the replicated surface applied on a cylinder is shown in Figure (4.15), and represents an old rough surface of a cast iron propeller blade.

Measurements of torque/speed on the rough rotors were conducted in the same manner as those on the smooth rotors. The data have been tabulated in Appendix E and also plotted in Figure (4.16). The mean values of ΔT at each speed are also shown. Analysis of the data is given in Table (4.6) in which the roughness function is obtained at the same Reynolds number from:

$$\Delta u/u^* = (U_1/u^*)_S - (U_1/u^*)_R \quad (4.37)$$

where,

$(U_1/u^*)_S$ is given by equation (4.36).

Figure (4.17) shows the resistance characterisation of smooth and rough rotors. The velocity loss can be seen as a constant offset of the smooth friction line for values of $R_1 u^*/\nu > 2 \cdot 10^4$. On the other hand, the surface roughness of the Poole River has no drag increasing effect if the value of the Reynolds number $R_1 U_1/\nu$ is less than $5 \cdot 10^5$. It is interesting

to observe also that the drag penalty depends upon both the roughness magnitude and Reynolds number. This has been expected since the flow behaviour of the present test should be similar to that of irregularly-rough engineering surfaces.

In figure (4.18), the roughness function of the Poole River surface $\Delta u/u^*$ is plotted to a base of $\text{Log}(u^*h'/mV)$. It can be seen that although there is some scatter at low speeds, the majority of the data are sufficient to obey the Colebrook-White form:

$$\Delta u/u^* = 1/K \ln(1 + u^*h'/0.62V) \quad (4.38)$$

where $h' = 36.6$ micron for the measured surface. When Ra and Pc are used instead of h' , see Figure (4.19), the roughness function becomes:

$$\Delta u/u^* = 1/K \ln(1 + u^*h^*/33.9V) \quad (4.39)$$

where,

$$h^* = Ra^2(2.5) Pc$$

The drag measurements indicated a very large added resistance in the order of 34% at Reynolds number of 2×10^6 . This may be far greater than that of today's operating propellers with finer texture. However, the results should still be useful to present in a quantitative way such effects of propeller roughness. It is also difficult to generalise from one surface test in relating the surface roughness to drag increment. In this context, the present experimental work should be repeated for more

and different propeller surfaces to establish a universal propeller roughness function.

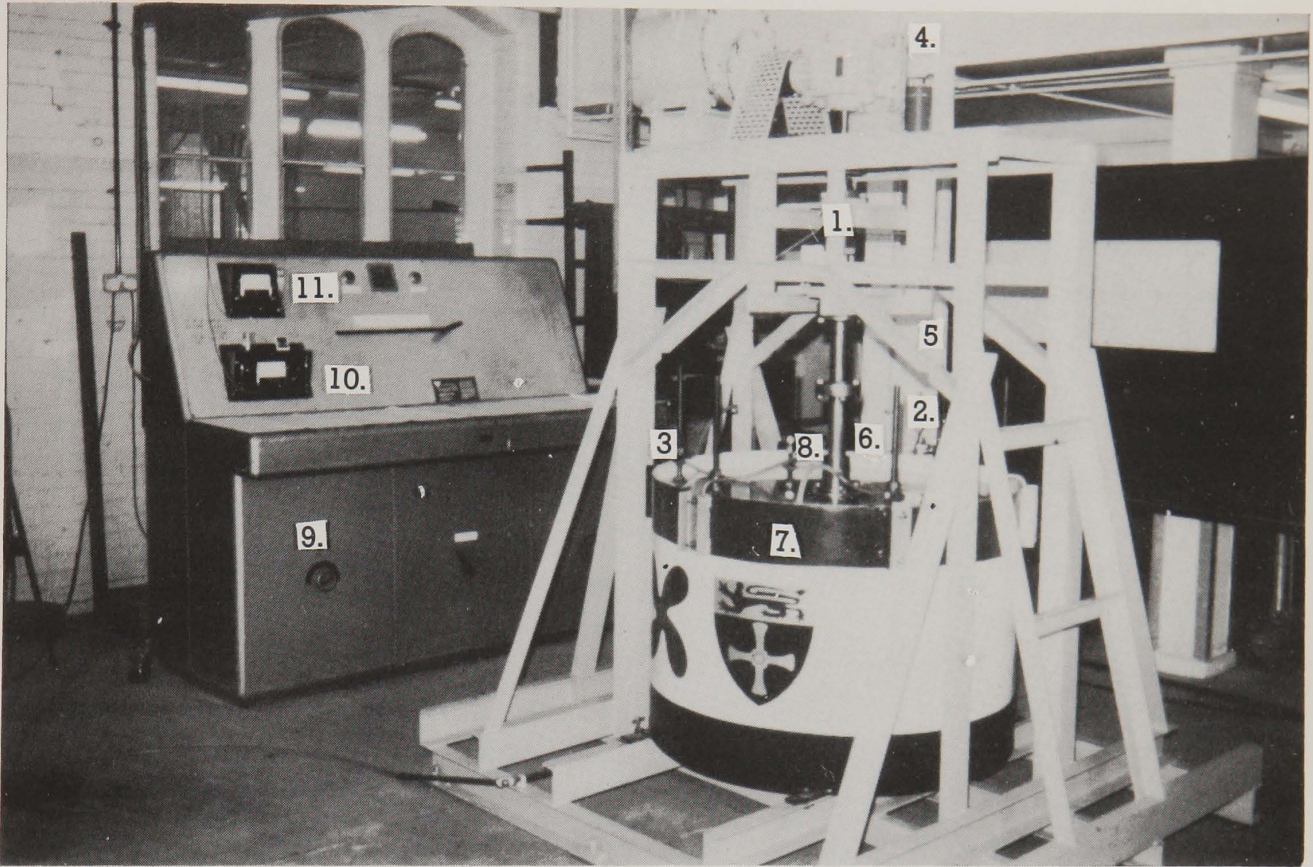


Figure (4.12) Newcastle University Rotor Apparatus

1. Torque transducer & speed pickup.
2. Perspex cover. 3 Inflatable rubber seal.
4. Motor & gearbox platform. 5 Compression legs. 6. Rotating test cylinder. 7. Fixed outer cylinder. 8. Fluid reservoir. 9. Motor/Generator Set.
10. Tachometer. 11. Indicator

ROTORQUE.- Friction Rotor Analysis Package
 EXPERIMENT.- SMOOTH ROTOR EXPERIMENTS

DATE/VENUE.- 29-11-85

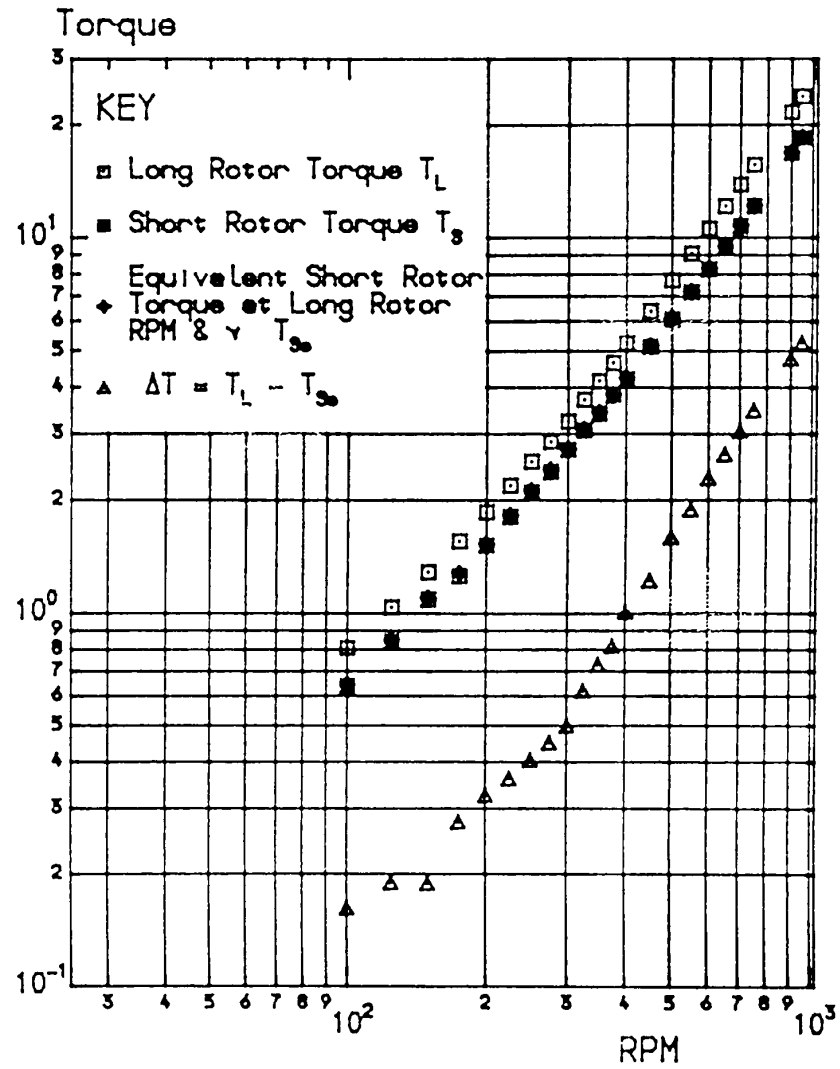
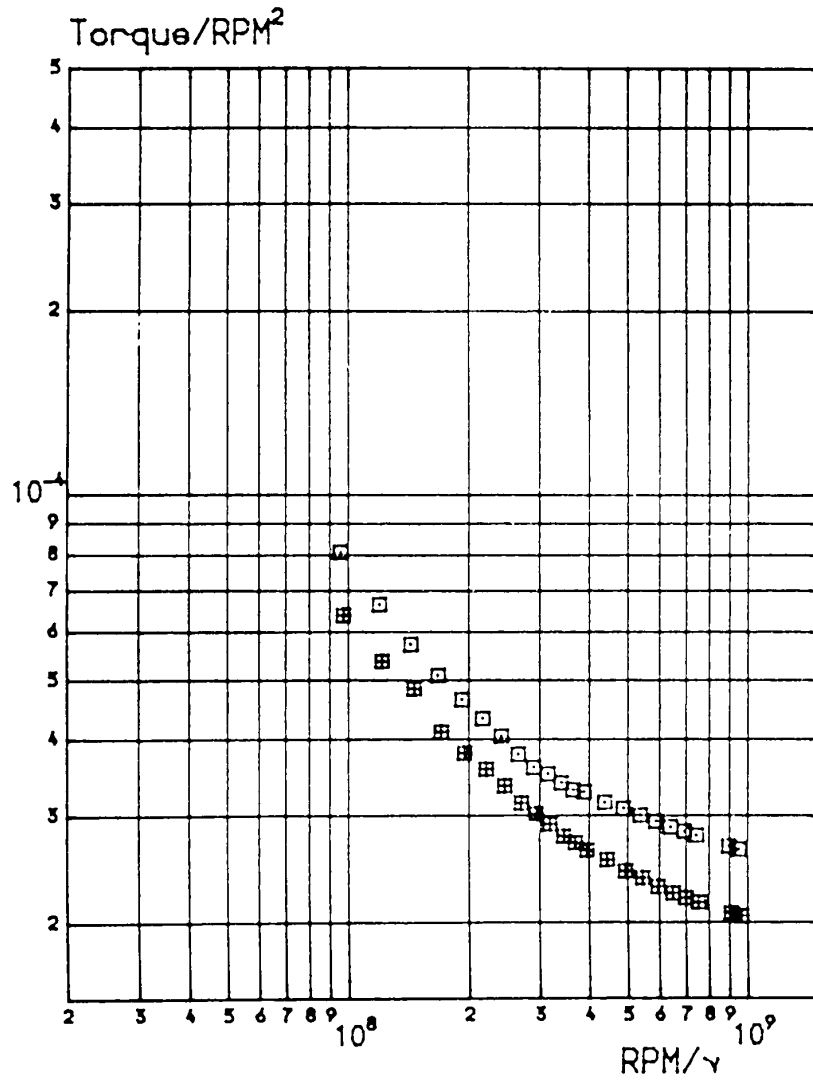


Figure (4.13) Torque/Speed Plots of Smooth Rotor Experiments

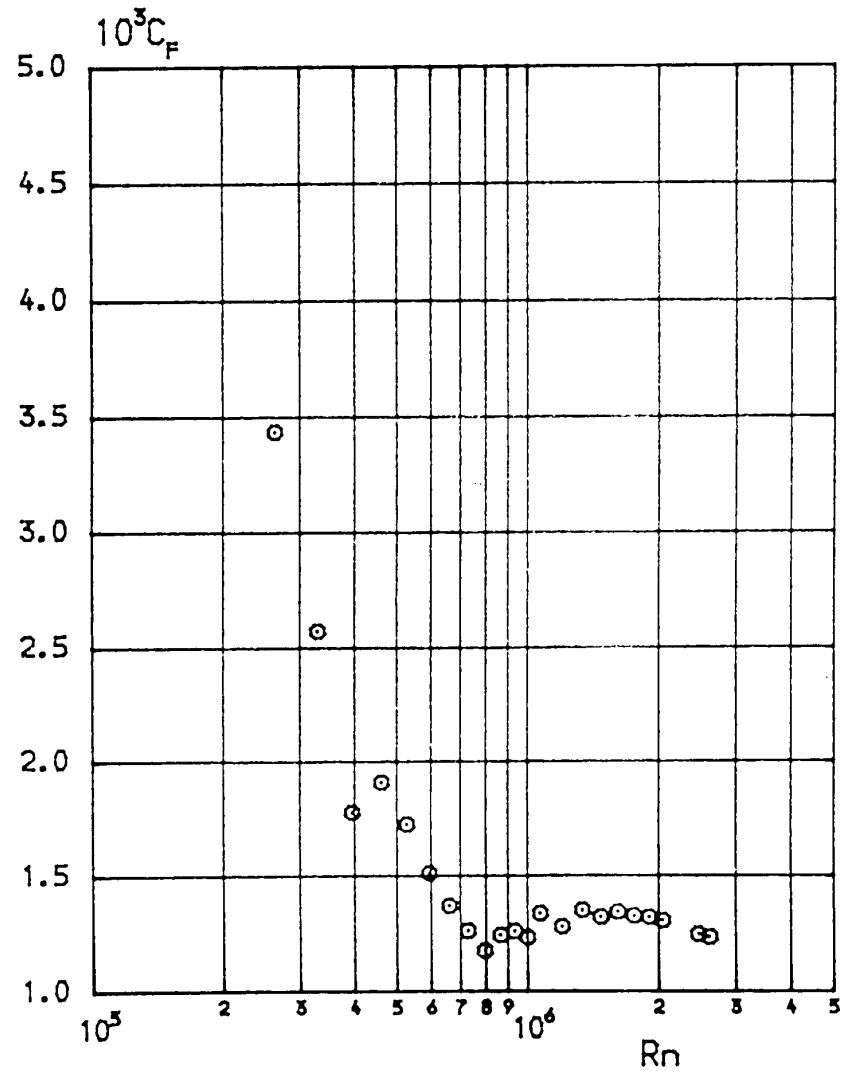
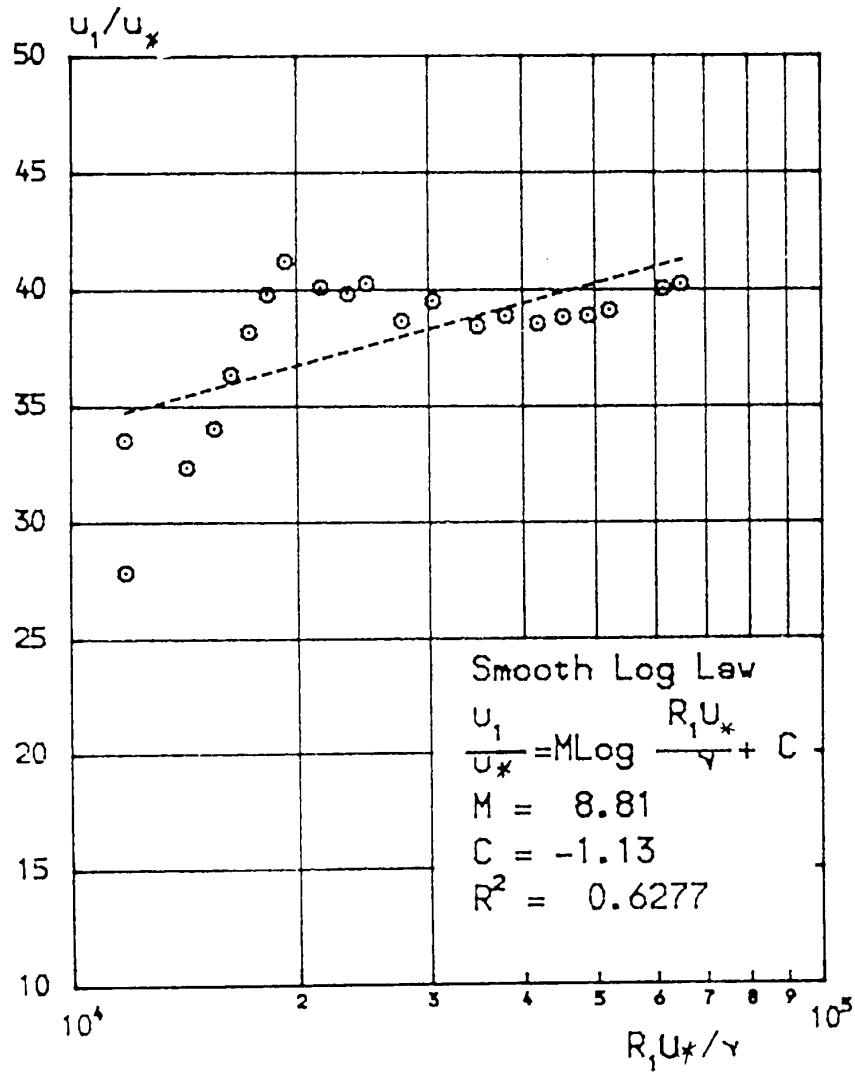


Figure (4.14) Smooth Friction Plots of Rotor Experiments



Figure (4.15) Photograph of "Poole River" Replicated Surface Applied on a Cylinder of the Rotor.

ROTORQUE.- Friction Rotor Analysis Package
 EXPERIMENT.- POOLRIVER PROPELLER

DATE/VENUE.- CAV.TUNNEL JAN 1985

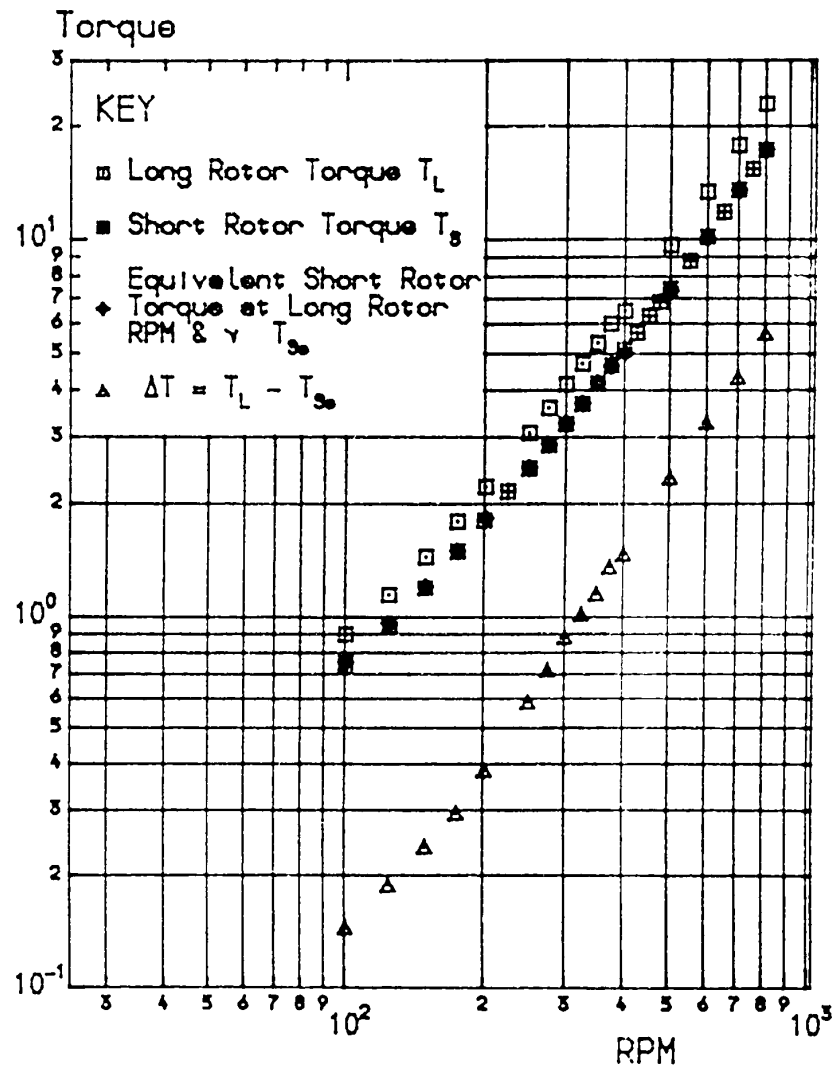
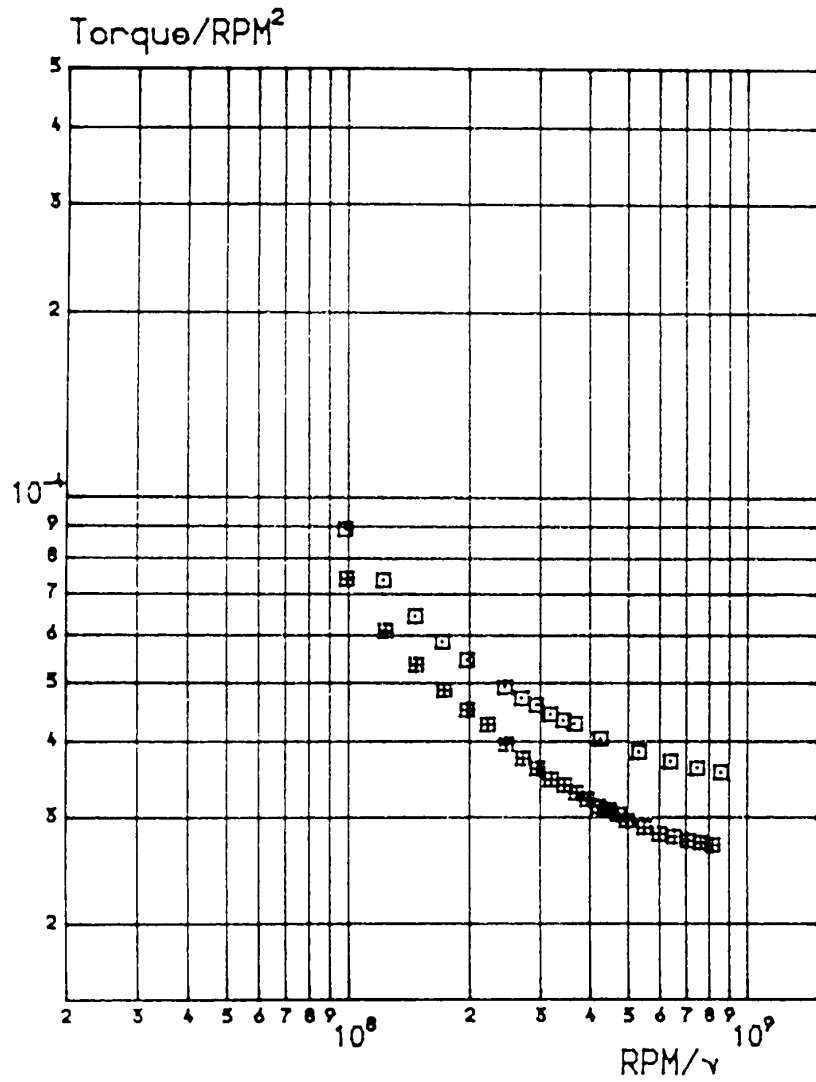


Figure (4.16) Torque/Speed Plots of "Poole River" Experiments

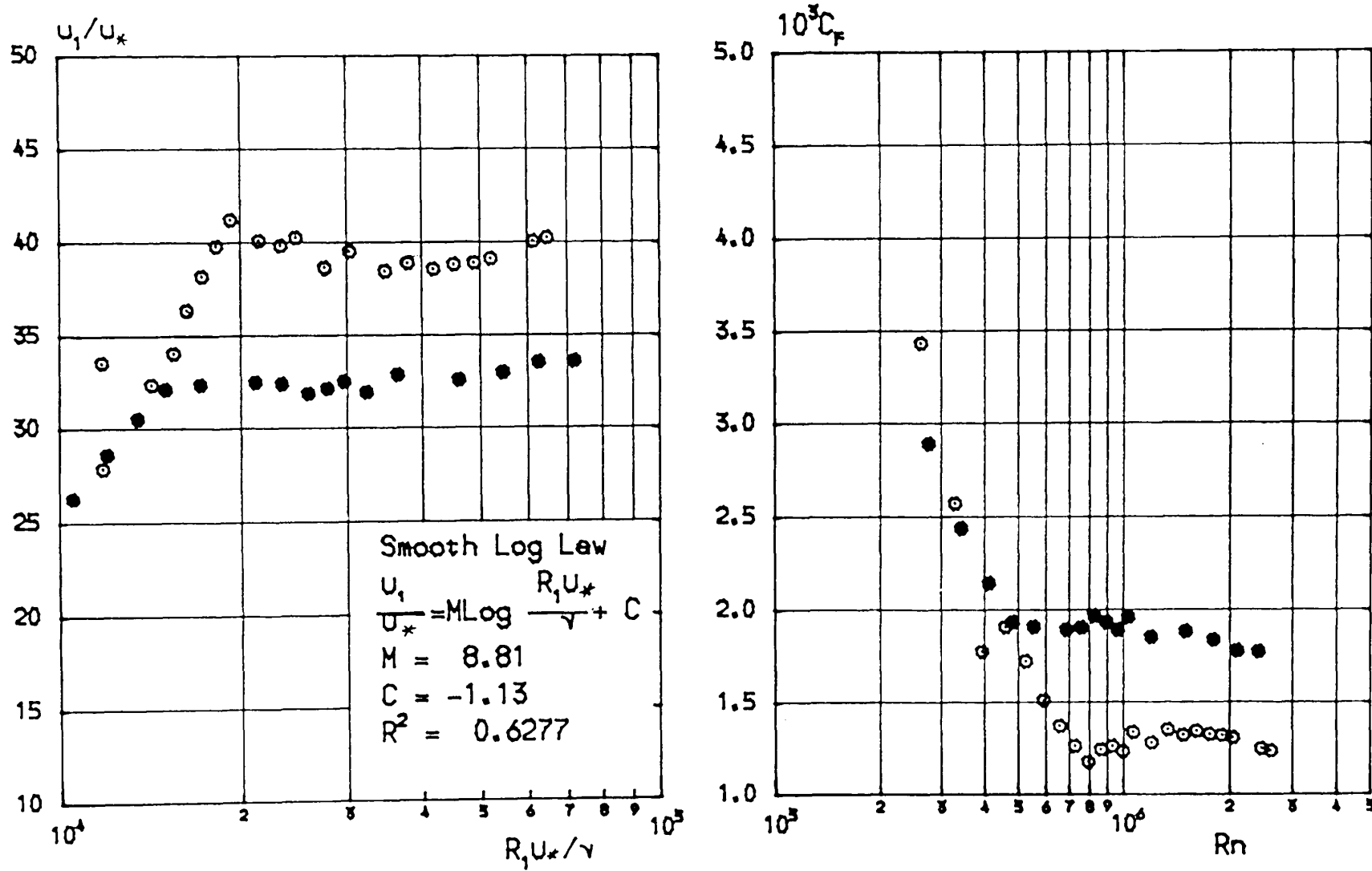


Figure (4.17) Friction Plots of "Poole River" Experiments

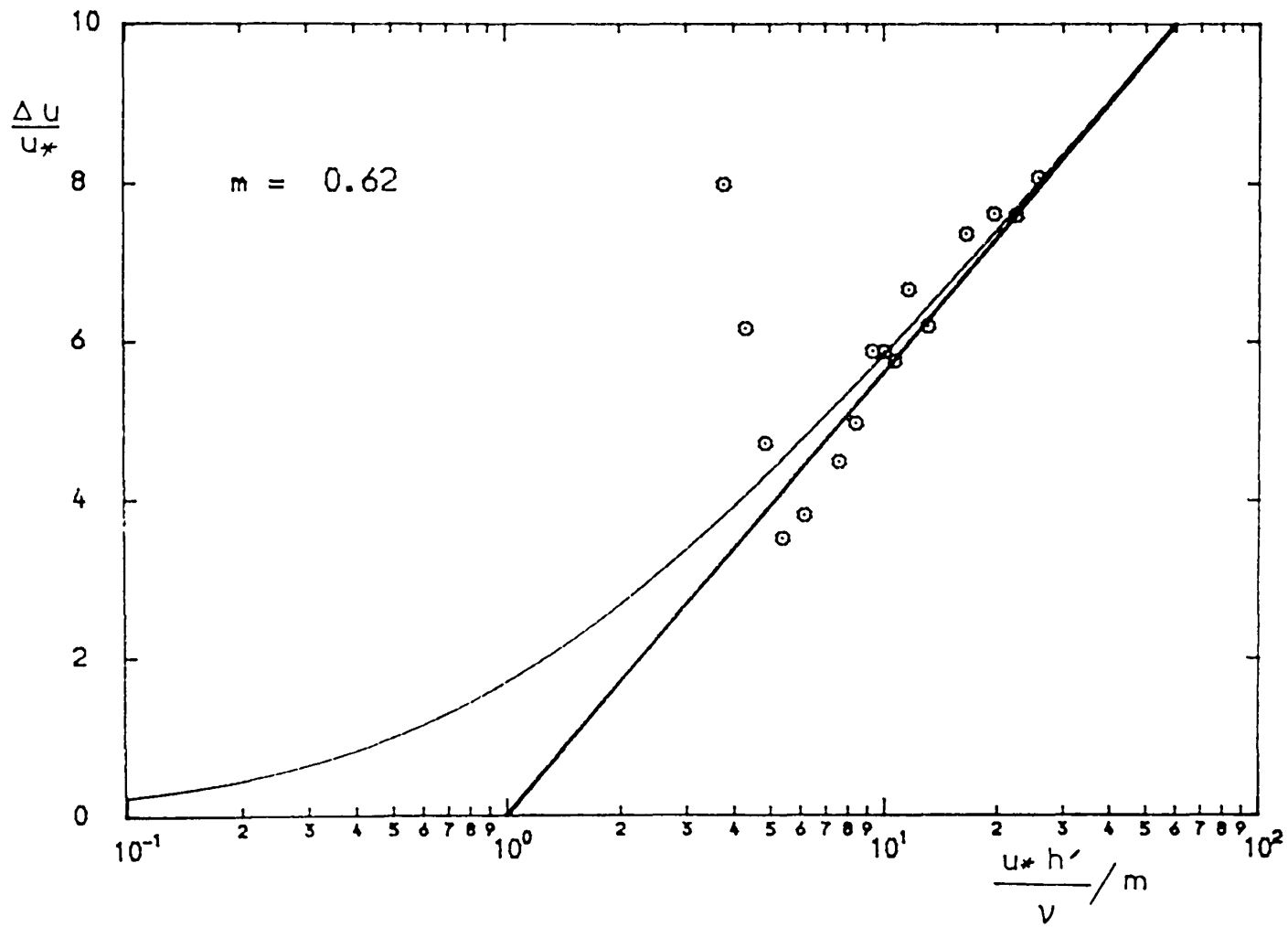


Figure (4.18) "Poole River" Roughness Function Correlated with h'

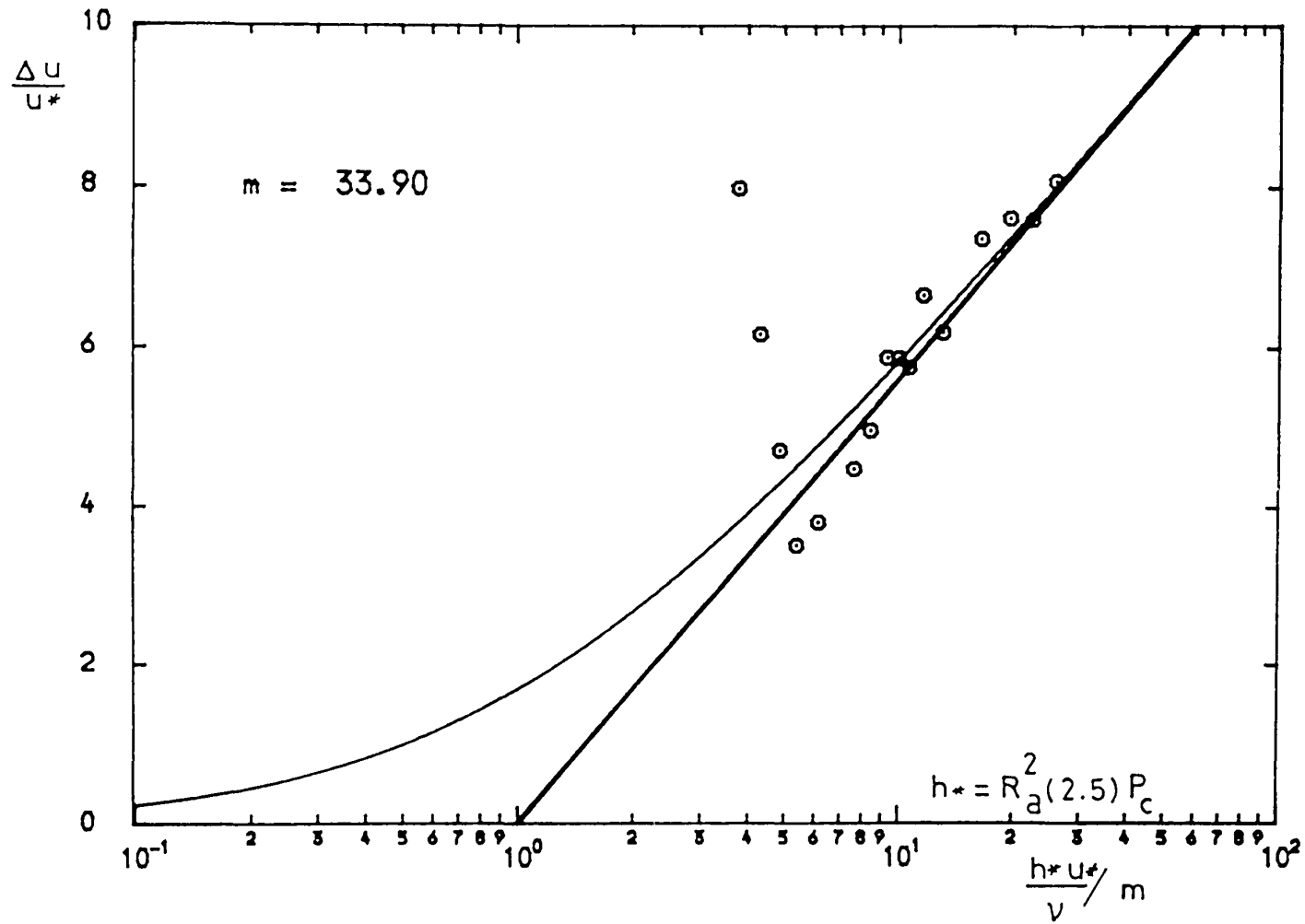


Figure (4.19) "Poole River" Roughness Function Correlated with $R_a(2.5)$ and P_c

Table (4.5)

 Fluid Friction Rotor Analysis

Analysis of Data for Smooth Cylinder Experiment

Cylinder Set Identifiaction:- SMOOTH ROTOR EXPERIMENTS

Measurement Date/Venue:- 29-11-85

Centre (Test) Cylinder Length:- 200.0 mm.

Centre (Test) Cylinder Radius:- 162.0 mm.

ΔT	RPM	Rn	C_f	U_1	u^*	U_1/u^*	$R_1 u^*/\nu$
0.16	100.0	0.26323E+06	0.34349E+01	1.70	0.0703	24.13	0.10909E+05
0.19	125.0	0.32903E+06	0.25725E+01	2.12	0.0761	27.88	0.11800E+05
0.19	150.0	0.39484E+06	0.17781E+01	2.54	0.0759	33.54	0.11773E+05
0.28	175.0	0.46065E+06	0.19090E+01	2.97	0.0917	32.37	0.14232E+05
0.33	200.0	0.52776E+06	0.17252E+01	3.39	0.0996	34.05	0.15500E+05
0.36	225.0	0.59373E+06	0.15118E+01	3.82	0.1049	36.37	0.16324E+05
0.41	250.0	0.65970E+06	0.13708E+01	4.24	0.1110	38.20	0.17271E+05
0.45	275.0	0.72748E+06	0.12620E+01	4.67	0.1172	39.81	0.18274E+05
0.50	300.0	0.79559E+06	0.11770E+01	5.09	0.1235	41.22	0.19300E+05
0.62	325.0	0.86403E+06	0.12435E+01	5.51	0.1375	40.10	0.21545E+05
0.73	350.0	0.93280E+06	0.12605E+01	5.94	0.1491	39.83	0.23417E+05
0.82	375.0	0.99943E+06	0.12328E+01	6.36	0.1579	40.28	0.24813E+05
1.01	400.0	0.10687E+07	0.13379E+01	6.79	0.1755	38.66	0.27640E+05
1.23	450.0	0.12023E+07	0.12804E+01	7.63	0.1932	39.52	0.30420E+05
1.60	500.0	0.13392E+07	0.13523E+01	8.48	0.2206	38.46	0.34823E+05
1.89	550.0	0.14767E+07	0.13224E+01	9.33	0.2399	38.89	0.37973E+05
2.29	600.0	0.16149E+07	0.13447E+01	10.18	0.2639	38.57	0.41875E+05
2.65	650.0	0.17581E+07	0.13264E+01	11.03	0.2840	38.83	0.45276E+05
3.06	700.0	0.19026E+07	0.13216E+01	11.88	0.3053	38.90	0.48909E+05
3.48	750.0	0.20437E+07	0.13065E+01	12.72	0.3252	39.13	0.52235E+05
4.78	900.0	0.24642E+07	0.12468E+01	15.27	0.3812	40.05	0.61527E+05
5.27	950.0	0.26138E+07	0.12351E+01	16.12	0.4005	40.24	0.64953E+05

Table (4.6)

Fluid Friction Rotor Analysis

Analysis of Data for Rough Cylinder Experiment

Cylinder Set Identifiaction:- POOLERIVER PROPELLER

Measurement Date/Venue:- CAV.TUNNEL JAN 1985

Centre (Test) Cylinder Length:- 200.0 mm.

Centre (Test) Cylinder Radius:- 164.0 mm.

Nominal Test Cylinder Roughness:- $h' = 36.60$ microns

Grigson "m" (computed) = 0.62

ΔT	RPM	$Rn \cdot 10^{-6}$	$\frac{1000}{C_f}$	U_1	u^*	$\frac{U_1}{u^*}$ rough	$\frac{R_1 u^*}{\nu}$	$\frac{U_1}{u^*}$ smooth	$\frac{\Delta u}{u^*}$	$\frac{h' u^*}{\nu}$
0.16	100.5	0.27654	2.891	1.73	0.0656	26.30	10513	34.30	8.00	2.35
0.19	124.8	0.24402	2.440	2.14	0.0749	28.63	11995	34.81	6.18	2.68
0.24	149.9	0.41247	2.144	2.57	0.0843	30.54	13505	35.26	4.72	3.01
0.30	175.3	0.48236	1.936	3.01	0.0937	32.14	15008	35.66	3.52	3.35
0.39	201.5	0.55445	1.910	3.46	0.1070	32.36	17136	36.17	3.82	3.82
0.59	250.0	0.68791	1.895	4.29	0.1321	32.49	21173	36.98	4.49	4.73
0.72	275.7	0.75862	1.906	4.73	0.1462	32.39	23421	37.37	4.98	5.23
0.88	300.2	0.82604	1.970	5.16	0.1618	31.87	25923	37.75	5.89	5.79
1.02	325.6	0.89593	1.935	5.59	0.1739	32.15	27869	38.03	5.88	6.22
1.16	350.7	0.96500	1.893	6.02	0.1853	32.51	29686	38.27	5.77	6.63
1.37	374.3	1.03250	1.962	6.43	0.2013	31.93	32335	38.60	6.67	7.22
1.48	400.5	1.19840	1.853	6.88	0.2094	32.85	36477	39.06	6.21	8.14
2.35	501.2	1.49980	1.884	8.61	0.2642	32.58	46032	39.95	7.37	10.27
3.29	600.2	1.80020	1.839	10.31	0.3126	32.98	54588	40.60	7.63	12.18
4.34	701.0	2.10250	1.779	12.04	0.3591	33.53	62710	41.13	7.61	14.00
5.67	802.1	2.41690	1.774	13.78	0.4103	33.58	71981	41.66	8.08	16.06

CHAPTER FIVE

CALCULATION OF PROPELLER FLOW AND PROPELLER CHARACTERISTICS

5.1 BLADE SECTION VELOCITY DISTRIBUTIONS

The boundary layer procedures, outlined before, required a knowledge of the surface variation of pressure on the propeller blade, which has a general aerofoil geometry. The calculation of the velocity distribution about such profiles in inviscid flow is one of the classic problems of fluid motion theory. A large number of calculation methods have been devised for two-dimensional aerofoils. The method needed here should be sufficiently accurate, and have a quick and simple calculation procedure to make it suitable for practical application. Riegels method [4] meets the requirement fairly well and is chosen for use in this work, in which the potential flow results have to be corrected for viscosity and cascade effects in order to be applied to the screw propeller. A summary of this method is in Appendix F.

The accuracy of Riegels method is dependent upon the magnitude of the incidence. Patience [5] examined this method for a large range of local nominal wake fraction and his results have been considered acceptable for marine propeller application. The Riegels method calculates the two-dimensional potential flow about an isolated profile in a steady stream. The real flow about a propeller blade is three-dimensional, non-steady and has the viscosity as well as the blade interaction

effects. However, in his approach Patience has reduced the problem to a two-dimensional quasi-steady model corrected only for viscosity and blade interference effects. He developed his correction factors on the basis that the integration of the pressure distribution for a profile at incidence should correspond to the total lift force. At the same time, the lift coefficient can be established from the propeller theories with reasonable accuracy. He also used the concept of the effective camber, the magnitude of which is established by consideration of the relevant expressions for the lift coefficient, as proposed by Burrill [63] .

Typical results of the velocity distribution on a surface of a propeller blade section have been presented in Figure (5.1). The main objective of calculating the velocity profile, in terms of U_s/V , is to use it in solving the boundary layer equations to obtain the difference in drag between smooth and rough blade sections. Alternatively, a similar calculation procedure can be carried out twice, once for the smooth blade and the other for the rough condition. Since we are interested only in the difference, the inaccuracy of the method in the calculation of the blade section velocity distribution is less critical.

The above method has been programmed in FORTRAN and now modified and included in the boundary layer procedures which form the "PROFNESS" package.

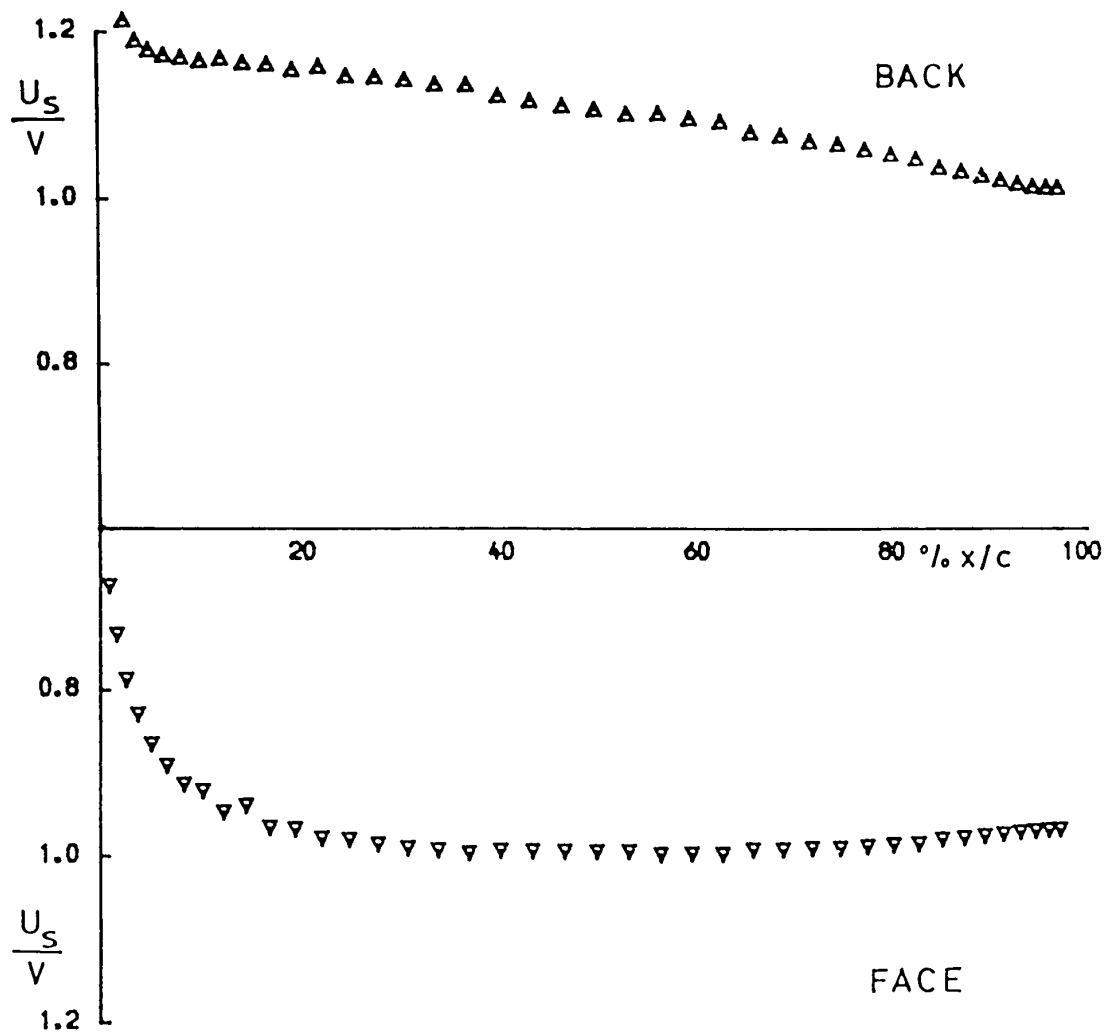


Figure (5.1) Velocity Distribution of Blade Section at 0.7R for "VLCC" Propeller

5.2 THE SHIP WAKE FIELD

5.2.1 Introduction

The propeller works in the water wake which has been created by the moving ship. Like all objects moving in a fluid, the ship has a boundary layer formed around its hull. The result is that the speed of the propeller relative to water is less than that of the ship relative to water. The speed of the water at the propeller disc is related to the wake and therefore, the difference between the ship's speed and the speed of the propeller, which is called the speed of advance, can be defined as the wake fraction (in Taylor's notation) by the equation:

$$w_T = 1 - V_a/V_s \quad (5.1)$$

5.2.2 Nominal and Effective Wake

The nominal wake belongs to the basic flow, i.e. to the flow caused by a towed ship or model at the place where the propeller is going to work. The wake field at the propeller is not uniform, but it varies around the propeller disc. The non-uniformity of the wake field is the cause of many undesirable effects like vibration and cavitation. The effective wake fraction is obtained when the wake fraction of a ship model is measured by the propeller acting as a wake meter and integrater.

There are two types of wake fraction, the thrust identity and the torque identity wake fraction. They are somewhat different because of the difference in flow conditions behind the ship and in open water.

5.2.3 Formation and Determination of Wake

The formation of the wake comprises axial, tangential and radial components together with a component due to motion in seaway. The axial component is the most important and is an accepted part of current propeller design practice. For analysis procedures, the tangential component can be introduced but it is only recently that model wake surveys include the measurement of this component.

Because of scaling effects the distribution of the wake measured behind a model hull is not necessarily a true representation of the wake distribution at full scale. It is therefore considered invalid to design a propeller by wake-adapting the sections to suit the model wake distribution without correcting the wake survey results. Such wake correction may be given by the following formulae:

$$(1 - w'_{NS}) = (1 - w'_{NM}) (1 - w_{NS}) / (1 - w_{NM}) \quad (5.2)$$

or

$$(1 - w_{NS}) = (1 - w_{NM}) (1 - w_{QS}) / (1 - w_{QM}) \quad (5.3)$$

where,

- w'_{NS} and w'_{NM} represent the local magnitude of the nominal wake

fraction for ship and model respectively.

- w_{NS} and w_{NM} represent the moment-mean nominal wake fraction for ship and model respectively.
- w_{QS} and w_{QM} represent the moment-mean effective wake fraction for ship and model respectively.

5.3 BASIC PROPELLER CHARACTERISTICS

Propeller characteristics have been calculated using the Burrill's vortex method [6] . This method was developed to calculate torque-thrust characteristics based on NACA aerofoil data of standard roughness [64] . Therefore, it is valid only for the case of smooth propellers. However, Burrill's method can be modified to take into account the blade surface roughness. Alternatively, it is possible to calculate for each section the contributions to the drag coefficient due to roughness from the upper and lower surfaces using the program "PROFNESS". This value can then be added to the total drag coefficient for smooth sections before estimating the modification to the lift coefficient due to the contraction of the slip stream.

It has been generally accepted that an increase in propeller roughness is followed by an increase in torque and a decrease in thrust. The circulation around the propeller blade will also be affected and hence the lift coefficient. Abbott and Doenhoff [64] have concluded that propellers having a roughness comparable with NACA standard roughness,

will not experience a change in characteristics due to a reduction of section lift caused by the roughness. In the proceedings of the 1978 ITTC, the effects of various roughnesses on model propellers indicated that the changes in the lift and drag coefficients can be related as follows:

$$\Delta C_L = -1.1 \Delta C_D \quad (5.4)$$

Since the above equation has been deduced from the model tests results, the extrapolation to full scale is not easy. However, the absolute magnitude of changes to C_L is small and the effects upon propeller characteristics can be assumed negligible for moderate values of blade surface roughness [58] .

5.4 EFFECTS OF PROPELLER ROUGHNESS UPON PROPELLER CHARACTERISTICS

Propeller roughness has two effects on blade section performance. Firstly, it increases the section drag coefficient; secondly it reduces the lift coefficient due to the reduction in the circulation around the propeller blade. Figure (5.2) shows a description of propeller blade section geometry and the forces acting on it. It is clear that increases in the section drag not only increases the torque but also reduces the thrust. However, the decreasing lift reduces both thrust and torque. Therefore, the equations of torque and thrust for a roughened propeller may be expressed as follows:

$$K_{QR} = K_{QS} + \Delta K_{QD} + \Delta K_{QL} \quad (5.5)$$

$$K_{TR} = K_{TS} + \Delta K_{TD} + \Delta K_{TL} \quad (5.6)$$

where,

ΔK_{QD} = change in torque coefficient due to a change in drag coefficient

ΔK_{QL} = change in torque coefficient due to a change in lift coefficient

ΔK_{TD} = change in thrust coefficient due to a change in drag coefficient

ΔK_{TL} = change in thrust coefficient due to a change in lift coefficient

the subscript "S" denotes the smooth propeller condition and the subscript "R" denotes the rough propeller condition.

If the assumption of constant lift for smooth and rough propeller is applied, i.e.

$$\Delta K_{QL} = \Delta K_{TL} = 0.0 \quad (5.7)$$

thus

$$K_{QR} = K_{QS} + \Delta K_{QD} \quad (5.8)$$

and

$$K_{TR} = K_{TS} + \Delta K_{TD} \quad (5.9)$$

It can be seen from Figure (5.3) that the thrust and torque characteristics were found to be changed, slightly in the case of K_T and significantly for K_Q , due to propeller roughness.

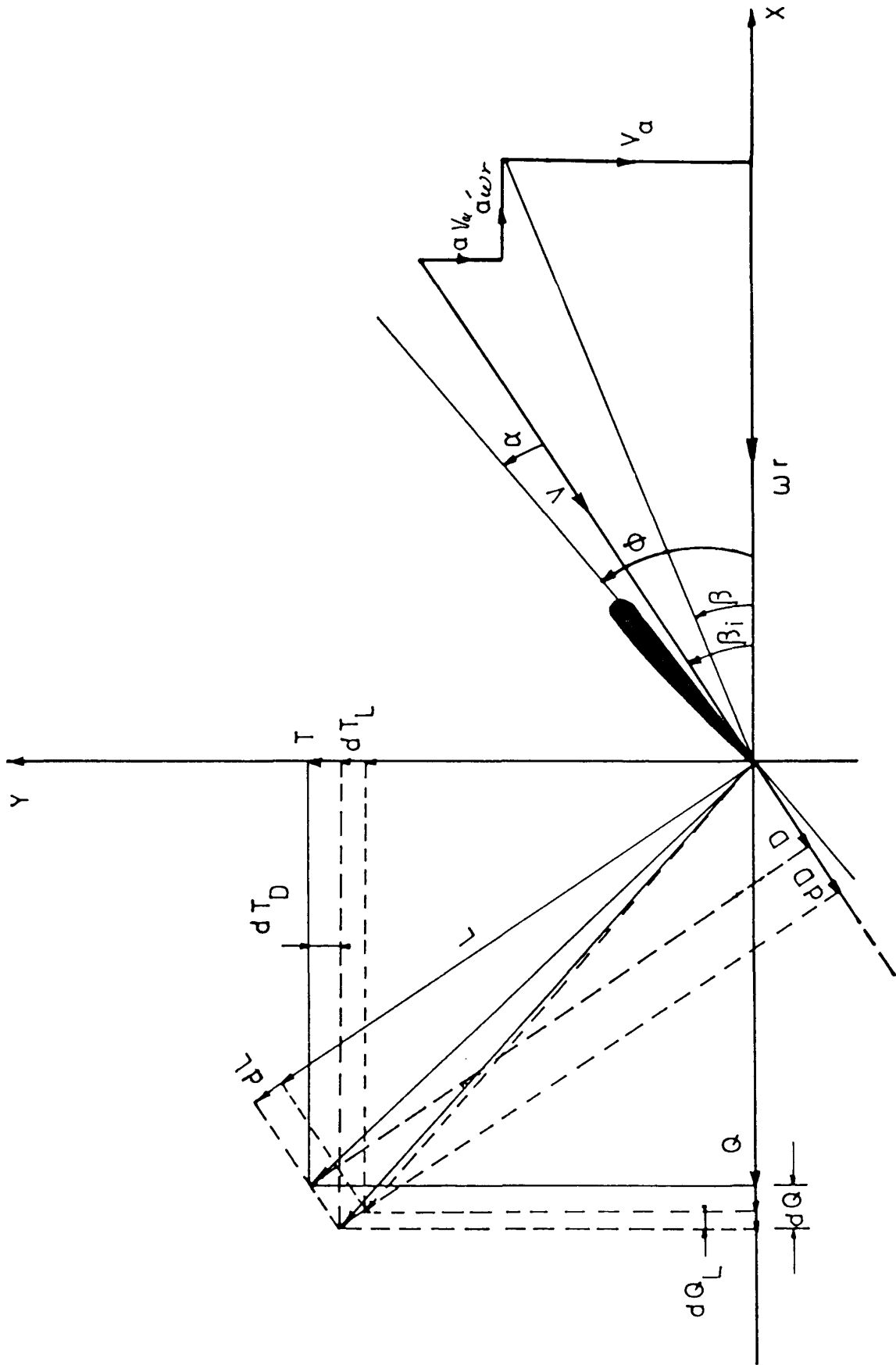


Figure (5.2) Speed and Force Diagram

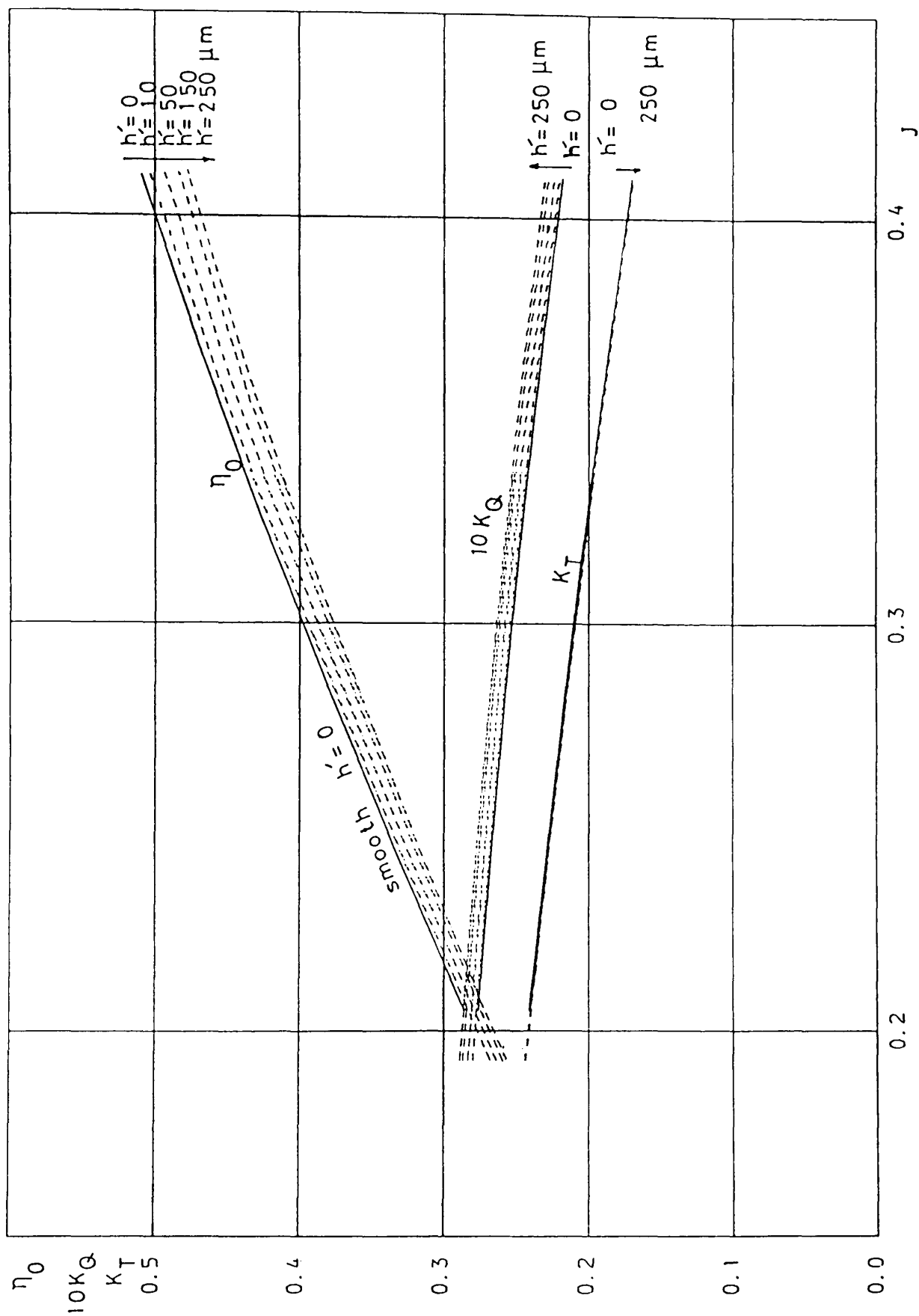


Figure (5.3) Effect of Propeller Roughness upon K_T , K_Q and η_0

5.5 THE EFFECT OF PROPELLER ROUGHNESS ON SHIP SPEED AND POWER

5.5.1 Power Penalty

In order to relate the effects due to the propeller roughness to actual RPM and power, it is assumed that the propeller develops a constant thrust in order to maintain the same ship speed for a variety of blade surface roughness. At the same time the hull surface roughness remains unchanged or in other words, the resistance of the ship remains the same. The ship speed will of course vary with the hull roughness for the same thrust. The effect of hull roughness upon the ship performance is discussed in chapter 6.

The power absorbed by a smooth propeller operating behind a ship can be written as:

$$P_S = 2 \pi \rho K_{QS} n_S^3 D^5 \quad (5.10)$$

and for a roughened propeller as:

$$P_R = 2 \pi \rho K_{QR} n_R^3 D^5 \quad (5.11)$$

The percentage increase in power due to roughness is

$$\frac{P_R - P_S}{P_S} * 100\% = \frac{\Delta P}{P} * 100\% = \left(\frac{P_R}{P_S} - 1 \right) * 100\% \quad (5.12)$$

Substituting equations (5.10) and (5.11) into (5.12) gives:

$$\frac{\Delta P}{P} \% = \frac{K_{QR}}{K_{QS}} \left[\frac{n_R}{n_S} \right]^3 - 1 * 100\% \quad (5.13)$$

In general,

$$K_T = T / \rho n^2 D^4 \quad (5.14)$$

or

$$T / \rho D^4 = K_T (V_a/J)^2 \quad (5.15)$$

Assuming that the deduction factor t and the wake fraction w_T remain unchanged due to propeller roughness, and applying the constant thrust-speed,

$$T_R = T_S \quad (5.16)$$

equation (5.14) can be written as:

$$K_{TR} \rho n_R^2 D^4 = K_{TS} \rho n_S^2 D^4 \quad (5.17)$$

or

$$K_{TR} / J_R^2 = K_{TS} / J_S^2 \quad (5.18)$$

i.e

$$K_{TR} / K_{TS} = (n_S/n_R)^2 = (J_R/J_S)^2 \quad (5.19)$$

equations (5.13) and (5.19) yield,

$$\frac{\Delta P}{P} = \frac{K_{QR}}{K_{QS}} \left[\frac{K_{TR}}{K_{TS}} \right]^{-3/2} - 1 * 100\% \quad (5.20)$$

To find the variables in equation (5.19), an iterative solution is made.

5.5.2 Speed Penalty

In order to calculate the speed loss at constant power, it is also assumed that the hull roughness remains unchanged. Generally, the essential controlling feature in the calculation of speed loss at constant power is the slope of the P~V curve in the range of the speed of interest. This is largely determined by the speed index, n of the resistance-speed curve. The speed index may vary from ship to ship and even within a ship speed range. Convenient methods of determining n from the power-speed curves are given by Lackenby [65] .

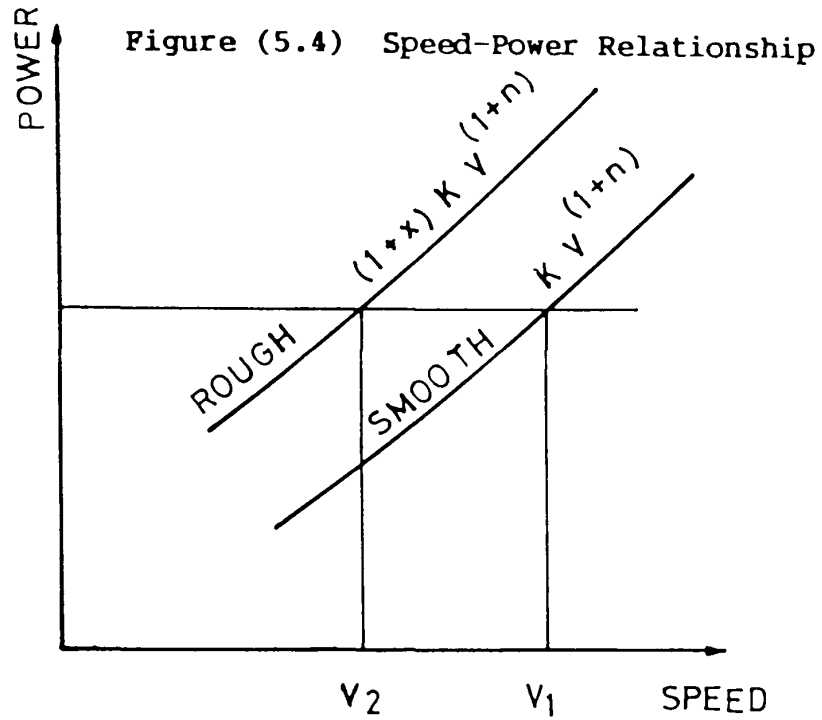
The power-speed relationship of a vessel can be expressed by:

$$P = k v^{(n+1)} \quad (5.21)$$

where k is a constant and n is the local speed exponent of the resistance curve in the range of operation.

In Figure (5.4) the power-speed relationship for two different propeller surface conditions can be demonstrated. The power in the case of smooth propeller is given by:

$$P_1 = k v_1^{(n+1)} \quad (5.22)$$



It is shown that, over the speed range of interest, say V_2 to V_1 , the ordinate of the smooth propeller curve is increased by the constant percentage of power. The equation of the rough propeller curve can therefore be expressed by:

$$P_2 = (1+x) k v_2^{(n+1)} \quad (5.23)$$

where,

$$x = \Delta P/P \text{ calculated at constant speed.}$$

At constant power, $P_1 = P_2$, i.e.,

$$(1+x) k v_2^{(n+1)} = k v_1^{(n+1)} \quad (5.24)$$

or

$$v_2/v_1 = [1+x]^{-1/(n+1)} \quad (5.25)$$

If x is relatively small, which is the case here, equation (5.25) can be approximated by:

$$V_2/V_1 = 1 - [1/(n+1)] x \quad (5.26)$$

i.e.

$$(V_2-V_1)/V_1 = - [1/(n+1)] x \quad (5.27)$$

It is to be noted that the value of x has been assumed constant in the region of interest for speed changes. The validity of this assumption may lie in the fact that the change of the open water efficiency, due to the roughened propeller, and hence the propulsive efficiency is relatively small in the given region and therefore less critical for the present calculation. Equation (5.27) can be written in the following form:

$$\frac{\Delta V}{V} = - \frac{1}{(1+n)} \left[\frac{\Delta P}{P} \right]_{\text{constant speed}} \quad (5.28)$$

The value of $\Delta P/P$ at constant speed may be calculated from equation (5.20).

The above method has been applied for the VLCC case and $(n+1)$ has been taken as 2.91 for the laden condition as given in [66] for the same vessel.

5.6 APPLICATION STUDIES

5.6.1 Program "PROFNESS"

The purpose of the program "PROFNESS" is to calculate the increment in frictional drag, ΔC_F , of a propeller blade section due to the blade surface roughness. From ΔC_F , the increment of overall drag coefficient, ΔC_D can be estimated using the results of Squire and Young [33] for aerofoil sections. Generally, it is sufficient to perform calculations for sections at $r/R = 0.3, 0.4, 0.5, 0.6, 0.7, 0.8, 0.9$ and 0.95 in order to obtain a complete picture of the performance of a propeller blade.

The data required for "PROFNESS" are basically the full scale propeller particulars, including section geometry, and the propeller surface measure with its roughness function. The main calculations in the program can be summarised by two principal steps:

1. Calculation of the flow around a propeller blade section.
2. Calculation of the development of turbulent boundary layer over smooth/rough blade surface section to estimate ΔC_F and hence ΔC_D .

The velocity distribution over each blade section can be calculated using tabulated data for NACA sections, with corrections for the angle of attack, camber, etc., as it has been made by Svensen [58]. In "PROFNESS", analytical procedures based on Riegels method and developed by Patience for marine propellers is used. It is to be noted that the velocity distributions expressed non-dimensionally in terms of U_S/V ,

velocity at the edge of the boundary layer divided by section velocity. This section velocity is the vector resultant of V_a and $2\pi nr/60$, where n is the speed of rotation in RPM.

To reduce the input data to a minimum the computer program includes a numerical interpolation routine to define completely the section geometry. The values of Burrill correction factors, Goldstein factors and smooth drag coefficients are stored in tabulated information within the program. Glauert formulation is used to calculate the zero-lift angle. An iterative solution of the Burrill equations is then followed to establish the local incidence. Integration routines are also included for calculation of the section lift coefficient.

The integral boundary layer method used in "PROFNESS" has been described in chapter 3. The integration of the boundary layer starting with values of x, π , and a single value of the propeller roughness for each section; the parameter h' is used incorporated with Musker's roughness function obtained in chapter 4. This follows with calculation of the starting values of δ and C_f . Modification of K and B_0 at low Reynolds numbers will be made if R_θ is less than 6000. Before calling the subroutine of the Runge-Kutta method, the velocity U_s is calculated and then differentiated to get the velocity gradient dU_s/dx and hence the term $1/U_s(dU_s/dx)$. A check on the error in C_f will be made before the calculation proceeds to the next step. The calculated average values of C_f along the blade section are integrated to give the total C_F . To find the propeller drag penalty, (ΔC_F and hence ΔC_D) the calculation

should be repeated for roughened blade condition. Figure (5.5) shows the local skin friction, C_f , of blade section at 0.7R for "VLCC" propeller.

An outline of the program "PROFNESS" is presented by means of flow diagrams in Figure (5.6).

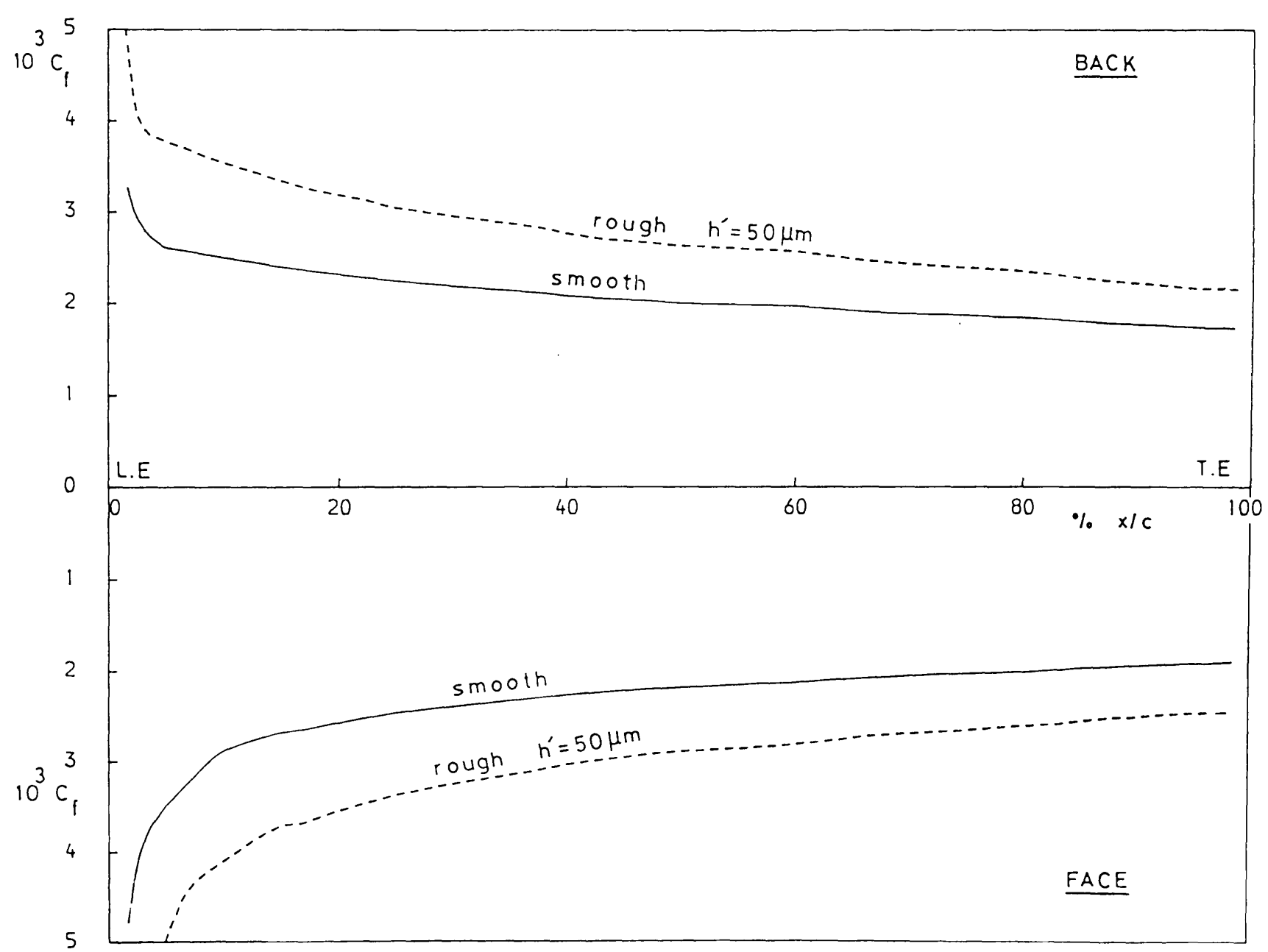


Figure (5.5) Local Skin Friction Coefficient of Blade Section at 0.7R for "VLCC" Propeller

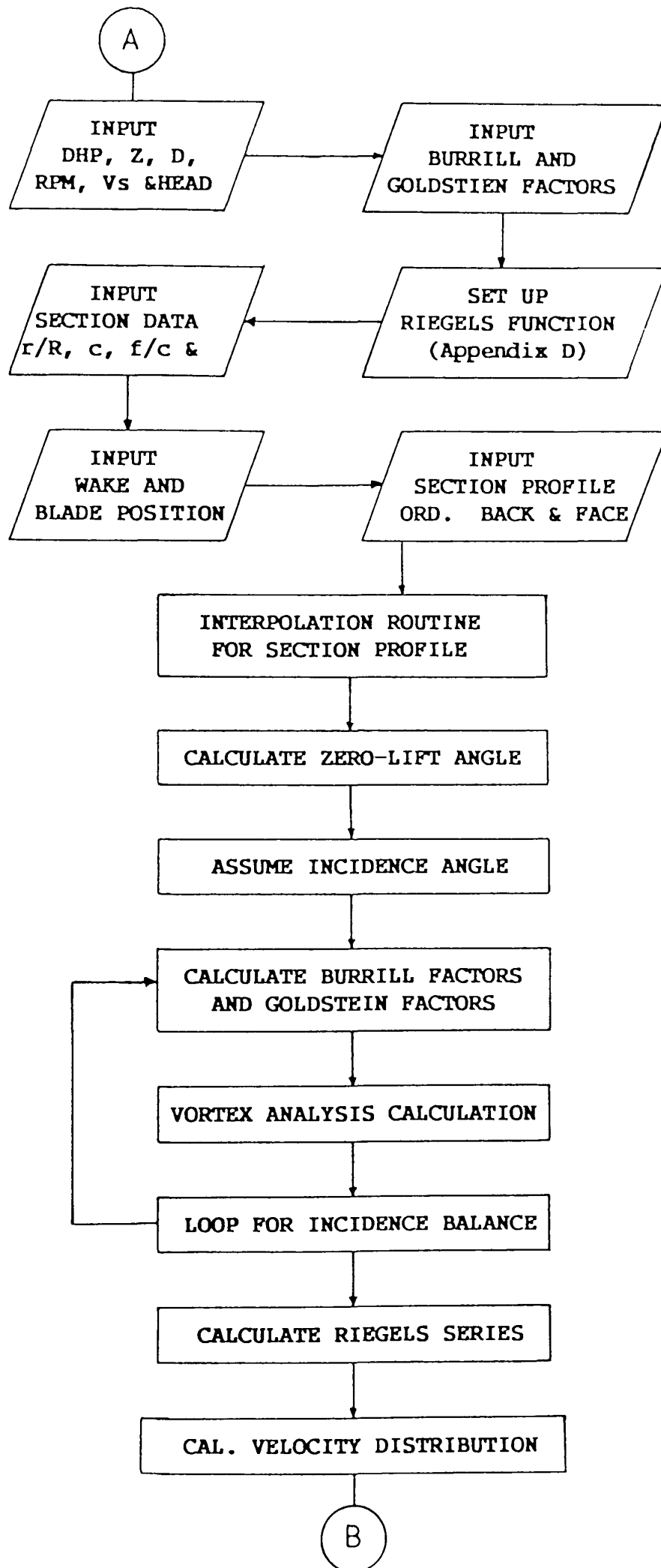
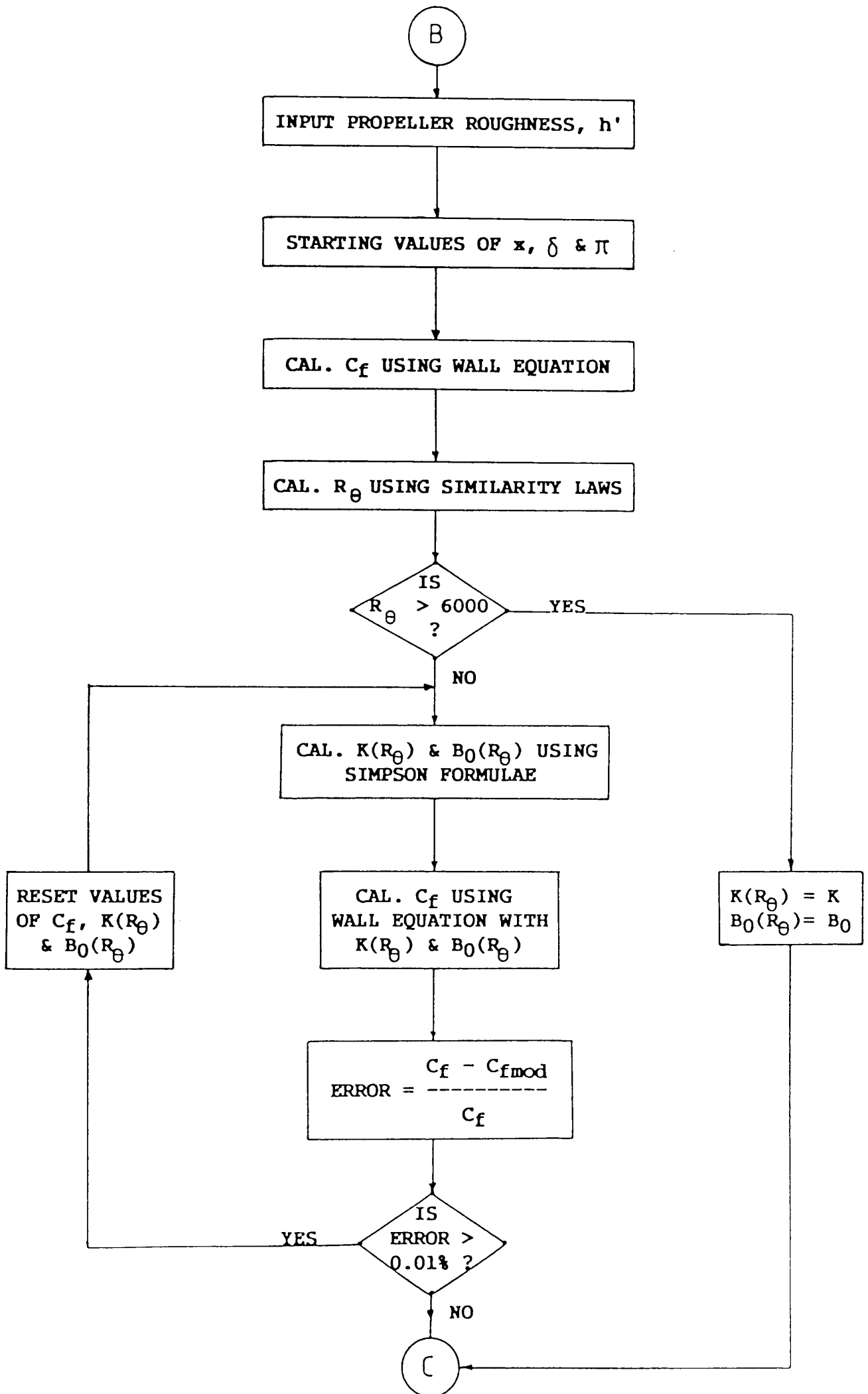
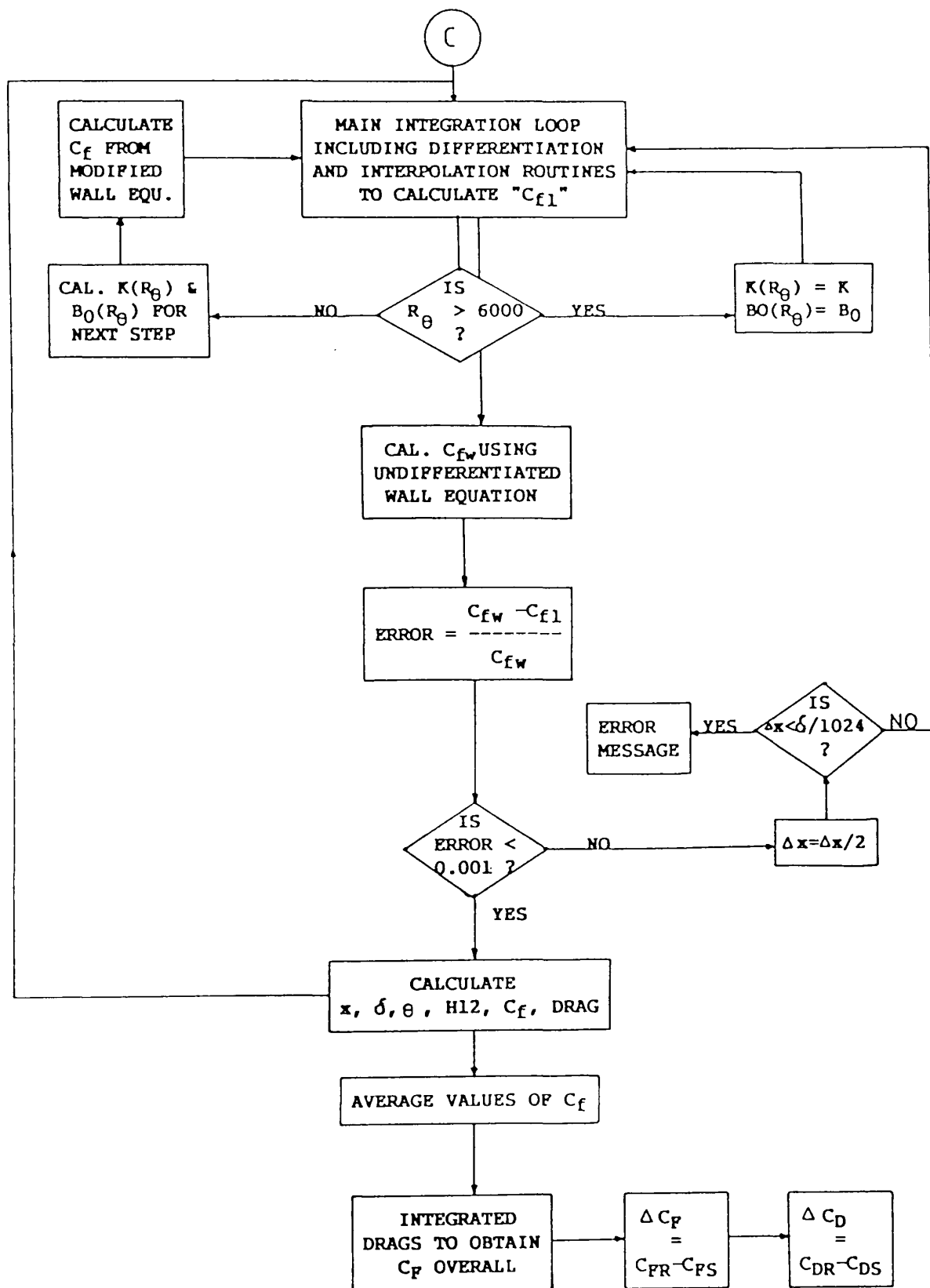


Figure (5.6) Flow Diagram of "PROFNES"





5.6.2 Case Studies

The objective of performing a series of case studies was to identify the principal variables associated with the propeller roughness penalties and their evaluation. It is hoped that some general conclusions can be obtained to develop a simple and reliable method which can be used by the shipowner or ship operator to quantify the benefits and hence justify the cost of regular blade surface maintenance.

The choice of suitable propeller for the case studies was mainly determined by the availability of data and information. However, considerations for obtaining a representative sample of different types of ship have also been taken into account. For each propeller, the local wake and the mean wake fractions were scaled from the model wake distribution using equations (5.2) and (5.3). Samples of a model wake distribution of a VLCC is shown in Figure (5.7). The necessary information about the propeller blade section characteristics was obtained from the propeller drawing. Appropriate extrapolations were made to suit the corresponding calculations. The task of extracting the required information in this manner was very difficult and time consuming.

Altogether five propellers were chosen for the case studies. Their characteristics are summarised in Table (5.1).

Table (5.1)

 Propeller Characteristics of Case Studies

Ship Type	z	P/D	D	RPM	Power	Speed
VLCC	6	0.738	8.65	87	32234	15.5
PRODUCT CARRIER	4	0.758	6.00	128	13890	16.9
CONTAINER SHIP	6	1.243	7.50	93.5	33740	24.5
CAR FERRY*	4	1.090	3.24	225	5287	21.0
FRIGATE*	5	1.340	3.66	130	3300	17.0

* Twin Screw

The results obtained from the computer program "PROFNESS" are given in Tables (5.2)-(5.6), for each of the five propellers. In each table, the results are presented in terms of ΔC_D for each section at a range of propeller roughness h' . Using Burrill vortex analysis, the propeller thrust and torque are evaluated for each of these roughness values. The effect of propeller roughness on thrust and torque characteristics, for the VLCC propeller, is shown in Figure (5.3). The change of thrust, torque and RPM are then transformed into ship power penalties at constant speed, for all propellers, as well as speed loss at constant power for the VLCC propeller. Tables from (5.7) to (5.13) present the results in terms of percentage increase in power, $\Delta P/P$ and speed loss, $\Delta V/V$ for a range of h' between 0 and 300 μm . For the VLCC propeller, an attempt has been made to examine roughness effects on only the outer half of the propeller blade. The results are given in Tables (5.8) and (5.9). It is shown also from Figure (5.8) that the outer half of propeller blade constitutes about 90% of the total power penalty and should therefore be reflected in the maintenance procedures adopted.

The power penalty, $\Delta P/P$ has been plotted against $(h'/c)^{1/3}$ for each propeller and the results are shown in Figure (5.9) to be linear which can be approximated by:

$$\Delta P/P \% = A (h'/c)^{1/3} - B \quad (5.29)$$

where, h' is the propeller roughness measure in microns and the chord length, c is taken at the equivalent radius, $r/R=0.7$.

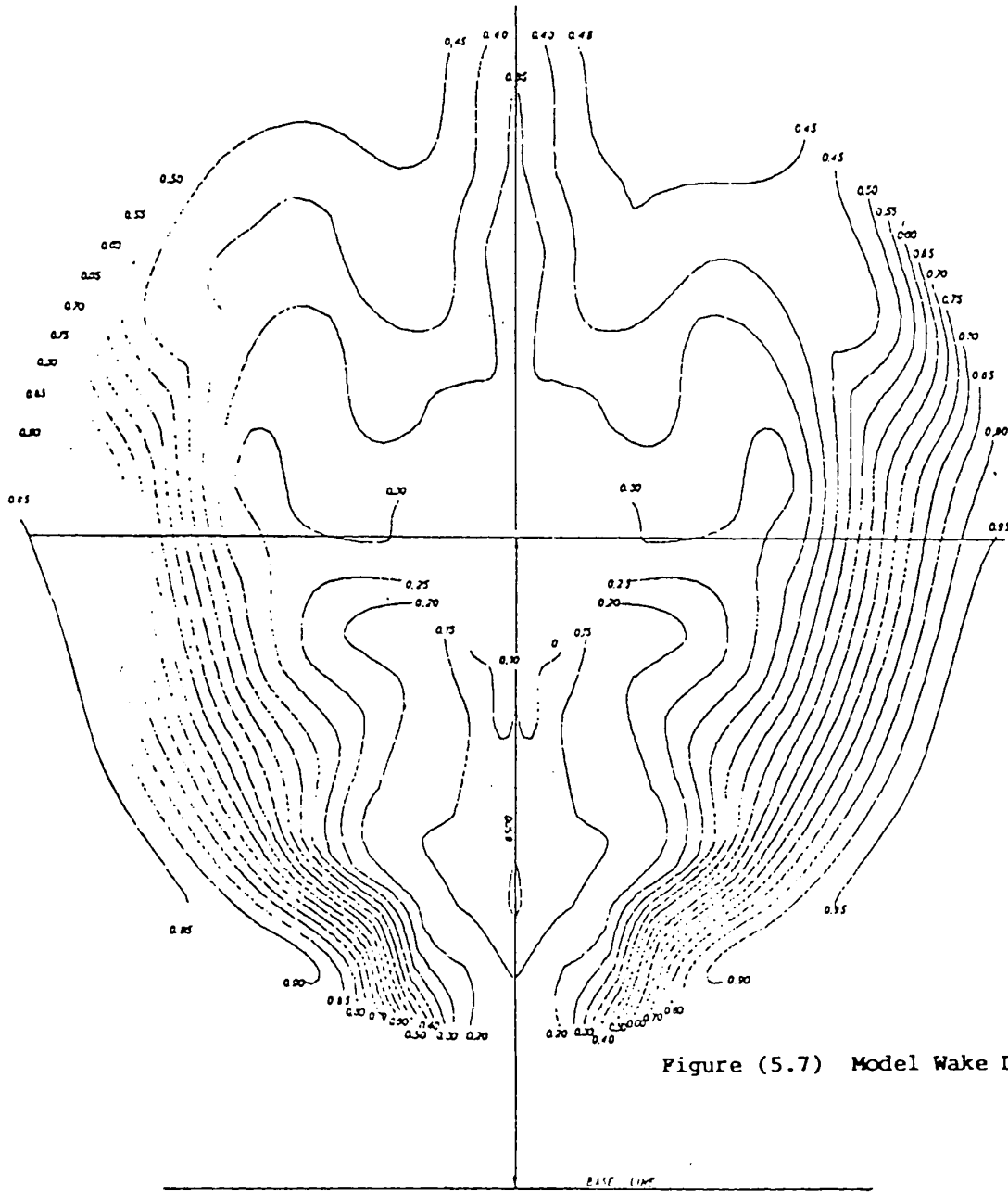
It is to be noted that, the slope A and the intercept B , in equation (5.29) are different for each propeller. However, ignoring the result of the propeller used for the "Frigate", which is special type of ship, the results of the others can be analysed together to find an average value of A and B . From a simple regression analysis of the data, equation (5.29) can be rewritten as:

$$\Delta P/P \% = 1.69 (h'/c)^{1/3} - 1.84 \quad [\text{for } (h'/c)^{1/3} > 1.1] \quad (5.30)$$

As the plots for the four propellers are within 10% of the above fitted equation, it can be used as approximate penalty estimations for similar types of propeller.

More rigorous relationships can be found also by relating A and B to propeller parameters (P/D , BAR , Z ,...). In this case numerous case studies should be done in order to find accurately A and B in terms of the above parameters. A simplified method involving such propeller

parameters has been developed in chapter 6 to determine the effect of propeller roughness on ship power.



LINES OF EQUAL AXIAL VELOCITY COMPONENTS $\frac{V_x}{V}$

DERIVED FROM RESULTS OF A VELOCITY SURVEY
BY MEANS OF A FIVE HOLES PITOT TUBE

SHIP MODEL No. 4496

DRAFT: 22.35 m.

IMMERSED DISPLACEMENT VOLUME: 340944 m³

SPEED 15 1/2 KNOTS.

TEST No. 31640

MODEL CONDITION

SCREW APERTURE I

BULBOUS BOW I

OUTLET SCOOP SITUATED AT PORT SIDE

THE VELOCITY SURVEY WAS MADE IN A PLANE

PERPENDICULAR TO THE SHAFT AXIS IN

WAY OF THE PROPELLER

Figure (5.7) Model Wake Distribution of a VLCC Propeller

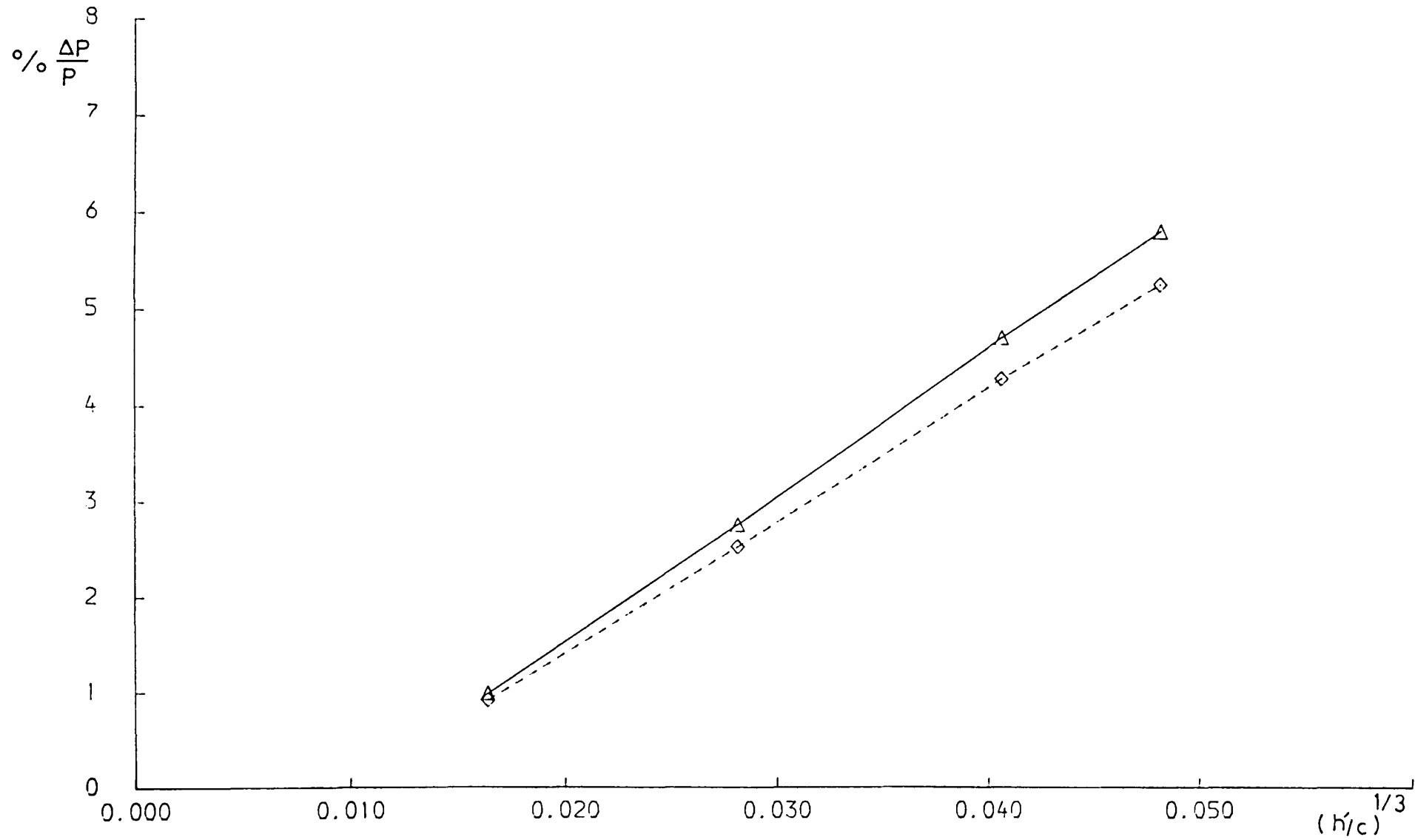


Figure (5.8a) Roughness Effects on Only the Outer Half of a Propeller Blade (Power Penalty)

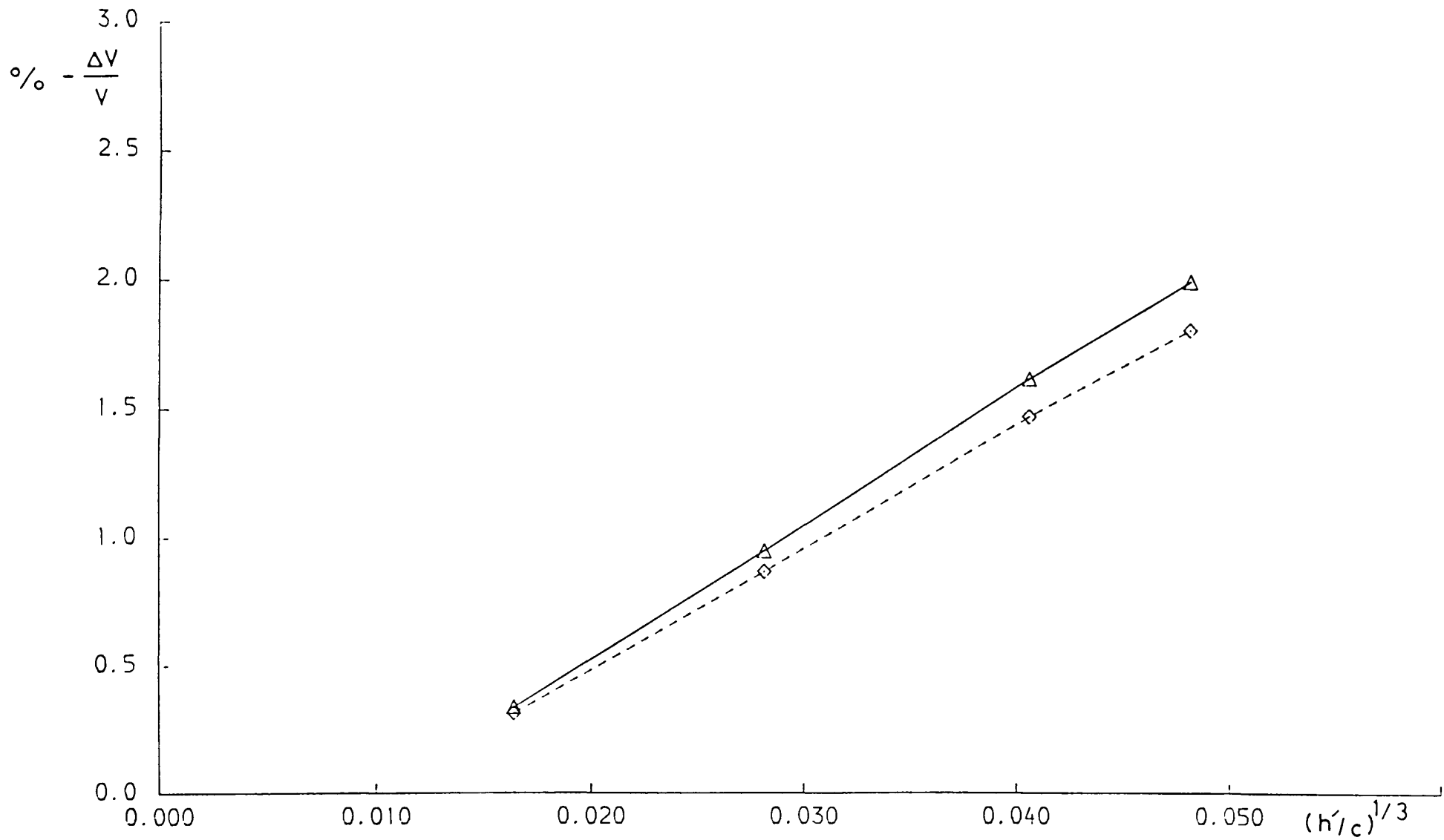


Figure (5.8b) Roughness Effects on Only the Outer Half of a Propeller Blade (Speed Penalty)

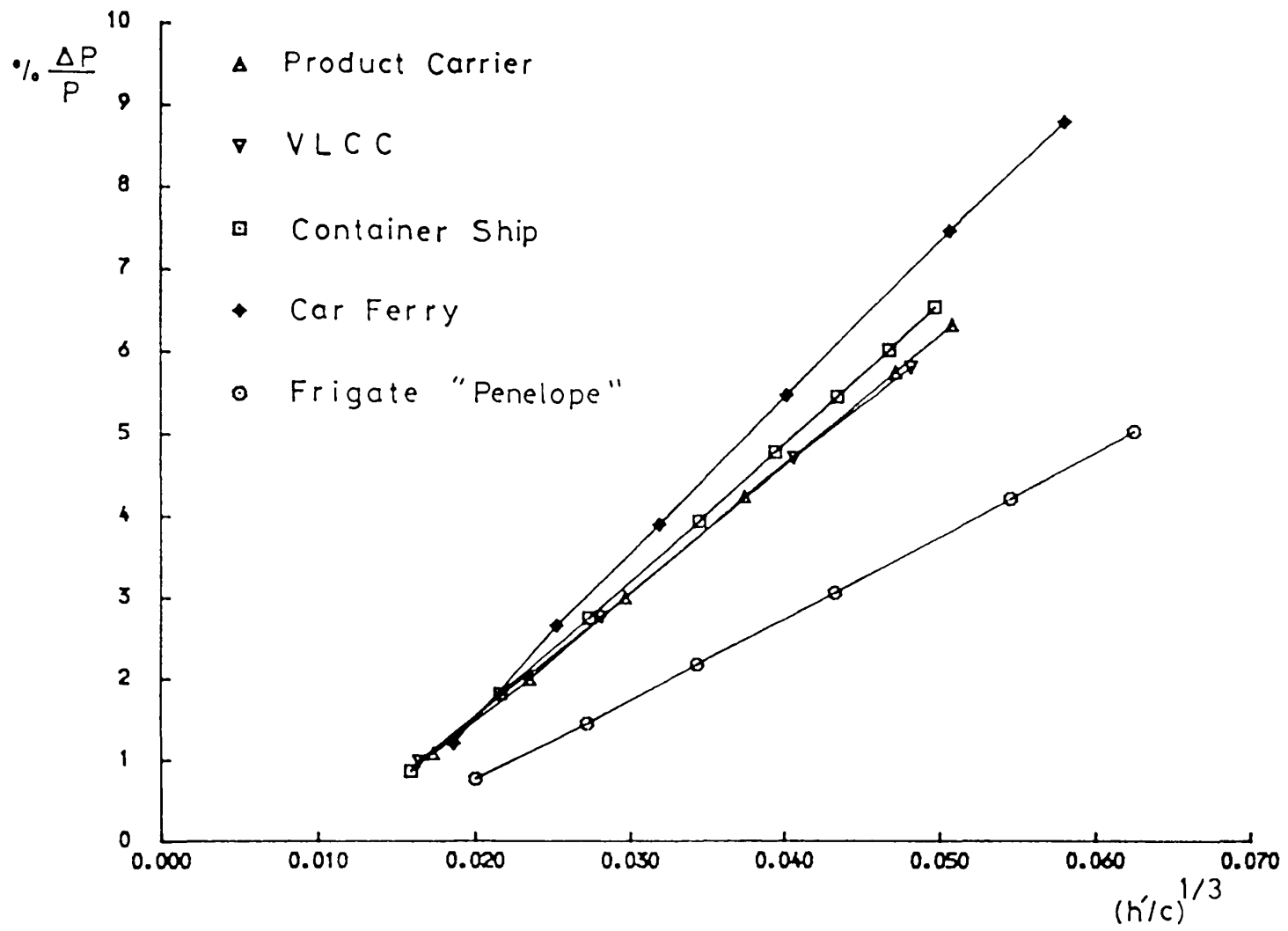


Figure (5.9) Power Penalty Due to Propeller Roughness

Table (5.2)

Section Drag Penalites of VLCC

h'	$10^3 \Delta C_D$						
	Sec0.3	sec0.4	sec0.5	sec0.6	sec0.7	sec0.8	sec0.9
10	0.5045	0.5238	0.5304	0.5773	0.5651	0.5967	0.6401
50	1.7356	1.6597	1.6081	1.5969	1.6048	1.6508	1.7325
150	3.1807	2.9937	2.8263	2.7649	2.7400	2.7858	2.8946
250	4.100	3.800	3.5000	3.4000	3.5000	3.4400	3.4500

Table (5.3)

Section Drag Penalites of Product Carrier

h'	$10^3 \Delta C_D$						
	Sec0.3	sec0.4	sec0.5	sec0.6	sec0.7	sec0.8	sec0.9
10	0.612	0.610	0.621	0.630	0.643	0.678	0.678
25	1.210	1.175	1.815	1.195	1.121	1.261	1.239
50	1.866	1.815	1.788	1.792	1.802	1.861	1.821
100	2.737	2.631	2.570	2.550	2.545	2.611	2.534
200	3.842	3.649	3.534	3.420	3.453	3.525	3.405
250	4.250	4.035	3.880	3.800	3.794	3.855	3.723

Table (5.4)

Section Drag Penalites of Container Ship

h'	$10^3 \Delta C_D$						
	Sec0.3	sec0.4	sec0.5	sec0.6	sec0.7	sec0.8	sec0.9
10	0.650	0.570	0.500	0.460	0.404	0.450	0.540
25	1.290	1.160	1.050	0.990	0.950	0.971	1.090
50	1.920	1.740	1.600	1.510	1.462	1.481	1.631
100	2.720	2.471	2.290	2.180	2.110	2.121	2.314
150	3.280	2.990	2.780	2.640	2.560	2.580	2.790
200	3.732	3.400	3.160	3.010	2.923	2.940	3.180
250	4.010	3.740	3.49	3.320	3.220	3.240	3.500
300	4.490	4.040	3.770	3.590	3.494	3.500	3.783

Table (5.5)

Section Drag Penalites of Car Ferry

h'	$10^3 \Delta C_D$						
	Sec0.4	sec0.5	sec0.6	sec0.7	sec0.8	sec0.9	sec0.95
10	0.863	0.778	0.698	0.690	0.708	0.759	0.818
25	1.581	1.454	1.319	1.292	1.300	1.378	1.478
50	2.268	2.206	1.985	1.918	1.918	2.019	2.146
100	3.121	3.118	2.806	2.709	2.693	2.818	2.990
150	3.724	3.757	3.388	3.251	3.228	3.363	3.566
200	4.301	4.247	3.842	3.680	3.639	3.774	4.018
250	4.608	4.560	4.211	4.021	3.974	4.129	4.386
300	4.962	4.876	4.522	4.323	4.272	4.428	4.705

Table (5.6)

Section Drag Penalites of the Frigate

h'	$10^3 \Delta C_D$						
	Sec0.3	sec0.4	sec0.5	sec0.6	sec0.7	sec0.8	sec0.9
10	1.005	0.785	0.649	0.611	0.615	0.685	0.811
25	1.856	1.484	1.240	1.174	1.188	1.285	1.493
50	2.810	1.961	1.912	1.805	1.798	1.932	2.221
100	3.224	2.842	2.769	2.589	2.596	2.765	3.152
200	4.483	3.928	3.839	3.507	3.568	3.780	4.278
300	5.331	4.625	4.583	4.219	4.254	4.485	5.064

Table (5.7)

Power Penalites of VLCC

h'	$10^{-6} h'/c$	$(h'/c)^{1/3}$	K_T	$10K_Q$	η_0	RPM	$\Delta P/P$
0	0.0	0.0	0.2044	0.2478	0.4176	87.0	0.0
10	4.43	0.0164	0.2042	0.2498	0.4136	87.065	0.9886
50	22.14	0.0281	0.2038	0.2533	0.4065	87.187	2.7769
150	66.40	0.0405	0.2033	0.2570	0.3990	87.319	4.7396
250	110.70	0.0480	0.2030	0.2591	0.3950	87.395	5.8390

Table (5.8)

Power Penalites of VLCC
(outer part of the blade is only roughened)

h'	$10^{-6} h'/c$	$(h'/c)^{1/3}$	K_T	$10K_Q$	η_0	RPM	$\Delta P/P$
0	0.0	0.0	0.2044	0.2478	0.4176	87.0	0.0
10	4.43	0.0164	0.2042	0.2496	0.4138	87.055	0.9165
50	22.14	0.0281	0.2039	0.2529	0.4073	87.152	2.5407
150	66.40	0.0405	0.2035	0.2565	0.4005	87.256	4.3097
250	110.70	0.0480	0.2032	0.2583	0.3968	87.316	5.2909

Table (5.9)

Speed Penalites of VLCC

h'	$10^{-6} h'/c$	$(h'/c)^{1/3}$	$\Delta V/V\%$	$\Delta V^*/V\%$
0	0.0	0.0	0.0	0.0
10	4.43	0.0164	-0.3397	-0.3149
50	22.14	0.0281	-0.9543	-0.8731
150	66.40	0.0405	-1.6287	-1.4810
250	110.70	0.0480	-2.0065	-1.8182

* outer part of the blade is only roughened

Table (5.10)

Power Penalites of Product Carrier

h'	$10^{-6} h'/c$	$(h'/c)^{1/3}$	K_T	$10K_Q$	η_0	RPM	$\Delta P/P$
0	0.0	0.0	0.1645	0.2088	0.5410	128.0	0.0
10	5.19	0.0173	0.1643	0.2107	0.5354	128.107	1.083
25	12.97	0.0235	0.1642	0.2122	0.5307	128.199	1.998
50	25.93	0.0296	0.1640	0.2139	0.5255	128.302	3.015
100	51.87	0.0373	0.1639	0.2160	0.5194	128.429	4.260
200	103.70	0.0470	0.1636	0.2185	0.5122	128.584	5.781
300	129.70	0.0506	0.1636	0.2194	0.5095	128.643	6.353

Table (5.11)

Power Penalites of Container Ship

h'	$10^{-6} h'/c$	$(h'/c)^{1/3}$	K_T	$10K_Q$	η_0	RPM	$\Delta P/P$
0	0.0	0.0	0.2015	0.4264	0.6737	93.50	0.0
10	3.19	0.0159	0.2015	0.4294	0.6683	93.610	0.8660
25	9.77	0.0216	0.2016	0.4327	0.6626	93.730	1.8178
50	19.53	0.0273	0.2017	0.4390	0.6570	93.879	2.7625
100	39.06	0.0344	0.2017	0.4399	0.6502	93.999	3.9603
150	58.59	0.0393	0.2018	0.4428	0.6454	94.105	4.8069
200	78.13	0.0433	0.2018	0.4451	0.6417	94.189	5.4843
250	97.66	0.0466	0.2019	0.4470	0.6387	94.258	6.0482
300	117.19	0.0495	0.2019	0.4487	0.6359	94.325	6.5668

Table (5.12)

 Power Penalites of Car Ferry

h'	$10^{-6} h'/c$	$(h'/c)^{1/3}$	K_T	$10K_Q$	η_0	RPM	$\Delta P/P$
0	0.0	0.0	0.1609	0.3138	0.6513	225.0	0.0
10	6.42	0.0186	0.1609	0.3170	0.6440	225.27	1.2020
25	16.05	0.0252	0.1609	0.3207	0.6356	225.70	2.6647
50	32.09	0.0318	0.1609	0.3239	0.6285	226.02	3.9199
100	64.18	0.0400	0.1610	0.3279	0.6198	226.43	5.5041
200	128.37	0.0504	0.1610	0.3329	0.6094	226.95	7.4965
300	192.55	0.0577	0.1610	0.3361	0.6027	227.28	8.8211

Table (5.13)

 Power Penalites of the Frigate

h'	$10^{-6} h'/c$	$(h'/c)^{1/3}$	K_T	$10K_Q$	η_0	RPM	$\Delta P/P$
0	0.0	0.0	0.2386	0.5629	0.7083	130.0	0.0
10	8.067	0.0200	0.2385	0.5661	0.7034	130.16	0.7678
25	20.170	0.0272	0.2385	0.5689	0.6991	130.31	1.4484
50	40.336	0.0343	0.2385	0.5719	0.6944	130.46	2.1875
100	80.671	0.0432	0.2384	0.5755	0.6890	130.64	3.0796
200	161.342	0.0544	0.2384	0.5801	0.6821	130.88	4.2345
300	242.013	0.0623	0.2383	0.5834	0.6773	130.05	5.0541

5.6.3 Comparison of Flat Plane and Section Profile Roughness Drag

Penalty

An attempt has been made to apply the program "PROFNESS" to cover a sufficient number of cases to enable interpolations to be made on the propeller drag penalty for a range of Reynolds number, profile thickness and roughened blade surface, at the same time to compare the results with the corresponding rough flat plane. The numerical results show that a

"rough" flat plane calculation is quite adequate for calculating the effect of roughened blade surfaces.

Figure (5.10) represents the increment of C_F for a flat plate and propeller section profile for varying values of Reynolds number. It may be observed from the figures that the relation between ΔC_F and $(h'/c)^{1/3}$ is fairly linear. From Figure (5.11) it is also clear that the effect of the pressure distribution about the aerofoil sections, particularly for a moderately roughened propeller, is not significant, say about 6% or less in ΔC_F at the same value of Reynolds number.

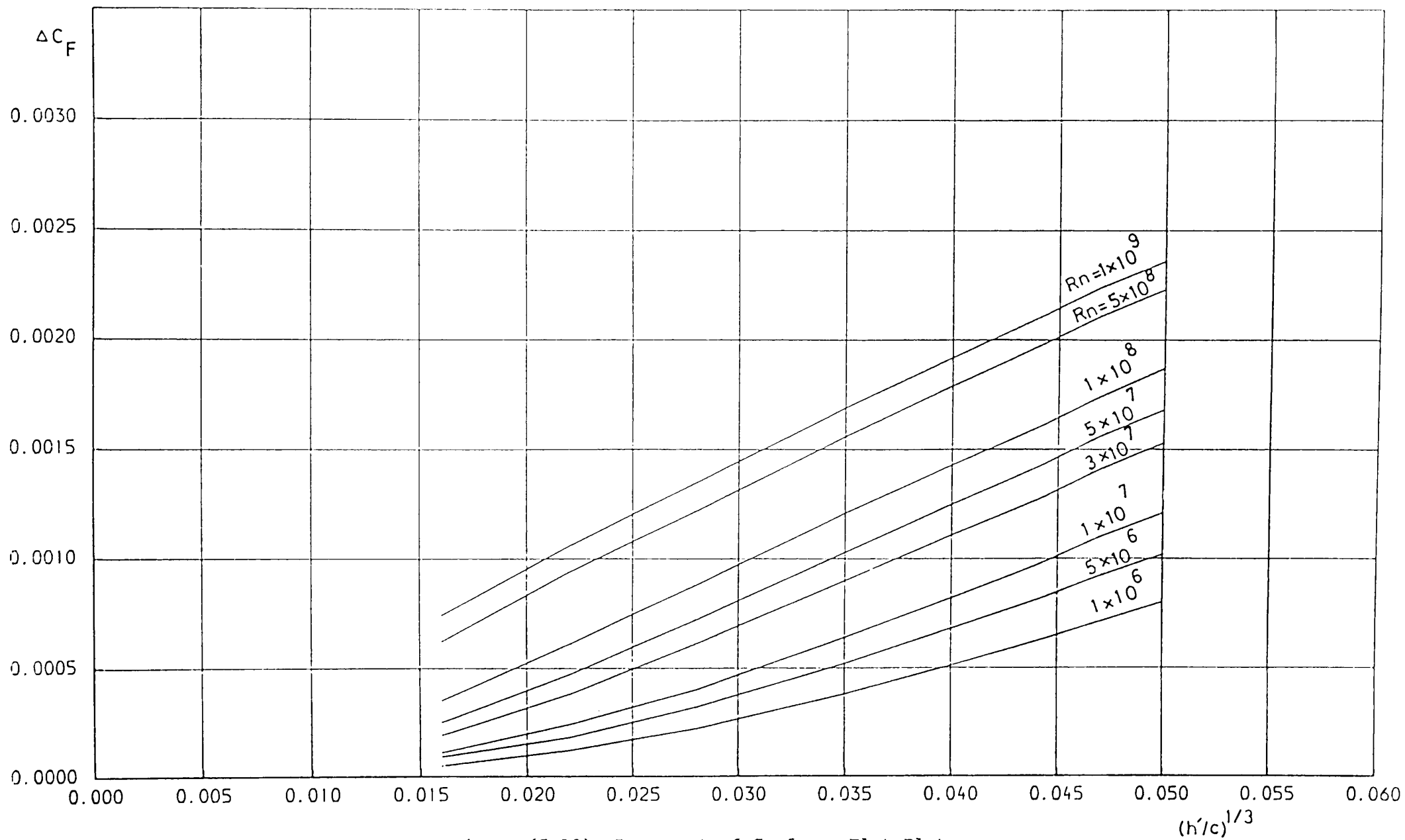


Figure (5.10) Increment of C_F for a Flat Plate

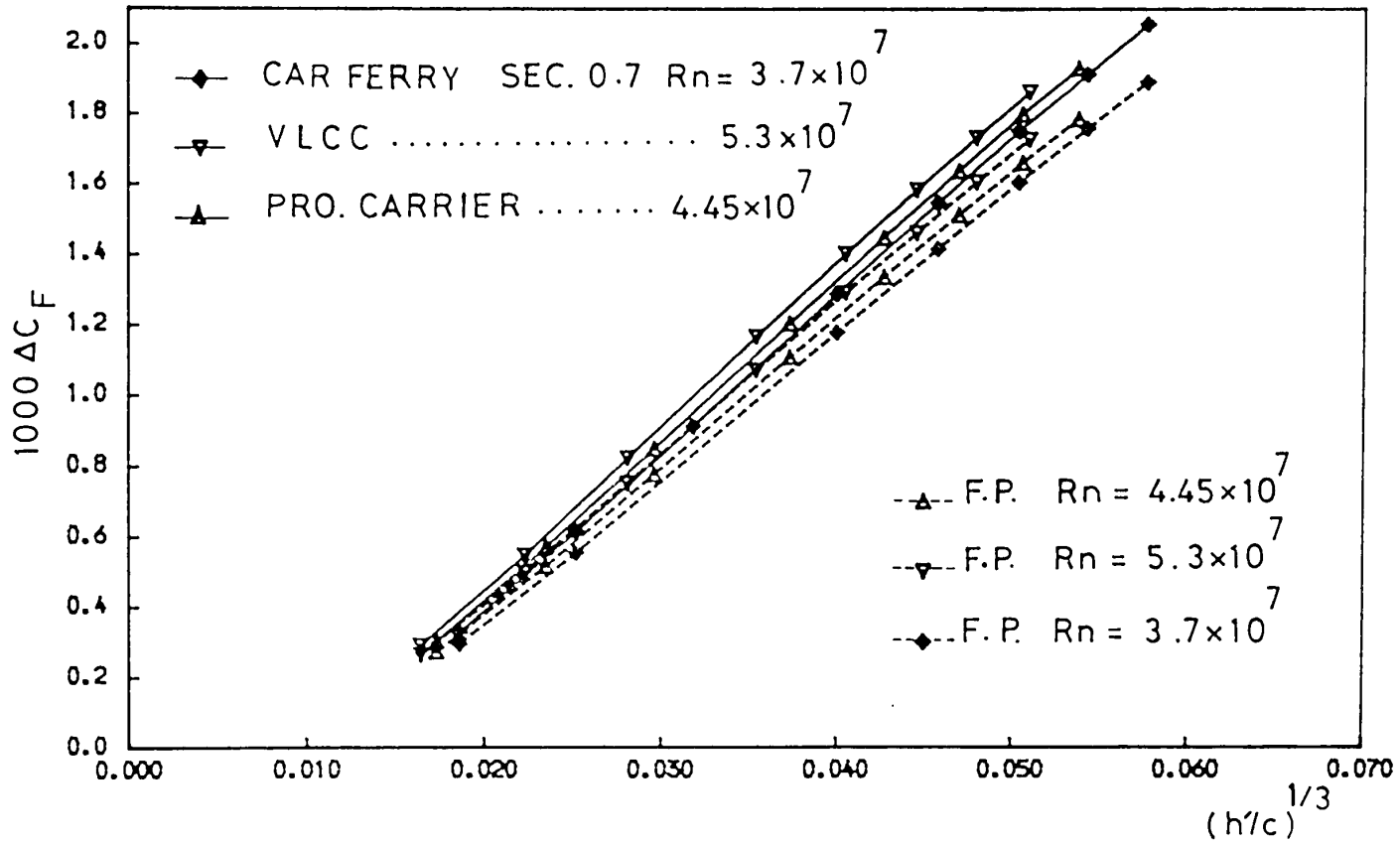


Figure (5.11) Effect of Pressure Distribution on Drag Penalty

CHAPTER SIX

SIMPLIFIED METHODS FOR THE ESTIMATION OF HULL AND PROPELLER ROUGHNESS

PENALTIES

6.1 ADDED RESISTANCE OF HULL ROUGHNESS

6.1.1 Introduction

Since the combined effect of rough hulls and rough propeller is to be considered later some background discussion of hull roughness drag is appropriate.

Added resistance to fluid flow of roughened surfaces has been a continuing concern since Froude's towing tank experimental work in 1872. However, the problem of achieving and maintaining a smooth ship's hull has recently been the subject of detailed study because of possible economies to ship operators. A popular method with a long history is the towing of a flat plate of surface area A in a large towing tank. The drag force F on the carriage and its speed V are measured. The overall coefficient of friction is given by:

$$C_F = F / (0.5 \rho A V^2) \quad (6.1)$$

as a function of length Reynolds' number LV/ν . In the case of uniform roughness of sand-grain type, the drag coefficient is nearly constant

with increasing R_n . However, engineering surfaces, like ship hull surfaces, are irregularly rough in nature in which the flow regimes at the ship normal service speeds are usually "transitional" rather than "fully rough" and the drag is therefore Reynolds' number dependent. The friction line of a fairly well maintained surface can lie between the uniform roughness line and the smooth turbulent line.

The ITTC Ship-Model Correlation Line was established in 1957 [67] for the calculation of smooth skin friction. The line is called a ship-model correlation line and not a frictional resistance line representing the frictional resistance of plane or curved surfaces. For surfaces that are not plane, Hughes [68] defined a form factor correction r :

$$r = (1+k) = C_v/C_F \quad (6.2)$$

where C_F is the two dimensional flat plate resistance coefficient given by his formula:

$$C_F = 0.067/(\log R_n - 2)^2 \quad (6.3)$$

and C_v is the viscous resistance coefficient. It is assumed that r is independent of R_n and is the same for all similar models and ships. It is to be noted also that the ITTC correlation line merges with Hughes line for form factor $r=1.12$.

There has since been a growing use of the ship-model correlation formula together with a form factor analysis and some work has been carried out to test its validity. The principal test was carried out by Bowden and Davison [69] on a number of single screw ships using the corresponding predictions by the ITTC method. Initially the form factor correction $(1+k)$ was ignored in the analysis. However, a later analysis using three different form factor corrections was carried out [70]. It led to the adoption by ITTC in 1978 of a Correlation Allowance:

$$10^3 \Delta C_F = 105 (AHR/L)^{1/3} - 0.64 \quad (6.4)$$

It is clear that this allowance will depend only on the length of the ship, L and the hull surface defined by the the average hull roughness, AHR . More recent works from performance monitoring [18] and boundary layer integration method [38] produce ΔC_F values between half and two-third of these predicted by the ITTC allowance formula.

The purpose of this section is to reconsider any inadequacies in the ITTC Ship-Model Correlation line in the light of recent work on hull roughness [38] and developments in the analytical prediction of flat plane drag by the Author.

6.1.2 The Hull Roughness Allowance

It is clear from reference [70] that the ITTC correlation allowance is based on only ten sets of ship trials data on similar types of clean new ships, having values of AHR between 140 and 230 μm . The analysis was carried out using three different form factors. It has been generally found that the model to ship correlation coefficient is too low [66] .

An integral boundary layer method has been used in [38] to calculate the roughness drag penalty for a variety of ship types. The method takes into account the effect of hull form, ship speed, ship length and surface roughness. Using the height parameter AHR, it was found that the ΔC_F would increase with increasing ship speed. The result was given as a simple formula of Reynolds' number dependency:

$$10^3 \Delta C_F = 44 [(AHR/L)^{1/3} - 10 R_n^{-1/3}] + 0.125 \quad (6.5)$$

Equation (6.5) appears to give a roughness drag penalty some half to two-third of the ITTC correlation allowance. Townsin and the Author [71] showed that for a typical new ship, roughness constitutes only part of the correlation allowance. For a products carrier only one-third of the correlation allowance would be due to roughness and the ship speed should be included in the correlation. It should also be noted that with new ship-building techniques AHR values between 107 and 113 μm are becoming more common on new ships [72] and the old figure of 150 μm can no longer be assumed.

6.1.3 The ITTC Ship Correlation Line

Hughes friction method was very much discussed during the eighth ITTC from which the ITTC model-ship correlation line was adopted as an interim solution for practical engineering purposes. Correction to the deficiency in the slope of the ITTC line may be sought in the interpretation and extrapolation of Hughes smooth plane data.

For the friction resistance coefficient, Hughes proposed an important correlation in the form:

$$C_F = a (\log R_n - b)^c \quad (6.6)$$

where a , b and c are constants of 0.066, 2.03 and -2, respectively. The formula agrees reasonably well with the experimental curve. It is interesting to note that the form of equation (6.6) was first proposed by Prandtl in 1932, ($b=0.0$), as a convenient interpolation formula [73]. This form was used by Schultz-Grunow [74] as an approximate fit to his calculated results in the range $10^6 < R_n < 10^9$:

$$C_F = \frac{0.427}{(\log R_n - 0.407)^{2.64}} \quad (6.7)$$

On the basis of Schultz-Grunow results a new formulation was proposed by Troost in 1948 [75] as follows:

$$C_F = \frac{0.0725}{(\log Rn - 2)^2} \quad (6.8)$$

Surprisingly, some ten years later in 1957 ITTC adopted a correlation line that was very similar to Troost's.

Each of the empirical formulations above yields slightly different numerical values of C_F . This will no doubt cause some uncertainty and confusion with regard to what is the real value of the friction drag coefficient. This question was discussed by Gadd [76]. He reanalysed Hughes' experimental data and carried out supplementary tests to provide further evidence on the details of the edge effect of the flat plane, similar to that provided by Davies and Young [77]. Gadd found that the edge effects on both wide and narrow plates are roughly the same contrary to Hughes' idea. This then led to a new turbulent skin friction formulation for flat plates using the same form of equation (6.6) as:

$$C_F = \frac{0.0113}{(\log Rn - 3.7)^{1.15}} \quad (6.9)$$

This equation was suggested to be approximately valid for Reynolds numbers between 10^6 and 10^8 . It can only be extrapolated with caution to higher values of Rn bearing in mind that most ships are in the range of $10^8 < Rn < 10^{10}$. It is very difficult to confirm experimentally the C_F values at ship Reynolds' numbers and one of the problems in ship-model correlation was to account for added resistance due to hull roughness.

Assuming that Gadd's analysis of Hughes' experimental data is an improvement of the original, Townsin and the Author [71] compared Gadd's extrapolation with the corresponding ITTC prediction using form factors which make the model C_v values the same in both cases. It was found that at lower end of the R_n range equations (6.4) and (6.9) together give a slightly lower prediction than ITTC but at the upper end they give over 10% greater values than ITTC using the standard roughness ($AHR=150 \mu m$). The influence of R_n on the roughness allowance is also shown in the calculated results.

6.1.4 Proposed Smooth Friction Line

Coles [7] analysed a large amount of experimental data which covered the range $425 < R_\theta < 29000$. The result showed considerable consistency from which Coles produced tabular data given in Table (6.1). In this table a relationship between the momentum thickness Reynolds' number, R_θ and C_f is given. A difficulty with the R_θ - C_f relationship is that it depends on the manner in which transition from laminar to turbulent flow is supposed to occur in the leading length. The result is that whilst naval architects can agree about high Reynolds number values of C_f there is a divergence of views concerning C_f for $R_n < 10^6$.

According to Newton's law, the drag D for a plate of unit width can be given by:

$$D = \int_0^{\delta} \rho u (U-u) dy \quad (6.10)$$

This equation may be expressed in the following form :

$$D = \rho U^2 \delta \int_0^1 u/U (1-u/U) d(y/\delta) \quad (6.11)$$

which can be rewritten as :

$$D = \rho U^2 \theta \quad (6.12)$$

where

$$\theta/\delta = \int_0^1 u/U (1-u/U) d(y/\delta)$$

Alternatively, the drag D is usually given as :

$$D = C_F \cdot 1/2 \rho U^2 x \quad (6.13)$$

therefore, C_F can be described as :

$$C_F = 2 \theta / x \quad (6.14)$$

hence,

$$C_F = 2 R_\theta / R_n \quad (6.15)$$

The shear stress at the wall for a plate of unit width is given by:

$$\tau_w = dD/dx = \rho U^2 d\theta/dx \quad (6.16)$$

in which it gives the von Karman momentum equation for a flat plane

$$d\theta/dx = \tau_w/\rho U^2 \quad (6.17)$$

where x is the streamwise distance along the flat plate, measured from the leading edge.

In order to evaluate C_F , it is necessary to obtain the plate Reynolds number R_n as a function of the local friction coefficient C_f . From the momentum equation, R_n may be found as :

$$R_n = \int (2/C_f) dR_\theta \quad (6.18)$$

In order to perform integration on Coles data, the assumption shown in Figure (6.1) for the lowest R_θ - C_f values is made. The calculated results are given in Table (6.2) and Figure (6.2). It shows a close agreement with the ITTC correlation line.

From the above results a relationship between R_θ and R_n for Coles data can be deduced in the form:

$$R_\theta = 0.03781 R_n^{0.8} \quad (6.19)$$

More importantly, by using Prandtl's interpolation form of equation (6.6), the results can be accurately interpreted by:

$$C_F = \frac{0.0762}{(\log R_n - 1.94)^2} \quad (6.20)$$

Equation (6.20) is a new form of a flat plane skin friction coefficient at both low and high Reynolds numbers. The present method is in accord with the study by Granville [78] who also showed a close agreement between the analytical methods and the ITTC correlation line.

In view of the above the current solutions of the flat plane momentum integral equations provide strong support for the ITTC correlation line. Moreover, it perhaps removes any suspicion in regard to its slope particularly for use at ship model Reynolds numbers.

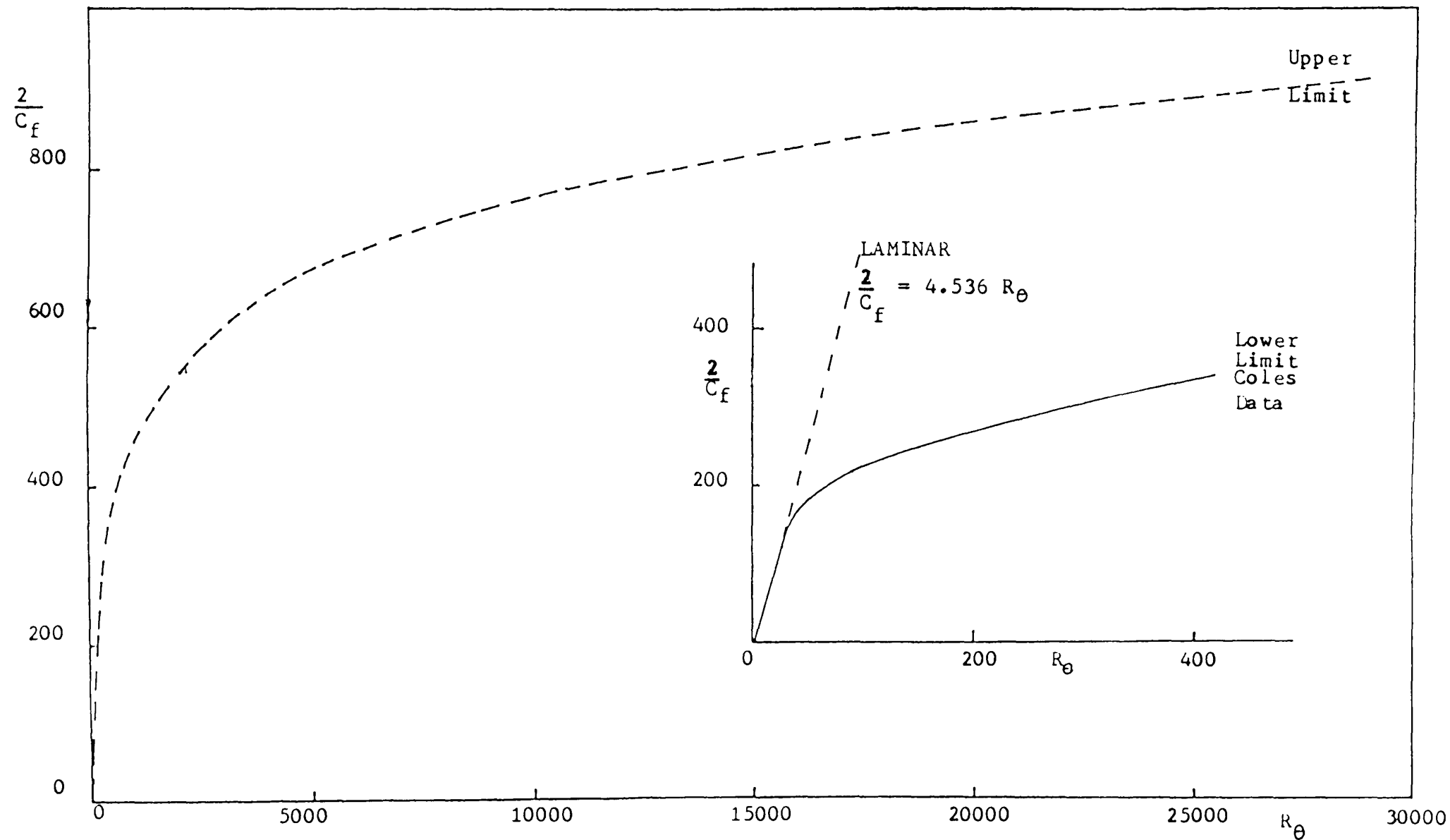


Figure (6.1) Assumption of $2/C_f \sim R_\theta$ Relationship Below $R_\theta = 425$

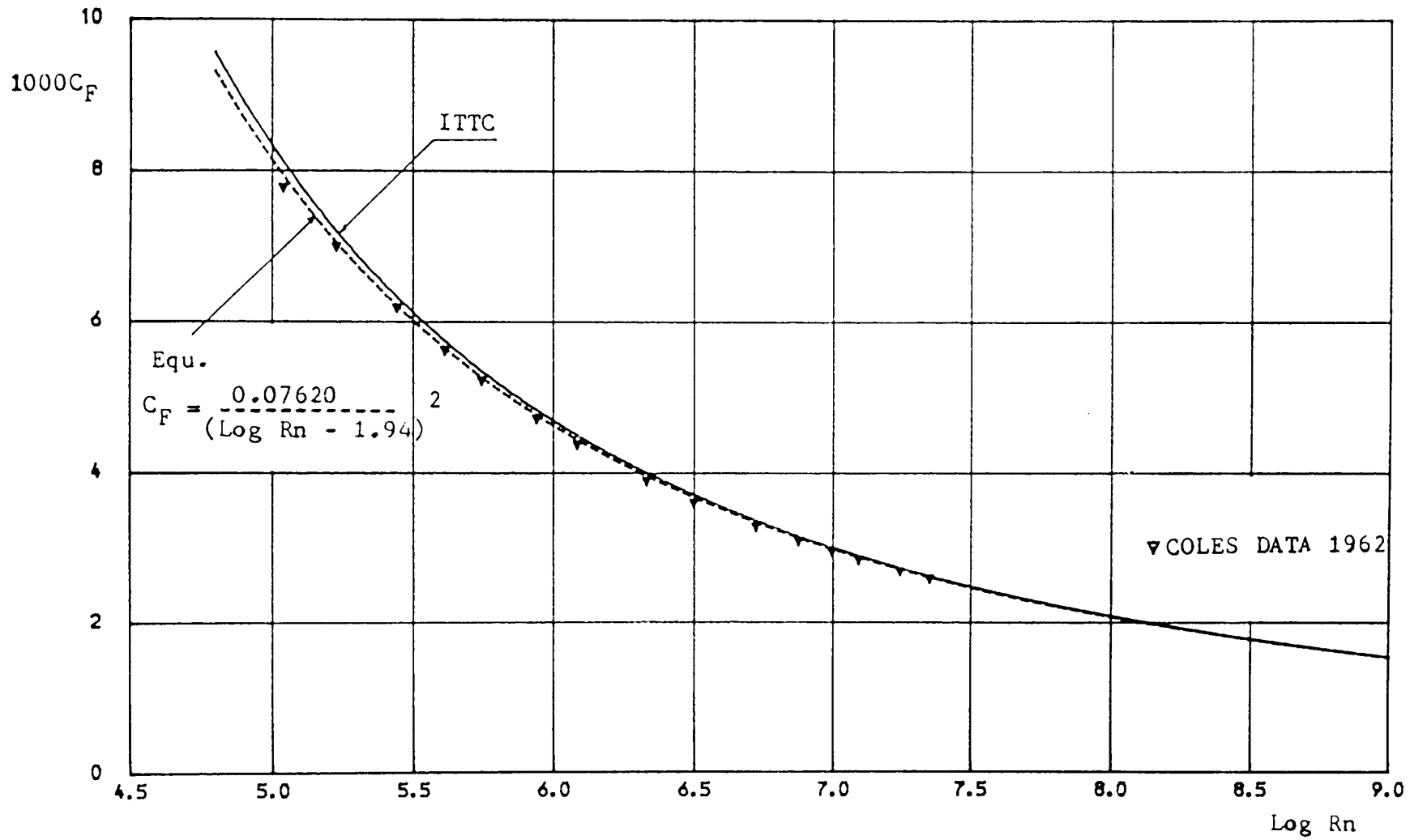


Figure (6.2) Integration of Coles Results

TABLE (6.1)

THE LOCAL FRICTION LAW FOR THE TURBULENT BOUNDARY LAYER
AT CONSTANT PRESSURE

$\delta u^*/\nu$	π	$1000C_f$	R_θ	δ^*/θ	$C_f R_\theta$
240	0	5.90	425	1.535	2.510
300	0.12	5.24	590	1.500	3.100
400	0.23	4.64	855	1.470	3.970
500	0.30	4.26	1150	1.445	4.880
600	0.36	5.98	1450	1.425	5.730
800	0.43	3.63	2050	1.405	7.410
1000	0.48	3.40	2650	1.390	8.940
1500	0.53	3.08	4150	1.365	12.750
2000	0.55	2.90	5650	1.350	16.360
3000	0.55	2.69	8600	1.325	23.200
4000	0.55	2.55	11500	1.315	29.600
5000	0.55	2.46	14500	1.305	35.900
6000	0.55	2.38	17500	1.295	41.800
8000	0.55	2.27	23500	1.290	53.600
10000	0.55	2.19	29000	1.285	64.800

Rewritten From Reference [7]

TABLE (6.2)

COLES C_F SMOOTH FLAT PLATE

σ^2	R_θ	$1000C_f$	$Rn \cdot 10^{-5}$	LOG. Rn	$1000C_F$
339	425	5.90	1.093	5.0380	7.7700
382	590	5.24	1.688	5.2270	6.9900
431	855	4.64	2.765	5.4420	6.1800
470	1150	4.26	4.093	5.6100	5.6200
503	1450	3.98	5.551	5.7440	5.2200
551	2050	3.63	8.711	5.9400	4.7100
588	2650	3.40	12.129	6.0840	4.3700
649	4150	3.08	21.411	6.3310	3.8800
690	5650	2.90	31.453	6.4980	3.5900
744	8600	2.69	52.592	6.7210	3.2700
784	11500	2.55	74.745	6.8740	3.0800
813	14500	2.46	98.705	6.9940	2.9400
840	17500	2.38	123.505	7.0920	2.8300
881	23500	2.27	175.147	7.2430	2.6800
913	29000	2.19	224.491	7.3510	2.5800

6.2 BOUNDARY LAYER PREDICTION METHOD ON ROUGH FLAT PLANE

6.2.1 Introduction

For accurate calculation of the effect of roughened blade surfaces a propeller analysis program is required together with a boundary layer integral prediction method to calculate the increased section drag. For this purpose the program "PROFNESS" has been developed. However, the study in chapter 5 showed that for many practical applications the flat plane calculation is quite adequate.

An attempt is therefore made, in this study, to develop a "rough" flat plate solution to the question of hull and propeller roughness penalty. It is intended to provide a valid, simple and practical solution to the problem of predicting the roughness drag.

Coles' velocity profile has been expanded to take into account the effect of surface roughness and expressed in slightly different form than that discussed in chapter 3. Some developments are introduced into Coles' velocity law in order to make it valid for both low and high Reynolds numbers. The engineering roughness function, equation (4.4) is used incorporating Musker's roughness parameter, h' and Grigson's dimensionless texture parameter, m . More details are discussed in chapters 3 and 4.

6.2.2 Summary of the Method

The following expression for the velocity profile is used:

$$u/u^* = 1/K \ln(yu^*/\nu) + B_0 + \pi/K w_k(y/\delta) - \Delta u/u^* \quad (6.21)$$

where,

$$\Delta u/u^* = 1/K \ln (C_1/B_1 \omega_1 R_h + 1)$$

and

$$\omega_1 = (u^*/U_S) \quad , \quad R_h = h'U_S/\nu$$

At the outer edge of the boundary layer, this equation may be written as:

$$1/\omega_1 = 1/k \ln(R_\theta \omega_1 / \theta / \delta) + B_0 + 2\pi/K - \Delta u/u^* \quad (6.22)$$

For large Reynolds' number the constants K and B₀ are "universal" of 0.41 and 5.0, respectively.

The velocity law is modified to account for the lower Reynolds number range ($R_\theta < 6000$) as has been suggested by Simpson that the constants K and B₀ in the law of the wall can be varied with R_θ as follows:

$$K(R_\theta) = K(6000/R_\theta)^{0.125} \quad (6.23)$$

and

$$B_0(R_\theta) = R_\theta^{0.125} (7.9 - 0.737 R_\theta) \quad (6.24)$$

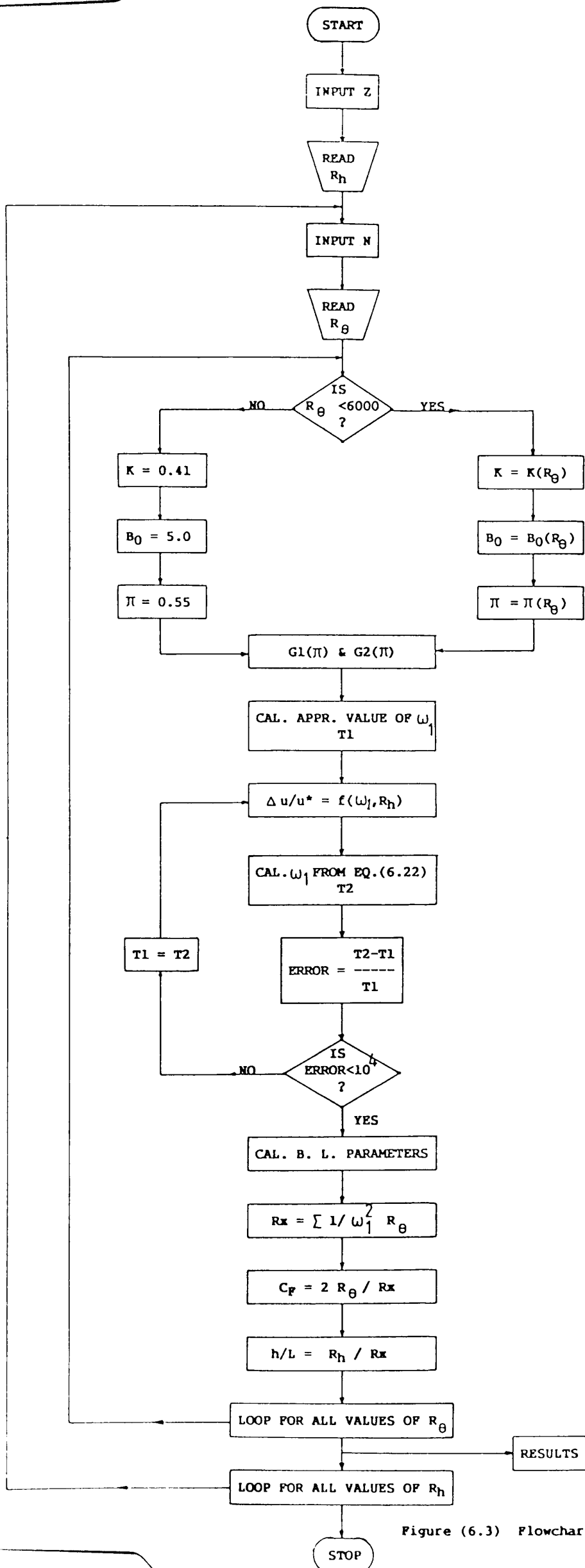


Figure (6.3) Flowchart of the Program "RPPBL"

6.2.3 Discussion and Applications

The main aim of this exercise is to determine the differences in skin friction coefficient with different surface roughness conditions on both hull and propeller. The basis of comparison, which is the case of a "hydraulically" smooth regime, has been calculated by exactly the same procedure as for the rough conditions. Since only differences are considered, exactness of the smooth plane flow results is less critical for calculating the roughness drag penalty. However, results from "RFPBL" for a smooth flat plate, which are shown in Figure (6.4), have demonstrated a good agreement with the ITTC standard skin friction line.

An attempt has been made to modify "RFPBL" to use R_n instead of R_θ as a practical input data. The flowchart for the algorithm of this modified program "FPBL" is given in Figure (6.5). The output of roughness drag penalty calculated from both "RFPBL" and "FPBL" may be accepted to be identical.

Comparison of the law of the wall for smooth and roughened hull is shown in Figure (6.6). For this purpose, equation (6.21) was used with the polynomial expression for the wake function given by equation (3.16). It can be seen that the effect of increasing surface roughness induces a downward shift in the velocity component, $\Delta u/u^*$. It is of interest to see how this velocity shift varies with increasing roughness.

The results obtained from the program "RFPBL" for given values of momentum thickness Reynolds' number, R_θ and roughness Reynolds' number, R_h are presented in figures to be explained later. These results can be classified for hull and propeller roughnesses. The only difference in the input data used in the two types of surface is the empirical constant C_1 in the roughness function $\Delta u/u^*$. The total friction coefficient C_F as a function of R_n with R_h as a parameter for hull and propeller surface roughness is given in Figures (6.7) and (6.8), respectively. These results may be used to calculate the roughness drag penalty as demonstrated in Figures (6.9) and (6.10) in which C_F has been plotted versus $(h/l)^{1/3}$ with R_n as a parameter. For hull, h is AHR, l is ship's length and for propeller h is Musker's parameter h' and l is the blade chord length. It may be seen that the relationship is linear at constant R_n but the slopes are different as R_n changes. Alternatively, the slope becomes smaller as R_n decreases.

Results from the program "FPBL" were compared with the roughness drag penalty obtained from "PROFNESS", for the different types of propeller given in Table (5.1), and are presented in Figure (6.11). This comparison shows a good agreement between the two methods.

It is intended to compare ΔC_F obtained from the present method with experimental data for flat plates having various surface roughnesses. For this purpose, extrapolated experimental data of Todd [79], Townsin et al [80] and Tokunaga [81] are compared with calculated ΔC_F , using "FPBL", in Figure (6.12). From this figure the validity of the flat

plate analogue method to predict the roughness drag may be confirmed.

The magnitude of speed dependency in calculating ΔC_F for a variety of ship types has been demonstrated in [38]. Using the flat plate analogue, variation of ΔC_F with speed for the different ships are represented in Figure (6.13). This shows that, ΔC_F is not only dependent on the roughness function used, but also on the Reynolds' number range. However, for propellers the flow over the blade sections may be assumed to be turbulent from the leading edge. For the propeller types used in this study, the Reynolds' number does not vary over a wide range, so that it is unlikely to be a very important parameter for simple calculation of the roughness drag penalty.

6.2.4 Approximate Equations

In the case of hull surface roughness, using a regression analysis, the following formula was found to give a good fit to the flat plate results presented in Figure (6.9):

$$10^3 \Delta C_F = 6 Rn^{0.093} [(AHR/L)^{1/3} - 5.8 Rn^{-1/3}] \quad (6.27)$$

This formula when used for the typical Rn range of the different ship types, used in [38], gives a good agreement with the formula proposed by Townsin in the same reference:

$$10^3 \Delta C_F = 44 [(AHR/L)^{1/3} - 10 Rn^{-1/3}] + 0.125 \quad (6.28)$$

Equation (6.27) may be used to calculate the roughness drag penalty for widely different ship types.

Similarly for propeller roughness, using the results in Figure (6.10) it was found that:

$$10^3 \Delta C_F = 8.1 R_n^{0.093} [(h'/c)^{1/3} - 4.5 R_n^{-1/3}] \quad (6.29)$$

Advantage may be taken from equations (6.27) and (6.29) to give a general form which can be used for both hull and propeller roughnesses drag penalty:

$$10^3 \Delta C_F = 6 n R_n^{0.093} [(\gamma/L)^{1/3} - (5.8/n) R_n^{-1/3}] \quad (6.30)$$

where

$$n = 2.82 m^{-1/3} \quad (n \text{ for hull surface} = 1.0)$$

m = Grigson's texture parameter

$$\gamma = \text{AHR (hull)} \quad \text{and} \quad \gamma = h' \quad (\text{propeller})$$

The surface roughness slightly affects the pressure distribution around the aerofoil sections of a propeller and hence the change in drag is due to only the increase in skin friction. However, unlike that of a flat plate flow the presence of the pressure distribution does increase ΔC_F of a propeller section. For the equivalent sections of three propellers, given in Figure (6.14), and their equivalent flat plates, two approximate equations have been deduced by the methods adopted in

"PROFNESS" and "FPBL" and may be represented respectively as follows:

$$10^3 \Delta C_{FP} = 44.5 [(h'/c)^{1/3} - 0.0107] \quad (6.31)$$

and

$$10^3 \Delta C_{Ff} = 43.0 [(h'/c)^{1/3} - 0.0107] \quad (6.32)$$

where,

ΔC_{FP} = roughness drag penalty for profile blade section.

ΔC_{Ff} = roughness drag penalty for flat plate.

c is the chord and h' should be greater than $c/10^6 \mu\text{m}$.

For the present purpose, ΔC_F in the above two equations are assumed to be independent of R_n , since its range are very small.

It may be noted that the above equations imply,

$$\Delta C_{FP} = k \Delta C_{Ff} \quad (6.33)$$

where,

k is a constant of 1.035

A similar relationship has been determined by Lerbs [82] :

$$\Delta C_{FP} = (1+2t/c) \Delta C_{Ff} \quad (6.34)$$

where,

t/c is the maximum thickness-chord ratio of a blade section.

Applying these equations for the "equivalent" profile section of the above three propellers, give an overestimation by equation (6.34). From the above consideration, equation (6.33) is proposed to be represented as:

$$\Delta C_{FP} = (1+t/c) \Delta C_{Ff} \quad (6.35)$$

omitting the constant 2 in equation (6.33).

In such work, the roughness drag coefficient increment may be considered as due to change in the friction drag only, therefore, ΔC_D may take the form:

$$\Delta C_D = 2 (1+t/c) \Delta C_{Ff} \quad (6.36)$$

This equation can be used to calculate the roughness drag penalty for the blade sections of propellers.

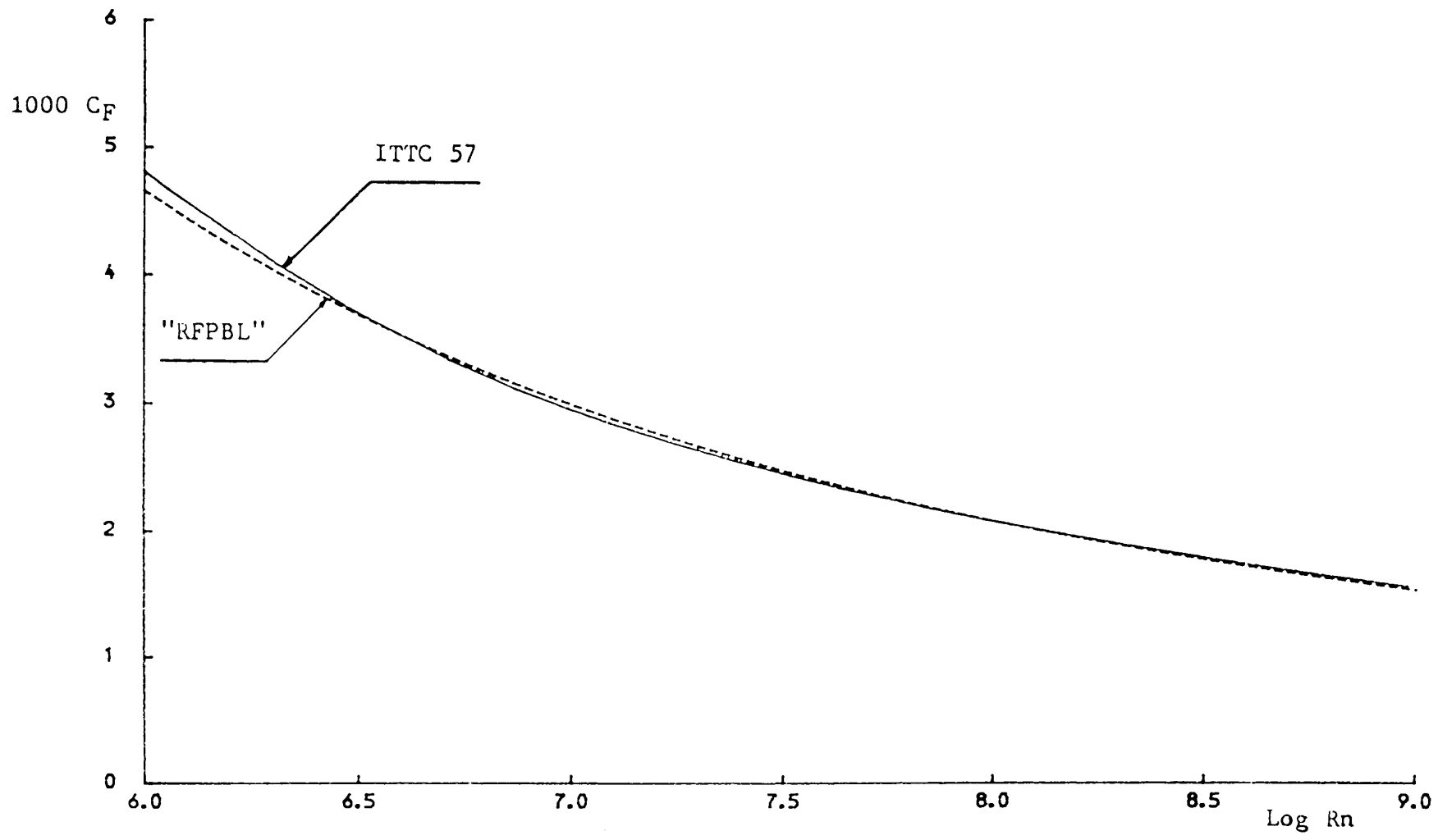


Figure (6.4) "RFPBL" Smooth Friction Results

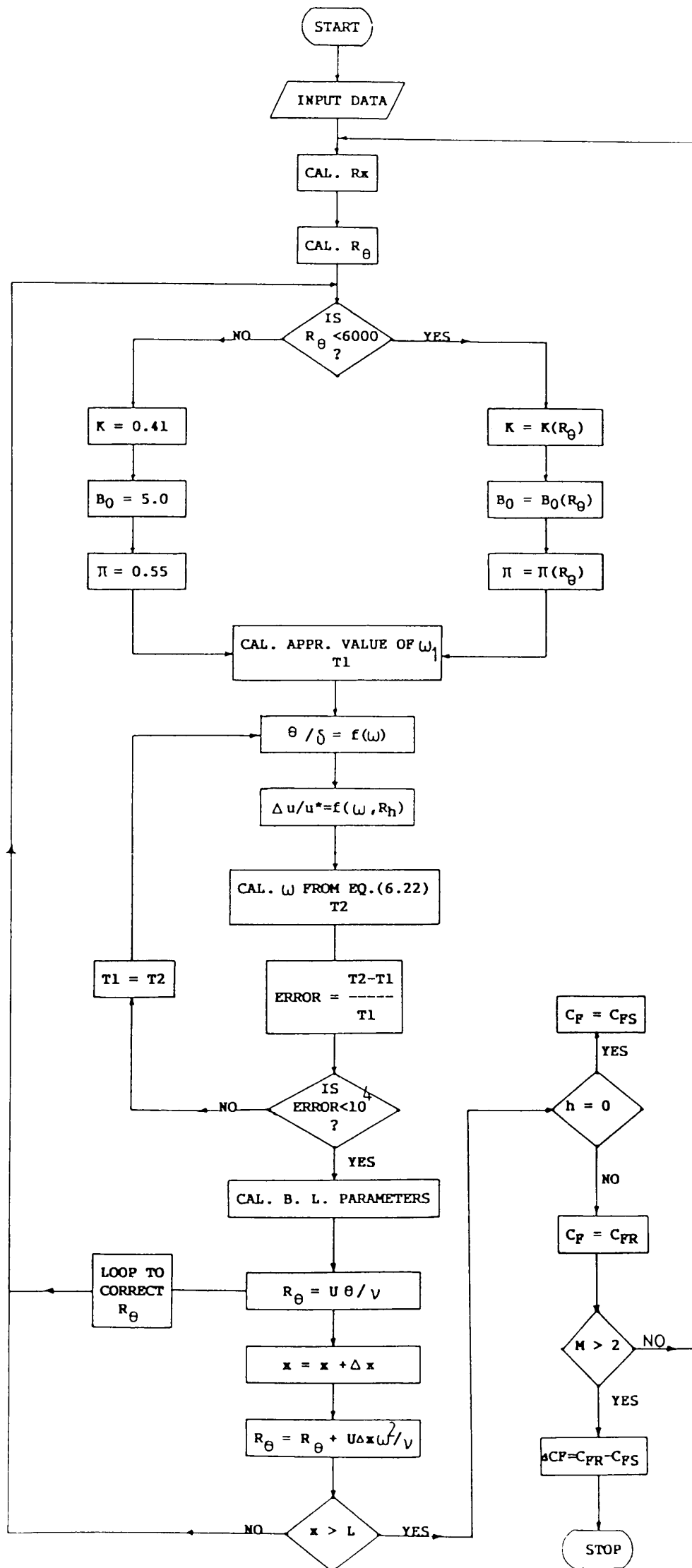


Figure (6.5) Flowchart of the Program 'RPP1'

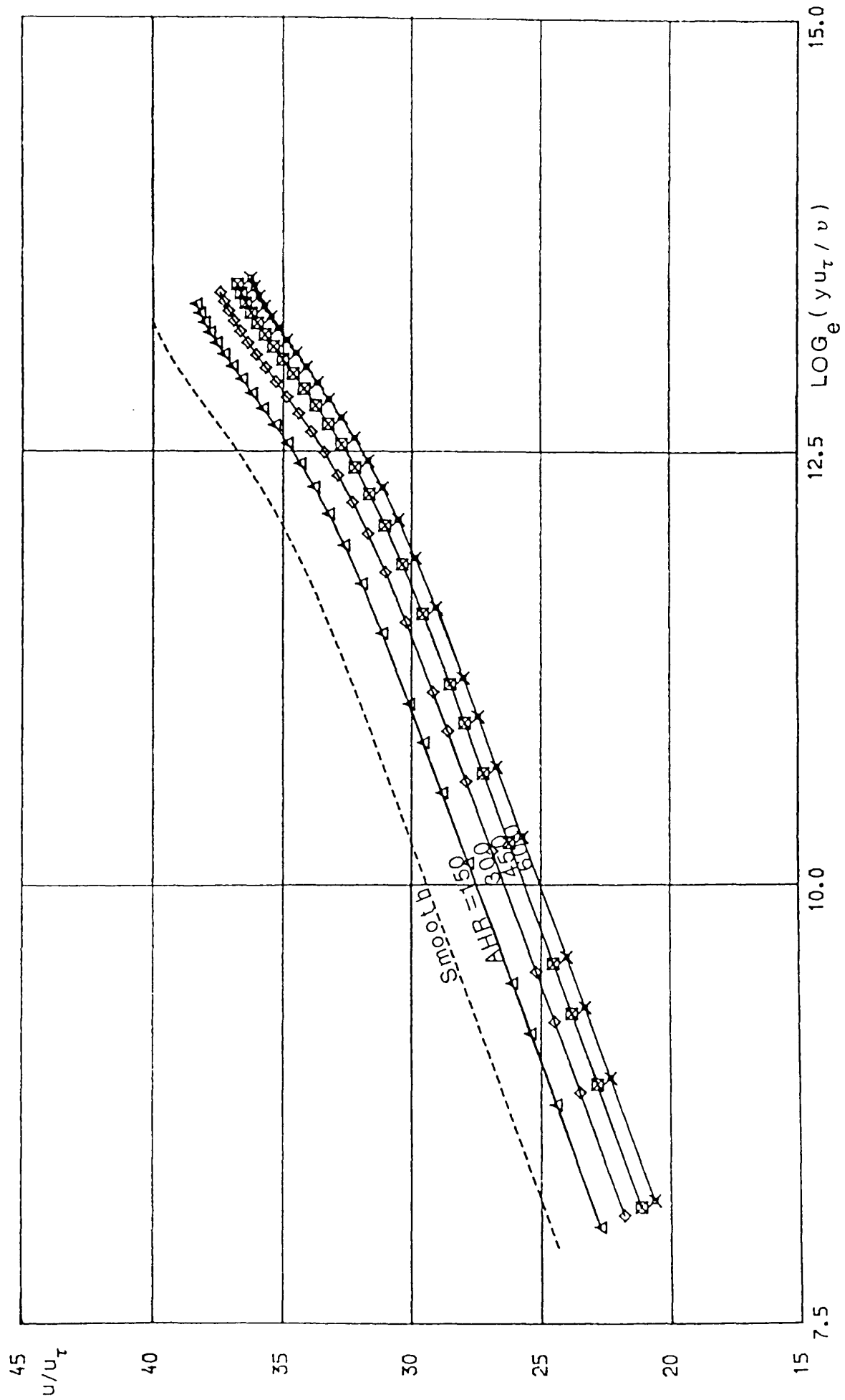


Figure (6.6) Universal Law of the Wall Plots

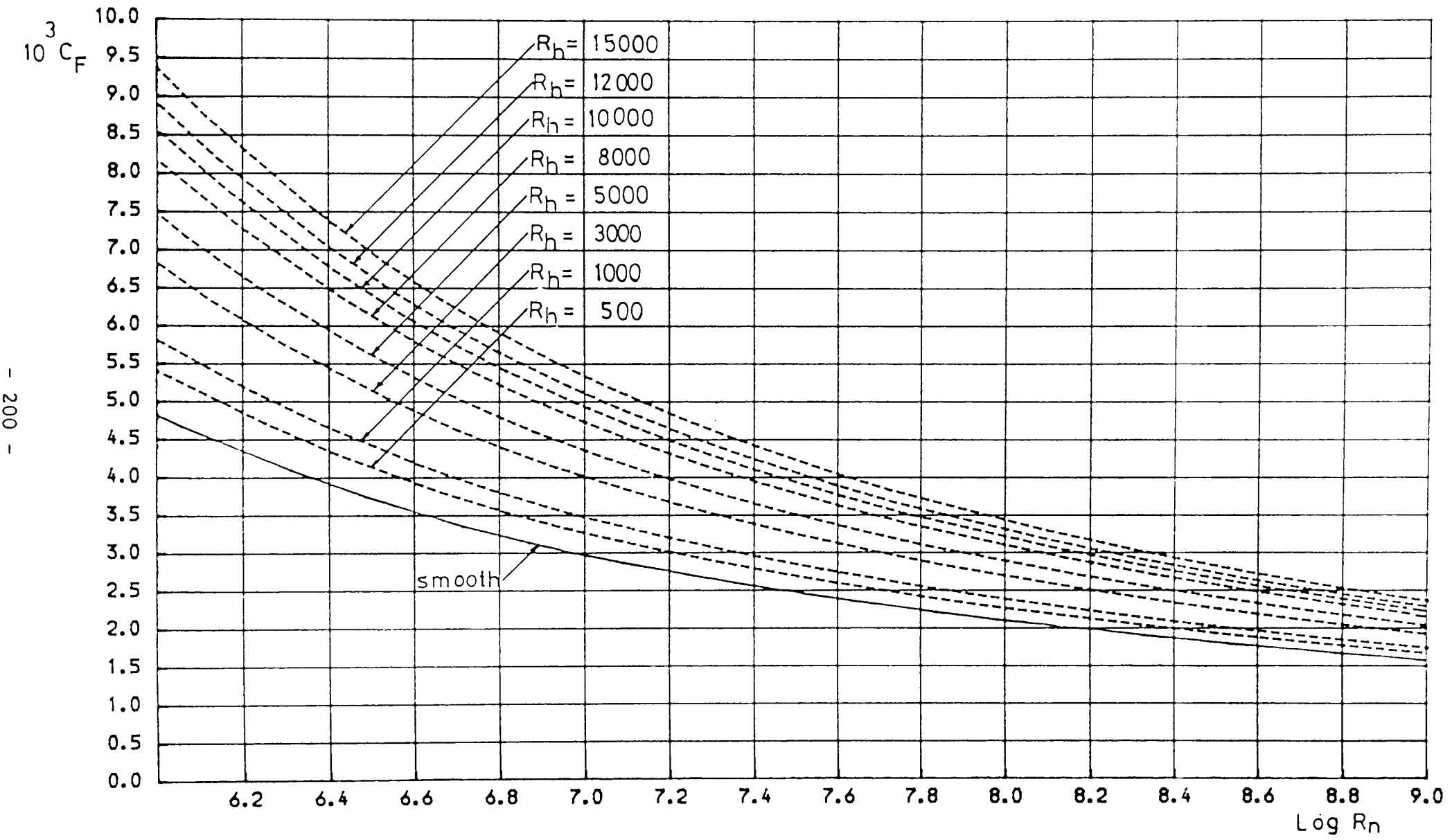


Figure (6.7) Hull Skin Coefficient C_F as a Function of R_n
 With R_h as a Parameter ($m = 22.5$)

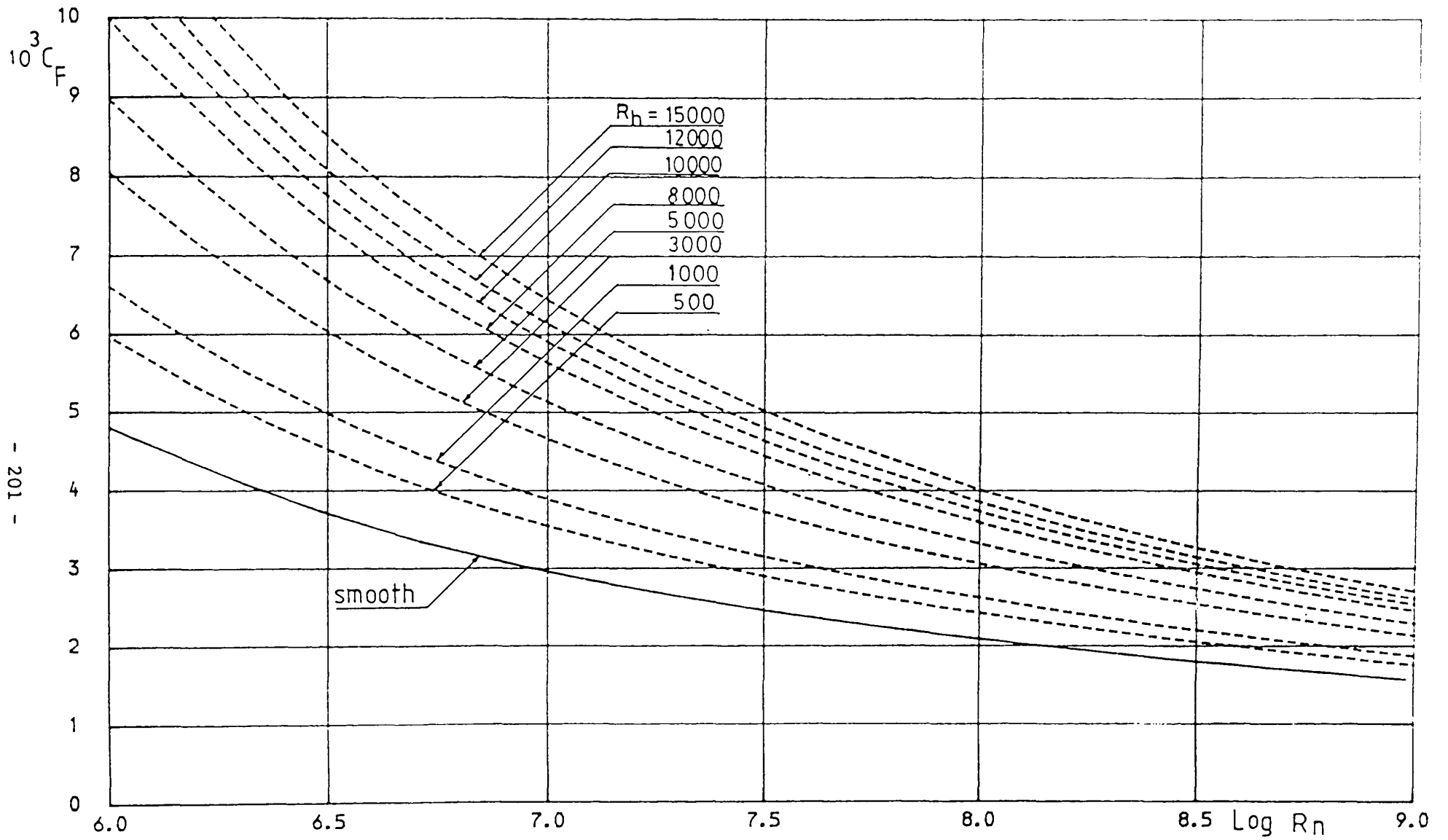


Figure (6.8) Propeller Skin Coefficient C_F as a Function of R_n
 With R_h as a Parameter ($m = 9.02$)

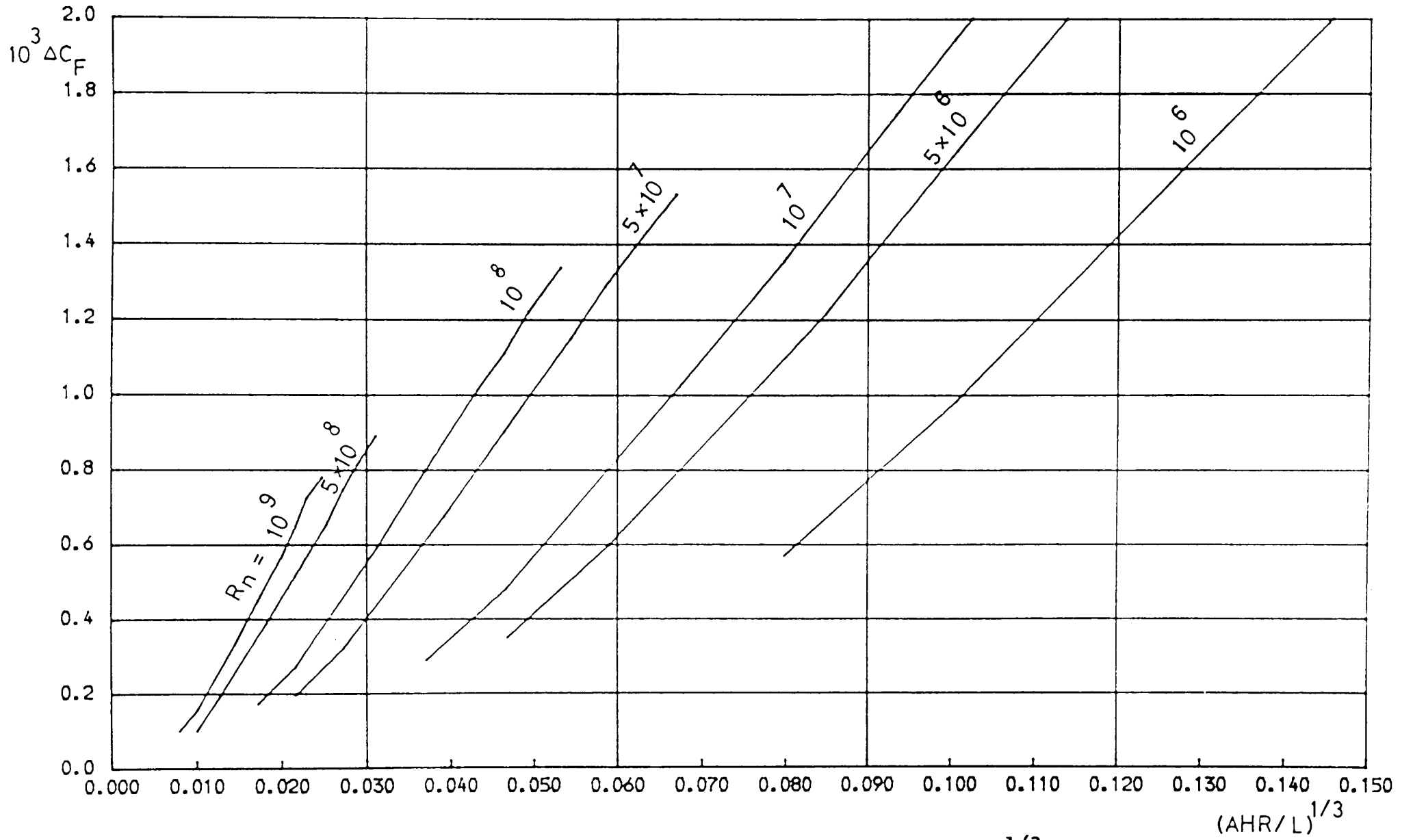


Figure (6.9) Hull Drag Penalty ΔC_F Versus $(AHR/L)^{1/3}$
With R_n as a Parameter ($m = 22.5$)

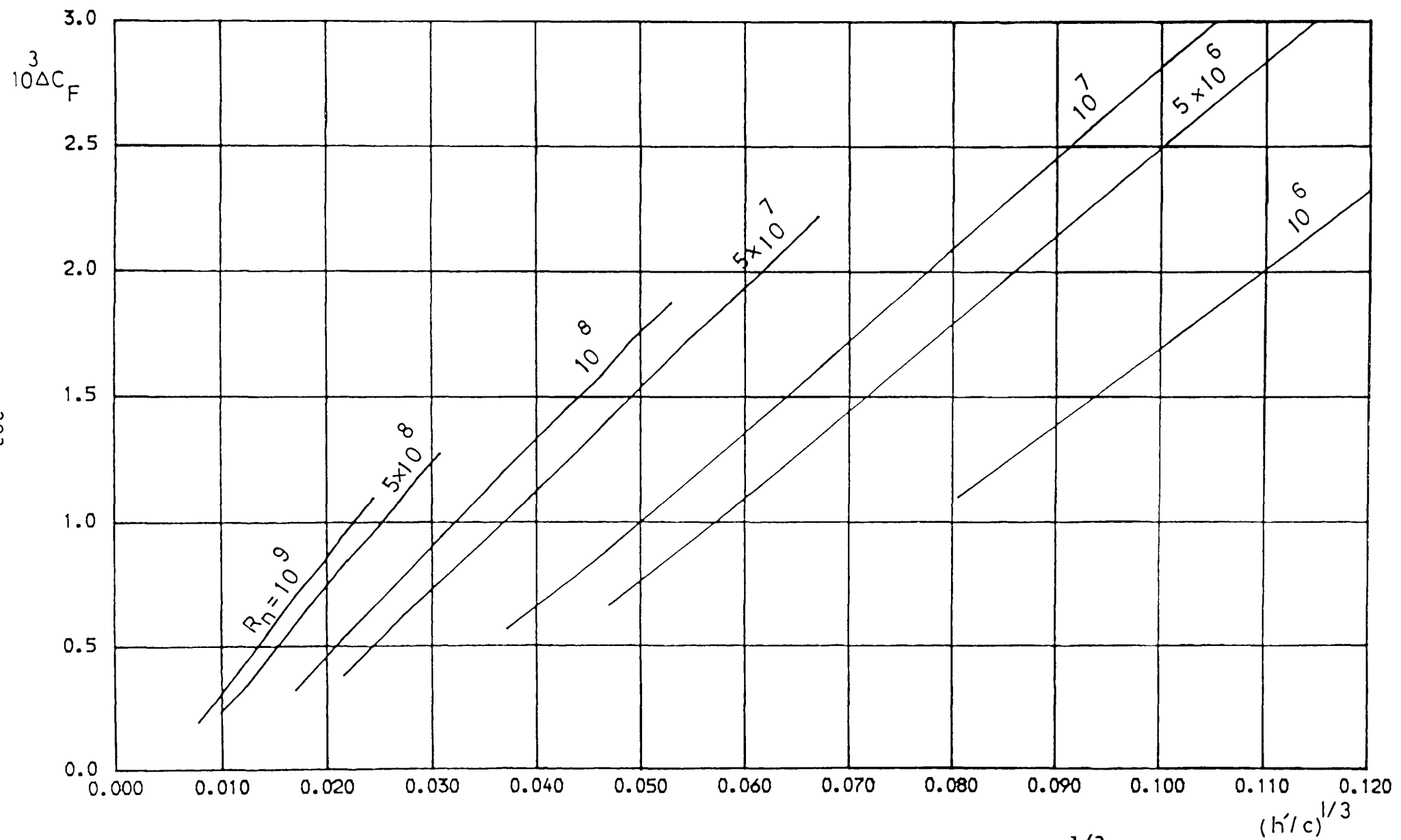


Figure (6.10) Propeller Drag Penalty ΔC_F Versus $(h'/c)^{1/3}$
With R_n as a Parameter ($m = 9.02$)

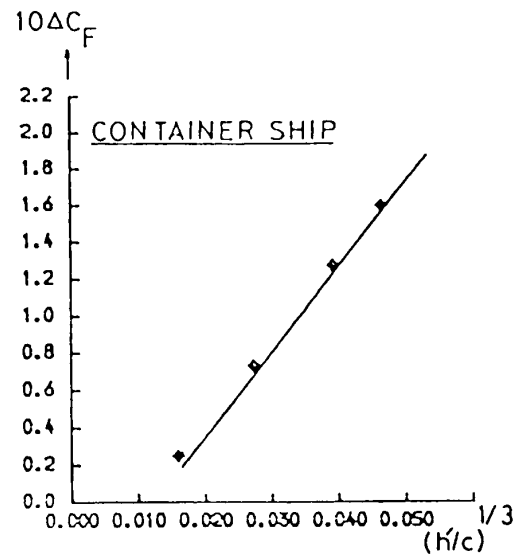
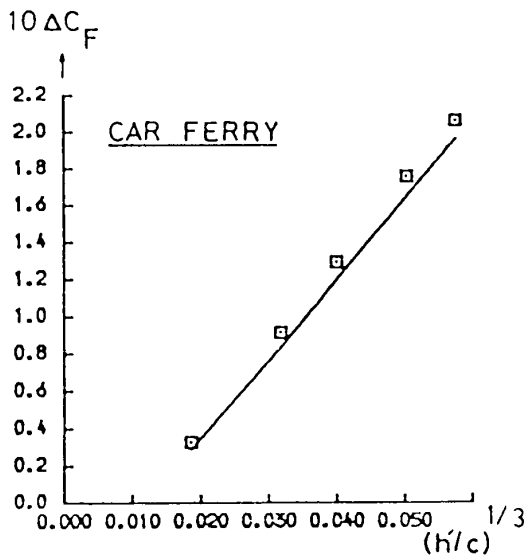
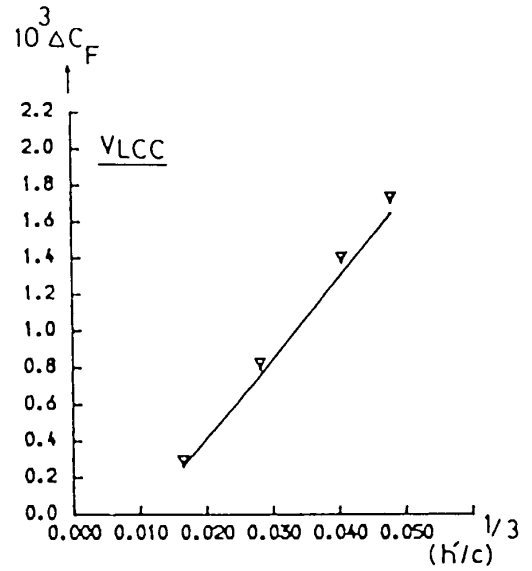
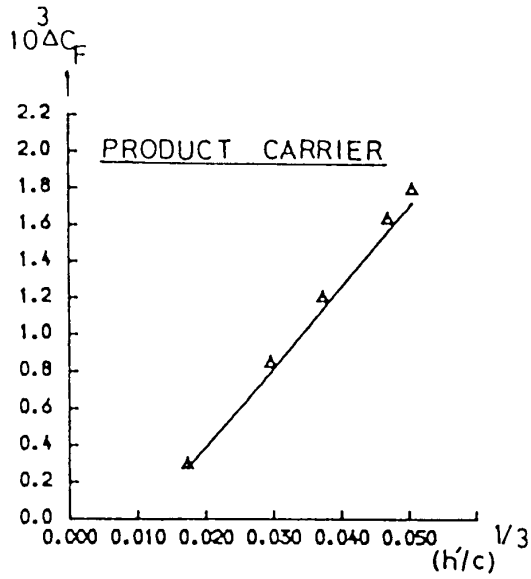


Figure (6.11) Results of C_F Obtained From "PROFNESS" and "FPBL" at 0.7R Blade Section For 4 Types of Propeller

(Key: continuous line for "FPBL" & individual points for "PROFNESS")

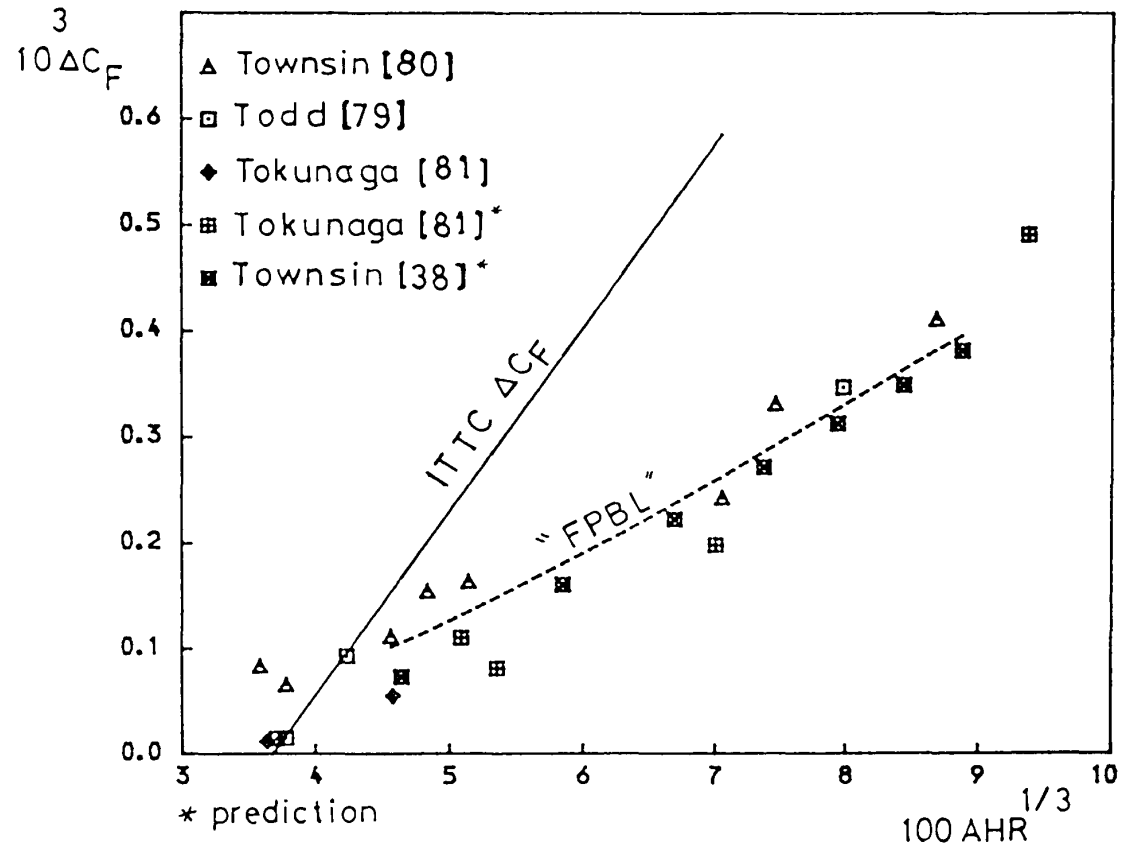


Figure (6.12) Comparison of "FPBL" Results With Experimental Data

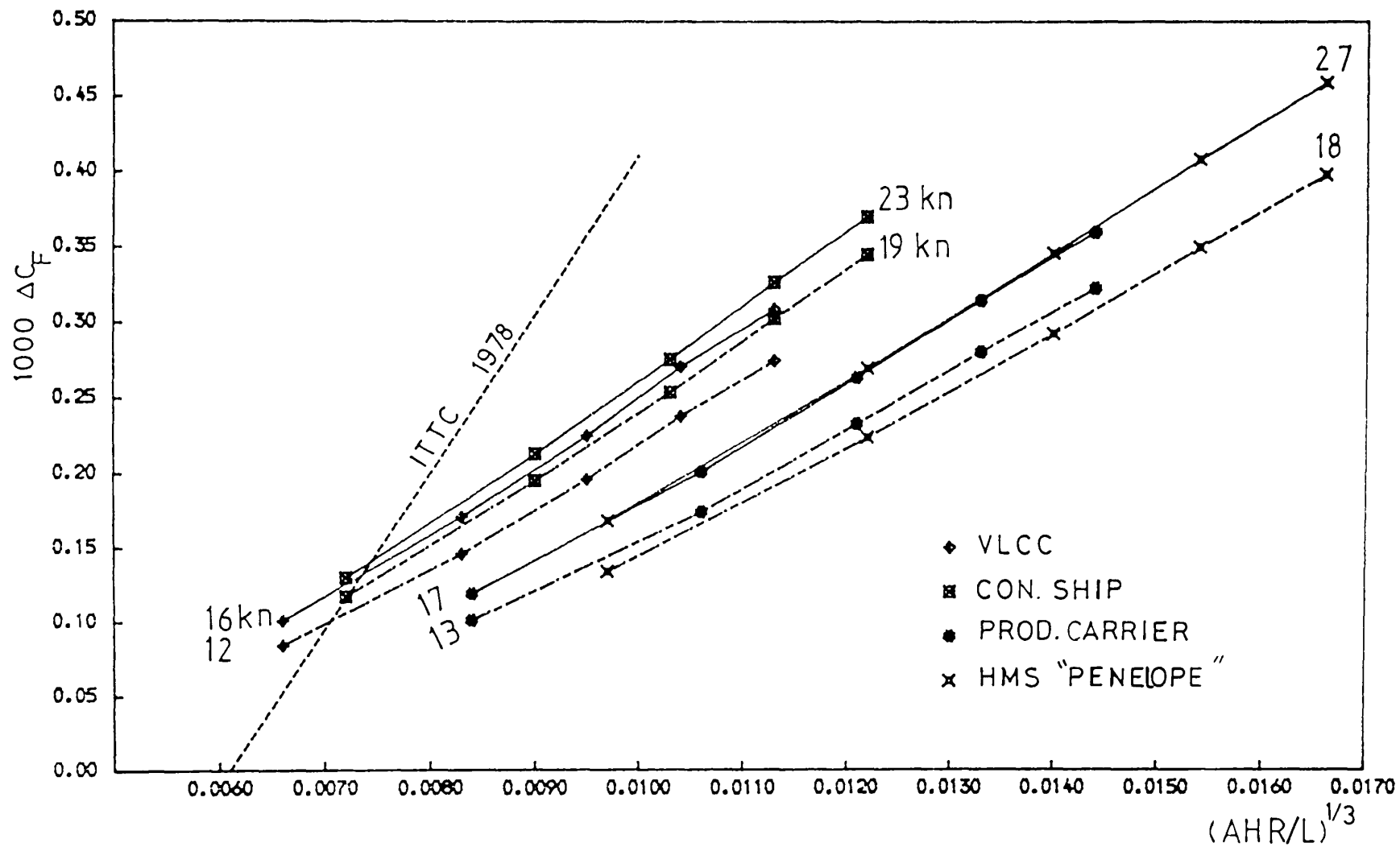


Figure (6.13) ΔC_F Versus $(AHR/L)^{1/3}$ For 4 Types of Ships Using "FPBL" Prediction Method

(Distributed Roughness, 100-500 μm AHR)

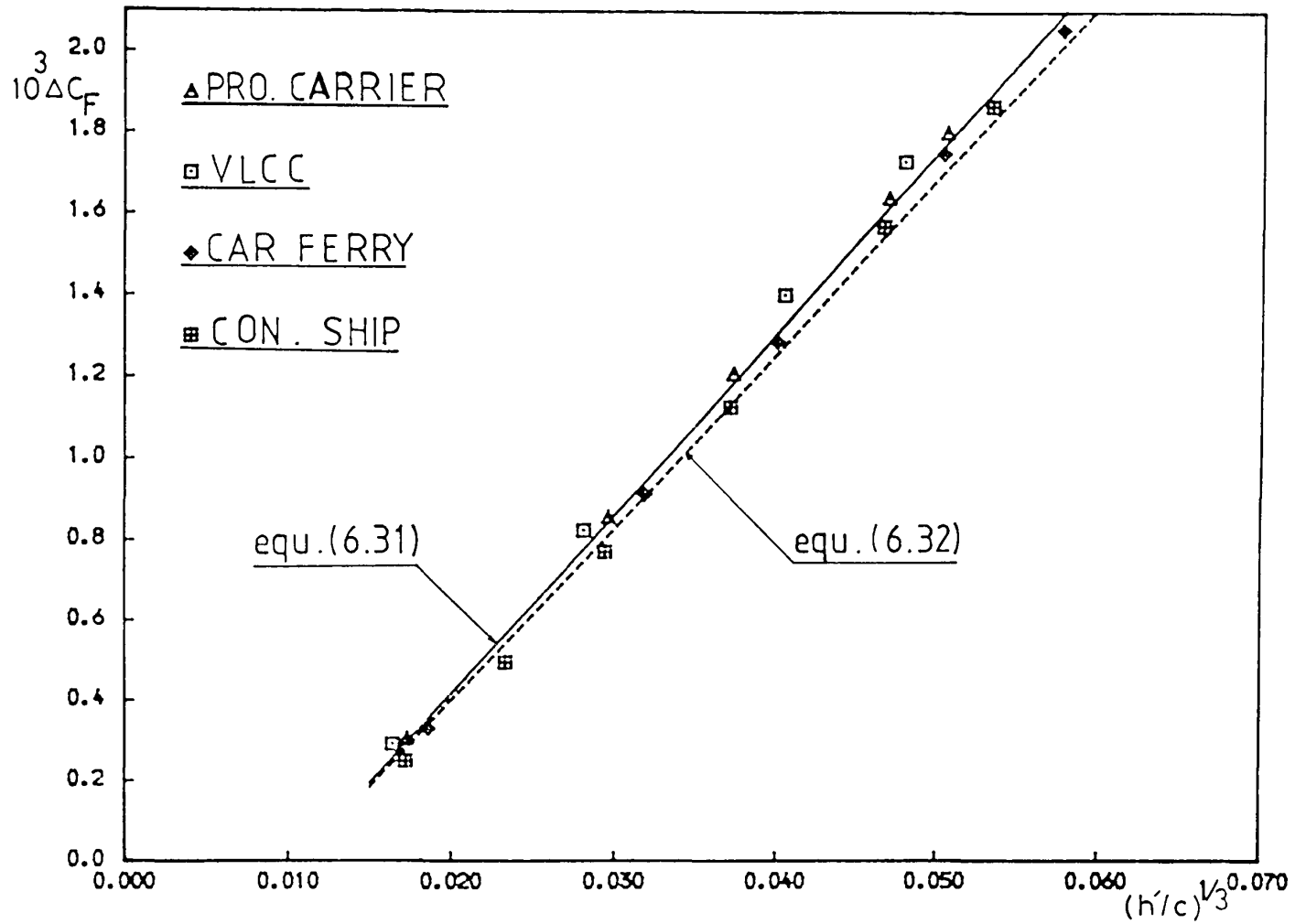


Figure (6.14) $\Delta C_F \sim (h'/c)^{1/3}$ Plots of Propeller Foils and Their Equivalent Flat Plate

6.3 A SIMPLIFIED METHOD TO DETERMINE THE EFFECT OF PROPELLER ROUGHNESS
ON SHIP POWER

6.3.1 Calculation of Thrust and Torque Coefficient of Equivalent Profile

The method is to establish the elementary forces on a blade element, then the integration of these forces will give the total thrust and torque in non-dimensional form. A blade element of length dr is considered at r of a z -bladed propeller. When the propeller is working at ω and V_a , the axial and tangential induced velocities aV and $a'\omega r$ are generated and the resultant inflow velocity is given by:

$$v = \sqrt{V_a^2(1+a)^2 + \omega^2 r^2(1-a')^2} \quad (6.37)$$

However, in the case of lightly loaded propellers the induced velocities are small and hence the resultant inflow velocity V may be approximated by:

$$v = \sqrt{V_a^2 + (\omega r)^2} \quad (6.38)$$

In Figure (5.2), the thrust and torque due to the lift and drag may be expressed separately as follows:

$$dT_L = C_L \frac{1}{2} \rho v^2 c(r) \cos \beta_i dr$$

$$dT_D = C_D \frac{1}{2} \rho v^2 c(r) \sin \beta_i dr$$

$$dQ_L = C_L \frac{1}{2} \rho v^2 c(r) \sin \beta_i dr$$

$$dQ_D = C_D \frac{1}{2} \rho v^2 c(r) \cos \beta_i dr$$

where,

$$C_L = dL/0.5 \rho v^2 c(r) dr \quad , \quad C_D = dD/0.5 \rho v^2 c(r) dr$$

The overall thrust and torque of the propeller are then:

$$T = z \int_h^R (dT_L/dr) dr - z \int_h^R (dT_D/dr) dr \quad (6.39)$$

$$Q = z \int_h^R (dQ_L/dr) dr + z \int_h^R (dQ_D/dr) dr \quad (6.40)$$

In order to calculate T and Q using equations (6.39) and (6.40), some assumptions are necessary. The relation between the thrust of a z-bladed propeller and that of a blade section element can be described by:

$$K_{TL} = z \int_h^1 dK_{TL}/dx \quad dx \quad (6.41)$$

Following Lock [83], the radial distribution of the thrust coefficient dK_{TL}/dx^2 is assumed to be elliptical. Then equation (6.41) can be expressed by:

$$K_{TL} = z (dK_{TL}/dx)_x m(x) \quad (6.42)$$

where,

$$m(x) = \frac{\pi}{16} \frac{1}{x^2 \sqrt{1-x^2}} \quad (6.43)$$

and

$$x = r/R$$

Similar assumption may be made for the torque coefficient,

$$K_{QL} = z \int_0^1 (dK_{QL}/dx)_x m(x) dx \quad (6.44)$$

Following Yamasaki [84], the radial distribution of the thrust and torque due to the drag, dK_{TD}/dx and dK_{QD}/dx , may be assumed to be:

$$K_{TD} = z \int_0^1 (dK_{TD}/dx)_x dx = z \int_0^1 (dK_{TD}/dx)_x j(x) dx \quad (6.45)$$

and

$$K_{QD} = z \int_0^1 (dK_{QD}/dx)_x dx = z \int_0^1 (dK_{QD}/dx)_x g(x) dx \quad (6.46)$$

where,

$$j(x) = 0.267/x\sqrt{1-x} \quad , \quad j(0.7) = 0.696$$

and

$$g(x) = 0.102/x^3\sqrt{1-x} \quad , \quad g(0.7) = 0.543$$

Arranging dT_L and dQ_L in dimensionless form and substituting them in equations (6.42) and (6.44), the following may be obtained:

$$K_{TL} = C_L z c/D \pi^2/4 m(x) x^2 (1+\mu^2)/\mu^2 \cos Bi \quad (6.47)$$

and

$$K_{QL} = C_L z c/D \pi^2/8 m(x) x^3 (1+\mu^2)/\mu^2 \sin Bi \quad (6.48)$$

where,

$$\mu = \omega r/Va = \omega R x/Va = \pi x/J$$

Similarly, the thrust and torque coefficient due to the drag are:

$$K_{TD} = C_D z_{c/D} \pi^2/4 j(x) x^2 (1+\mu^2)/\mu^2 \sin Bi \quad (6.49)$$

and

$$K_{QD} = C_D z_{c/D} \pi^2/8 g(x) x^3 (1+\mu^2)/\mu^2 \cos Bi \quad (6.50)$$

and the resultant K_T and K_Q of the propeller are found to be:

$$K_T = F1 [m(x) C_L \cos Bi - j(x) C_D \sin Bi] \quad (6.51)$$

and

$$K_Q = 1/2 F1 x [m(x) C_L \sin Bi + g(x) C_D \cos Bi] \quad (6.52)$$

where,

$$F1 = \pi^2/4 z_{c/D} x^2 (1+\mu^2)/\mu^2$$

6.3.2 Change of Thrust and Torque Coefficient Due to Propeller Roughness

Starting with the thrust coefficient, equation (6.51) can be written in general form as:

$$K_T = f (C_L, C_D, Bi, x, J) \quad (6.53)$$

at fixed values of x and J , the variation of K_T is:

$$\Delta K_T = (\partial K_T / \partial C_L) \Delta C_L + (\partial K_T / \partial C_D) \Delta C_D + (\partial K_T / \partial Bi) \Delta Bi \quad (6.54)$$

for a fixed propeller blades with moderate surface roughness,

$$\Delta Bi = - \Delta \alpha = 0.0$$

and hence from equations (6.51) and (6.54)

$$\Delta K_T = F l m(x) \cos Bi [\Delta C_L - j(x)/m(x) \tan Bi \Delta C_D] \quad (6.55)$$

or

$$\Delta K_T/K_T = \frac{\Delta C_L/C_L - j(x)/m(x) \tan Bi (\Delta C_D/C_L)}{1.0 - j(x)/m(x) \tan Bi (C_D/C_L)} \quad (6.56)$$

assuming, $\Delta C_L = -1.1 \Delta C_D$ and $\tan Bi = 1/\pi x (P/D)i$

the value of P/D can be written as:

$$P/D = \pi x \tan Bi \left(1 + \frac{\Delta P/D}{P/D}\right) = k (P/D)i \quad (6.57)$$

therefore,

$$\Delta K_T/K_T = - \frac{\Delta C_D/C_L [1.1 + j(x)/m(x) (P/D)/\pi x k]}{1.0 - j(x)/m(x) (P/D)/\pi x k C_D/C_L} \quad (6.58)$$

In similar way $\Delta K_Q/K_Q$ can be derived to be:

$$\Delta K_Q/K_Q = - \frac{\Delta C_D/C_L [1.1 - g(x)/m(x) \pi x k / (P/D)]}{1.0 + g(x)/m(x) \pi x k / (P/D) C_D/C_L} \quad (6.59)$$

P/D in equations (6.58), (6.59) is the average value of the propeller blade and x takes the values of 0.7 to 0.75 as shown by Lerbs. However, preliminary results indicate that:

$$x = 0.7 \quad , \quad (P/D)_{av} = (P/D)^{0.7} \quad , \quad 1.01 < k > 1.04$$

To calculate the power increment due to propeller roughness equation (5.20) can be rewritten in a simpler form:

$$\Delta P/P = [\Delta K_Q/K_Q - 3/2 \Delta K_T/K_T] \quad (6.60)$$

in which equations (6.58) and (6.59) can be used. To express equation (6.60) in terms of roughness drag penalty, the term $(\Delta C_D/C_L)(C_D/C_L)$ may be neglected and the following formula can be used for very simple calculations at $x=0.7$,

$$\Delta P/P = \Delta C_D/C_L [2.13/(P/D) + 0.55 + 0.85 P/D] \quad (6.61)$$

To estimate $C_L(0.7)$, if unknown, we can start from equation (6.52) which can be rewritten, assuming $m(x)=g(x)$, as follows:

$$K_Q = 1/2 F_l x C_L g(x) [\sin Bi + C_D/C_L \cos Bi] \quad (6.62)$$

Hence C_D/C_L is very small,

$$\sin(C_D/C_L) = C_D/C_L \quad \text{and} \quad \cos(C_D/C_L) = 1.0$$

therefore,

$$K_Q = 1/2 F_l x C_L g(x) \sin (Bi + C_D/C_L) \quad (6.63)$$

also assuming,

$$\tan (Bi + C_D/C_L) = P/D \ 1/\pi x$$

i.e.

$$\sin (Bi + C_D/C_L) = P/D [(\pi x)^2 + (P/D)^2]^{-1/2}$$

and

$$(1+u^2)/u^2 = [(\pi x)^2 + J^2] / (\pi x)^2$$

but

$$K_Q = Q / n^2 D^5 \quad \text{and} \quad Q = P_D / 2\pi n$$

so that

$$C_L = 2.37 \cdot 10^5 \text{ KL } (\text{SHP}/n^3 D^5) (P/D)^{-1} (z_c/D)^{-1} \quad (6.64)$$

where,

$$\text{KL} = \sqrt{1 + 0.207(P/D)^2} / (1 + 0.207J^2)$$

The section chord c is also required for the calculations and should be given. However, if it is unknown it may be estimated by the equation:

$$c(0.7) = D \sqrt{4.15 (\text{BAR}/z)^2 + 0.01} \quad (6.65)$$

This equation is derived with the assumption that, the maximum chord length of the blade is at $x=0.625$ and the upper part from 0.625 to the tip of the blade is a semi-circle. The chord $c(0.75)$ is taken from the equation

$$c(0.75) = 2.037 \text{ BAR } D/z \quad (6.66)$$

given in [85] , assuming 0.75 R is equivalent to the whole blade.

To calculate ΔC_D from ΔC_F , the section thickness, t_c , is also required. If t_c is unknown it may be estimated [86] by:

$$t_c(0.7)/D = 0.00255 + 0.092 [\text{SHP}/D^3 \text{ RPM } S_c (P/D)]^{-1/3} \quad (6.67)$$

where,

S_c = the design yield stress of propeller material.

(86 MPa for Manganese Bronze)

To evaluate the annual cost saving due as a result of grinding and polishing a propeller surface, the following equations can be used:

$$\text{AFCS} = 24 \cdot 10^{-6} \text{ SFC SHP SDPA FPPT } \Delta P/P\% \quad (6.68)$$

$$\text{GPC} = \pi/2 D^2 \text{ BAR GPCM} \quad (6.69)$$

$$\text{PBP} = 52.0 \text{ GPC/AFCS} \quad (6.70)$$

where,

AFCS = annual fuel cost saving.

SFC = specific fuel consumption in gm/SHP/hr.

SDPA = sea days per annum.

FPPT = fuel price per tonne.

GPC = grinding and polishing cost of propeller.

GPCM = grinding and polishing cost per m^2 .

PBP = pay back period in weeks.

6.3.3 Average Propeller Roughness APR

In chapter 5, the contribution to the power penalty of each roughened propeller section is shown to be varied especially in the outer half of the blade in which about 90-95% of the power loss are found. For the equivalent propeller section method, account must be taken of the roughness distribution over the whole blade. In [28] one single

roughness measure, APR has been devised to represent the state of the whole blade surface by weighting the roughness effects on each section. The average propeller roughness is defined as:

$$APR = \left[\sum_1^5 W_i (h'_i)^{1/3} \right]^3 \quad (6.71)$$

The weights W_i are evaluated so that for uniform distribution of roughness ($h'(x)=\text{constant}$), $APR=h'$. This allows APR to be used directly in place of h' . For calculating APR, the weights are given in Table (6.3).

Table (6.3)

Weights for Calculating APR

i	Region	Weight
1	0.2 - 0.5	0.07
2	0.5 - 0.7	0.22
3	0.7 - 0.8	0.21
4	0.8 - 0.9	0.27
5	0.9 - TIP	0.23

Sometimes readings for a certain roughness area could not be taken. In this case, as the missing values could not be assumed zero, an alternative formula for APR is used:

$$APR = \left[\frac{\sum_m^n W_i (h'_i)^{1/3}}{\sum_m^n W_i} \right]^3 \quad m < n < 5 \quad (6.72)$$

6.3.4 Applications and Economic Evaluations of Propeller Maintenance

The proposed simplified procedures described above have been programmed "SIMPWR" which includes "FPBL" as a routine to calculate C_D . The method is applied to the same propellers used in chapter 5 and their particulars given in Table (5.1). In the last two columns in Table (6.4) a comparison between the lift coefficient calculated by equation (6.64) and that calculated by the propeller analysis program in chapter 5 is made. Figures (6.15) to (6.19) give a comparison between the power penalty calculated using both the simplified method and the more rigorous version of chapter 5. There is a reasonable agreement between the two results. Moreover, if the actual lift coefficient is used instead of that given by equation (6.64) the two curves become very similar.

Table (6.4)

Lift Coefficient calculations

Ship Type	z	P/D	D	RPM	Power	Speed	C_L	C_L^+
VLCC	6	0.738	8.65	87	32234	15.5	0.223	0.231
P. CARRIER	4	0.758	6.00	128	13890	16.9	0.222	0.243
CON. SHIP	6	1.243	7.50	93.5	33740	24.5	0.188	0.172
CAR FERRY*	4	1.090	3.24	225	5287	21.0	0.144	0.167
FRIGATE*	5	1.340	3.66	130	3300	17.0	0.302	0.259

* Twin Screw

+ actual values

To demonstrate the economic effects of propeller roughness, the power penalties can be related conveniently to roughness assessments by the

Rubert roughness comparators as given in Table (4.4). The results are then transformed into economic terms using equation (6.70). Assumed values of technical and operational variables of the case studies used in this calculation are given in Table (6.5). The polishing cost in the dry dock is assumed to be \$180/m² or \$100/m² if polishing afloat [29]. Sample of costs of the excessive roughness of Grade D relative to Grade A at bunker cost of \$180/tonne are presented in Table (6.6). It is shown that maintenance of propeller smoothness represents an enormous return for a relatively cheap investment.

Table (6.5)

 Technical and Operational Variable

Ship Type	Type of Operation	SDPA	SFC+	BAR
VLCC	con. power (n+1=2.91)	300 (24)	254	0.689
PR. CARRIER	con. power (n+1=3.22)	250 (24)	163	0.576
CON. SHIP	const. speed	200 (24)	185	0.870
CAR FERRY*	const. speed	340 (12)	104	1.000
FRIGATE*	const. speed	180 (24)	100	0.650

* Twin Screw
 + in gm/SHP hr

Table (6.6)

 Economic Evaluation of Propeller Roughness

Ship Type	ΔP/P %	AFCS \$	DRY DOCK		AFLOAT	
			GPC	PBP	GPC	PBP
VLCC	2.77	316005	14582	2.40	8101	1.33
PR. CARRIER	2.81	44342	5865	6.88	3259	3.82
CON. SHIP	2.57	138576	13842	5.20	7690	2.89
CAR FERRY	3.83	31638	2988	4.90	1660	2.73
FRIGATE	1.68	8619	2460	14.0	1367	8.25

In Table (6.6), the calculated penalties at constant speed for the VLCC and the products carrier have been transformed to economic penalties at constant power, using the simplified method proposed by Svensen [66] as:

$$C_s/C_p = 3.1 F/I \quad (6.73)$$

where,

C_s = cost saving at constant speed.

C_p = cost saving at constant power.

F = daily fuel cost at sea.

I = daily average income after deductions for cargo handling and port charges.

and since we are looking for only an approximate answer, the ratio F/I is assumed 0.3 for the VLCC and 0.5 for the products carrier.

The present method is in accord with the simplified procedure developed by the Ship Performance Group for the calculation of rough propeller penalties using the "nomograph" in [28] .

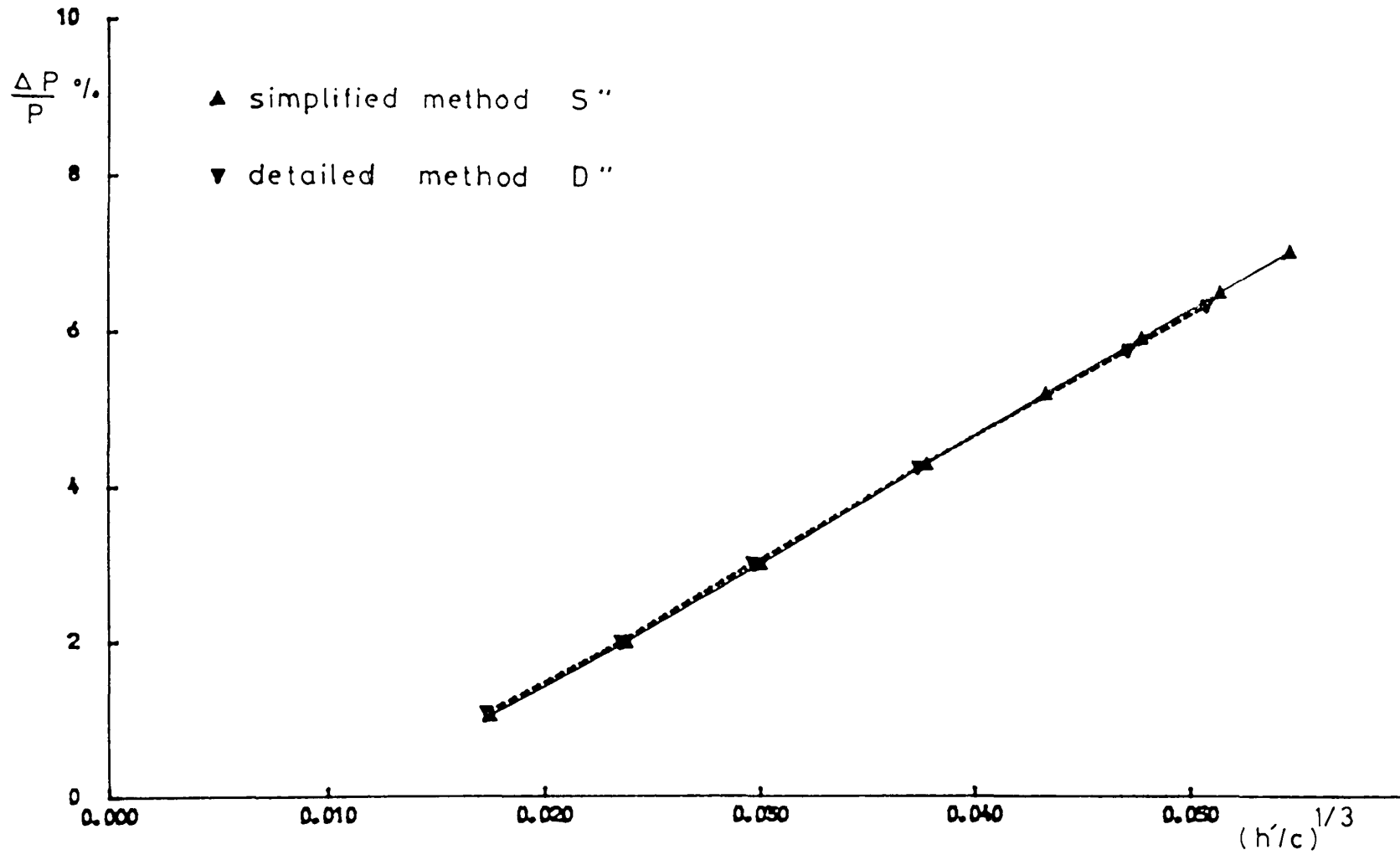


Figure (6.15) Propeller Power Penalty of "Product Carrier"

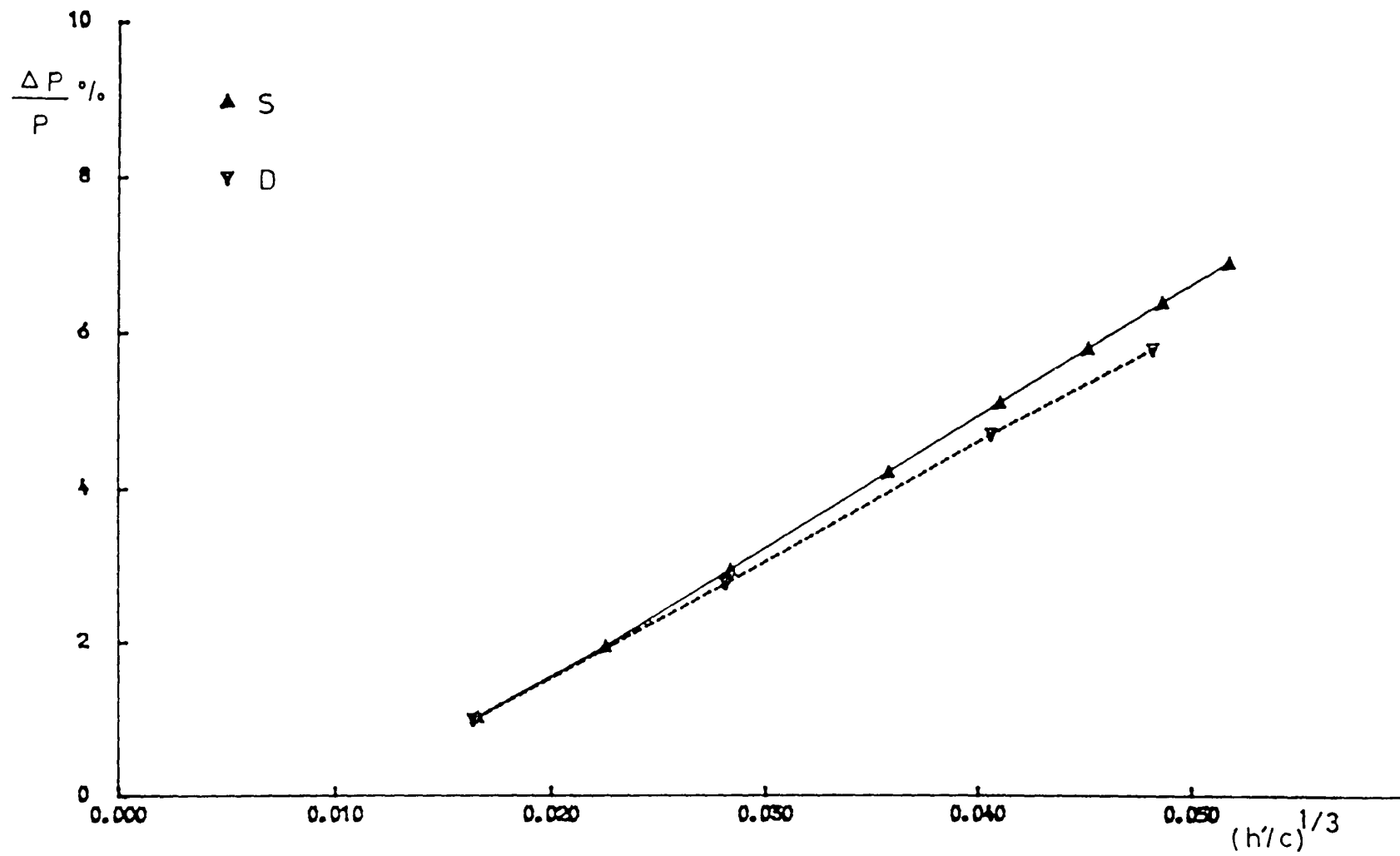


Figure (6.16) Propeller Power Penalty of "VLCC"

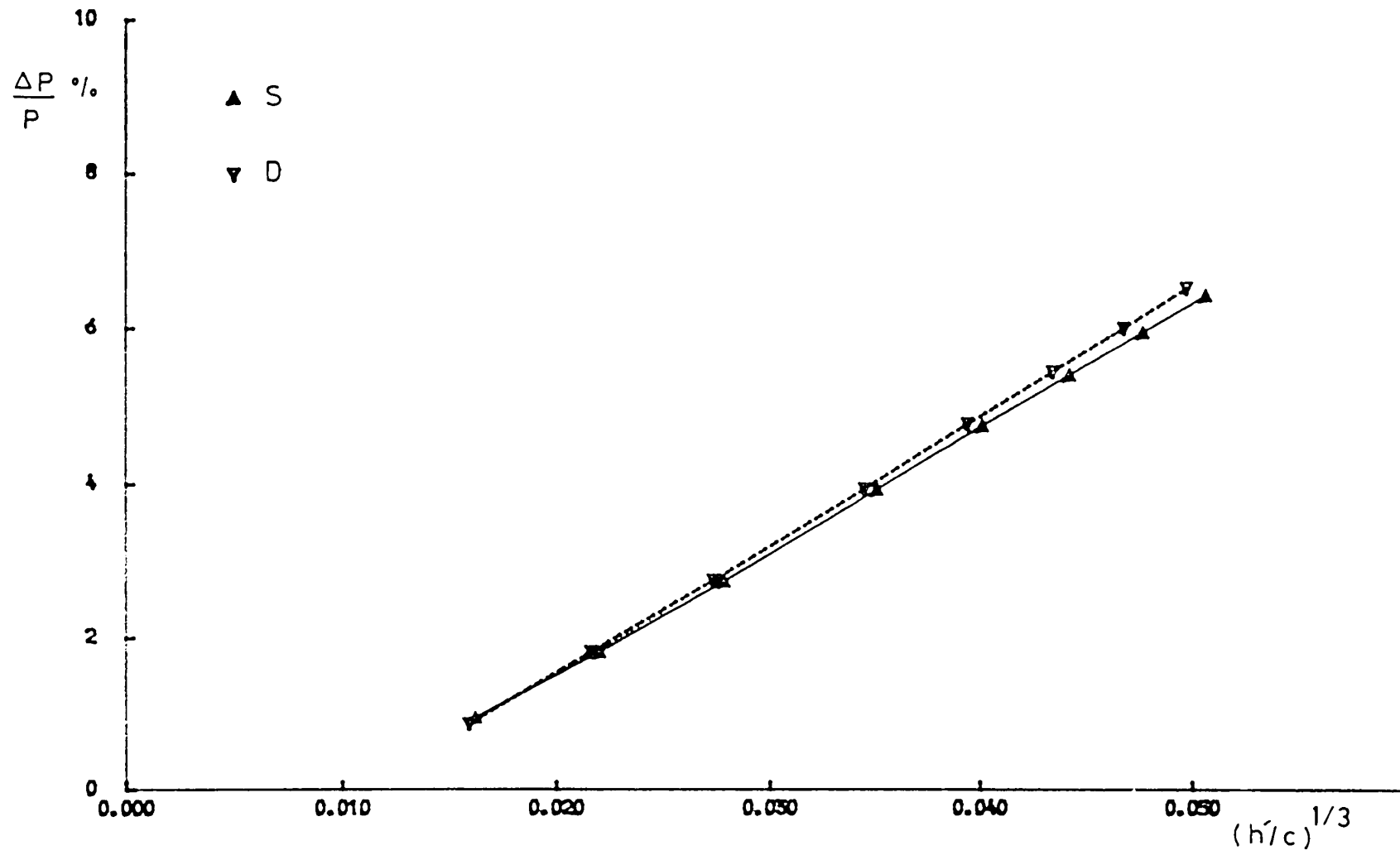


Figure (6.17) Propeller Power Penalty of "Container Ship"

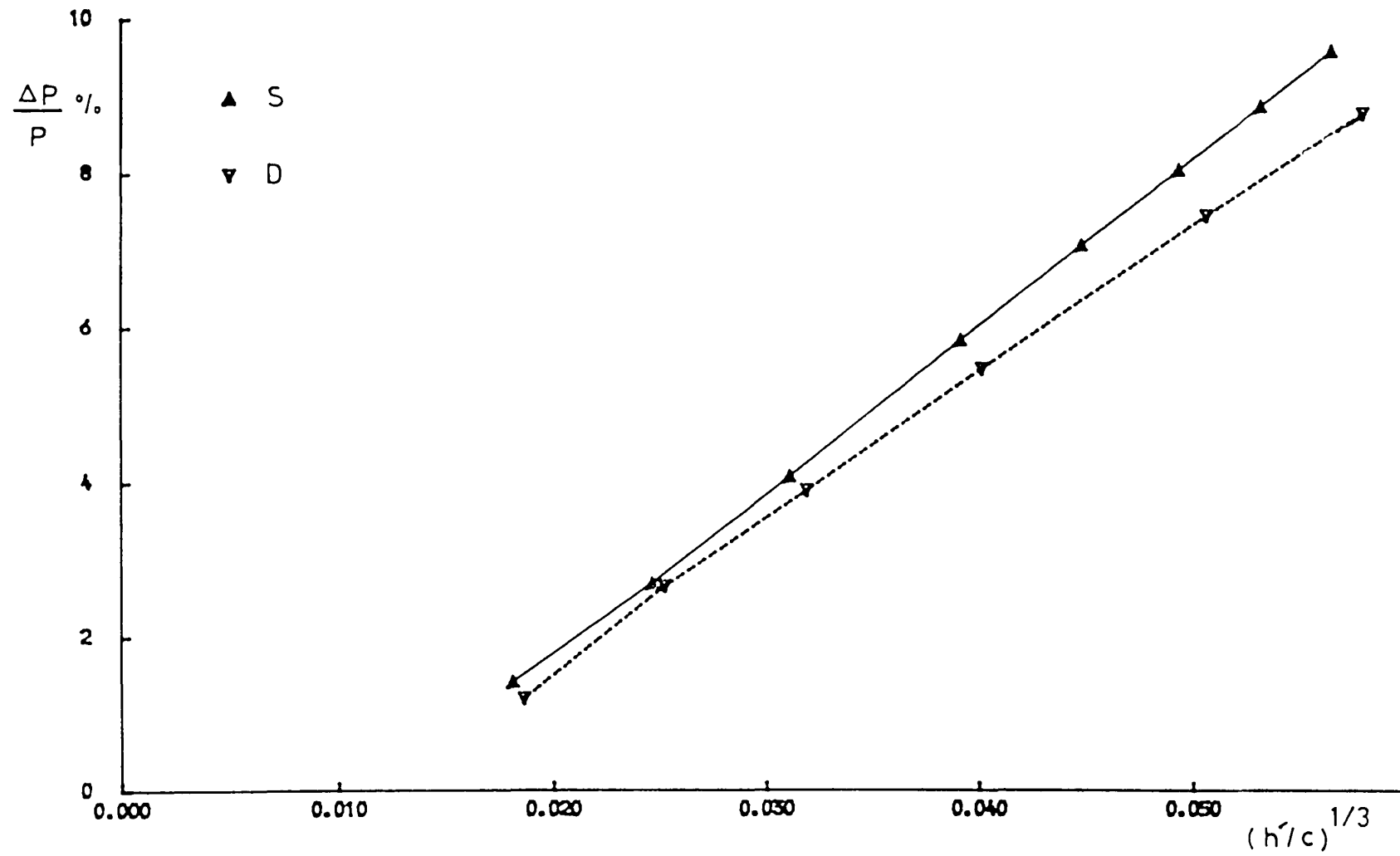


Figure (6.18) Propeller Power Penalty of "Car Ferry"

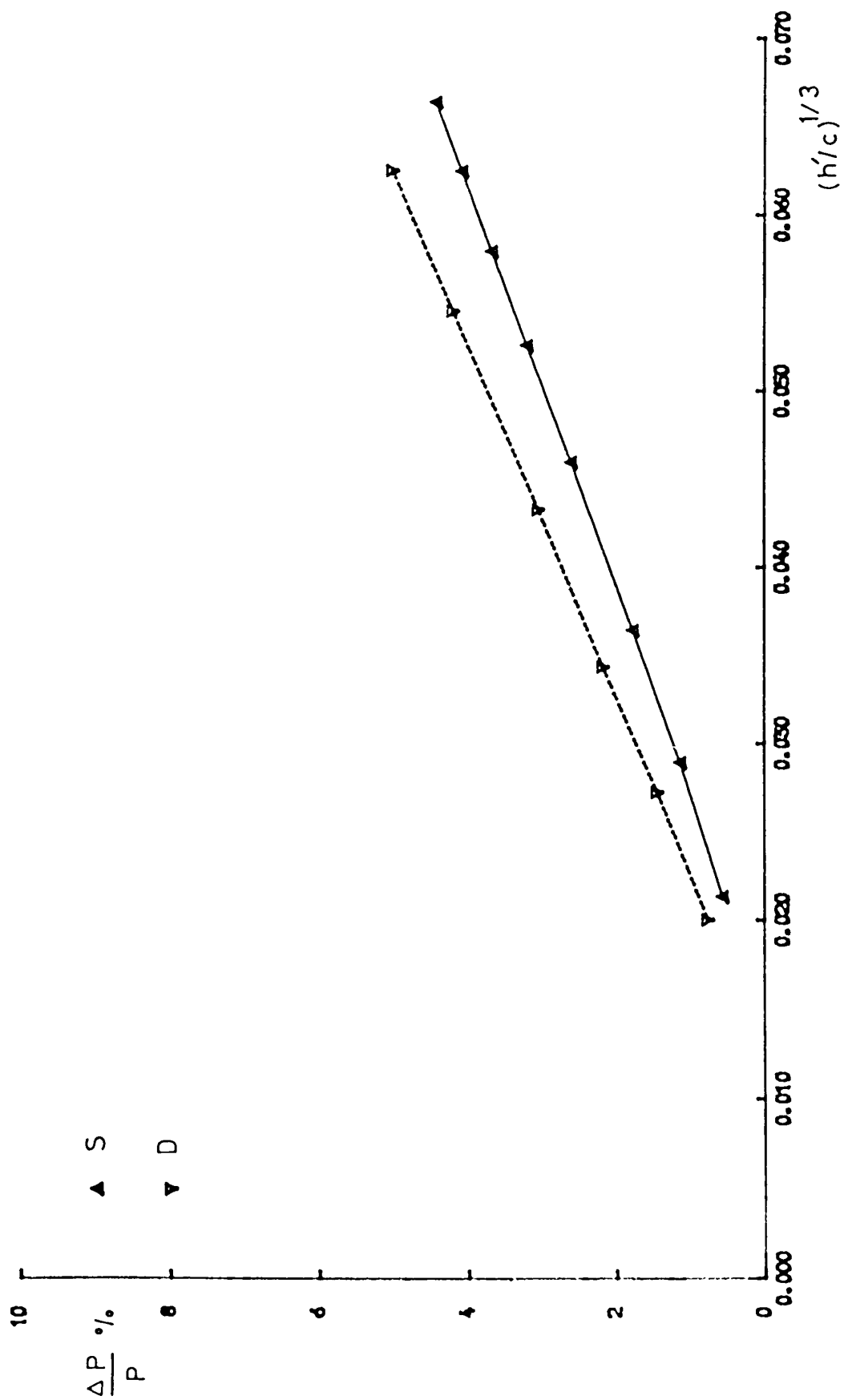


Figure (6.19) Propeller Power Penalty of "Frigate"

6.4 COMBINED EFFECT OF PROPELLER AND HULL ROUGHNESSES ON THE SHIP

PERFORMANCE

6.4.1 The Effect of Hull Roughness upon the Propulsion Factors

It is known that the propeller efficiency depends on the propeller loading or indirectly on the total resistance of the ship. The effect of the added resistance due to the hull roughness is to increase the propeller loading and hence a change in propeller efficiency. Moreover, the changing of hull flow characteristics influences the propeller wake field. The overall picture is therefore too complicated and more information is needed about how the various components of the propulsive coefficient are affected by the presence of hull roughness and fouling.

It is common practice to assume that the total efficiency, η_{tot} consists of three constituent parts:

1. the hull efficiency, $\eta_H = (1-t)/(1-w_T)$
2. the propeller efficiency for propeller working aft the ship η_B , which is the the product of the open water efficiency, η_0 and the relative rotative efficiency, η_R ,

i.e.

$$\eta_B = \eta_0 \eta_R = T v_a / 2\pi Q n$$

3. the shaft transmission efficiency, η_S and hence η_{tot} can be obtained

by:

$$\eta_{tot} = \eta_H \eta_B \eta_S$$

The propulsive efficiency or Quasi-propulsive coefficient is usually expressed as:

$$\eta_D = \eta_0 \eta_H \eta_R$$

To investigate the effect of surface roughness on propulsive performance, 3 factors should be involved:

1. the thrust deduction fraction, t
2. the relative rotative efficiency, η_R
3. the effective wake fraction, w_T

Many researchers have assumed that there is a close relationship between t and w_T . However, there is as yet no convenient answer to this question. Van Lammeren [75] investigated this relationship and found that there is no simple relation between t and w_T ; but both the two fractions depend to a large extent on the same factors. An examination of this problem has also been made by Harvald [87] and no proportionality between t and w_T can be found from his results. With regard to roughness effects, Tokunaga [81] concluded that the thrust deduction and the relative rotative efficiency remained unaffected by hull roughness, while the wake fraction does experience an increase with increasing hull roughness. A similar result has been found from testing a small size ship [27] to study the effect of fouling severity upon propulsive performance.

From the above discussion t and η_R can be assumed constant with the increase in the hull roughness. Therefore, the change of propulsive

efficiency depends only on the resulting change in open water efficiency and the wake fraction or the hull efficiency. To estimate the changes in the effective wake fraction due to the hull roughness, the ITTC-1978 formula for full scale wake prediction can be modified as follows:

Starting with the original ITTC-1978 form:

$$w_{TS} = (t+0.04) + (w_{TM}-t-0.04) \frac{(1+k)C_{FS}+\Delta C_F}{(1+k)C_{FM}} \quad (6.74)$$

where,

t = thrust deduction fraction for model and ship, assumed to be independent of scale

(1+k) = form factor

C_{FS} = frictional coefficient of ship, ITTC-1957 Line

C_{FM} = frictional coefficient of model, ITTC-1957 Line

ΔC_F = roughness allowance, ITTC-1978

and since the changes are due to roughness in service, we have:

$$w_{TR} = (t+0.04) + (w_{TM}-t-0.04) \frac{(1+k)C_{FS}+\Delta C_F + C_s}{(1+k)C_{FM}} \quad (6.75)$$

$$w_{TS} = (t+0.04) + (w_{TM}-t-0.04) \frac{(1+k)C_{FS}+\Delta C_F}{(1+k)C_{FM}} \quad (6.76)$$

from which by division the following is obtained:

$$w_{TR} = (t+0.04) + (w_{TS}-t-0.04) \left[1 + \frac{C_s}{(1+k)C_{FS}+\Delta C_F} \right] \quad (6.77)$$

where,

$$C_s = \Delta C_{FR} - \Delta C_{FS}$$

In fact equation (6.77) is slightly different from that proposed by Kresic [35] for the same purpose:

$$w_{TR} = t + (w_{TS}-t) \left[1 + \frac{C_s}{(1+k)C_{FS}} \right] \quad (6.78)$$

However, the total friction resistance on trials in the denominator of the last part of equation (6.78) has been modified to include the roughness allowance as suggested by Townsin in the discussion of [35] and hence,

$$w_{TR} = w_{TS} + \frac{C_s}{C_{vis}} (w_{TS}-t) \quad (6.79)$$

where,

$$C_{vis} = [(1+k)C_{FS} + \Delta C_F]$$

Using this equation it is possible to estimate the effective wake fraction of the ship for various degrees of hull roughness. Svensen [66] examined the effects of hull roughness upon propulsive efficiency. He found that the open water efficiency is reduced significantly by the roughness of the ship hull due to the increased loading on the propeller. At the same time the hull efficiency experiences an increase due to the increase in the effective wake fraction, while the resultant change in the total efficiency was assumed to be minimal.

6.4.2 Estimation of Combined Propeller and Hull Roughness Penalties

In the following section it is shown that the total power penalty associated with a rough propeller operating behind a rough hull can be calculated by summing each of the propeller and hull power penalties together. It is also shown that the initial assumption of no change in η_D due to hull roughness may not be valid, and hence a new method with equation (6.27) is used to estimate the hull roughness power penalty.

In general a rough propeller is usually accompanied by a rough hull with corresponding changes in the resistance and wake characteristics. The interesting point is to study the combined effect of these factors upon the propeller performance. In fact there are four cases which should be considered when tackling this problem:

1. Smooth propeller operating behind smooth hull.
2. Rough propeller operating behind smooth hull.
3. Smooth propeller operating behind rough hull.
4. Rough propeller operating behind rough hull.

The first case is the basic one for calculation of the torque and thrust characteristics for a new propeller behind smooth hull, and any subsequent changes in the propulsion characteristics can be related to it. To examine cases 2, 3 and 4 the following assumptions are made:

- Ship speed will remain constant for all roughness conditions of hull and propeller.
- Trial or smooth ship hull roughness $AHR=125 \mu\text{m}$.
- The water density ρ , wetted surface S , thrust deduction fraction t ,

relative rotative efficiency η_R and transimssion efficiency η_S remain unchanged by changes in surrounding conditions, while the wake fraction is affected by the ship hull roughness.

- Zero power penalty means smooth propeller of Rubert Grade A and smooth hull of AHR=125 μm .

The required power P at the speed V in case 1 can be written as:

$$P = R V / \eta_D \quad (6.80)$$

In the general case 4, the relative change in power can be given by:

$$\Delta P/P = [(1+\Delta C_T/C_T) / (1+\Delta\eta_0/\eta_0)(1+\Delta\eta_H/\eta_H)] - 1.0 \quad (6.81)$$

where, the relative change in the open water efficiency, which itself is a function of the advance constant, the thrust and torque coefficient of the propeller, can also be given by:

$$\Delta\eta_0/\eta_0 = [(1+\Delta J/J) (1+\Delta K_T/K_T) / (1+\Delta K_Q/K_Q)] - 1.0 \quad (6.82)$$

If the relative changes in the above equations are small compared to the value of one, as this is the present case, equation (6.81) can be approximated, using the binominal theorem, by:

$$\Delta P/P = \Delta C_T/C_T - \Delta J/J - \Delta K_T/K_T + \Delta K_Q/K_Q - \Delta\eta_H/\eta_H \quad (6.83)$$

Equation (6.83) gives the total hull and propeller roughness power penalty which can be analysed term by term as follows:

- The first term is the relative change in the total ship resistance coefficient $\Delta C_T/C_T$ in which the total resistance coefficient in the denominator is given by:

$$C_T = (1+k)C_{FS} + \Delta C_F + C_R + C_{AA} \quad (6.84)$$

where,

$(1+k)$ = the form factor and is not a function of the roughness.

C_{FS} = the smooth hull friction coefficient, equation (6.20) may be used.

ΔC_F = the additional component due to roughness.

C_R = the residual resistance coefficient and is function only of the Froude number.

C_{AA} = the weather allowance coefficient.

and the hull roughness friction drag penalty, $\Delta C_F = \Delta C_T$, may be calculated directly using equation (6.27).

- The relative change in the advance constant $\Delta J/J$, at constant speed operation is:

$$\Delta J/J = [(1-w_{TR})/(1-w_{TS})] (n_S/n_R) - 1.0 \quad (6.85)$$

and

$$n_S/n_R = (1+\Delta K_T/K_T)^{1/2} / (1+\Delta C_T/C_T)^{1/2} \quad (6.86)$$

Since the relative changes in both thrust and total resistance

coefficients are relatively small, equation (6.85) can be approximated also by:

$$\Delta J/J = (1-w_{TR})/(1-w_{TS}) [1+1/2(\Delta K_T/K_T - \Delta C_T/C_T)] - 1 \quad (6.87)$$

- The relative changes in the thrust and torque coefficients can be divided into two components one due to propeller roughness and the other due to change in operating point:

$$\Delta K_T/K_T = (\Delta K_T/K_T)_P + (\Delta K_T/K_T)_J \quad (6.88)$$

and

$$\Delta K_Q/K_Q = (\Delta K_Q/K_Q)_P + (\Delta K_Q/K_Q)_J \quad (6.89)$$

the terms $(\Delta K_T/K_T)_P$ and $(\Delta K_Q/K_Q)_P$ can be estimated using equations (6.58) and (6.59), respectively. In the operation region K_T/K_Q may be assumed constant, and hence;

$$(\Delta K_T/K_T)_J = (\Delta K_Q/K_Q)_J \quad (6.90)$$

However, the relative changes in the thrust coefficient due to change in operation can be written in the form:

$$(\Delta K_T/K_T)_J = 1/K_T \, dK_T/dJ \, \Delta J = J/K_T \, dK_T/dJ \, \Delta J/J \quad (6.91)$$

From equations (6.87), (6.88) and (6.91) the total changes in $\Delta J/J$ can be found as:

$$\Delta J/J = \frac{(1-w_{TR})/(1-w_{TS}) \{1+1/2[(\Delta K_T/K_T)_P - \Delta C_T/C_T]\} - 1}{1 - 1/2 (1-w_{TR})/(1-w_{TS}) J/K_T dK_T/dJ} \quad (6.92)$$

The above equation can be separated into two terms, one for hull roughness effects (C_T and wake) and the other for propeller roughness effect ($\Delta K_T/K_T$). Therefore, equation (6.92) becomes:

$$\Delta J/J = \frac{WK[1-1/2(\Delta C_T/C_T)]-1}{1-1/2 WK J/K_T dK_T/dJ} - \frac{1/2(\Delta K_T/K_T)_P}{WK - 1/2 J/K_T dK_T/dJ} \quad (6.93)$$

where,

$$WK = (1-w_{TR})/(1-w_{TS})$$

It can be seen from the above equation that the first term is a function of the hull roughness only while the second one is a function only of the propeller roughness assuming $WK=1$ in the denominator. Thus:

$$\Delta J/J = (\Delta J/J)_H + (\Delta J/J)_P \quad (6.94)$$

This relationship can be used to calculate the power penalty, equation (6.83), by summing the hull and propeller penalties;

$$\Delta P/P = (\Delta P/P)_H + (\Delta P/P)_P \quad (6.95)$$

where,

$$(\Delta P/P)_H = \Delta C_T/C_T - (\Delta J/J)_H - \Delta \eta_H/\eta_H \quad (6.96)$$

and

$$(\Delta P/P)_P = (\Delta K_Q/K_Q)_P - (\Delta J/J)_P - (\Delta K_T/K_T)_P \quad (6.97)$$

The value of the term $J/K_T dK_T/dJ$, in the denominator of equation (6.93) has been found [28] to be:

$$1/K_T dK_T/dJ = - (1.1 P/D - J)^{-1} \quad (6.98)$$

Equation (6.97) is similar to equation (6.60) assuming the relative change of the advance coefficient due to propeller roughness, in the second term of equation (6.93), is:

$$(\Delta J/J)_p = 1/2 (\Delta K_T/K_T)_p$$

- The relative change in the hull efficiency can be given by:

$$\Delta \eta_H / \eta_H = (w_{TR} - w_{TS}) / (1 - w_{TR}) \quad (6.99)$$

in which both sides of equation (6.76) can be divided by the term $(1-w_{TR})$ to give:

$$\Delta \eta_H / \eta_H = C_s / C_{vis} [(w_{TS} - t) / (1 - w_{TR})] \quad (6.100)$$

To calculate the speed penalty at constant power, the method described in chapter 5 and given by equation (5.28) can be used in a similar way.

A complete worked example is provided in Appendix G to show the combined effects on ship performance of propeller blade and ship hull

surface roughnesses.

CHAPTER SEVEN

CONCLUSIONS AND RECOMMENDATIONS

Propeller surface maintenance has been identified in this work as an appropriate matter concerned with the fuel efficiency of ships. The project involved extrapolation beyond the experience of naval architecture in both surface roughness topography, its effect on drag and application of boundary layer theory. The conclusions are summarised below and also certain aspects are identified which the Author considers should be developed in future work.

- From extensive measurements of the surface topography of new and in-service propellers, a standard roughness survey using either a stylus instrument or a comparator gauge has been developed.
- The analysis of the surface measurements has shown that the effect of increasing the long wavelength cutoff is generally to increase the mean and variation of height roughness parameters. Moreover, the increase in the ratio of various height parameters results from an increase in the long wavelength cutoff.
- Examination of the ISO requirements indicated that the 1966 standard for class I is better than the 1981 class S specified for finer propeller surface finish. Consequently, the current 1981 standard for propeller surface finish is a step backward as far as improvement of the ship fuel consumption and propeller hydrodynamic smoothness are concerned.
- Excluding considerations of cavitation pitting marine propellers

become rougher with time in service(not smoother as reported in [25]) and the change in roughness occurs most rapidly in the outer half of the blades. Usually the roughness on the back of the blade is greater than that on the face, and the surface deterioration also depends on the propeller alloy.

- The velocity law of Coles as modified by the Author, following Simpson [46], becomes valid for turbulent flow in both low and high Reynolds number ranges. It improves the slope of the skin friction line in the smooth flat boundary layer solution.
- From the experimental data of Musker, empirical relations have been found which can be used in the boundary prediction methods on rough surfaces. In addition, a simpler version of Musker's 4-parameters h' is deduced in terms of only 2-parameters, which can be found by a portable stylus instrument.
- The present experimental work shows that the nature of in-service propeller surface roughness is irregular and similar to surfaces of the Colebrook-White type. They should be characterised by height and texture parameters. Although the surface replicated and used on the rotor is uncharacteristically rough for today's propeller surfaces the results can still be useful as a test case for assessing the propeller roughness function.
- A hydrodynamic prediction model to estimate the propeller roughness penalties for a given blade geometry has been developed. Results from the case studies show that the relation between the power penalty and the relative blade roughness measure can be expressed by a linear relationship. It is also shown that a rough flat plane

calculation is quite adequate for such work.

- A new formula is derived from the present integration of Coles' friction results. It provides a strong support to the ITTC correlation line and may remove any residual suspicion in regard to the slope of the ITTC line, particularly at ship model Reynolds numbers.
- Formulae are presented for calculating the propeller and hull roughness drag penalty for widely different ship types. Results obtained in the case of hull roughness have shown that the added resistance is much smaller than that predicted by the ITTC roughness allowance. Moreover, the drag penalty is not only dependent on the roughness function used but also on the Reynolds number range.
- A simplified method has been developed to determine the effect of the propeller roughness on ship performance. The results obtained from this method are in good agreement with that obtained from the complete method of chapter 5. In simple economic terms the results show a high return for a small cost.
- An analytical routine has been developed which can be used to calculate the effect on ship performance for a rough propeller working behind a rough hull. It is shown that the power penalty can be calculated by summing each of the propeller and hull power penalties together. It is also shown that the assumption of no change in the total propulsive efficiency consequent upon a change in hull roughness may be inaccurate and hence the present method is proposed to calculate the hull roughness penalty.
- The present ISO recommendations of new surface finish to 1981 class S

- standard should be specified for manufacturing all merchant ship propellers. In service, the propeller should be cleaned and polished not only when the ship is drydocked but also during the inter-docking intervals. The intermediate propeller servicing can be carried out every year by specialist diving companies working particularly in propeller surface maintenance. Whatever the method, the propeller surface roughness should be measured before and after the polishing. These measurements are required to be reported clearly and accurately, not only for the operator's immediate concern but also for continuing research investigation on the behaviour of propeller surface with time in service. At the same time, more research work for long-term anti-fouling propeller coating systems is also needed.
- The experimental work undertaken in this study should be repeated for different propeller surfaces to establish a universal propeller roughness function.

Although this work is principally about propeller roughness inevitably conclusions have also been drawn about hull roughness as follows:

- Although the new relationship between the hull roughness and added resistance is believed to be sufficiently accurate, there is a need for further model test-ship trial correlation analysis.
- More data is required to search for a roughness function involving two-parameters measurement applicable to ship hull roughness. For this purpose, rotor experiments together with a recent development of the BSRA Hull Roughness Analyser undertaken by the Newcastle ship performance group for drydock survey, can be used.

- There is a need also for further understanding of the influence of slimes. This includes measuring and defining the slimes together with experimental work to determine their roughness function.
- Finally, the underwater surfaces damage and its associated fouling should be investigated with a view to improving the husbandry of these surfaces.

REFERENCES

- [1] Coles, D.
The Law of the Wake in the Turbulent Boundary Layer
Journal of Fluid Mechanics, pp 191-226, 1956.
- [2] Colebrook, C. H. & White, C. M.
Experiments with Fluid Friction in Roughened Pipes
Proc. Roy. Soc., London, A161, pp 367-381, 1937.
- [3] Musker, A. J.
Turbulent Shear-Flows Near Irregularly Rough Surfaces with Particular Reference to ships hulls
University of Liverpool, Ph.D. Thesis, Dec., 1977.
- [4] Riegels, F. W.
Aerofoil Sections
Butterworths, 1961.
- [5] Patience, G.
A Criterion for the Avoidance of Cavitation, Erosion of Marine Propellers
University of Newcastle upon Tyne, Ph.D Thesis, 1973.
- [6] Burrill, L. C.
Calculation of Marine Propeller Performance
Trans. NECIES, Vol. 60, 1943.
- [7] Coles, D.
The Turbulent Boundary Layer in a Compressible Fluid
RAND Report, R-403-pr, California, 1962.
- [8] Thomas, T. R.
Rough Surfaces
Longman Inc., New York, 1982.
- [9] Thomas, T. R.
Characterization of Surface Roughness
Precision engineering, pp. 97-103, 1981.
- [10] BSRA
The BSRA Propeller Roughness Gauge

- BSRA, Report 347, 1961.
- [11] Lackenby, H.
Resistance of Ships with Special Reference to Skin Friction and Hull Surface Condition
Proc. Inst. Mech. Engrs, Vol. 176, 1962.
- [12] Byrne, D.
Hull Roughness of Ships in Service
University of Newcastle Upon Tyne, M.Sc Thesis, 1980.
- [13] Nayak, P. R.
Random Process Model of Rough Surfaces
Trans. ASME, J. Lub. Technology, Vol. 93F, 1971, pp. 398-407.
- [14] Byrne, D. & Ward, G.
The Cost of Hull Roughness Versus the Cost of Hull Smoothness
Trans. IMarE(TM), Vol. 94, paper C98, 1982.
- [15] Longuet-Higgins, M. S.
Statistical Properties of an Isotropic Surface
Trans. Roy. Soc., A250, 1957.
- [16] Vorburger, T. V. & Scire, F. E. & Teague, E. C.
Hydrodynamic Drag Versus Roughness for Rotating Disks
Leicester Polytechnic, 2nd.I.C.on Meteology, 1982.
- [17] Medhurst, J. S.
VARICUT Surface Metrology Program-Users Guide on Programming Manual
Newcastle University, Internal Report, Nov., 1984.
- [18] Townsin R. L. & Byrne, D. & Svensen, T. E. & Milne, A.
Estimating the Technical and Economic Penalties of Hull and Propeller Roughness
SNAME, Vol. 89, 1981, pp. 295-318.
- [19] Wellman, F.
A Survey of Hull and Propeller Roughness Data
The Shipbuilder and Marine Engine-Builder, July, 1963.
- [20] Broesma, G. & Tasseron, K.
Propeller manitenance, propeller efficiency and blade roughness
I.S.P., Vol. 14, No. 157, 1967, pp. 347-356.
- [21] Grigson, C. W. B.
Propeller Roughness, its Nature, and its Effect upon the Drag Coefficients of Blades and Ship Power
RINA, 1981.
- [22] Sinclair, L. & Eames, C. F.
Propeller for Economy

- SNAME, Shipboard Energy Conservation Symposium, Sep., 1980.
- [23] Byrne, D. & Fitzsimmons, P. A. & Brook, A. K.
Manitaning Propeller Smoothness: a Cost Effective Means of Energy Saving
SNAME, Ship Costs and Energy Symp., New York, 1982.
- [24] Patience, G.
The Contribution of the Propeller to Energy Conservation in Ship Operation
Trans.IMarE(c), Vol. 94, paper c99, 1982.
- [25] Meyne, K. J. & Blaurock, J. & Kohl, H.
Long Term Roughness Measurements and Cavitation Erosion Observations on Ship Propellers
SNAME, Propeller 84 symposium, May, 1984.
- [26] Callis, F. T.
The Maintenance and Repair of Bronze Propellers
The Shipuilder and Marine Engine-Builder, March, 1963.
- [27] Kan, S. & Shiba, H. & Tsuchida, K. & Yokoo, K.
Effect of Fouling of a Ship's Hull and Propeller upon Propulsive Performance
I.S.P., Vol. 5, No. 41, Jan., 1958.
- [28] Townsin, R. L. & Spencer, D. & Mosaad, M. & Patience G.
Rough Propeller Penalties
SNAME, Annual Meeting, New York, Nov. 13-16, 1985.
- [29] Jones, D. F.
Underwater Propeller Polishing
Underwater Maintenance Company Limited, private comm., 1985
- [30] Dashnaw, F. J. & Hochrein, A. K. & Weinreich, R. S. & Conn, P. K.
Development of Pritective Covering Systems for Steel and Bronze Ship Propellers
Trans. SNAME, Vol. 88, 1980.
- [31] Beauchamp K. G. & Yuen, C. K.
Digital Method for Signal Analysis
George Allen and Unwin, London, 1979.
- [32] Thomas, T. R. & Charlton, G.
Variation of Roughness Parameters on Some Typical Manufactured Surfaces
Precision engineering, 1981.
- [33] Squire, H. B. & Young, A. D.
The Calculation of the Profile Drag of Aerofoil
Aeronautical Research Council, R&M 1838, London, 1937.

- [34] Schlichting, H.
Boundary Layer Theory
Translated by J. Kestin, 6th ed., McGraw-Hill Book
Company, Inc., 1968.
- [35] Kresic, M. & Haskell, B.
Effects of Propeller Design-Point Definition on the Performance
of a Propeller/Diesel Engine System with Regard to In-Service
Roughness and Weather Conditions
Trans. SNAME, 1984.
- [36] Von Karman, T.
Über Laminare und Turbulente Reibung
ZAMMI, pp 233-252, 1921.
- [37] Musker, A. J. & Lewkowicz, A. K.
The Effect of Ship Hull Roughness on the Development of the
Turbulent Boundary Layer
SSPA, International Symposium on Ship Viscous Resistance,
Gothenberg, paper 11, 1978.
- [38] Townsin, R. L. & Medhurst, J. S. & Hamlin, N. A. & Sedat, R.
Progress in Calculating the Resistance of Ships with Homogeneous
or Distributed Roughness
NECIES, Centenary Conference May 1984.
- [39] Clauser, F. H.
Turbulent Boundary Layers in Adverse Pressure Gradients
Journal of Aero. Sci., Vol. 21, pp 91, 1954.
- [40] Hinze, J. O.
Turbulence
McGraw-Hill, New York, 1959.
- [41] Moses, H. L.
The Behaviour of Turbulent Boundary Layers in Adverse Pressure
Gradients
Gas Turbine Laboratory, M.I.T., Rep. 73, Jan., 1964.
- [42] Bull, M. K.
Velocity Profiles of Turbulent Boundary Layers
Aero. J. of the Roy. Aero. Soc., Vol. 73, pp 143, 1969.
- [43] Granville, P. S.
A Modified Law of the Wake for Turbulent Shear Layers
ASME Journal of Fluids Engineering, Vol. 98, No. 3, 1976, pp
478-480.
- [44] Strehle, E.
Zur Integration der Bewegungsgleichungen für ebene turbulente
Wandgrenzen
Wiss., Zeitschrift der T.U. Dresden-23, Heft 1, 1974.

- [45] Mosaad, M. A.
On the Suction of the Boundary Layer When the Free Stream Velocity is Random
Dept. of Mech. Eng., Mansoura University (Egypt), M.Sc. Thesis, 1981.
- [46] Simpson, R. I.
Characteristics of Turbulent Boundary Layers at Low Reynolds Numbers With and Without Transpiration
Journal of Fluid Mech., Vol. 42, 1970.
- [47] Head, M. R.
Entrainment in the Turbulent Boundary Layer
Ministry of Aviation A.R.C., R&M No. 3152, 1960.
- [48] Dvorak, F. A.
Calculation of Turbulent Boundary Layers on Rough Surfaces on Pressure Gradient
AIAA Journal, Vol. 7, No. 9, pp 1752-1759, 1969.
- [49] Sayre, C. L. & Duerr, R. J.
Boundary Layer Investigation on U.S.S. Timmerman
DTMB, Report 1170, 1960.
- [50] Hama, F. R.
Boundary Layer Characteristics for Smooth and Rough Surfaces
SNAME Trans., Vol. 62, pp 333-358, 1954.
- [51] Nikuradse, J.
Stromungsgesetze in Rauhen Rohren
Forsch Arb. Ing. Wes., No. 361, 1933.
- [52] Colebrook, C.
Turbulent Flow in Pipes, with Particular Reference to the Transition Region Between the Smooth and Rough Pipe Laws
J. of Institution of Civil Engineers, Vol. 11, paper 5204, 1938, pp 133-156.
- [53] Altshul, A. D.
Frictional Resistance of Plates with Process Roughness at Turbulent Boundary Layer
Proc. USSR Academy of Sciences, BSRA Translation No. 3967, 1955.
- [54] Grigson, C. W. B.
The Drag Coefficients of a Range of Ship Surfaces
Trans. RINA, 1982.
- [55] Kauczynski, W. & Walderhang, H.
Effect of Paint Roughness on the Skin Friction of Ships
3rd Congress of Int. Mar. Ass. of East Medit., Athens, 1984.

- [56] Johansson, L. E.
The Local Effect on Hull Roughness on Skin Friction. Calculation Based on Floating Element Data and Three-Dimensional Boundary Layer Theory
 RINA, Spring Meetings, 1985.
- [57] Streeter, V. L.
Frictional Resistance in Artificially Roughened Pipes
 Proc. Am. Soc. Civ. Engrs., Vol. 61, pp 163-186, 1935.
- [58] Svensen, T. E. & Medhurst, J. S.
A Simplified Method for the Assessment of Propeller Roughness Penalties
 SNAME, Vol. 21, No. 1 Jan., 1984.
- [59] Theodorsen, T. & Regier, A.
Experiments on Drag of Revolving Discs, Cylinders and Streamline Rods at High Speeds
 N.A.C.A., Report no. 793, 1944.
- [60] Smith, G. P. & Townsend, A. A.
Turbulent Couette Flow Between Concentric Cylinders at Large Taylor Number
 J. Fl. Mech., Vol. 123, pp 187-217, 1982.
- [61] Medhurst, J. S.
Polishing Characteristics and Their Influence on Fluid Drag
 Newcastle University, Navel Arch. Dept., Short Progress Report, 1983.
- [62] Dorfman, L. A.
Hydrodynamic Resistance and the Heat Loss of Rotating Solids
 Oliver and Boyd, 1963.
- [63] Burrill, L. C.
Aerodynamics and Marine Propeller Design
 Trans. NECIES, 1965.
- [64] Abbott, I. H. & Doenhoff, A. E.
Theory of Wing Sections
 Dover Pub., New York, 1959.
- [65] Lackenby, H.
On the Acceleration of Ships
 Institution of Engrs. and Shipbuilders in Scotland, Paper No. 1155, 1952.
- [66] Svensen, T. E.
The Economics of Hull and Propeller Maintenance Examined in the Face of Uncertainty
 Trans. NECIES, Oct., 1983.

- [67] I.T.T.C
Proc. 8th ITTC
Madrid, 1957.
- [68] Hughes, G.
Friction and Form Resistance in Turbulent Flow, and a Proposed Formulation for Use in Model and Ship Correlation
Trans. RINA, Vol. 96, 1954.
- [69] Bowden, B. S. & Davison, N. J.
Ship Resistance and Hull Roughness
Ship TM 356 (NMI), July, 1973.
- [70] Bowden, B. S. & Davison, N. J.
Resistance Increments Due to Hull Roughness Associated with Form Factor Extrapolation Methods
Ship TM 380 (NMI), Jan., 1974.
- [71] Townsin, R. L. & Mosaad, M.
The ITTC Line - Its Genesis and Correlation Allowance
RINA, September, 1985.
- [72] Townsin, R. L. & Byrne, D. & Svensen, T E. & Milne, A.
Fuel Economy Due to Improvements in Ship Hull Surface Condition 1976-1986
I.S.P. , July, 1986.
- [73] Prandtl, L.
Zur Turbulenten Stromung in Rohren und Langsplatten
Erg. Aerodyn. Vers. Anst. zu Gottingen, IV, 1932.
- [74] Schultz-Grunow, F.
New Friction Resistance Law for Smooth Plates
Transl. NACA T.M. 986, Washington, 1941.
- [75] van Lammeren, W. P. A. & Troost, L. & Koning, J. G.
Resistance, Propulsion and Steering of Ships
Tech. Pub. , pp. 43, Holland, 1948.
- [76] Gadd, G.
A New Turbulent Friction Formulation based on a Re-Appraisal of Hughes' Results
Trans. RINA, Vol. 109, 1967.
- [77] Davies, E. B. & Young, A. D.
Streamwise Edge Effects in the Turbulent Boudary Layer on a Flat Plate of Finite Aspect Ratio
Aeronautical Research Council, R&M no. 3367, 1963.
- [78] Granville, P. S.
Drag and Turbulent Boundary Layer of Flat Plates at Low Reynolds Numbers

SNAME, JSR, 21 March, 1952.

- [79] Todd, F. H.
Skin Friction Resistance and the Effects of Surface Roughness
Trans. SNAME Vol. 59, pp. 315, 1951.
- [80] Townsin, R. L. & Byrne, D. & Milne, A. & Svensen, T.
Speed, Power and Roughness: the Economics of Outer Bottom Maintenance
Trans. RINA, Vol. 122, 1980.
- [81] Tokunaga, K. & Baba, E.
Approximate Calculation of Ship Frictional Resistance Increase due to Surface Roughness
J. Soc. N. A., Japan, 152, 1982.
- [82] Lerbs, H. W.
On the Effects of Scale and Roughness on Free Running Propellers
J. Amer. Soc. N. Eng., V. 63, 1951.
- [83] Lock, M. A.
Graphical Method of Calculating the Performance of Airscrews
Aeronautical Research Council, R&M no. 1675, 1934.
- [84] Yamasaki, T.
A Method of Estimating the Ship Propeller Characteristics
Trans. Soc. N. A., Japan, No. 62, Aug., 1981.
- [85] Oosterveld, M. W. & Van Oossanen, P.
Further Computer - Analysed Data of the Wageningen B-Series
International Shipbuilding Progress, Vol. 22, No. 251, 1975.
- [86] Eckhardt, M. K. & Morgan, W. B.
A Propeller Design Method
Trans. SNAME, Vol. 63, 1955.
- [87] Harvald, Sv. Aa.
Resistance and Propulsion of Ships
John Wiley and Sons Pub., New York, 1983.

Appendix A

PROPELLER ROUGHNESS MEASUREMENT

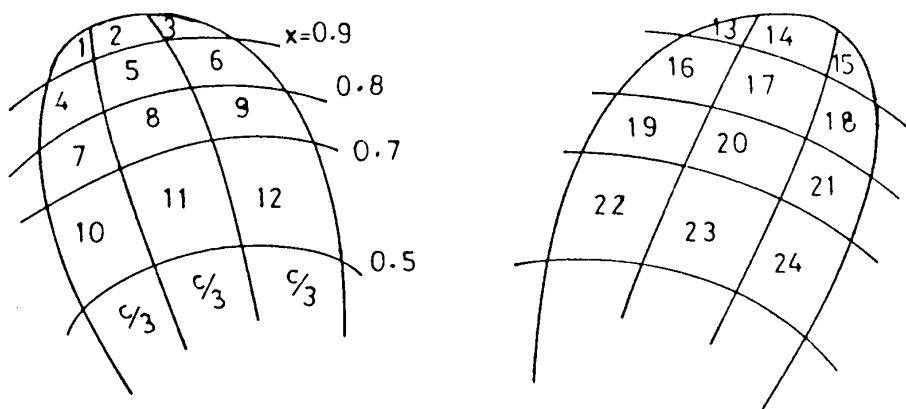
JOB NUMBER: _____ DATE: _____
PROPELLER IDENTIFICATION NO: _____
DIAMETER: _____ P/D: _____ NO. OF BLADE: _____ BAR: _____
SHIP NAME (TYPE): _____
REASON FOR REPAIR (IF ANY): _____

NOTE:

At indocking, after recording fouling extent and severity, the fouling should be removed from this area randomly selected for measurement. This may be done by scrubbing or light scraping but not by abrasive or metallic implements.

Prior to roughness measurements of the propeller surface, an inspection should be made to ensure that each of the blades has the same roughness character.

Three* roughness measurements shall be taken (widely and evenly spaced in the direction of a streamline) within each grid outlined below. Care should be taken to avoid measurements of cavitation eroded areas.



PROCEDURE

- a) Set long wavelength 'cut off' to 2.5 millimeter setting.
- b) Record Ra within the grid.
- c) Set bandwidth "b" on parameter box to Ra then switch to measure peak count 'Pc'.
- d) Record Ra and Pc.
- e) Move the instrument to a new location within the grid and repeat b, c and d for each of the three* measurement locations within the grid.

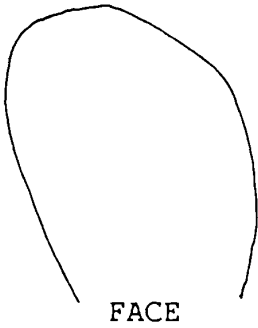
*Short Procedure: Only one location would be sampled per grid located roughly at the center of the area.

FOULING:

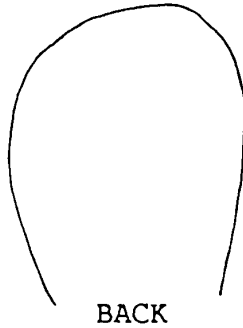
NUMBER OF YEARS IN SERVICE:

MATERIAL:

COATING (if any):



FACE



BACK

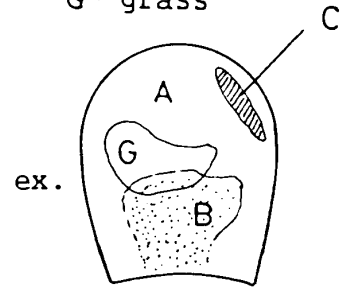
legend:

A- clean

B- barnacles

c- cavitation

G- grass



indicate fouling on sketches

run loc 'n	1			2			3		
	Ra(b)	Ra	Pc	Ra(b)	Ra	Pc	Ra(b)	Ra	Pc
face									
1									
2									
3									
4									
5									
6									
7									
8									
9									
10									
11									
12									
back									
13									
14									
15									
16									
17									
18									
19									
20									
21									
22									
23									
24									

Appendix B

POOLE RIVER SURFACE ROUGHNESS PROFILES

SURFPACK RUN NO. 104

PROFILE I/D. POOLE1

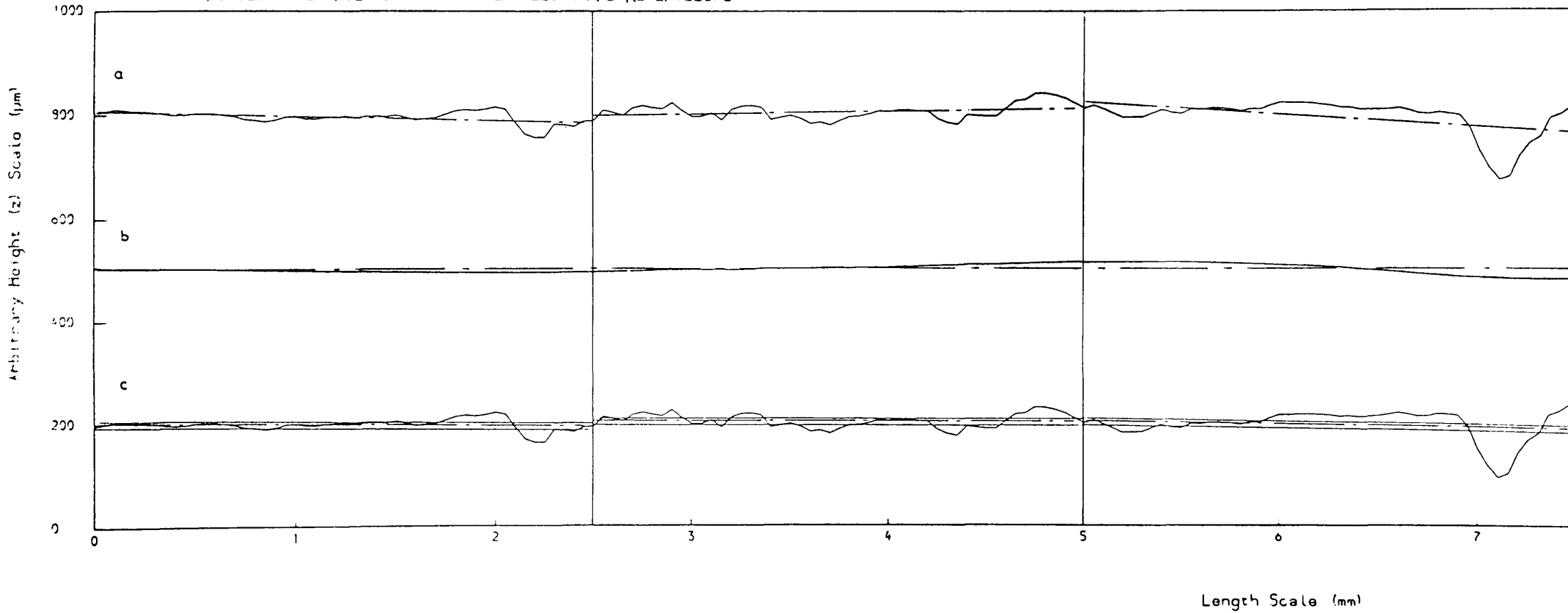
VENUE. 30-4-85

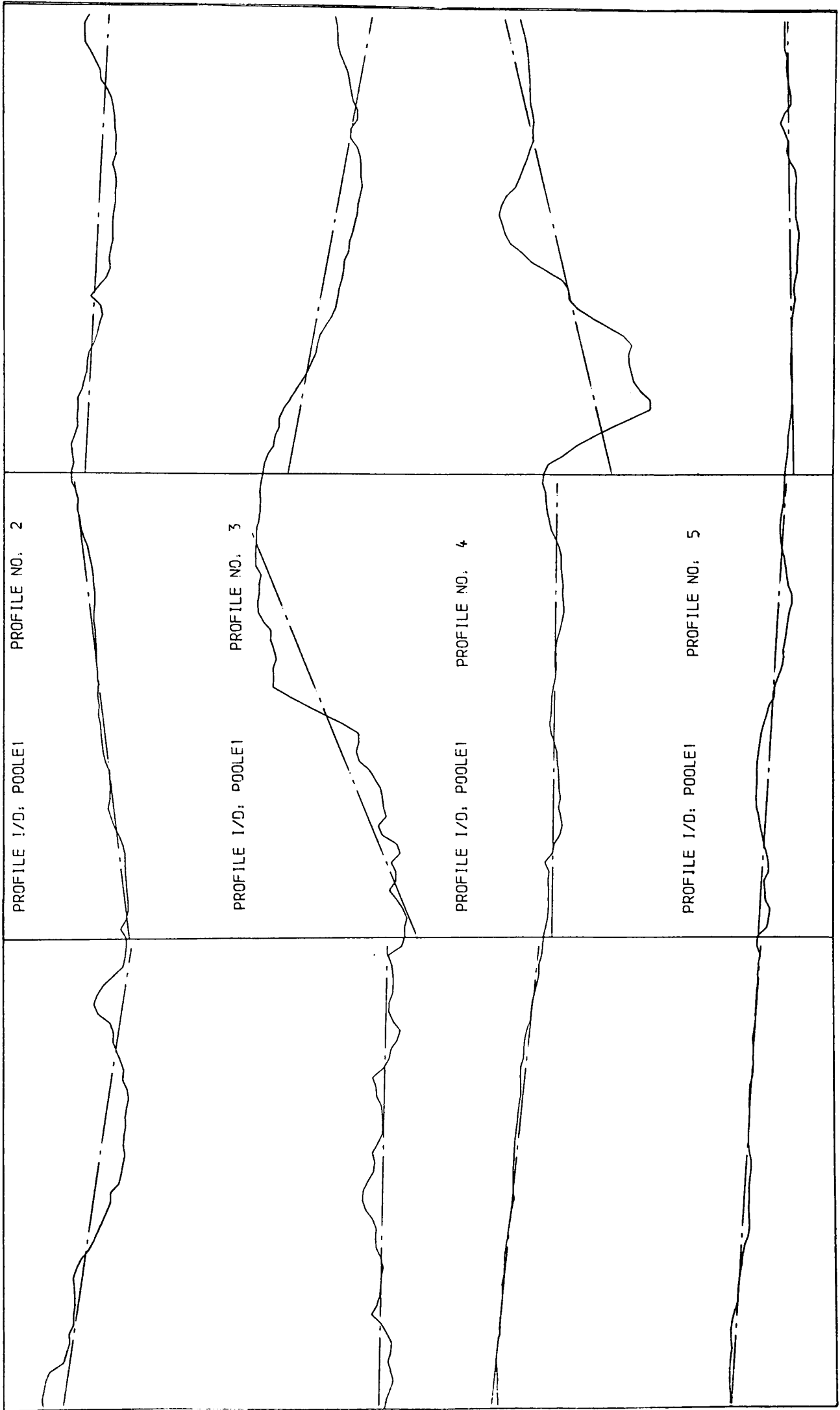
PROFILE NO. 1

a - UNFILTERED PROFILE WITH CENTRELINE Vertical/Horizontal Magnification Factor: 2.6

b - SIGNAL REJECTED BY RECURSIVE I.I.R. FILTER

c - PROFILE AFTER FILTERING WITH CENTRELINE AND R_a ENVELOPE





PROFILE 1/D: POOLE2

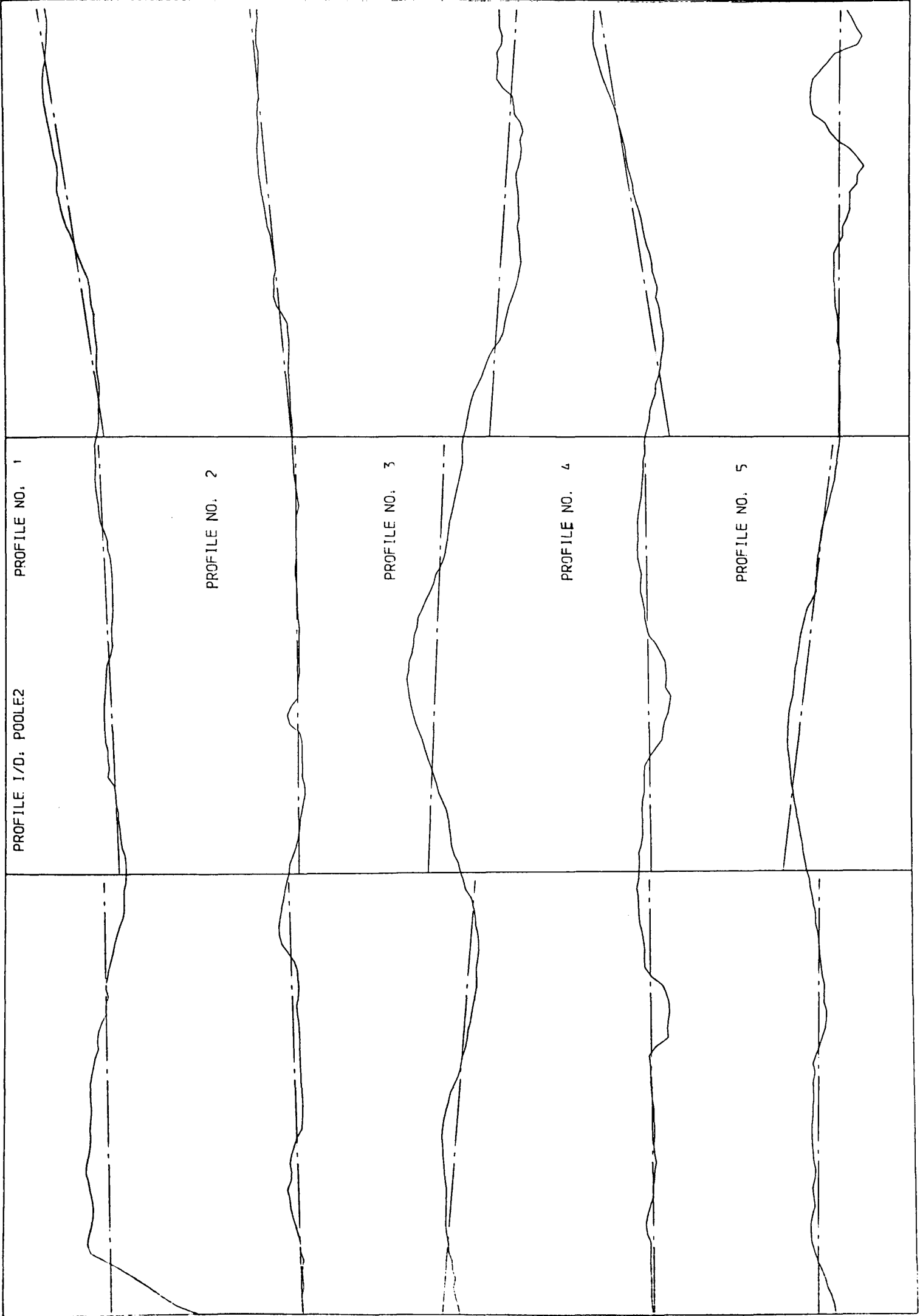
PROFILE NO. 1

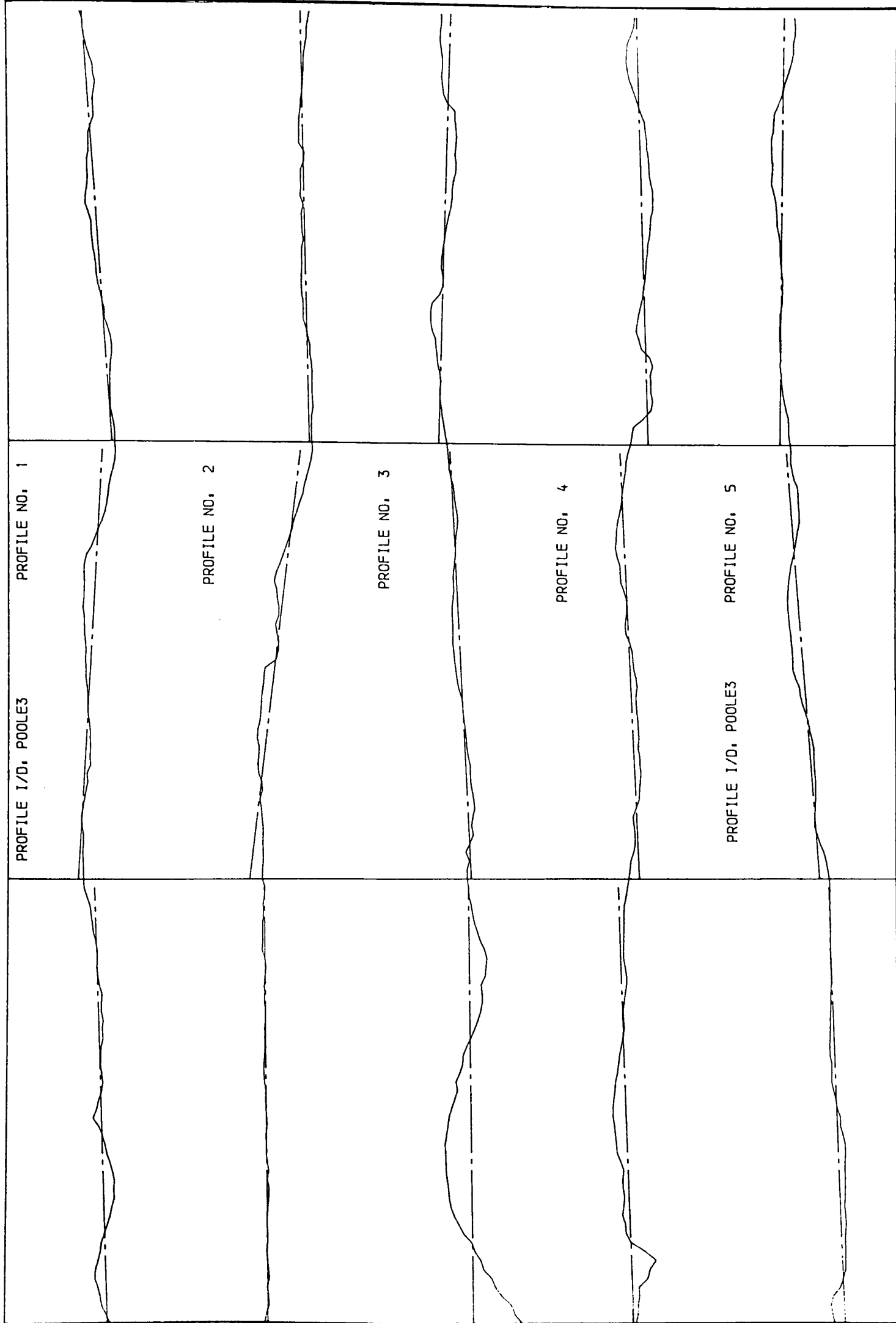
PROFILE NO. 2

PROFILE NO. 3

PROFILE NO. 4

PROFILE NO. 5



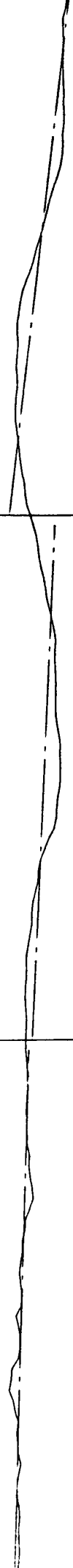


PROFILE I/D, POOLE4

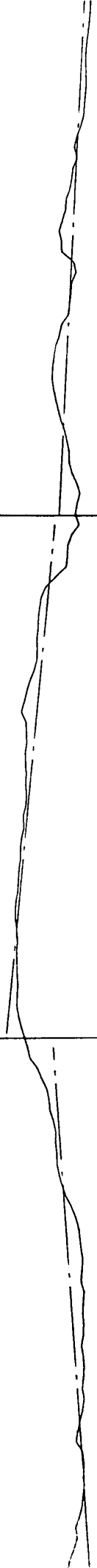
PROFILE NO. 1



PROFILE NO. 2



PROFILE NO. 3

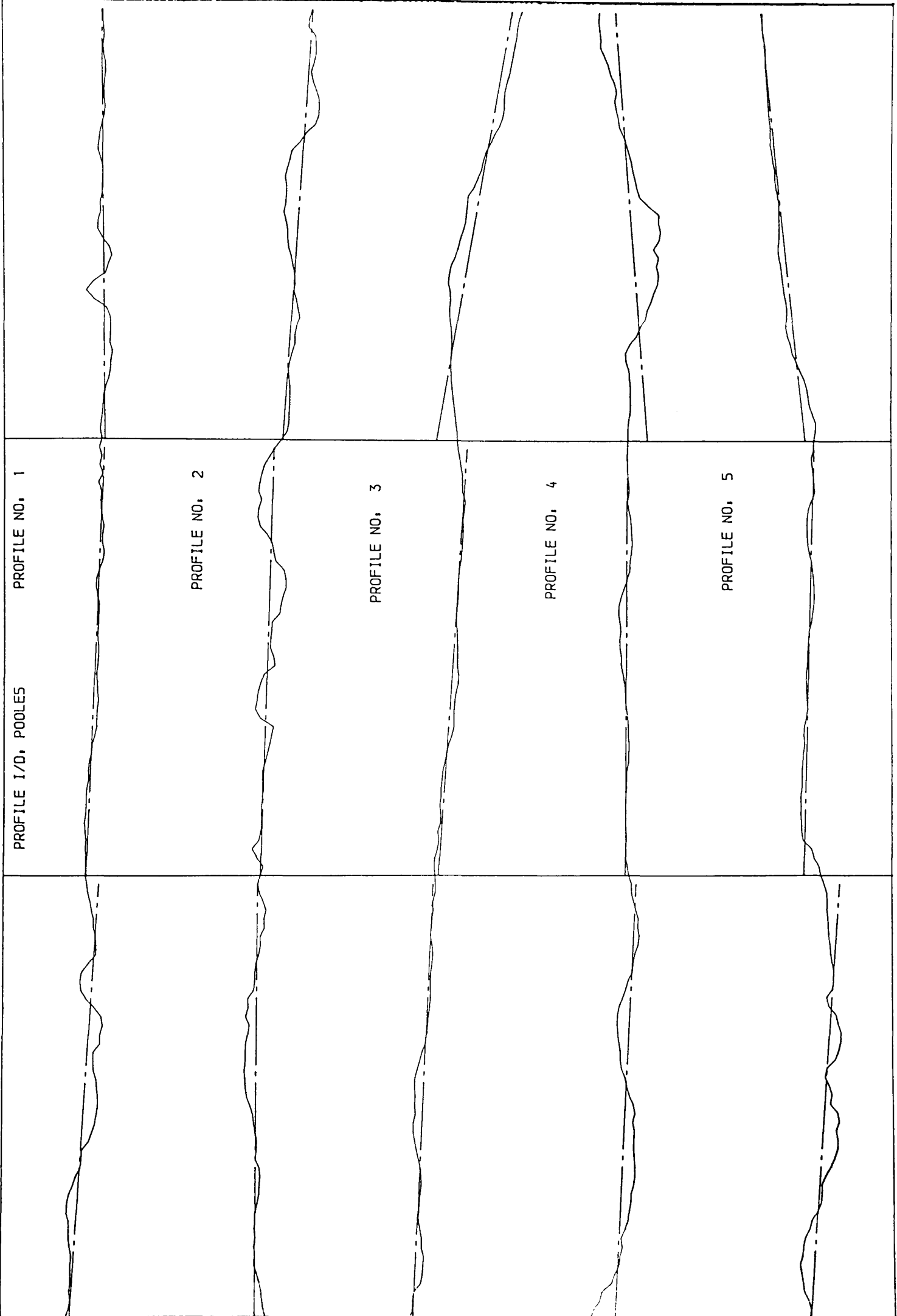


PROFILE NO. 4



PROFILE NO. 5





Appendix C

ALGORITHM SOLUTION OF THE BOUNDARY LAYER INTEGRAL EQUATIONS

C-1 THE CRAMER'S RULE SOLUTION

The boundary layer equation has been derived in chapter 3 in the following form:

$$f_{11} \frac{d\delta}{dx} + f_{12} \frac{d\pi}{dx} + f_{13} \frac{d\omega}{dx} = f_{14}$$

$$f_{21} \frac{d\delta}{dx} + f_{22} \frac{d\pi}{dx} + f_{23} \frac{d\omega}{dx} = f_{24}$$

$$f_{31} \frac{d\delta}{dx} + f_{32} \frac{d\pi}{dx} + f_{33} \frac{d\omega}{dx} = f_{34}$$

Using CRAMER'S RULE to find the first order differential equations in terms of $d\delta/dx$, $d\pi/dx$ & $d\omega/dx$ as follows:

$$\frac{d\delta}{dx} = \frac{\begin{vmatrix} f_{14} & f_{12} & f_{13} \\ f_{24} & f_{22} & f_{23} \\ f_{34} & f_{32} & f_{33} \end{vmatrix}}{|D|}$$

$$\frac{d\pi}{dx} = \frac{\begin{vmatrix} f_{11} & f_{14} & f_{13} \\ f_{21} & f_{24} & f_{23} \\ f_{31} & f_{34} & f_{33} \end{vmatrix}}{|D|}$$

$$\frac{d\omega}{dx} = \frac{\begin{vmatrix} f_{11} & f_{12} & f_{14} \\ f_{21} & f_{22} & f_{24} \\ f_{31} & f_{32} & f_{34} \end{vmatrix}}{|D|}$$

where,

$$|D| = \begin{vmatrix} f_{11} & f_{12} & f_{13} \\ f_{21} & f_{22} & f_{23} \\ f_{31} & f_{32} & f_{33} \end{vmatrix}$$

The above solution is expressed in the the following set of equations:

$$d\delta/dx = f_1(x, U_S, h, \delta, \pi, \omega)$$

$$d\pi/dx = f_2(x, U_S, h, \delta, \pi, \omega)$$

$$d\omega/dx = f_3(x, U_S, h, \delta, \pi, \omega)$$

This equations can be simplified in the following notations:

$$d\delta/dx = F_1(x, \delta, \pi, \omega)$$

$$d\pi/dx = f_2(x, \delta, \pi, \omega)$$

$$d\omega/dx = f_3(x, \delta, \pi, \omega)$$

C-2 FOURTH RANGE-KUTTA ALGORITHM

For the integrations from step 0 to step 1, the RUGE-KUTTA METHOD

ALGORITHM proceeds as follows:

$$\begin{aligned} K_1 &= F_1(x_0, \delta_0, \pi_0, \omega_0) \Delta x \\ L_1 &= F_2(x_0, \delta_0, \pi_0, \omega_0) \Delta x \\ M_1 &= F_3(x_0, \delta_0, \pi_0, \omega_0) \Delta x \end{aligned}$$

$$\begin{aligned} K_2 &= F_1(x_0 + \Delta x/2, \delta_0 + K_1/2, \pi_0 + L_1/2, \omega_0 + M_1/2) \Delta x \\ L_2 &= F_2(x_0 + \Delta x/2, \delta_0 + K_1/2, \pi_0 + L_1/2, \omega_0 + M_1/2) \Delta x \\ M_2 &= F_3(x_0 + \Delta x/2, \delta_0 + K_1/2, \pi_0 + L_1/2, \omega_0 + M_1/2) \Delta x \end{aligned}$$

$$\begin{aligned} K_3 &= F_1(x_0 + \Delta x/2, \delta_0 + K_2/2, \pi_0 + L_2/2, \omega_0 + M_2/2) \Delta x \\ L_3 &= F_2(x_0 + \Delta x/2, \delta_0 + K_2/2, \pi_0 + L_2/2, \omega_0 + M_2/2) \Delta x \\ M_3 &= F_3(x_0 + \Delta x/2, \delta_0 + K_2/2, \pi_0 + L_2/2, \omega_0 + M_2/2) \Delta x \end{aligned}$$

$$\begin{aligned} K_4 &= F_1(x_0 + \Delta x, \delta_0 + K_3, \pi_0 + L_3, \omega_0 + M_3) \Delta x \\ L_4 &= F_2(x_0 + \Delta x, \delta_0 + K_3, \pi_0 + L_3, \omega_0 + M_3) \Delta x \\ M_4 &= F_3(x_0 + \Delta x, \delta_0 + K_3, \pi_0 + L_3, \omega_0 + M_3) \Delta x \end{aligned}$$

$$\begin{aligned} \Delta\delta &= 1/6 (K_1 + 2K_2 + 2K_3 + K_4) \\ \Delta\pi &= 1/6 (L_1 + 2L_2 + 2L_3 + L_4) \\ \Delta\omega &= 1/6 (M_1 + 2M_2 + 2M_3 + M_4) \end{aligned}$$

$$\begin{aligned} \delta_1 &= \delta_0 + \Delta\delta \\ \pi_1 &= \pi_0 + \Delta\pi \\ \omega_1 &= \omega_0 + \Delta\omega \end{aligned}$$

Appendix D

ESTIMATING THE BOUNDARY LAYER THICKNESS

On the basis of the power law assumptions, Schlichting [34] has given the following formula to estimate the growth of the turbulent boundary layer for smooth flat plate:

$$\delta_{fp} = 0.37 \times R_x^{-0.2}$$

The above equation was derived on the basis of $n=7$ in the following equation:

$$u/U_s = (y/\delta)^{1/n}$$

and hence is valid for only a limited range of Reynolds numbers. To determine whether δ_{fp} would give a useful estimate for the magnitude of δ on an engineering surface, a general expression has been derived by Sayere and Duerr [49] for δ_{fp} as a function of n :

$$\delta_{fp}(x,n) = [(2+n)(3+n)/n]^{(n+1)/(n+3)} [1/c(n)]^{2n/(3+n)} x^{n-2/(3+n)}$$

where,

$c(n)$ is a dimensionless empirical coefficient related to the friction velocity.

However, the above equation is applicable to only the two-dimensional turbulent flow over a smooth flat plate, it gives a more realistic estimate of δ than Schlichting's formula. To calculate the velocity profile exponent n and the empirical coefficient $c(n)$ with the variation of the Reynolds number, approximation relationships based on the work made by Sayre and Duerr are used:

$$n = 1.4795 \log Rn - 3.247$$

and

$$c(n) = 0.02167 n^3 - 0.575 n^2 + 5.9333 n - 12.03$$

and hence δ_{fp} can be calculated to use as a starting value in the method of calculations.

Appendix E

ROTOR EXPERIMENTS DATA

SMOOTH SURFACE EXPERIMENTS

DATA OF SMOOTH SHORT ROTOR

N_a	N_{mi}	N_{mx}	Q_a	Q_{mi}	Q_{mx}	$T^{\circ}C$
100.0	100.0	100.0	0.64	0.61	0.67	19.0
125.0	125.0	125.0	0.84	0.83	0.86	19.0
150.0	150.0	150.0	1.09	1.08	1.11	19.1
175.0	175.0	175.0	1.26	1.20	1.32	19.2
200.0	200.0	200.0	1.52	1.47	1.55	19.2
225.0	225.0	225.0	1.81	1.79	1.82	19.3
250.0	250.0	250.0	2.10	2.07	2.11	19.3
275.0	275.0	275.0	2.38	2.35	2.40	19.3
300.0	300.0	300.0	2.72	2.70	2.74	19.4
325.0	325.0	325.0	3.07	3.03	3.11	19.4
350.0	350.0	350.0	3.40	3.30	3.50	19.5
375.0	375.0	375.0	3.81	3.77	3.89	19.5
400.0	400.0	400.0	4.21	4.14	4.29	19.6
450.0	450.0	450.0	5.14	5.10	5.17	19.6
500.0	500.0	500.0	6.08	6.02	6.18	19.7
550.0	550.0	550.0	7.17	6.96	7.32	19.8
600.0	600.0	600.0	8.25	8.23	8.23	19.9
650.0	650.0	650.0	9.45	9.41	9.50	20.1
700.0	700.0	700.0	10.76	10.70	10.80	20.2
750.0	750.0	750.0	12.15	12.10	12.20	20.4
900.0	900.0	900.0	16.81	16.73	16.90	20.6
950.0	950.0	950.0	18.50	18.40	18.60	20.8

SMOOTH SURFACE EXPERIMENTS

DATA OF SMOOTH LONG ROTOR

N_a	N_{mi}	N_{mx}	Q_a	Q_{mi}	Q_{mx}	$T^{\circ}C$
100.0	100.0	100.0	0.81	0.79	0.83	18.4
125.0	125.0	125.0	1.04	1.02	1.05	18.4
150.0	150.0	150.0	1.29	1.26	1.31	18.4
175.0	175.0	175.0	1.56	1.48	1.61	18.4
200.0	200.0	200.0	1.86	1.83	1.89	18.5
225.0	225.0	225.0	2.19	2.18	2.20	18.5
250.0	250.0	250.0	2.53	2.52	2.55	18.5
275.0	275.0	275.0	2.86	2.83	2.90	18.6
300.0	300.0	300.0	3.24	3.21	3.27	18.7
325.0	325.0	325.0	3.71	3.66	3.77	18.8
350.0	350.0	350.0	4.16	3.93	4.41	18.9
375.0	375.0	375.0	4.65	4.59	4.68	18.9
400.0	400.0	400.0	5.25	5.20	5.30	19.0
450.0	450.0	450.0	6.39	6.33	6.45	19.0
500.0	500.0	500.0	7.71	7.64	7.76	19.1
550.0	550.0	550.0	9.09	8.80	9.35	19.2
600.0	600.0	600.0	10.58	10.52	10.62	19.3
650.0	650.0	650.0	12.14	12.10	12.16	19.5
700.0	700.0	700.0	13.85	13.81	13.92	19.7
750.0	750.0	750.0	15.66	15.61	15.69	19.8
900.0	900.0	900.0	21.64	21.55	21.73	20.0
950.0	950.0	950.0	23.83	23.75	23.86	20.2

POOLE RIVER PROPELLER SURFACE EXPERIMENTS

DATA OF ROUGH SHORT ROTOR

N_a	N_{mi}	N_{mx}	Q_a	Q_{ni}	Q_{mx}	$T^{\circ}C$
100.5	100.2	100.8	0.75	0.71	0.78	19.5
125.4	125.1	125.6	0.96	0.95	0.97	19.5
149.5	149.4	150.3	1.20	1.19	1.21	19.5
175.5	175.2	175.7	1.50	1.40	1.62	19.5
200.2	200.0	200.0	1.81	1.78	1.88	19.5
224.9	224.8	225.1	2.16	2.14	2.17	19.5
250.1	249.7	250.4	2.48	2.47	2.48	19.5
275.8	275.3	276.3	2.86	2.84	2.90	19.5
299.8	299.6	300.5	3.25	3.24	3.28	19.5
325.2	324.8	325.3	3.67	3.62	3.71	19.5
350.5	350.2	350.8	4.17	3.95	4.33	19.5
375.6	375.0	376.2	4.65	4.51	4.75	19.5
399.2	398.4	400.4	5.12	5.05	5.17	19.6
425.3	425.0	425.7	5.67	5.62	5.71	19.7
451.0	450.8	451.3	6.29	6.23	6.33	19.8
474.9	474.8	475.4	6.85	6.80	6.91	19.9
499.6	498.9	500.1	7.41	7.39	7.46	19.9
551.2	550.4	552.1	8.78	8.58	9.01	20.0
600.2	599.8	601.2	10.16	10.13	10.24	20.1
651.2	649.5	652.2	11.83	11.78	11.91	20.4
701.0	700.9	701.7	13.52	13.60	13.60	20.6
751.0	750.4	751.9	15.38	15.33	15.46	20.9
799.7	799.1	800.3	17.27	17.23	17.31	21.1

POOLE RIVER PROPELLER SURFACE EXPERIMENTS

DATA OF ROUGH LONG ROTOR

N_a	N_{mi}	N_{mx}	Q_a	Q_{mi}	Q_{mx}	$T^{\circ}C$
100.5	100.3	100.7	0.90	0.86	0.93	19.2
124.8	124.7	125.0	1.15	1.14	1.16	19.2
149.9	149.7	150.1	1.45	1.43	1.46	19.2
175.3	175.1	175.7	1.80	1.69	1.91	19.2
201.5	201.0	201.8	2.22	2.15	2.23	19.2
250.0	249.7	250.3	3.08	3.05	3.11	19.2
275.7	275.3	276.0	3.59	3.54	3.63	19.2
300.2	300.0	300.5	4.15	4.13	4.17	19.2
325.6	325.3	326.3	4.71	4.66	4.80	19.2
350.7	350.2	351.0	5.34	5.10	5.58	19.2
374.3	373.8	375.0	6.00	5.77	6.27	19.3
400.5	400.1	400.7	6.49	6.43	6.53	22.7
501.2	500.8	501.6	9.67	9.63	9.69	22.7
600.2	600.0	600.4	13.37	13.32	13.45	22.8
701.0	700.8	701.5	17.78	17.72	17.82	22.8
802.1	802.8	802.8	22.93	22.88	22.96	23.0

Appendix F

SUMMARY OF THE RIEGELS METHOD

Riegels method is based on the assumption that, the arbitrary profile contour with co-ordinates x and y in a free stream velocity V with incidence α to the x -axis is represented by:

1. a source distribution for the case of a thin profile in symmetrical flow, with a strength given by

$$2 V \cos\alpha \, dy/dx$$

2. a vortex distribution to account for unsymmetrical flow, with a strength given by

$$2 V \cos\alpha \frac{c/2 - x}{c/2 + x} \quad (c \text{ is the chord})$$

3. a vortex distribution to include the effect of finite thickness, with a strength given by

$$2 V \sin\alpha \, dy/dx$$

By introducing the boundary conditions, summing all the system of distribution and resolving for the velocity tangential to the profile contour U_s , and including the free stream component $V \cos\alpha$. This gives:

$$\frac{U_s}{V} = \frac{\cos\alpha [\pm a_n - C_n + A_n + C_0] + \sin\alpha [b_n \mp D_n + B_n - B_0]}{[a_n + (B_n \mp D_n)^2]}$$

where,

$$A_n = \sum A_{mn} (Y_m - Y_{2N-m})$$

$$B_n = \sum B_{mn} (Y_m - Y_{2N-m})$$

$$C_n = \sum C_{mn} (Y_m + Y_{2N-m})$$

$$D_n = \sum D_{mn} (Y_m + Y_{2N-m})$$

$$a_n = -1/2 \sin$$

$$b_n = -1/2 + 1/2 \cos \phi$$

$$\phi = \pi m/N \quad (n = 0, 1, 2, 3, \dots, N)$$

and

$Y_m - Y_{2N-m}$ is the profile thickness

$Y_m + Y_{2N-m}$ is the profile camber

Using Bernolli's equation, the local pressure change Δp can be obtained as:

$$\Delta p = 1/2 \rho v^2 [1 - (U_s/v)^2]$$

and the pressure coefficient can be expressed by:

$$C_p = p/q_0 = 1 - (U_s/v)^2$$

where q_0 is the dynamic pressure equal to $1/2 \rho v^2$.

Appendix G

PROPELLER/HULL ROUGHNESS PENALTIES - NUMERICAL EXAMPLE

The vessel chosen to demonstrate the combined effects on ship performance of propeller blade and ship hull surface roughness was built in 1978, and is a general cargo ship. The surface roughness of its propeller was measured by courtesy of S.M.M.Ltd., using a Surtronic 3, in accordance with the procedure developed by the Ship Performance Group.

Main Ship Particular:

Overall Length	=	163.150	m
Length B. P.	=	155.000	m
Breadth	=	22.860	m
Depth	=	13.420	m
Max. Summer Draught	=	9.727	m
Deadweight at Max. Summer Draught	=	9015.000	tonnes
Block Coefficient	=	0.710	
Watted Surface Area (at T=9.727)	=	5079.000	m ²
Design Speed	=	16.75	knots
Taylor Wake	=	0.38	
Thrust Deduction	=	0.195	
Relative Rotative Efficiency	=	1.030	

Machinery:

6 Cylinder Sulzer 2SA

Max. output 8952 KW / 12000 BHP 122 RPM

Design output 85% MCR 7610 KW / 10200 BHP 122 RPM

Propeller Characteristics:

Diameter D = 5.5 m

Pitch 0.7R P = 4.758 m

Pitch Ratio P/D = 0.865

Developed Blade Area Ratio BAR = 0.660

Number of Blades Z = 4

t/c 0.7R [equation(6.67)] = 0.04

G-1 PROPELLER ROUGHNESS MEASUREMENT

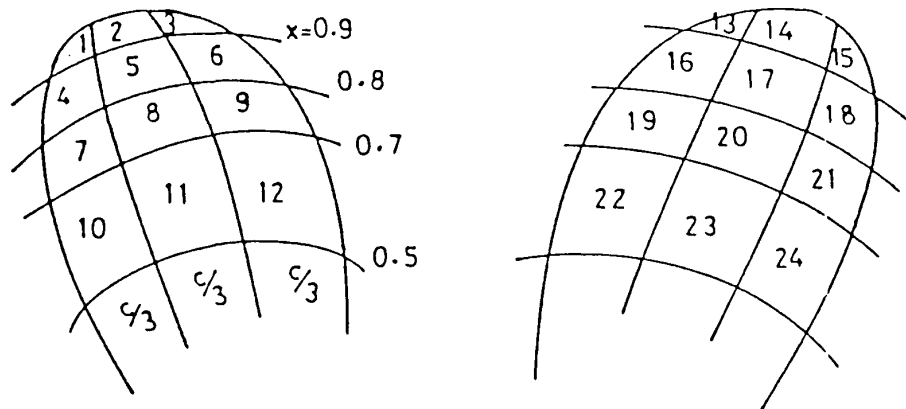
JOB NUMBER: _____ DATE: _____
PROPELLER IDENTIFICATION NO: _____
DIAMETER: 5.5 m P/D: 0.865 NO. OF BLADE: 4 BAR: 0.66
SHIP NAME (TYPE): "General Cargo Ship"
REASON FOR REPAIR (IF ANY): _____

NOTE:

At indocking, after recording fouling extent and severity, the fouling should be removed from this area randomly selected for measurement. This may be done by scrubbing or light scraping but not by abrasive or metallic implements.

Prior to roughness measurements of the propeller surface, an inspection should be made to ensure that each of the blades has the same roughness character.

Three* roughness measurements shall be taken (widely and evenly spaced in the direction of a streamline) within each grid outlined below. Care should be taken to avoid measurements of cavitation eroded areas.



PROCEDURE

- a) Set long wavelength 'cut off' to 2.5 millimeter setting.
- b) Record Ra within the grid.
- c) Set bandwidth "b" on parameter box to Ra then switch to measure peak count 'Pc'.
- d) Record Ra and Pc.
- e) Move the instrument to a new location within the grid and repeat b, c and d for each of the three* measurement locations within the grid.

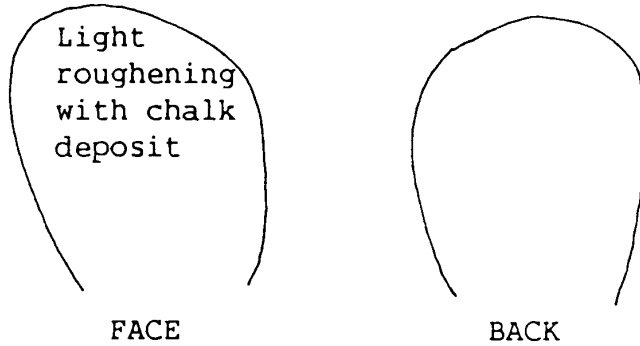
*Short Procedure: Only one location would be sampled per grid located roughly at the center of the area.

FOULING:

NUMBER OF YEARS IN SERVICE: 7

MATERIAL: Manganese Bronze

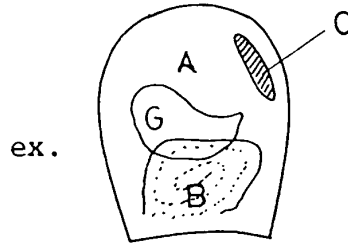
COATING (if any): Light Chalk



indicate fouling on sketches

legend:

- A- clean
- B- barnacles
- c- cavitation
- G- grass



run loc'n	1			2			3		
	Ra(b)	Ra	Pc	Ra(b)	Ra	Pc	Ra(b)	Ra	Pc
face									
1	14.4	13.5	43	14.0	12.4	53.0			
2	17.4	15.6	22	16.5	15.1	22.0			
3	18.0	18.3	24	18.1	17.6	22.0			
4	19.9	19.1	19	19.6	19.1	19.0			
5	27.0	26.7	24	26.9	27.9	17.0			
6	22.8	24.5	10	23.6	20.8	16.0			
7	26.7	28.0	32	27.3	22.2	19.0			
8	10.1	10.9	15	10.5	10.0	24.0			
9	9.7	10.0	34	9.8	9.4	29.0			
10	8.2	6.7	17	7.5	6.6	32.0			
11	5.6	5.0	51	5.3	5.1	68.0			
12	10.8	10.2	39	10.5	10.6	17.0			
							in general direction of lay		
back									
13	21.7	20.3	29	20.7	20.6	29.0			
14	17.0	16.6	19	16.8	16.8	24.0			
15	21.5	20.0	27	20.7	19.8	24.0			
16	18.0	21.1	28	19.5	21.8	19.0			
17	46.4	46.8	17	46.6	47.0	14.0			
18	25.1	24.9	10	25.0	26.5	15.0			
19	23.1	21.0	15	22.0	20.2	24.0			
20	21.7	22.1	19	21.9	24.6	27.0			
21	17.4	17.8	27	17.6	18.3	22.0			
22	22.6	22.5	36	22.5	20.6	36.0			
23	7.9	8.0	56	7.9	7.9	44.0			
24	8.0	8.2	46	8.1	8.4	36.0			
							generally at right angle to lay		

G-2 CALCULATION OF APR

SET 1 TRACE 1 FACE

1	2	3	4	5	6	7	8
	Ra	Pc	h'	(h') ^{1/3}	(h') ^{1/3}	Wi	6*7
1	13.9	43.0	123.0	5.0			
2	16.5	22.0	88.0	4.4	4.77	0.23	1.10
3	18.1	24.0	116.2	4.9			
4	19.5	19.0	106.2	4.7			
5	26.8	24.0	254.3	6.3	5.14	0.27	1.39
6	23.6	10.0	82.2	4.3			
7	27.3	32.0	351.9	7.1			
8	10.5	15.0	24.3	2.9	4.53	0.21	0.95
9	9.8	34.0	48.5	3.6			
10	7.4	17.0	13.9	2.4			
11	5.3	51.0	21.1	2.8	3.05	0.22	0.67
12	10.5	39.0	63.2	4.0		----	----
						0.93	4.11

$(h')^{1/3} = 4.11/0.93 = 4.42$

SET 2 TRACE 2 FACE

1	2	3	4	5	6	7	8
	Ra	Pc	h'	(h') ^{1/3}	(h') ^{1/3}	Wi	6*7
1	13.2	53.0	135.8	5.1			
2	15.8	22.0	80.7	4.3	4.72	0.23	1.08
3	17.9	22.0	103.0	4.7			
4	19.4	19.0	104.6	4.7			
5	27.4	17.0	187.6	5.7	5.10	0.27	1.38
6	22.2	16.0	115.9	4.9			
7	24.8	19.0	171.1	5.6			
8	10.3	24.0	37.1	3.3	4.10	0.21	0.86
9	9.6	29.0	39.3	3.4			
10	7.1	32.0	23.4	2.9			
11	5.2	68.0	27.0	3.0	2.96	0.22	0.65
12	10.5	17.0	27.8	3.0		----	----
						0.93	3.97

$$(h')^{1/3} = 3.97/0.93 = 4.27$$

SET 3 TRACE 1 BACK

1	2	3	4	5	6	7	8
	Ra	Pc	h'	(h') ^{1/3}	(h') ^{1/3}	Wi	6*7
13	21.0	29.0	188.0	5.7			
14	16.8	19.0	78.8	4.3	5.19	0.23	1.19
15	20.8	27.0	170.9	5.5			
16	19.6	28.0	157.3	5.4			
17	46.6	17.0	542.7	8.2	6.02	0.27	1.63
18	25.0	10.0	91.9	4.5			
19	22.1	15.0	107.2	4.8			
20	21.9	19.0	134.0	5.1	4.95	0.21	1.04
21	17.6	27.0	122.9	5.0			
22	22.6	36.0	269.1	6.5			
23	7.9	56.0	52.0	3.7	4.28	0.22	1.01
24	8.1	46.0	44.4	3.5		----	----
						0.93	4.87

$$(h')^{1/3} = 4.87/0.93 = 5.23$$

SET 4 TRACE 2 BACK

1	2	3	4	5	6	7	8
	Ra	Pc	h'	(h') ^{1/3}	(h') ^{1/3}	Wi	6*7
13	20.6	29.0	181.8	5.7			
14	16.8	24.0	99.6	4.6	5.18	0.23	1.19
15	20.3	24.0	144.7	5.2			
16	20.6	19.0	119.1	4.9			
17	46.8	14.0	450.8	7.7	5.95	0.27	1.61
18	25.8	15.0	146.2	5.3			
19	21.1	24.0	157.1	5.4			
20	23.3	27.0	214.5	6.0	5.36	0.21	1.13
21	17.9	22.0	104.2	4.7			
22	21.6	36.0	245.8	6.3			
23	7.9	44.0	40.4	3.4	4.33	0.22	0.95
24	8.3	36.0	36.0	3.3		0.93	4.88

$$(h')^{1/3} = 4.88/0.93 = 5.25$$

APR FOR ENTIRE PROPELLER

Trace	Face	Back
1	4.42	5.23
2	4.27	5.25
Average (h') ^{1/3}	4.25	5.24

$$\text{Overall Average (APR)}^{1/3} = 4.74; \text{ APR} = 110.0 \mu\text{m}$$

G-3 CALCULATION OF ROUGHNESS PENALTIES

1000 C _{FS}	(ITTC 57)	=	1.5100
(1+k)	(Watanabe Formula)	=	1.1630
1000 ΔC _F	(Flat Plane, AHR=125μm)	=	0.1559
1000 ΔC _F	(Ship) = 1.1 ΔC _F (Plane)	=	0.1715
1000 C _{vis}	= (1.163*1.51) + 0.1715	=	1.9276
Volume of Displacement, ∇		=	24470.0 m ³
L/∇ ^{1/3}		=	5.340
Fn		=	0.221
1000 C _R	(Reference [87])	=	1.100
1000 C _{AA}		=	0.150
1000 C _T		=	3.177
1000 C _s	= 1000[ΔC _F (AHR300)-ΔC _F (AHR125)]	=	0.1315
Hull Efficiency	= (1 - t)/(1 - w _{TS})	=	1.300
Propeller Efficiency	(Bp-δ Diagram)	=	0.530
Propulsive Efficiency		=	0.710
w _{TR}	[equation (6.79)]	=	0.393
WK	= (1 - w _{TR})/(1 - w _{TS})	=	0.980
1/K _T dK _T /dJ	[equation (6.98)]	=	-2.111
Advance Constant; (J = Va/RPM*D)		=	0.478
C _L	[equation (6.46)]	=	0.229
Chord	[equation (6.66)]	=	1.928 m
1000 ΔC _F	[Flat Blade, equation (6.29)]	=	1.050
1000 ΔC _D	[equation (6.36)]	=	2.188

Propeller/Hull Penalties

Sign	Item	Propeller	Hull	Propeller/Hull
(+)	$\Delta K_Q/K_Q$ %	(+) 1.42	-	1.42
(-)	$\Delta K_T/K_T$ %	(-) -1.54	-	1.54
(-)	$\Delta J/J$ %	(-) -0.51	(-) -2.72	3.23
(+)	$\Delta C_T/C_T$ %	-	(+) 4.14	4.14
(-)	$\Delta \eta_H/\eta_H$ %	-	(-) 2.08	-2.08
<hr style="border-top: 1px dashed black;"/>				
(+)	$\Delta P/P$ %	3.470	4.780	8.25
<hr style="border-top: 1px dashed black;"/>				
(-)	$\Delta V/V$ % *	1.157	1.593	2.75
<hr style="border-top: 1px dashed black;"/>				

* (n+1) = 3.0

Propeller Roughness Penalty Using Rubert Gauges

Rubert Surface	A	B	C	D	E	F
Musker 's h'	1.1	5.4	17.3	61.0	133	311
Change in Drag Coef.	-	0.0001	0.0007	0.0016	0.0024	0.0036
$\Delta P/P$ %	-	0.144	1.060	2.540	3.830	5.6500
$\Delta V/V$ % *	-	0.048	0.353	0.847	1.273	1.8830
<hr style="border-top: 1px dashed black;"/>						
(+) $\Delta P/P$ % equ.(6.61)	-	0.148	1.080	2.620	3.940	5.8300
<hr style="border-top: 1px dashed black;"/>						
(-) $\Delta V/V$ % *	-	0.049	0.360	0.873	1.313	1.9430
<hr style="border-top: 1px dashed black;"/>						

* (n+1) = 3.0